Validation Test Report for the 1/16° East Asian Seas Navy Coastal Ocean Model Nowcast/Forecast System

SHELLEY RIEDLINGER
RUTH PRELLER
PAUL MARTIN

Ocean Dynamics and Prediction Branch
Oceanography Division

September 27, 2006

REPORT DOCUMENTATION PAGE

Public reporting burden for this collection of information is estimated to average 1 hour per response, including the time for reviewing instructions, searching existing data sources, gathering and maintaining the data needed, and completing and reviewing this collection of information. Send comments regarding this burden estimate or any other aspect of this collection of information, including suggestions for reducing this burden to Department of Defense, Washington Headquarters Services, Directorate for Information Operations and Reports (0704-0188), 1215 Jefferson Davis Highway, Suite 1204, Arlington, VA 22202-4302. Respondents should be aware that notwithstanding any other provision of law, no person shall be subject to any penalty for failing to comply with a collection of information if it does not display a currently valid OMB control number. **PLEASE DO NOT RETURN YOUR FORM TO THE ABOVE ADDRESS.**

1. REPORT DATE (DD-MM-YYYY)	2. REPORT TYPE	3. DATES COVERED (From - To)
27-09-2006	Memorandum Report	

4. TITLE AND SUBTITLE

Validation Test Report for the 1/16° East Asian Seas Navy Coastal Ocean Model Nowcast/Forecast System

5a. CONTRACT NUMBER

5b. GRANT NUMBER

5c. PROGRAM ELEMENT NUMBER
0603207N

6. AUTHOR(S)

Shelley Riedlinger, Ruth Preller, and Paul Martin

5d. PROJECT NUMBER

5e. TASK NUMBER

5f. WORK UNIT NUMBER
73-5097-16-5

7. PERFORMING ORGANIZATION NAME(S) AND ADDRESS(ES)

Naval Research Laboratory
Oceanography Division
Stennis Space Center, MS 39529-5004

8. PERFORMING ORGANIZATION REPORT NUMBER

NRL/MR/7320--06-8978

9. SPONSORING / MONITORING AGENCY NAME(S) AND ADDRESS(ES)

Space & Naval Warfare Systems Command
2451 Crystal Drive
Arlington, VA 22245-5200

10. SPONSOR / MONITOR'S ACRONYM(S)

SPAWAR

11. SPONSOR / MONITOR'S REPORT NUMBER(S)

12. DISTRIBUTION / AVAILABILITY STATEMENT

Approved for public release; distribution is unlimited.

13. SUPPLEMENTARY NOTES

14. ABSTRACT

The East Asian Seas (EAS) model is a regional application of the Navy Coastal Ocean Model (NCOM) in the Western Pacific (WESTPAC). The EAS model domain includes the South China Sea, the East China Sea, the Yellow Sea, and the Japan/East Sea. This model was developed by the Naval Research Laboratory (NRL) as part of a forecast system to predict ocean currents, temperature, salinity, and elevation for the WESTPAC region. This forecast system addresses the Navy requirements for Littoral Salinity Prediction (METOC 9902), Numerical Modeling (METOC 9801), High Resolution Surface and Subsurface Currents (METOC 9308), and Air-Sea Drift Prediction (METOC 9115). The EAS model is scheduled for transition into operations at the Naval Oceanographic Office in 2006. This validation test report will describe the EAS forecast system and discuss the evaluation of this system performed by NRL including comparison to observations as well as other Navy operational forecast systems in the WESTPAC region.

Other detailed descriptions of the EAS forecast system are available from the EAS Software Design Description (SSD), Software Requirements Specification (SRS), Software Test Description (STD), and User's Manual (UM).

15. SUBJECT TERMS

NCOM   MODAS
EAS

16. SECURITY CLASSIFICATION OF:			17. LIMITATION OF ABSTRACT	18. NUMBER OF PAGES	19a. NAME OF RESPONSIBLE PERSON
a. REPORT	**b. ABSTRACT**	**c. THIS PAGE**	UL	143	Shelley Riedlinger
Unclassified	Unclassified	Unclassified			**19b. TELEPHONE NUMBER** (include area code) (228) 688-4277

CONTENTS

VALIDATION TEST REPORT FOR THE 1/16° EAST ASIAN SEAS NAVY COASTAL OCEAN MODEL NOWCAST/FORECAST SYSTEM

Introduction

The East Asian Seas (EAS) model is a regional application of the Navy Coastal Ocean Model (NCOM) in the Western Pacific (WESTPAC). The EAS model domain includes the South China Sea, the East China Sea, the Yellow Sea and the Japan/East Sea. This model was developed by the Naval Research Laboratory (NRL) as part of a forecast system to predict ocean currents, temperature, salinity and elevation for the WESTPAC region. This forecast system addresses the Navy requirements for Littoral Salinity Prediction (METOC 9902), Numerical Modeling (METOC 9801), High Resolution Surface and Subsurface Currents (METOC 9308), and Air-Sea Drift Prediction (METOC 9115). The EAS model is scheduled for transition into operations at the Naval Oceanographic Office in 2006.

This validation test report will describe the EAS forecast system and discuss the evaluation of this system performed by NRL including comparison to observations as well as other Navy operational forecast systems in the WESTPAC region.

Other detailed descriptions of the EAS forecast system are available from the EAS Software Design Desciption (SDD), Software Requirements Specification (SRS), Software Test Description (STD) and User's Manual (UM).

EAS Model Description

The EAS model is an adaptation of the Navy Coastal Ocean Model (NCOM) to the WESTPAC region. The EAS NCOM model uses NCOM version 2.3 (NCOM 2.3). The physics and numerics of NCOM (Martin, 2000), are based largely on the Princeton Ocean Model (POM) as described in Blumberg and Mellor (1987), with some aspects from a sigma-z model developed by Paul Martin at NRL (Martin *et al.*, 1998), and other additional features. Detailed descriptions of the controlling equations and numerical implementations are given in Martin (2000).

NCOM has a free surface and is based on the primitive equations and the hydrostatic, Boussinesq, and incompressible approximations. Mixing is defined by horizontal mixing coefficients that are calculated with the Smagorinsky (1963) scheme or a grid-cell Reynolds number scheme where the mixing coefficients are determined from a specified grid-cell Reynolds number. Minimum values for the coefficients are specified for both schemes. Vertical mixing coefficients are calculated using the Mellor-Yamada Level 2 (Mellor and Yamada, 1974) or Level 2.5 (Mellor and Yamada, 1982) turbulence models. The Level 2 model can optionally include the Richardson-number-based mixing enhancement scheme of Large *et al. (*1994), which provides for weak mixing at the edge of a turbulent boundary layer for Richardson numbers above the normal critical value of about 0.25 up to a value of 0.7. For the Level 2.5 scheme, the surface flux of turbulent kinetic energy is specified as in Craig and Banner (1994). The EAS

NCOM system utilizes Smagorinsky horizontal mixing and Mellor-Yamada Level 2 vertical mixing with the Large *et al.* enhancement. Two density options are available in NCOM 2.3: the Friedrich and Levitus (F-L) (1972) polynomial approximation of the equation of state, and the adaptation by Mellor (1991) of the United Nations Educational Scientific and Cultural Organization (UNESCO) equation of state (Millero *et al.,* 1980; Millero and Poisson 1981). EAS NCOM opts for the F-L equation, which is faster but less accurate at depth than the Mellor equation. We have assumed that F-L has sufficient accuracy relative to the other sources of error in the model, but have not performed a detailed analysis quantifying the time benefit versus performance cost in NCOM.

The spatial finite differences are mainly second order with options for some higher-order differences. There is an option for the quasi-third order upwind advection scheme described by Holland *et al. (*1998) for momentum and/or scalars, and an option for the Flux-Corrected Transport (FCT) advection scheme (Zalesak, 1979) for scalars. The FCT scheme avoids advective overshoots but increases running time by about 50%. EAS NCOM employs the third-order upwind advection for the horizontal. Temporal differencing is leapfrog with an Asselin (1972) filter to suppress time splitting. All terms are treated explicitly in time except for the solution for the free surface and vertical diffusion. In the solution for the free surface, the horizontal surface pressure gradient terms in the depth-averaged momentum equations and the divergence terms in the depth-averaged continuity equation are evenly split between the old and new time levels to minimize the damping of surface waves. In the vertical diffusion terms, the field being diffused is evaluated fully at the new time level to avoid diffusive overshoots and vertical gradient reversals.

The free-surface mode is calculated implicitly; therefore, the surface pressure gradients and the divergence terms in the surface elevation equation have a component at the new time level being calculated. Horizontal mixing and quadratic bottom drag are time-lagged as required for stability, avoiding time splitting problems. Vertical mixing is fully implicit with vertical eddy coefficient evaluated using time-lagged values of the model fields to avoid exciting the time splitting behavior of the leap-frog scheme.

NCOM includes a hybrid vertical coordinate system that consists of z (fixed) coordinates with a free surface, full σ (terrain following) coordinates, or hybrid σ/z coordinates. These vertical grid configurations are depicted in Fig.1. The EAS application of NCOM uses a vertical grid with σ coordinates from the surface down to a user-specified depth z_s and z-levels below (Fig. 1c). The upper, σ portion of the grid is divided into layers as in POM with each σ layer being a fixed fraction of the total depth occupied by the σ layers. On the lower, z-level portion of the grid, the bottom depth is rounded to the nearest specified z-level. The model can be configured to run completely in σ mode or with any number of σ over z-levels, i.e., as long as at least one σ layer is included to accommodate the free surface. For the σ-level portion of the grid, the form of the NCOM equations is similar to that presented by Blumberg and Mellor (1987) except that the depth in the equations is replaced by min(H, z_s), where H is the bottom depth.

The East Asian Seas model grid was designed to fit easily into the Global NCOM model. NCOM is coded for an orthogonal curvilinear horizontal grid, as is POM (Blumberg and Herring 1987). Fig 2 depicts the horizontal grid used in the EAS NCOM. The model domain was chosen

to encompass the South China Sea, the East China Sea, the Yellow Sea and the Japan/East Sea and for the ease of providing open boundary information. The model extends east to 158° E longitude into the deep mid-Pacific Ocean and west to 98° E longitude to include the western boundary of the South China Sea. The model's northern boundary is located at 52° N latitude, to include the entire Japan/East Sea, and its southern boundary is located at 17° S latitude to include a buffer area around key open ocean regions that affect the South China Sea. The grid cell size varies due to stretching from 6-10 km based on the mapping of the grid.

The EAS horizontal grid is twice that of the global model (1/16 degree versus 1/8 degree) while the vertical coordinate system is the same as for the Global NCOM. This consists of 41 σ-z level surfaces, resulting in 40 material levels in the vertical. Of these 41 surfaces, 19 are σ-coordinate interfaces in the upper 137 m, and 21 are z-coordinate levels from 137 to 5500 m, and one, surface 21, behaves as a σ-coordinate on the bottom for depths shallower than 137 m and as a fixed 137 m z-coordinate for deeper depths. Interfaces are at depths determined by logarithmic stretching such that the uppermost material layer thickness is 1 m and the bottom z-interface is at 5500 m. The 137 m σ-z interface is selected as a surface that generally intersects an isobath close to or shallower than the shelf break. Thus the σ-z transition lies between the inner and middle shelf, where σ coordinates are clearly appropriate, and the shelf break and slope, where z-levels are desired to maintain minimum upper level thickness and avoid the problems associated with σ coordinates in regions of steep topography. Where the water is shallower than 137 m, primarily in the shelf region, the σ-coordinate levels follow the bottom to improve representation of response to topographic features. In deeper water, the vertical resolution of the σ-coordinate layers at rest increases from 1m at the surface to about 20 m at the σ-z interface. The sigma layers adjust in response to sea surface changes in a set relationship to the total water depth. Grid cell wetting or drying is not supported, and the shallowest total depth allowed is 5 m, which is divided into 19 material σ-levels. The model depth and coastline (Fig. 3) are based on NRL DBDB2, a global, 2-minute gridded bottom topography produced at NRL (D. Ko, personal communication).

Boundary values at open ocean areas are obtained from the operational global $1/8^o$ NCOM system. Surface elevation, 3D temperature, salinity and velocity as well as the vertically integrated velocity are extracted from the global model and interpolated to the EAS domain. A Flather type boundary condition is used for the sea surface heights, zero gradient for the vertically integrated velocities, advective for the 3D velocities perpendicular to the boundary, and zero gradient for 3D velocities parallel to the boundary. Scalar values (temperature and salinity) use Orlanski type boundary conditions. The frequency at which the boundary values are applied depends on the availability of global output varying from once a day in the early simulations to 3 hourly in most recent simulations. The NCOM model linearly interpolates inputs in time to the model time.

Surface boundary conditions for NCOM are wind stress for the momentum equations, surface heat flux for the temperature equation, and for the salinity equation, a surface salt flux via relaxation to surface salinity from a combination of MODAS and climatology. The bottom boundary conditions are the bottom drag for the momentum equations, which is parameterized by a quadratic drag law, and zero flux for the temperature and salinity equations.

For the EAS version of NCOM, atmospheric forcing is supplied by FNMOC Navy Operational Global Atmospheric Prediction System (NOGAPS) (Rosmond *et al.*, 2002). This consists of atmospheric fields of wind stress, surface air pressure, total surface heat flux, and net solar radiation. These fields are provided at a 3-hour time interval and linearly interpolated to each model time step.

The total surface heat flux field is a sum of latent, sensible, longwave and shortwave radiation. A separate solar radiation file is used to allow for solar heating with depth. Thus solar radiation must be removed from the total surface heat flux field. A 2-band approximation to Jerlov extinction profiles, assuming a water type of 2, is used for solar heating with depth (Simpson and Dickey, 1981). Presently in EAS16 the extinction profiles do not vary spatially. This option exists in NCOM, but is not presently implemented. The remaining surface heat flux is modified by subtracting a "relaxation heat flux" from it which is proportional to the difference between the model sea surface temperature (SST) and the MODAS SST. This flux is of the form

$$\text{relaxation heat flux} = r * (T\_model - T\_MODAS) \qquad\qquad (1)$$

The constant "r" has units of m/s, which gives a heat flux in units of ^{o}C-m/s. A value of r=4.0 m/day is used for hindcasts and r=1.0 is used for forecasts. This assumes an average surface layer of 10 m and a correlation time of 2.5 days for the SST analysis. A longer correlation time is assumed for the forecast (Chapman et al. 2004).

The surface salinity is relaxed via a surface salt flux to a blend of the MODAS sea surface salinity (SSS) and a climatological SSS (Chapman et al., 2004). For this relaxation, a value of r=0.1 m/d is used for hindcasts and r=0.05 m/d is used for forecasts. The MODAS SSS correlation time is 30 days, but since there are larger relative errors in the MODAS SSS, it was decided to back-off the relaxation and use 100 days for SSS. All forcing input are interpolated to the EAS16 model grid and linearly interpolated in time.

NCOM Data Assimilation

NCOM assimilates real-time satellite derived observations through the Modular Ocean Data Assimilation System (MODAS). Developed at NRL (Fox *et al.*, 2002a), MODAS consists of climatological databases plus over 200 programs and utilities for combining irregularly sampled remote-sensed data and in-situ measurements to create 2-D and 3-D estimates of temperature and salinity over the global ocean. MODAS performs quality checking and optimum interpolation of ocean observations (Bretherton *et al.*, 1976), including temperature, salinity, and sea surface height (SSH).

The MODAS 2-D SSH and SST are gridded by optimum interpolation using altimeter (Jacobs *et al.*, 2002) and Multi-Channel SST (MCSST) data products from NAVOCEANO (Fox *et al.*, 2002b). MCSST data are obtained from multiple 5-channel Advanced Very High Resolution Radiometer (AVHRR) instruments aboard polar orbiting satellites (May *et al.*, 1998).

MODAS uses these two dimensional fields of SST and SSH to estimate three-dimensional fields of temperature and salinity based on regression models derived from historical profiles. The regression models are based on the steric height component of the SSH, where the steric height anomaly is the integrated difference of the actual specific volume anomaly minus the specific volume anomaly of an ideal water column with 35 salinity and 0°C potential temperature, in this case integrated over the upper 1000 m (Boebel and Barron, 2003).

Given the real time SST and steric SSH, MODAS computes anomalies by subtracting from these real time values a mean SST and mean steric SSH, respectively, taken from the MODAS bimonthly climatological database. MODAS then uses equations determined from historical correlations of surface and sub-surface temperatures to project the surface anomalies downward through the water column at standard depths. At a given location, the bimonthly climatological temperature profile is added to the profile of estimated anomalies to produce a profile of synthetic temperature. MODAS estimates synthetic salinity profiles by use of location-specific climatological temperature-salinity relationships at standard depths.

Since the altimeters measure total SSH, errors can arise where non-steric contributions are relatively large, such as in shelf regions. At present there is no operational method of directly distinguishing the steric and non-steric contributions from the altimeter data. An indirect method must be used. This indirect method may be via a statistical model or a numerical model. For the EAS16 model (and for Global), MODAS uses SSH from the assimilative $1/16^o$ NRL Layered Ocean Model (NLOM), another U.S. Navy operational product (Smedstad et al., 2003). Use of the NLOM SSH takes advantage of the improved nowcast skill of the NLOM dynamics, over statistical models, and the ability of NLOM to quantify the steric component of SSH. Changes in steric SSH do not produce changes in bottom pressure, so a model can calculate a steric SSH by subtracting the height proportional to the calculated bottom pressure anomaly from the total height. Thus NLOM assimilates the total SSH from the altimeter and internally attributes the signal to the dynamically appropriate sources. MODAS then uses the steric SSH anomaly determined from NLOM SSH, as discussed earlier, to produce the synthetic temperature and salinity profiles.

NLOM SSH does not extend over regions shallower than 200m or north of 66°N, and it is not reliable south of 55°S, as outcropping of layers is not allowed in NLOM. Because the non-steric component of total SSH is proportionally larger in shallow water and in high latitudes (Shriver and Hurlburt, 2000), direct use of MODAS2D SSH is problematic in the same areas in the absence of information on how to partition the signal between steric and non-steric components. Thus in these regions, MODAS synthetic profiles are calculated using SST only, and a linear blend is applied to transition between regions of SST only and full SSH/SST synthetics.

Within MODAS is the ability to assimilate available in-situ observations into the 3D analyses of synthetic temperature and salinity profiles. For the present study, no *in situ* data have been included, allowing all *in-situ* observations to be used for independent validation. After converting temperature to potential temperature, the 3D potential temperature and salinity fields are interpolated to the model grid. These T&S values are linearly interpolated in time as the model runs.

Data assimilation used in NCOM is done using two mechanisms: (1) adjustment of heat and salinity fluxes at the surface, and (2) relaxation toward subsurface temperature and salinity profiles. In both cases, the assimilation is applied each time step with strength proportional to the product of the deviation field multiplied by the gridded weighting function, where the deviation field is the difference between the model and assimilation fields, and the weighting field reflects the relative confidence between the model and the data. This slow data insertion technique allows the model to incrementally adjust to the data with minimal dynamic disruption (Rhodes *et al.*, 2002). Preparation of the data fields for assimilation is independent of the NCOM assimilation itself, allowing the model to accommodate a variety of approaches to preparing the observational analyses.

NCOM River Database

Monthly river outflow can contribute to a more accurate seasonal representation of areas near coastlines. Nearshore distribution of salinity in a model using river sources is likely to be superior to the distribution based on gridded global climatologies. These are likely to smooth out or miss nearshore gradients inadequately sampled by sparse historical hydrographic observations. Although relaxation to MODAS surface salinity does produce realistic salinity distribution in the open ocean, in coastal regions, inclusion of major rivers significantly modifies nearshore salinity stratification.

The EAS16 model uses monthly river flow rates from the World Meteorological Office (WMO) database. There are 51 rivers in the EAS domain (Fig. 4) from the WMO database. The Yangtze is the largest with respect to freshwater discharge, with an annual average flow rate of 29,432 m^3/sec. The next largest is the Pearl (Zhu) with an annual average flow rate of 10,030 m^3/sec. Both of these rivers are located on the Chinese coast and are denoted by a red stars in Fig. 4. Rivers with moderate flow rates (1000 to 2000 m^3/sec) are denoted by the blue triangles. The smaller rivers are denoted by the green diamonds. Salinity at the river mouth is set to 0 and temperature is from Levitus climatology. The river flow is partitioned from the surface to the bottom or 50 m, whichever is shallowest, using a linear weighting with depth, from a maximum at the surface to zero at $z = -50.0$ or bottom if shallower than 50 m. The river inflow in the EAS16 model will be updated in the future by using a newly developed NRL river database. The NRL data base includes monthly mean river discharge and was derived by augmenting the Perry et al. (1996), containing estimates of annual mean river discharges for 981 of the world's largest rivers, with data from multiple internet sources and other published data sets.

Tidal Model

A three-year simulation of the EAS16 model with atmospheric forcing, data assimilation and open boundary conditions from Global NCOM, as described previously, was performed before the addition of tides. Tides were added to NCOM by providing (1) tidal potential forcing, which is applied at each interior open water point, and (2) tidal boundary condition forcing, which is applied at each open water point on the open boundary.

Tidal potential forcing is due to the gravitational pull of the sun and moon and is the force that directly drives the global tides. Tidal potential forcing is needed to simulate tides in domains that contain significant areas of deep water. The tidal potential routine in NCOM can provide potential forcing for up to 10 tidal constituents (K1, O1, P1, Q1, K2, M2, N2, S2, MF, and MM), however for the EAS16 model only the first 8 major constituents are used. The total tidal potential is computed by summing the tidal potential of the individual constituents, calculated by analytical formulas. Implementation of the tidal potential forcing in NCOM is controlled by setting an input parameter (tidpot=T) and providing an input file (optcn_1.D) that lists the tidal constituents for which tidal potential forcing is to be calculated.

To compute tidal boundary condition forcing, NCOM stores harmonic tidal constituent elevation and depth-averaged velocity data at each of its open boundary points. Note that the velocity data are stored as transports, i.e., velocity multiplied by depth, for the components of the velocity normal and tangential to the open boundary of the model domain. These data were obtained (interpolated) from the Oregon State University (OSU) global tidal database (Egbert, et al., 1994; Egbert and Erofeeva, 2002). At each model timestep, the elevation and velocity due to the tide at the open boundary points are computed from the harmonic tidal constituent data by summing the contributions from each of the constituents. The total elevation and velocity at the open boundary points are then obtained by combining the values due to the tide with the elevation and velocity at the open boundary points obtained from global NCOM, which contain contributions from the non-tidal aspects of the ocean circulation. The implementation of tidal boundary conditions in NCOM is controlled by setting an input parameter (indtide=1) and by providing input files for the harmonic tidal constituent data at the open boundary points (otide_1.D) and a list of the corresponding tidal constituents (otide_1.B).

Tidal forcing of EAS16 was initiated on Oct 1, 2003. Tidal initial conditions (surface elevation and depth-averaged currents) for this date were computed by spinning up a barotropic tidal solution on the EAS16 grid over a 10-day period ending on Oct 1, and this tidal solution was then added to the existing EAS16 model solution for Oct 1 to create a set of initial conditions containing both the non-tidal circulation and the tides.

East Asian Seas Nowcast/Forecast system

The EAS model was originally developed and tested at $1/8^o$ horizontal resolution (EAS8), coupled to a $1/4^o$ North Pacific Princeton Ocean Model (Ko et al., 2003 and Chapman et al. 2004). The North Pacific model was used to provide boundary conditions as a demonstration of the coupling that would be used with the Global NCOM. The EAS8 was run in a spinup mode using NOGAPS forcing for the years 1994-2000. EAS8 was run in a data assimilative mode using NOGAPS forcing from Sept 2000 through Dec 2003. This system provided a nowcast/forecast and was viewed as a beta-test of the NCOM to NCOM coupled forecast system. The circulation of the EAS8 model was evaluated and discussed in several manuscripts that were produced as part of the ONR/NRL Dynamical Linkage of the Asian Marginal Seas (LINKS) project (Jacobs et al., 2005; Teague et al., 2003)

The Global NCOM was initially tested at 1/4° horizontal resolution. However, with the advent of more available computer power, the decision was made to double the resolution of the global model to 1/8° and at the same time to double the resolution of the EAS model to 1/16° (EAS16).

NCOM was then adapted to a 1/16° horizontal resolution over the EAS domain. The EAS16 model was initialized from Global NCOM fields for December 30, 2000 and a spin-up run with surface forcing and data assimilation was begun using the Global NCOM fields as boundary conditions. This spin-up run continued from December 30, 2000 through February 22, 2003. On February 23, 2003, NRL began to run EAS16 in a nowcast/forecast mode. In this mode, the EAS16 model run consists of a 48-hr hindcast and a 72-hr forecast. That is, the time that the model run is assumed to be valid for is the analysis or nowcast time. A short spin-up run (hindcast) beginning with the nowcast model fields from two days prior to the analysis time is run out to the analysis time using the forcing and data assimilation fields valid for the hindcast time period. Then starting from the end of the hindcast run (i.e. at the analysis time) a 72-hour forecast is run. The forecast run uses forecast atmospheric fields and very weak relaxation to MODAS synthetic profiles valid at the analysis time.

The application of tides in EAS16 nowcast/forecast runs was started with the October 1, 2003 model simulation. A spin-up tidal solution with 8 tidal constituents was started 10 days prior to the October 1 date. This tidal solution, valid for October 1, 2003, consisted of elevations and barotropic currents. This solution was added to the model temperature, salinity and velocities from October 1, 2003 to create a set of initial conditions with both the non-tidal circulation and tides. The EAS16 model continues to run in the nowcast/forecast mode but now with tides.

Evaluation of the EAS16 Nowcast/Forecast System (EAS16NFS)

Validation testing of the EAS16 Nowcast/Forecast system will build upon the previous validation of Global NCOM. Global NCOM was spun-up for 6 years from a static climatological initial state to statistical energy equilibrium. Global NCOM was run in modes both with and without data assimilation. The results of these experiments proved the credibility of the NCOM model and will not be repeated with the EAS16 model; rather the interested reader should refer to the Global NCOM Validation Test Report (Barron, et. al., 2004).

The EAS16 model was initialized from Global NCOM and run for almost 3 years assimilating data before tides were added to the system. Therefore this evaluation will examine different issues for the tidal verses non-tidal results. The evaluation of the non-tidal EAS16 will focus on the general circulation within the model domain, a comparison to sea level data, a comparison to CTD data, comparison to drifter data and an evaluation against the Global NCOM. The tidal EAS16 will be evaluated against, hourly sea level data, co-tidal charts for EAS16 and two state of-the-art global tidal models, International Hydrographic Office (IHO) data, glider and drifter data.

Non-Tidal EAS16

The general circulation of the EAS16 model is shown as a three-year mean of ocean currents near the surface in Figure 5. EAS16 reproduces the location of many of the observed circulation features of the western Pacific (Fig. 6) including the Kuroshio, the North Equatorial Current and Counter Current, the cyclonic Mindanao Eddy and the anticyclonic Halmahera Eddy and the general circulation of the South China Sea, the Yellow Sea/East China Sea and the Japan Sea. A zoomed view of the EAS16 monthly mean near surface currents from February 2003 and August 2003 for the South China Sea (Figs. 7a&b), Yellow Sea, East China Sea (Figs. 8a&b) and the Japan Sea (Figs. 9a&b) reproduce many of the circulation patterns reported in the literature. Examples of observed seasonal surface circulation of the marginal seas are shown in Figs 7, 8, 9c and d. For example, the model reproduces the winter/summer reversal in the current along the coast of Vietnam, also the reduced inflow of the Kuroshio into the South China Sea in summer. In the Yellow Sea/East China Sea region, the model has southward flow along the Chinese coast in winter and predominately northward flow through the Taiwan Strait in summer.

The accuracy of the general circulation of the EAS16 is shown by comparing modeled transports against observations of transport through several key straits included in the model domain. The observed values were derived from open published literature and consist of averaged values as well as year/season specific values. Figure 10 includes transports from the three-year EAS16 assimilative run and the Global NCOM assimilative run for the year 2000. Note that the EAS16 results show a stronger circulation through the Luzon strait, for the Kuroshio east of Luzon and for the North Equatorial Current than that associated with the observed values. This larger transport is probably specific to the years being evaluated (2000-2003). The larger modeled transport through the Luzon Strait is at least partly a result of the larger modeled transport of the North Equatorial Current.

One of the most easily available data sets for model comparison is sea level data. This data may be used for comparison on short time scales to model tidal prediction and when de-tided, may be used to look at the longer time scale changes in sea level. The EAS16 results of sea level were evaluated against observations from 10 stations available through the Joint Archive of Sea Level (JASL) at the University of Hawaii. The JASL archive consists of hourly mean and daily mean SSH. A daily average of the SSH computed from the non-tides EAS16 run is compared to the daily mean SSH from JASL. Figure 11a shows the location of the 10 tidal stations available from JASL in the EAS16 region in 2001. Figures 11b-f show the daily values and a 30-day running mean for the model and data at five representative stations from the JASL archive. Table 1 shows the statistics comparing the model to the observations using the daily fields and the 30-day means for all 10 stations. The statistics shown are the root mean square difference (RMSD), the standard deviation of the data (σ_x), the standard deviation of the model (σ_y), correlation coefficient (R) and the skill score (SS).

The statistics are computed from the following equations (Kara et al, 2006):

$$\sigma_x = [1/n \sum_{i=1}^{n} (X_i - \bar{X}_i)^2]^{1/2}, \qquad (2)$$

$$RMSD = [1/n \sum_{i=1}^{n} (Y_i - X_i)^2]^{1/2}, \qquad (3)$$

$$R = 1/n \sum_{i=1}^{n}(X_i - \overline{X})\,(Y_i - \overline{Y})/\,(\sigma_x\,\sigma_y), \qquad (4)$$

$$SS = R^2 - [R - (\sigma_y/\sigma_x)]^2 - [(\overline{Y} - \overline{X})/\,\sigma_x]^2, \qquad (5)$$

where X denotes the data values and Y denotes the model values, the over bar denotes means, σ_x and σ_y are the standard deviation of the data and model values respectively. A skill score of 1.0 indicates a perfect model prediction. A negative skill score indicates that the model may have normalized amplitudes larger than the correlation or large biases in the mean (Murphy and Epstein, 1989). Most of the stations listed in Table 1 have high correlation coefficients and high skill scores, indicating that the EAS16 model reproduces the sea surface height quite well at these locations. Guam is the only location with a negative skill score. Indicating that there are biases at this location. In the SSH plot for Guam (Fig. 11f) one sees that the model's SSH is often several centimeters different from the data. The 30-day running mean shows that the model is 1-8cm lower than the data from Jan through mid-May and 1-8cm higher from mid-May on. The exact location of tidal stations is important to model/data comparisons. Stations located in small bays, narrow channels etc. will not agree well with model data as the EAS16 resolution, bathymetry etc. will not reproduce the conditions in these areas well. The Guam station is an example of this. According to the Gloss Station Handbook this station is located at the entrance to a boat channel within Apra Harbor. The model does not resolve this harbor so the nearest model wet point is outside the harbor. EAS16 SSH will agree best with stations that tend to be more open water in nature.

The EAS16 model was also evaluated against several Profiling Autonomous Lagrangian Circulation Explorers (PALACE) Floats and CTD observations of temperature and salinity profiles as well as profiles from moored buoys such as the NOAA Tropical Atmosphere-Ocean (TAO) array. As mentioned in the data assimilation section, these data sets are not included in the MODAS analysis of synthetic temperature and salinity fields. Figures 12-15 show the observed temperature and salinity profiles from 10 PALACE floats in the Japan Sea and the Pacific south of the Ryukyu Islands, plotted against the EAS16 and MODAS profiles for the region. Note that the EAS16 temperature profiles agree well with the observations at all locations except those in the Japan Sea close to the Tsushima Strait (Fig. 12). This is a region of high variability and neither EAS16 nor MODAS are able to capture the depth and sharp gradient of the thermocline. As with the temperatures, the salinity profiles for the location near Tsushima have the poorest comparison. The modeled salinity is often an improvement over the MODAS salinity profile, especially near the surface. However, overall agreement is not as good as in the temperature profile comparison. This is likely due to two factors: the lack of real time, or even inter-annual variability in the river outflow data and the lack of salinity data that is associated with the MODAS system and the generation of the MODAS salinity profiles.

Subsurface Temperature

The TAO array (McPhaden et al. 1998) offers a long-term data set of temperatures, both surface and sub-surface, for the tropical Pacific. There are 12 TAO moorings located within the EAS16

10

domain (Figure 16). These moorings are north and east of New Guinea. The eastern most moorings are approximately 220 km from the model's eastern open boundary. Temperatures at depths from 1.5m to 750m, are recorded at each location. Temperature time series for the upper 150m from the data, the model (Nowcast) and MODAS synthetic profiles for 2003 as well as the climatology are shown for three of these moorings in Figs 17 through 19. The black line in each figure represents the mixed layer depth. The mixed layer is best obtained using density values, which can be computed from temperature and salinity. Without salinity, the temperature can be used to estimate the mixed layer depth, or more precisely the isothermal layer depth (ILD). The ILD is used, since most of the TAO arrays do not include salinity values. The ILD is calculated using a method described in Kara et al., 2000. This method defines the ILD as the depth at the base of an isothermal layer, where the temperature has changed by a fixed value (0.5^o C) from the temperature at a reference depth of 10 m.

Model output was saved at 12 hour interval (00Z and 12Z of each model day). The TAO data used here is the daily averaged temperature (beginning at 00Z and time-stamped as 12Z), so a daily average for the model was obtained by computing a 24 hour mean of the model data centered at hour 12 (Shapiro type filter). The 00Z and 12Z times correspond to approximately 10 am and 10 pm local time for the TAO moorings. Thus the warmest part of day is omitted in the model average suggesting that the model average temperatures used in this comparison may be biased toward the cooler times of day. MODAS and climatology are essentially daily temperatures as well.

Three mooring locations (northeast, center and southwest part of the array) were chosen for a discussion of the model/TAO comparison in this section. Statistics for the remaining mooring and model comparisons are shown in the appendix. Figure 17 shows the temperature time series at one of the western locations of the TAO array (upper 150m), north of the equator (8^oN 137^oE). The model and the data show an upwelling event in the first three months of the year that is missed by both MODAS and the climatology. Immediately following the upwelling is a warming event in the upper 100 m of the water column. This event appears in both the model and the MODAS fields but not as deep as observed. Although the model fields are smoother than the observations and MODAS, the model still shows improvement over the MODAS fields.

Figure 18 represents the same data but at one of the TAO array locations along the equator (0^oN 147^oE). Both the model and the MODAS fields are too warm from $50 – 150$ m depth during the first four months of the year. Around day 140, the observed water temperature abruptly becomes warmer from about 70-150 m depths. The model also predicts a warming event at that time, but not as intense as observed. The MODAS temperatures show an even less intense warming. Through the remainder of the year, the model fields, slightly warmer then the observed temperatures are still closer to the observed values then the MODAS temperatures or climatology.

Figure 19 shows the same data at one of the eastern locations in the array, 2° west of the model open boundary and south of the equator (5^oS 156^oE). Both the model and MODAS are cooler than the observations at depth (100-150m) with MODAS colder than the model in the latter half of the year. However, both the model and MODAS capture the deep water cooling events

through the year, again with the model temperatures being closer to the observed then the MODAS.

A quantitative comparison of the data to the model, MODAS and climatology was also performed. Statistics were calculated for each of the observations along the TAO arrays in the EAS16 domain. These include the means of the model and the data, the mean error (ME), the root mean square difference (RMSD), the standard deviation (σ) of each data set, the correlation coefficient (R), and the skill score (SS)

$$ME = \overline{Y} - \overline{X}, \tag{6}$$

where $\overline{X}$ is mean of the data values, $\overline{Y}$ is the mean of the model values.

Table 2 shows the statistics of EAS16 vs. TAO at 12 depths calculated for the 3 locations shown in Figure 17-19. Table 3 contains these same statistics comparing MODAS to the TAO observations. These statistics for model, MODAS and climatology for these locations are shown graphically in Fig. 20-22.

The statistics, for the array located at 137° E, 8° N, show the model to be an overall improvement over MODAS, with smaller RMSD errors and better correlations and skill scores for most depths. At the array location near the equator the comparison is mixed. The model RMSD error is larger than the MODAS from 25-75 m depth but smaller from 100-250 m depth. At other depths at this location the RMS errors for MODAS and the model are similar. The correlation coefficient for MODAS and the model are comparable with the model being better except around 50 m depth. The skill score is not particularly good for either with several negative values. At this location MODAS is better than the model from 25 to 75 meters. Finally, at the eastern most array location (156° E, 5° S), the RMS error of the model is less than the MODAS error at all depths except 250-300m. The correlation coefficient is better for the model except at 50-75 m and the skill score for the model is the better in the upper 200 m. Both the model and MODAS have negative skill scores below 200m.

Summary statistics were calculated for the model, MODAS, and climatology versus the data. The temperatures from ten buoys were combined to create a long time series for each mooring depth (effectively a 10 year time series at 1m, at 5m etc.). Two of the buoys were not included in the time series (2^oN 147^oE and 2^oS 156^oE), as the depths of the measurements were different from each other as well as from the other buoys. The results of the summary statistics are shown in Figure 23. These overall statistics (Table 4) show that the largest mean difference is 0.7 degrees C and appears at 200m depth. The maximum RMS error is found between the depths of 100-200m and averages 1.4^oC. The standard deviation of the model is smaller than that of the data at all depths. The skill score for the model is 0.6 or greater at all points except the two deepest locations.

The mixed layer depth (or ILD) statistics computed for each location, for EAS16 vs. TAO are in Table 5 and the statistics for MODAS vs. TAO are in Table 6. The correlation coefficient and skill score for the ILD are not very good for either the model or MODAS. For the model, the

skill score is negative for all but four of the buoys, the two at 8°N, and the ones at 5n156e and 5s156e. For MODAS, the only non-negative skill scores occur at 2n137e and 5n156e. Figure 24 shows the ILD times series for each location and data type. The magnitude of the ILD fluctuations is much larger for the data than in either the model or MODAS. There are times when the EAS16 model reproduces changes in ILD rather well and are clearly better than MODAS. For example, from day 280 through day 350 at 8n137e, the first 60 days and the last 60 days at 2n156e and from day 90 to day 150 at 2n137e. Other ILD changes the model and MODAS both miss. One example is from day 220 through day 330 at 5°N 156°E. The ILD from the TAO mooring shows a significant shallowing, from 60m to 20m, while the model and MODAS stay deep (~50m).

Model Currents versus Drifter Observations

Model mean currents for the years 2001-2003 are compared to mean currents derived from drifter data; compiled and edited by Peter Niiler (Pazan and Niiler, 2004). The Niiler drifter data includes drifters from the 1970's through 2003 (when the data was requested). Much of the data included in the Meteorological and Environmental Data Set (MEDS) and the Atlantic Oceanographic and Meteorological Data Set (AOML) are included in the Niiler data set, but Niiler included other drifters as well. The Niiler data is quality controlled and corrected for wind-slip.

To compare with the model, u&v velocity components from drifters in the EAS16 region are averaged over 1°x1^{o} bins. An annual mean climatology for the data was computed by using all the available data. Similar means were computed for seasons, January-March, April-June, July-September, and October-December. Binned means from the model velocity were computed in a similar manner for model years 2001 through 2003; a model climatology. The model velocities were vertically averaged over the upper 15m before being averaged over the bins. This was done to better represent the surface currents measured by the predominately shallow drogued drifters. The annual mean velocity thus computed for the drifter data and for the model is shown in Figs 25 a & b. In these figures, the vector length is invariant with speed. The speed is shown via the color of the vector. The annual mean speed from the data (Fig 25a), over much the region, is 0.1 m/s or less. High speeds (greater than 0.7 m/sec) are seen in the Kuroshio, Mindanao current, Celebes Sea, off the coast of Vietnam and near Indonesia.

The annual currents from the model (Fig. 25b) are similar in many respects to that shown for the data. Both the Niiler data and the model show flow out of the Sea of Japan through the Tsugara Strait and southward along the northeast coast of Japan. Within the Sea of Japan both have southward flow along the Russian coast, northward flow along the east Korean coast and west coast of Japan. Flow in the central Sea of Japan tends to be eastward. Both show northward flow from the Kuroshio through the Tsusima Strait, and westward flow through the Luzon Strait and in the northern South China Sea. The major currents, Kuroshio, North Equatorial Current, North Equatorial Countercurrent, and South Equatorial Current are similar in both the data and model means. Differences are seen in the Yellow Sea where the model has a southward flow along the Chinese coast and the data is more mixed with some vectors going south, some north. South of Indonesia the model has westward flow and the data eastward flow.

The difference in annual mean current speed between model and data is shown in Fig. 26. Only those bins with greater than 50 data samples (i.e. u /v pairs) per bin are used to compute the difference. We see that the bins east of Vietnam and most of the South China Sea, in the Celebes Sea and around Indonesia are not shown in the difference plot as they have fewer than 50 data samples in those bins. Over a large portion of the region, the difference in speed between the model and data is 5 cm/sec or less (light and dark grays). Differences greater than 20 cm/sec occur in the Kuroshio and South Equatorial Current. The speeds in the Kuroshio from ~134°E to ~140°E are more than 40 cm/sec faster in the data than in the model. Farther east in the Kuroshio the model currents are greater by 20 to 40 cm/sec. In the South Equatorial Current and the Halmahera Eddy the model is stronger. Differences in speed of 10 to 20 cm/sec occur in between Taiwan and the Chinese coast and into the East China Sea.

Considering the number of samples per bin, the large differences in the Kuroshio and Equatorial currents occur in bins with fewer than 300 samples per bin. In other areas where there is poor agreement, e.g. the Yellow Sea, there are few samples or the samples are biased to a particular season. The number of samples per bin for all drifters and all years is shown in Fig. 27. The bins with fewer than 50 samples are colored gray. The bins in the Yellow Sea and much of the South China Sea are gray as are the seas around Indonesia. The bins with the highest number of samples are in the Sea of Japan and a few locations in the Kuroshio.

Seasonal biases occur as well. Table 7 lists the number of samples by season in certain regions. In the South China Sea most of the drifter samples occur in the winter and fall. In the southern part of the South China Sea there were no drifters in spring. There are changes in current speed and direction in the South China Sea due to the monsoons. Thus the data is biased toward the winter/fall monsoons. The East China Sea has more samples in the fall. In the other areas listed in Table 7 the distribution is more even. Though there may still be biases from bin to bin.

The kinetic energy computed from the mean currents in each bin is shown in Fig 28 a & b. The kinetic energy from both the data and the model show the highest energy in the Kuroshio, the Mindanao current and Halmahera eddy. The magnitudes are larger in the data in some portions of the Kuroshio and the model is larger in the Mindanao current and Halmahera eddy. In regions of high energy, small shifts in the position of a current can cause large changes in speed when comparing model and data.

The speeds from the model are within 5 cm/sec of the mean for the data in 57% of the bins and in 80% of the bins the difference between model and data is within 10 cm/sec. In 5% of the bins the speeds differ by 20 cm/sec or more (see Table 8). The root mean square difference (RMSD) for the annual mean speed is 9.7 cm/sec and the mean difference is 0.16 cm/sec. The RMSD for the seasons is a little higher 10 to 13 cm/sec.

EAS16 vs. Global NCOM

The Global NCOM 1/8° degree model is compared to the EAS16 model in several different ways. The first comparison is the mean position of the Kuroshio. The mean position is obtained

through frontal boguses derived from NAVOCEANO infrared imagery. A mean of these boguses for the years 2001 through 2003 along with +/- 1 standard deviation is shown in Fig. 29. The bogus (shown by the white lines) is plotted over the mean current vectors and mean speed for the EAS16 model (Fig 29a) and the Global model (Fig 29b). The strong current speeds fall within or very close to the bogus mean and the +/- 1 std. dev., showing that both models do a good job of reproducing the Kuroshio position. The mean currents for EAS16 and Global are similar, but a few differences are worth noting. The speed in the Kuroshio south of Japan around 131°E and in the Kuroshio extension near 150°E is greater for Global than for EAS16. There is slightly stronger flow in EAS16 on the north side of the Kuroshio, through the Korean strait and along the west coast of Japan. The flow through the Tsugara strait and down the east coast of Japan is also stronger in EAS16. These stronger flows are probably due to the higher horizontal resolution in EAS16 and thus better representation of the various straits than occurs in the Global model.

The next comparison is model SSH means. Both EAS16 and Global were averaged over the years 2001-2003. The mean sea surface height for EAS16 and Global and their difference (EAS16 – Global) are shown in Fig. 30. The difference is less than 3 cm over much of the EAS16 domain. Larger differences, up to 15 cm, occur in the Yellow Sea, East China Sea, Sea of Japan, and Kuroshio extension with lower elevations for EAS16. The lower elevations in the Yellow Sea and Sea of Japan for EAS16 can explain the slightly stronger flow north of the Kuroshio into the East China Sea and the Sea of Japan observed in the previous figures.

Temperature and temperature differences are shown in Fig. 31-33 at the surface, 100 m and 500 m. The temperature patterns and magnitudes are similar in both EAS16 and Global at each of the depths shown. At the surface EAS16 is warmer over much of the domain than Global, but particularly near the coasts, in several straits (e.g. Taiwan Strait) and in the Yellow/East China Seas, Sea of Japan and the Kuroshio extension. Warmer temperatures also occur near the eastern open boundary north of 15°N. The difference is often 0.5 to 1.0^{o}C. At 100 m depth the difference is somewhat smaller, up to 0.4^{o}C; with sometimes EAS16 being warmer and sometimes Global is warmer. A couple of areas where EAS16 is colder are east of Japan near the Kuroshio extension and east of the Tsugaru Strait. This is probably associated with the stronger flow through the straits in EAS16, which would bring colder water southward of the straits. At 500 m the major differences are in the Kuroshio extensions and eastward of the Tsugara strait, with the temperatures in EAS16 being colder. Again this is probably due to the stronger currents through the Tsugara strait in EAS16.

In Fig. 34-36 are shown the salinity and salinity differences at surface, 100 m and 500 m. As with the temperatures both models have generally the same patterns and magnitudes. Moderate differences occur at the northern boundary, with the Global being less saline here. Near the Yangtze, EAS16 is less saline than Global, and in the Gulf of Thailand and south of Vietnam Global is fresher. Differences are much smaller at 100 m and 500 m. Noticeable differences occur around the Kuroshio extension and east of the Tsugara strait as with the temperatures.

The U-component of velocity at the surface, 100 m and 500 m is shown in Fig. 37-39. As was mentioned previously the mean currents in the East China Sea through the Korean strait and along the west coast of Japan are stronger in EAS16 than in Global. The Global currents are

somewhat stronger in the Kuroshio south of the Ryukyu Islands and south of Japan. In the Kuroshio extension the EAS16 currents are stronger along the latitude 35°N with Global being stronger on either side of this latitude. In the North Equatorial Countercurrent and the Halmahera Eddy the Global currents are stronger. This pattern is true for the surface and 100 m.

The V-component of velocity at the surface, 100m and 500m is shown in Fig. 40-42. As discussed earlier the flow from the Tsugara Strait southward along the east coast of Japan is stronger in EAS16 than in Global. There are some large differences along the eastern and western open boundaries.

As has been discussed in previous sections there are several differences between the EAS16 model and the Global model, other than the horizontal resolution. Even though both models use NOGAPS atmospheric forcing (1° NOGAPS was used by both models prior to December 2004. After December 2004, both models use 0.5° NOGAPS), assimilate MODAS synthetic temperature and salinity, and include monthly river flow, there are differences in how these data are applied.

EAS16 includes surface air pressure in the surface fluxes while Global does not. EAS16 uses the total heat flux (minus the solar flux) and a separate solar flux field, while Global computes surface heat fluxes from bulk formulas using surface air temperature, vapor pressure, etc. While the wind stress fields are from the same source they may not be exactly the same. Global and EAS16 were not run at the same times, so the available atmospheric fields were not always the same. EAS16 fills in with forecast fields whenever analysis fields are not available. So if analysis fields were not available at the time EAS16 was run, then forecast fields from previous days would be used. If the EAS16 run was delayed then analysis fields for model analysis time and forecast may exist and would be used. Similarly there may be some small differences in the MODAS fields. Further, a heat flux correction, i.e. relaxing the surface heat flux to a flux correction computed from the difference in model SST and MODAS SST was used in EAS16 but not Global. Both models relax the sea surface salinity to MODAS SSS, but EAS16 blends salinity climatology with the MODAS SSS in the relaxation.

EAS16 was set-up before the NRL river database was completed, so there are differences in the rivers and river flows used in each. The salinity comparisons showed that for the most part, the difference in mean salinity is small except in the Gulf of Thailand, south of Vietnam and around the Yangtze. In the Gulf of Thailand both models have two rivers flowing into the gulf. Both have Choa Phraya while Global has Mae Klong and EAS16 has Tapi. Mae Klong has approximately a 4 time stronger flow rate than Tapi. Choa Phyraya in Global is about 9% stronger than in EAS16, so the Global model has fresher water in the Gulf of Thailand. South of Vietnam the fresh water is from the Mekong. Both models have this river but the flow rate in the Global model is an order of magnitude stronger than what is used in the EAS16 model. Thus Global is fresher where this river has influence. (A check of other sources of river flow indicates that the flow rate in the Global is more accurate.) Finally the area around the Yangtze is fresher in EAS16 than in Global. This occurs as the flow rate of the Yangtze is 2% stronger in EAS16 and EAS16 has the Huai He River and Global does not. The EAS16 river database will be updated/expanded beginning with the 2006 runs.

EAS16 with Tides

On October 1, 2003, NRL began running a second EAS16 model, identical to the original but with tidal potential forcing from 8 tidal constituents and tidal boundary conditions, both elevation and velocities. On December 20th, 2003 the tidal version of the EAS16 was implemented by NRL as a daily forecast system. On January 1, 2004, the EAS16 without tides was shut down and the tidal version became the new beta-test code.

Results from the EAS16 with tides code were compared to hourly sea level data from the Sea Level Center at the University of Hawaii (UH), to tidal amplitude and phase data from the IHO database and to two global tidal models. The sea level station data includes short time scale forcing (wind) while the IHO data is a tidal average with no wind/surge effects.

Sea Level Data

There were 23 active stations in the EAS16 region for 2004 in the UH sea level database. The location and station number of each is shown in Figure 43. A time series (covering 9 months) of EAS16 SSH variations and a time series of UH sea level variations were created at each location (the mean was removed from each time series). Statistics comparing EAS16 and the UH sea level data are shown in Table 9. The correlation coefficient (R) at 21 (91%) of the stations is 0.9 or greater, 15 (65%) of these stations have a skill score of 0.9 or greater and six stations have a skill score of 0.7 to 0.9. The root mean square difference (RMSD) is < 10 cm for 14 of the stations. The best agreement is at station h351 with SS of 0.97, R of 0.98 and RMSD of 6.3 cm. The poorest agreement is at station h049 with R of 0.531, SS of .198 and RMSD of 19.8 cm. The next poorest agreement is at stations h053 (Guam). There is some improvement at Guam with tides in 2004 over the run without tides in 2003.

A portion of the SSH time series for station h351 (best agreement) is shown in Fig. 44a. The sea level at this location has a semi-diurnal pattern much of the time, with an occasional diurnal signal. The rest of the time series resembles the segment shown. A portion of the time series for the station with the poorest agreement (h049) is shown in Fig. 44b. This time period was chosen to show that the model and data are in phase a good portion of the time but differ by a few centimeters in amplitude. However there are three events where the data SSH increases and remains high for a day or two, while the model SSH does not significantly increase and maintains a diurnal cycle. The cause of these events is not known but similar events (which the model did not capture) occur a few times during the year contributing to the poor agreement at this location. In Fig. 44c is a portion of the SSH time series at the station with the largest RMSD (46.4 cm). The SSH at this station has high amplitude variations, so even though the RMSD here is large, it is still only a fraction of the maximum amplitude (15%). R and SS at this location are both greater than 0.9. The time series in Fig. 44d is an example of the model capturing, reasonably well, two events where the SSH suddenly increases. The SS at this station is 0.77, R is 0.91 and RMSD is 6.7 cm.

Tidal amplitude and phase

Tidal amplitude and phase from a one-year hindcast of model SSH, with tides, were computed at each model point for the 8 major tidal constituents. Co-tidal plots for M2 and K1 are shown in Figures 45 and 46, respectively. Also shown are co-tidal plots for the OSU model and the Global Tide Finite Element Solution (Lefevre et. al, 2002) referred to as the FES99 model. OSU and FES99 are $1/4^o$ global tide models. Both assimilate TOPEX/Poseidon altimeter data and FES99 also assimilates data from select tide gauges. EAS16 does not assimilate SSH values from any external data source. EAS16 applies OSU values at the open boundaries.

The amplitude and phase for M2 and K1 are similar between each of the models. For M2 they all show a convergence of phase near 150^oE longitude. The biggest difference in this area is the 290° phase line. For EAS16 this phase line does not extend past 140^oE longitude. Each model has an amphidrome off the east coast of Sakhalin, the southern part of the Sea of Japan, north of the Korean strait and one north of Australia in the Timor Sea. Some differences are that there appears to be 4 amphidromes in the Gulf of Capentaria, Australia in the OSU model, but only 2 in the EAS16 and FES99 model. FES99 and EAS16 have two amphidromes in the Gulf of Thailand, one north and one south. OSU has one in the south. In the Yellow Sea, shown in more detail in Fig. 47, all three models have an amphidrome in the northern Yellow Sea east of Shandong peninsula. EAS and OSU have one in the western part of the sea between 34° and 35^oN. There is no amphidrome in this location in the FES99 model. All three models have high M2 amplitudes off the northwest coast of Australia, the east coast of China from Taiwan Strait northward to the Yangzte, and off the western coast of South Korea. EAS16 and FES99 have amplitudes up to 2.7m at Collier Bay Australia while the amplitude in OSU model is 2.0m. Off the east coast of China, south of the Yangtze, FES99 has maximum amplitude of 1.9m, EAS 1.6m and OSU 1.5m. In Korea Bay, both EAS16 and OSU have amplitudes up to 1.4m, but this value is confined to a small section of the coastline in OSU while for EAS16 it is spread along the northern and eastern portions of the bay. For FES99, a maximum of 2.1m is reached near the China/Korea boarder. FES99 has large amplitudes along the western Korean coast increasing to 2.3m at the mouth of Kyonggi Bay then decreasing to 0.6m in the southern part of the bay. For OSU the amplitude is 1.2m at the mouth of Kyonggi Bay and decreases slightly to 1.0m in the northern part of the bay. The amplitude in EAS16 decreases from 1.8m in the southern part of the bay to 1.4m to the north. The highest amplitude along the Korean coast in OSU is near 35.5^oN, a value of 1.5m. FES99 and EAS16 have maximum amplitude near 36^oN, 2.3m and 2.0m respectively.

For the K1 constituent, all three models have an amphidrome in the Sea of Japan, north of the Korean Strait. Also amphidromes exist in the Bohai Bay, Yellow Sea and Gulf of Carpentaria, Australia. One major difference is that FES99 and OSU have an amphidrome in the Gulf of Thailand, while in EAS16 this amphidrome is on land. Areas of large K1 amplitude are west of Kamchatka, between Chinese coast and Hainan Island, in southern South China Sea, Indonesia Sea south of Borneo, northwest Australia and Arafura Sea south of New Guinea. In Joseph Bonaparte Bay, Australia, EAS16 has the largest amplitude of 0.6m (FES99 and OSU, 0.4m). South of New Guinea FES99 has maximum amplitude of 1.1m, OSU, 1.0m and EAS16 0.9m. On the southern coast of Vietnam, EAS16 has maximum amplitude of 0.7m, while FES99 and OSU have 0.5m maximum amplitude. In Fig. 48 is a blow-up of the Yellow Sea K1 constituent. The maximum amplitudes for K1 are along the eastern side of the Yellow Sea. As with M2,

FES99 has the largest amplitudes reaching a maximum of 0.4m in the Korean Bay. EAS16 gets up to 0.34m and OSU reaches 0.3m before it decreases to 0.24m near the coast.

Amplitude and Phases (IHO vs. EAS16)

The EAS16 model amplitude and phase, discussed in the previous section, are compared to the amplitude and phase at several tidal stations from the IHO database. There are 1444 IHO stations in the EAS16 domain, less than half (690) are wet points relative to the EAS16 bathymetry. At these wet points, are computed the percent error in amplitude and phase between the data and EAS16 model [(data-model)/data*100.0]. Thus 100% error means that the EAS16 value is twice the IHO value or visa-a-versa even if the actual magnitudes are small. Table 10 presents the number of stations, for each tidal constituent, which fall within a % error range. (Note that not all the constituents were available at all the stations.) For M2, the percent error in amplitude is less than 10% at 227 stations, and for phase 426 stations have percent error <10%. For K1, 319 stations have <10% error in amplitude and 460 stations for phase. Forty-one stations have % error greater than 100% for M2 and 13 for K1. For phase large errors occur at 26 stations for M2 and 18 stations for K1. Furthermore, for M2 the amplitude percent error is positive in just over half of the stations (51%), i.e. EAS16 underestimates the amplitude. A similar percentage is found for phase (56%). For K1 the numbers are 43% for amplitude and 52% for phase.

To show where these stations are located, various colored symbols are plotted on domain maps in Figs. 49 – 52. The yellow diamonds denote locations where the percent error is less than 10% and the orange diamonds are for stations with percent error of 10-20%. The purple and green triangles along with the red squares denote extreme differences (>100%). In Fig. 49 and 50 are shown the percent error for M2 and K1 amplitudes, respectively. In Figs. 51 and 52 are shown the percent error for phase (M2 and K1).

For M2 amplitude, the EAS16 model agrees with the IHO data over a large portion of the model domain, demonstrated by the large number and wide distribution of yellow and orange diamonds in Fig 49. In a few areas the agreement is not as good. The northern Yellow Sea and Bohai Bay is one such area. Here most amplitude differences ranges from 20 to 50%. There are two locations in the Bohai Bay with difference <20 (two orange diamonds very close together). One of these is station #983 (119.6^{o}E, 39.9^{o}N). The M2 amplitude is 0.14m in the IHO database and 0.12m in the EAS16 model, a percent error of 12.7%. The phases, however, don't agree. The phase at this location from IHO is 76.1^o and for EAS16 it is 141.7^o. (Same situation for the near by station, #974). From Fig. 51 one sees that there are several stations in the Bohai Bay where the phase agrees within 20% though there is a larger error in amplitude. One example is station #999 (122.2^{o}E, 40.6^{o}N). Here the phases are 268.7^o from IHO and 270.0^o from EAS16 (-0.49% error). The amplitudes here are 1.17m and 0.67m for IHO and EAS16 respectively (42.7% error).

Many of the stations with large error have small amplitudes and/or are located in bays, narrow straits or other such restricted areas where the model's horizontal resolution can not sufficiently resolve the physical characteristics of the area. Small amplitudes, 5 cm or less, occur at 15 of the 41 stations with %error in M2 amplitude of 100% or greater. The stations with the poorest agreement, for M2 amplitude, are denoted by the two red squares (near Java) in Fig 49. One of these is station #1332 (113.7^{o}E, 7.1^{o}S), located on Madora Island, in the bay formed by this

island and Java. The amplitude at this station is 0.05m for IHO and 0.70m for EAS16 (-1292% error). For phase the values are 101.5^o and 168.0^o (-65.5% error). The other red square is for station #1293 (106.6^oE, 5.6^oS), which is within a group of small islands off the northwest coast of Java. Here amplitude from IHO is 1 cm and from EAS is 12 cm. The phase at this station is 52.8^o from IHO and 208.0^o for EAS.

The data/model agreement is good at more stations for K1 than for M2, both in amplitude and phase (see Table 10). An example is station #1320 (112.8^oE, 6.9^oS). Here the percent difference is 9.4 for amplitude and -3.8 for phase for K1. For M2 the errors are -424%, amplitude and -22.0%, phase. The actual values are for K1, amplitude of 0.52m for IHO and 0.47m for EAS and phase of 213.2^o for IHO and 221.2^o for EAS. For M2 the amplitude for IHO is 0.02m and for EAS it is 0.10m. For phases the values are 238.4^o for IHO and 290.9^o for EAS.

In some instances, the amplitude percent difference is good and the phase is not and visa versa, therefore the "best" stations will be defined as those where both amplitude and phase errors are less than 20% (Fig. 53 for M2 and Fig. 54 for K1). An example of good agreement for M2 and K1 is station #795 (139.8^oE, 35.3^oN). For M2 the amplitude is 0.450 for IHO and 0.447 for EAS. The M2 phases are 229.4 and 228.27, IHO and EAS respectively. For K1 the amplitude is 0.25 for IHO and 0.246 for EAS, while phases are 38.23 and 40.83. Just under half of the stations (327) fall into this best category for M2 and more than half (432) for K1. There are no best stations in the Bohai Bay, Gulf of Thailand and Gulf of Carpenteria for M2, but a few in Bohai Bay for K1. There are several best stations in the Strait of Malacca, between Malaysia and Sumatra for M2 ever though it is a relatively narrow strait. There are few best stations for K1 there.

Robertson and Ffield (2005) presented results from their tidal model of the Indonesian Seas and compared the amplitude and phase from their model to amplitude and phase computed at 13 TOPEX/Poseidon (T/P) crossover points. They agreed quite well with the T/P values, expect for one location (site 11) where their amplitude was too large. Excluding this site, their rms error for amplitude was 8 cm and for phase 13. We decided to see how EAS16 tidal values compared to the values at these crossover points. EAS16 values and the T/P values are listed in Table 11. Figure 55 shows the EAS16 amplitude and phase in the Indonesia Seas along with the location of the T/P crossover points. The EAS16 rms error for amplitude is 3.9 cm and 17.3 for phase. The largest error occurred in phase at site 8 with a phase difference of 60°. Excluding this site the EAS16 rms error for the remaining sites, for amplitude is 3.6 cm and 4.4 for phase.

Eddy Kinetic Energy

Eddy kinetic energy (EKE) is the kinetic energy (KE) of that part of fluid flow that represents a departure from the average kinetic energy. EKE is a measure of the degree of variability and may be used to identify regions with highly variable phenomena. In this section we will use EKE to identify regions within the model domain which are more energetic due to tides. The most accurate method of doing this is by comparing the EKE of model runs with tides to the EKE of runs without tides. However, there are only 2 months of overlapping runs that are available (October and November 2003). The average EKE for these two months (EKE_{2m}) are shown in Figure 56 a&b (with tides and without tides), their difference is shown in Figure 56c. Eddy

kinetic energy for these plots is computed by removing the kinetic energy computed with the mean velocity for these two months from the average kinetic energy over the same time period.

$$EKE_{2m} = [1/61 \sum_{d=1}^{61} KE_d] - KE_{2m}, \quad KE_d = 1/24 \sum_{h=1}^{24} KE_h = 1/24 \sum_{h=1}^{24} [\tfrac{1}{2}(U_h^2 + V_h^2)] \quad (7)$$

$$KE_{2m} = \tfrac{1}{2}(\overline{U}_{2m}^2 + \overline{V}_{2m}^2) \quad (8)$$

$$\overline{U}_{2m} = 1/61 \sum_{h=1}^{61}(U_h), \quad \overline{V}_{2m} = 1/61 \sum_{h=1}^{61}(V_h) \quad (9)$$

Where 2m = denotes the 2 month time period
      d = denotes daily
      h = denotes hourly
EKE_{2m} = is the average eddy kinetic energy for the 2 months
  KE_d = is the daily mean kinetic energy
  KE_h = is the kinetic energy each hour
  KE_{2m} = is the kinetic energy of the mean velocity

  $\overline{U}_{2m}$ = is the eastward component of the mean velocity

  $\overline{V}_{2m}$ = is the northward component of the mean velocity
  U_h = is the eastward component of the hourly velocity
  V_h = is the northward component of the hourly velocity

The Kuroshio extension, the currents north of Papua New Guinea and those along the east coast of Vietnam are a few of the areas where both model runs have high EKE. From the difference plot (Fig. 56c) one sees that the addition of tides has little effect in these areas. The Yellow Sea, Luzon strait, around Taiwan and the northwest Australian coast are a few of the areas which are more energetic with the addition of tides. The areas of increased EKE due to tides (Fig. 56c) are predominately is coastal or shallow areas where tidal amplitudes are significant. The EKE is also larger in straits, e.g. the Luzon strait. There is also increased EKE along some of the open boundaries due to the addition of the tidal boundary conditions.

For an annual average tidal EKE the best we can do is separate the short times scales (<24 hour) from the longer time scales (>24 hours but < 1 year) and assume that most of the tidal EKE will be captured in the short times scales. To accomplish this we first compute the average eddy kinetic energy (EKE$_a$) for one year. This is the same as equation 7 but for one year instead of two months.

$$\text{EKE}_a = \ [1/365 \sum_{d=1}^{365} \text{KE}_d \ ] - \text{KE}_y \ , \quad \text{KE}_y = \ ½ \ (\overline{U}_y{}^2 + \overline{V}_y{}^2 \ )] \tag{10}$$

Next we compute the annual mean of the daily eddy kinetic energy EKE$_s$ which is the EKE for short time scales.

$$\text{EKE}_s = 1/365 \sum_{d=1}^{365} \{[1/24 \sum_{h=1}^{24} \text{KE}_h] - \text{KE}_{dm} \} \ , \quad \text{KE}_{dm} = ½ \ (\overline{U}_d{}^2 + \overline{V}_d{}^2) \tag{11}$$

Finally the eddy kinetic energy for times scales longer than 24 hours (EKE$_l$) and less than one year are computed by subtracting the short times scales for the annual eddy kinetic energy.

$$\text{EKE}_l = \text{EKE}_a - \text{EKE}_s \tag{12}$$

The long time scale eddy kinetic energy (EKE$_l$) is plotted in Figure 57a and the short time scale EKE$_s$ is plotted in Figure 57b. EKE$_l$ highlights the variability in the Kuroshio extension, the Halmahera eddy and the Equatorial Countercurrent. Also shown is the coastal current off the east coast of Vietnam which changes direction with the monsoons. Some of these areas of variability were seen in Figure 56. As discussed earlier these areas of high EKE are not strongly influenced by tides.

The short time scale EKE shown in Figure 57b is similar in many ways to Figure 56c. They both show high EKE in the Yellow Sea, around Taiwan and the Luzon strait as well as the northwest coast of Australia. Clearly areas were tidal energy is important. One big difference is much lower EKE near the southwestern open boundary.

Glider Data Comparisons

During May, 2004, a technology demonstration of the Glider Operations and Data System (GODS) in the WESTPAC area was carried out in conjunction with the Naval Oceanographic Office. The objective of this effort was to quantify mesoscale variability in velocity and sound speed over a 100 km square box using glider technology as a synthetic moored array. The glider data was available for approximately one week, from May 8 – 16. Dr. Mike Carnes of the Naval Oceanographic Office compared velocity, temperature and salinity from the gliders to the Global NCOM and the EAS16 fields. The glider was programmed to dive to 200m depth and return to "near" the surface (5-11m). This process was repeated approximately every 40 minutes. Temperature and salinity measurements were made during the descent and ascent. However for the following discussion only the descending profiles were used. Approximately every 2 hours, the gilder returned to the surface to receive position information and transmit data. Water velocity was estimated using a combination of GPS locations and dead-reckoning calculations. Thus the current speeds from the glider are an estimated average over the time interval between surfacing (~2 hours) and an average over the depth of the dive. The model data is regridded to a horizontal spacing of $1/16^o$ and to fixed vertical levels. Then the matching velocity averages for the glider from the model fields are computed by averaging from 0 m to 200 m over the time interval between each time that the glider surfaces. The time for each average is set to the center

time between surfacing. For temperature and salinity comparisons, model (EAS and Global) temperature and salinity were extracted at the same time and location of each glider decent.

Figure 58 shows the location of the glider WE04 from May 8th through May 17th. Figures 59 a-c compares the observed currents, temperature and salinity from the glider to the EAS16 and Global NCOM derived fields. The glider data shows strong high frequency variability generated by tidal effects in the velocity data. This variability is represented in the EAS16 fields. The agreement with respect to phase is very good through the observational period; however, the amplitudes are underestimated during the first few days. The Global NCOM solutions do not agree as well as the EAS16 solutions as the Global NCOM does not include tidal forcing. (There is an option for adding a tidal solution from the OSU tide model to its fields after the fact.) The effect of the tides is also visible in the temperature and salinity observations (Fig. 59b). Again the EAS16 temperature fields are in closer agreement with the observations then the Global NCOM temperatures without tides. However, the EAS16 does not capture the strong high frequency effects seen in the observations.

Drifter Data Comparisons

During the same time as the glider operation, a number of Davis Drifters were released in the exercise area and several WOCE Argos drifters were available in the area. Davis Drifter measurements are considered valid at 1 m depth. The WOCE Argos drifters are designed to descend from the surface to a defined pressure, subsurface drift, ascend taking profile measurements, and then surface drift while transmitting data. The temperature and salinity values from both types of drifters are taken as surface values. The velocity measurements are surface (1 m) for the Davis Drifters and at 15 m for Argos. The first sigma level is used as the surface values for the models. In deep water, where the drifters are , the first sigma level is 1 meter thick. The 15 m velocity model values are taken from the regridded model fields described in the Glider section. Model values are interpolated to the location and time along the drifter path. Figure 60 shows the paths taken by two sample WOCE Argos drifters available in this area. The first drifter, #52513, Fig. 60a, began its path at 131.4^o E and 19.0^o N and drifted first west, then north and finally almost due east ending at 135.5^o E and 20.25^o N. The second drifter, #52521, Fig 60b, began near 132.0^o E and 19.5^o N and drifted south and west to 126.0^o E and 18.0^o N, before turning to the north and ending up at 126.0^o E, 19.5^o N. Figures 61 and 62 show time series of u and v components of the velocity, stick vector diagrams, speed, direction and SST comparisons of the EAS16 model results to the drifter data. Both the velocity and surface temperature data compare very well with the model. The largest differences in the comparison with drifter #52513 appear from May 3-10 when the u-component of the model velocities was substantially smaller than the observation. The largest difference between drifter #52521 and the model appear from April 27- May 6 when the u-component of the observed velocities is stronger than the modeled velocities. Again for drifter #52521, from April 23-25, the observed SST was warmer then the modeled SST and while from April 26 - 30, the modeled SST was warmer than the observed.

One of the Davis drifters released during the exercise is drifter #34851. The path taken by this drifter is shown in Figure 63. This drifter started at 124.3^o E and 28.3^o N and drifted east and north ending up at 126.7^o E and 29.0^o N. Figure 64a-b shows the u and v component of the

velocity and stick vector diagrams for the EAS16 and Global NCOM results compared to the drifter data. Figure 65a-b shows the speed, direction and SST from the two models versus the observations. The EAS16 model with tides well represents the phase and slightly underestimates the amplitude of the u and v components of the velocity. The Global NCOM solutions do not include the high frequency tidal effects and as such, underestimate the velocity and do not reproduce the phase well. The speed and direction plots also show that the EAS16 model agrees better with the data than does the Global model. These results clearly show the importance of including tidal effects in the velocity prediction. There is not such a significant difference in the SST values, but the SST from EAS is noticeably in better agreement with these observations than is Global.

Figure 66 is a second Davis drifter path, #34847. This drifter was released farther west (129.0^o E) and south (20.0^o N) than the previous example. During this time, Super Typhoon NIDA approached this region. Figure 67 shows the path taken by Super Typhoon NIDA (pink triangle) and the track of drifter #34847 (blue dots), while Table 12 quantifies the location and strength of the storm. The path of the storm curved around this drifter, first located south of the drifter, then west of the drifter and finally passing by north of the drifter. Super Typhoon NIDA was closest to this drifter on May 19th, passing to its west and therefore placing the drifter in its eastern and strongest quadrant. The effect of this storm caused this drifter to take a spiraling path to the southeast. Once the storm had passed and its effects had weakened, the drifter commenced its original path to the north-northeast. Note that the effect of this storm was not seen in the previous example as that drifter was located too far north to experience any strong effects from this storm.

Figure 68a-b shows the u and v component as well as the stick vector diagrams for the EAS16, Global NCOM and observation. Figure 69a-b shows the comparison of the speed and direction as well as the SST of the EAS16 and Global NCOM model to the drifter observations. Prior to May 19th, and similar to the previous example, the EAS16 results were in better agreement with the observations then the Global NCOM, due to the inclusion of tidal forcing. Starting at approximately May 19th, a large rotational effect appeared in the observations that eventually died out by May 27th. These inertial oscillations were excited by the passing of Super Typhoon NIDA. Both models reproduced the phase of this oscillation well, but the EAS16 reproduced the amplitude slightly better than the Global NCOM.

The third panel of Figure 69a & b, compares observed versus modeled SST. During the storm, EAS16 and Global NCOM both reproduced the cooling of the ocean surface reasonably well. EAS16 cools to 27.55^{o}C by May 20th. The drifter has the temperature cooling to 27.46^{o}C. After the storm, however both models warm rapidly. The temperature has reached 28.8^{o}C in the EAS16 model by day 21 06Z, while the drifter has a temperature of 27.7^{o}C at this time (1.1^{o}C difference). The drifter shows that the surface temperature stays under 28°C through May 26 while the model temperature stays above 28°C. Several factors affect the model's surface temperature; two are surface fluxes and relaxation to MODAS synthetic temperatures and salinities. The surface fluxes are also "corrected" using the SST from MODAS (see eq. 1). Closer exanimation suggest that surfaces fluxes are a significant contributor to the warming of the model temperatures after the storm and that MODAS temperatures can not help bring the

model temperatures down as the cooling from the storm is not reflected in the MODAS values until May 22 and MODAS temperatures do not remain lower as suggested by the drifter.

After the storm, beginning around the 21st, NOGAPS winds are weak and surface heating is strong from solar radiation and heat loss from sensible, latent and longwave are relatively weak. The average wind speed for the area encompassing the drifter is ~4 m/s. The average net heat flux (total of sensible, latent and longwave), is ~ 100 W/m^2 heat loss, and solar reaches ~800 W/m^2 , heat gain, on May 21st and ~700 W/m^2 on the 22nd and 23rd. The model responds by warming the surface layers. Figure 70 shows a closer examination of panel C of Figure 69a. In addition to drifter temperatures and model temperatures at the surface, are model temperatures at 1, 5, 15 and 40 meters. The surface and 1 meter temperatures increase the most with the peak temperatures occurring near the time of maximum solar flux each day. Temperatures at 5 and 15 meters warm as well but don't have the extreme peaks. Temperatures at 40 meters don't show any significant warming after the storm until the 24th. There is a surface cooling event on the 24th which is rather strong in the drifter temperatures but small in the model. This cooling occurs as typhoon OMAIS passed east of the drifter. OMAIS was weak when it passed the drifter. The model surface temperatures agree quite well with the drifter temperatures until after the passage of STY NIDA. The models warming in response to weak winds and strong surface heating is as expected for such conditions, but the drifter has the surface temperature staying cool. At this time there is not enough information to say exactly what is happening. Possibly the NOGAPS forcing did not adequately model cloud cover which would keep the solar heating down. Examinations of satellite images show considerable cloud cover over the region for several days after the typhoon passed. Cloud cover would also keep the MODAS temperatures from being updated with new information and thus revert to climatology. Or the model's vertical resolution is to coarse for this particular case. The first sigma level is 1 meter thick in the deep water where the drifter is located, with the first temperature at 0.5 m and the second at 1.6 m. Perhaps the solar heat is actually concentrated in a very thin surface layer and does not penetrate very deep. Maybe the drifter was damaged and is not reporting correct temperatures and/or location. This needs to be looked into further to see if this situation occurs following other storms.

Summary and Conclusions

This report has described the EAS16 NCOM model and presented the validation tests of the model. The model is NCOM version 2.3 implemented in the Western Pacific, referred to as the East Asian Seas region (98° to 158°E and 17°S to 52°N). The resolution of the model is 1/16° at mid-latitude horizontally and 40 sigma/z vertical levels. Data assimilation consists of 2D adjustment of surface fluxes using MODAS SST and climatological surface salinity and 3D relaxation to temperature and salinity fields produced by MODAS. Databases used in EAS16 are WMO river database, OSU global tide constituent data bases, and NRL DBDB2 bathymetry regridded to the NCOM grid. The model is forced by operational FNMOC wind stress and thermal fields. The model is run in a nowcast/forecast mode i.e. a two day hindcast is run up to analysis time using analysis forcing fields and MODAS. Then a 72 hour forecast is run beginning with the restart from the end of the hindcast run and using forecast fields from NOGAPS. Beginning with the October 1, 2003 run tides were added to the model. Some

validations were preformed with the no tides runs (2001-2003) and others with the tidal runs (2004).

The general circulation produced by the model was shown to agree reasonably well in location and strength to the major currents observed in the region. The model also reproduced the seasonal shifts in the currents, such as the southward current off the coast of Vietnam in the winter shifting to northward in summer in response to the monsoons. Transports at several straits agreed within a few Sverdrups to the values reported in the literature. Mean currents deduced from a drifter database compiled by Peter Niiler showed that in 57% of the samples examined the EAS16 model currents were within 5 cm/sec of the drifter data and in 80% of the samples the difference was within 10 cm/sec. Larger differences occurred in the Kuroshio, North Equatorial Current and Halmahera Eddy (20 cm/sec or greater). These are strong, highly variable currents so a small shift in location of the current can cause large difference. There were no comparisons in Yellow Sea, South China Sea and around Indonesia due to sparse data in these regions.

Model sea surface height (SSH) for runs with and without tides compared well with sea level data from the University of Hawaii Sea Level database. For the runs without tides the daily SSH from the model yielded correlations coefficients (R) of 0.8 or greater and skill scores (SS) of 0.6 or greater in 6 out of 10 of the data stations. At three stations the comparisons were moderate (R ~0.6 and SS ~0.3). The measurements at Guam were not reproduced well by the model. The station at Guam is located at the mouth of a channel in a small bay. The model can not adequately simulate SSH and other model products in restricted areas like small bays and channels due to the resolution of the model.

For the runs with tides comparisons of hourly SSH yielded correlations of 0.9 or greater and skill scores of 0.7 or greater in 21 out of 23 stations. Station h053 had moderate agreement (R = 0.76 and SS = 0.58). This station is Guam which had negative SS in the 2003 no tides run. Agreement in 2004 appears better however, there were several months of missing data at this station in 2004. The station with the poorest agreement (h049) was shown to have periods where the SSH in the data increased and stayed high for a day of two while the model SSH maintained a diurnal cycle.

Model temperature and salinity profiles compared well with several PALACE floats with temperatures having smaller differences than salinity. The model temperature was compared to the TAO array 2003 data. The model compared well in the upper ocean (above 50m) with high correlations and skill scores. The model did not do as well at 50 to 150m depths with negative SS occurring often at 50m. Exceptions were at buoy 8N137E and 5S156E with positive SS in the upper 200m and at 2N156E with positive SS in the upper 150m. The model did not adequately capture the variability of the mixed layer. However, there were times when the model did quite well, e.g. the mixed layer deepening at 2n137e around day 140 (Fig 24b) but some other events were missed or underestimated.

Tidal amplitude and phase from the EAS16 model were compared to two global tidal models, OSU and FES99. Both of these models include assimilation of tidal measurements, EAS16 does not. The tidal amplitude and phase for the EAS16 model are similar to those from the global models. The same areas of high amplitude and location of amphidromes agreed between the models. Some exceptions were the M2 amphidrome in the western part of the Yellow Sea.

EAS16 and OSU showed this amphidrome but FES99 did not, also the amphidrome in the Gulf of Thailand was shown in OSU and FES99, but EAS16 had this one on land. EAS16 amplitude and phase were compared to IHO data. Over half of the tidal stations in the IHO database are on land relative to the EAS16 bathymetry. Of the 688 usable stations the percent difference in amplitude and phase of just over half of the stations was less than 20%. These were called the best stations in Figs. 53 and 54. These "best" stations were distributed throughout the model domain. Some areas lacking "best" stations were the Bohai Bay, Gulf of Thailand, the Java Sea and Gulf of Carpenteria.

Tidal amplitude and phase at several TOPEX/Poseidon crossover points in the Indonesia seas were compared to EAS16 tidal values. EAS16 agreed quite well with the T/P values. The rms error for these sites was 3.9 cm for amplitude and 17.3 for phase. One location had a larger phase error than the others (site 8). Excluding this site slightly improved the amplitude rms (3.6 cm) and greatly improved the phase rms (4.4).

The model was compared to several drifters and data from a glider test run. The glider test covered the upper 200 meters of the water column. The model reproduced the temperature, salinity and mean currents reported by the glider reasonably well. The frequency of changes in temperature and salinity was captured by the EAS16 model but often the model underestimated the strength of the variability. For the drifter data, the model reproduced the temperatures and velocities reported by the drifters. A few large changes in temperature were underestimated by the EAS16 model. One such change occurred after the passage of Super Typhoon NIDA. The model captured the surface cooling as the typhoon passed by but following the typhoon EAS16 warmed up faster than indicated by the drifter data. A closer examination of the model response suggested that atmospheric forcing warmed the surface more than the data suggested and that MODAS temperatures were not update due to cloud cover after the storm and could not help the model reproduce accurate temperatures.

The non-tidal EAS16 and Global NCOM models yield similar results. Both models reproduce the mean position of the Kuroshio, have reasonable transports at major straits and reproduce the general structure in temperature and salinity. Some differences are lower SSH in the Yellow Sea and Sea of Japan in the EAS16 model. This results in stronger flow through the Korean Strait and along the west coast of Japan and reduced flow in the Kuroshio south of Japan (132° to 135^oE) in EAS16. Stronger flow through the Tsugara strait in EAS16 is a result of the stronger flow along the Japan coast and better resolution of the straits. This stronger Tsugara strait flow in EAS16 causes lower temperatures and salinities east of the strait and along the northeastern coast of Japan, particularly at depth. Difference in salinity between EAS16 and Global occur in some coastal locations as there are differences in the river flow database in EAS16 and Global. The biggest differences are in the Gulf of Thailand and south of Vietnam where Global salinities are lower and near the Yangtze where EAS16 salinities are lower. In the non-tidal EAS16 run the differences between EAS16 and Global are mainly due to the higher resolution of EAS16. More differences occur when tides are added to EAS16. As was seen with the glider and drifter data better agreement occurs with EAS16 as the frequency of the variability is captured better when tides are included.

The EAS16 model simulates oceanographic conditions in the EAS region reasonably well, such as the ability to reproduce currents, temperatures and tidal regimes. Instances when the model fails or falls short can often be attributed to resolution. That is, the model is not able to resolve some straits, bays etc. or adequately define some bathymetry. Other areas that affect the model's ability to reproduce adequate responses are atmospheric forcing, vertical mixing and data assimilation. NOGAPS forcing (0.5^o or 1.0^o) misses some of the finer scale forcing and may underestimate the strength of winds and heat exchange.

ACKNOWLEDGEMENTS

Table 1: Statistics for Sea Level Prediction

Statistics of daily ssh (JASL stations vs. EAS16 model) for 2001

Name	rmsd	σ_x	σ_y	r	ss
Kukup, Malaysia	5.32	6.78	3.69	0.62	0.38
Sedili, Malaysia	7.20	15.40	10.48	0.91	0.78
Tioman, Malaysia	6.43	13.99	10.04	0.91	0.79
Kuantan, Malaysia	6.90	16.48	11.83	0.93	0.82
Cendering, Malaysia	7.28	17.49	12.42	0.94	0.83
Geting, Malaysia	8.51	19.50	13.40	0.93	0.81
Naze, Japan	7.06	11.30	14.36	0.88	0.61
Miyzkejima, Japan	11.26	13.15	14.84	0.68	0.27
Lombrum, Papua New Guinea	4.08	5.75	3.76	0.71	0.49
Guam	6.19	4.83	7.44	0.56	-0.64

Statistics of 30day ssh (JASL stations vs. EAS16 model) for 2001

Name	rmsd	σ_x	σ_y	r	ss
Kukup, Malaysia	2.75	4.36	2.34	0.83	0.60
Sedili, Malaysia	5.19	12.44	7.49	0.99	0.83
Tioman, Malaysia	4.59	11.63	7.47	0.98	0.84
Kuantan, Malaysia	5.30	13.90	8.90	0.99	0.85
Cendering, Malaysia	5.36	14.60	9.54	0.99	0.87
Geting, Malaysia	6.15	16.00	10.12	0.99	0.85
Naze, Japan	4.35	10.83	12.88	0.95	0.84
Miyzkejima, Japan	7.01	8.51	10.38	0.74	0.32
Lombrum,Papua New Guinea	2.80	5.21	3.12	0.89	0.71
Guam	5.33	4.20	6.79	0.60	-0.62

rmsd : root mean square difference
σ_x : standard deviation of tide gauge
σy : standard deviation of model ssh
 r :   correlation coeff.
 ss: skill score
Station data from Univ. of Hawaii "Best" data

Table 2. Statistics - model vs. TAO mooring.

```
Location: 8n137e
No. samples: 360
 Depth  M_Mean  D_Mean M_diff  RMSD  stdm  stdd   R     SS
  -1.50  28.94  29.06  -0.11  0.31  0.62  0.69  0.91   0.79
 -25.00  28.77  28.90  -0.13  0.31  0.65  0.63  0.90   0.76
 -50.00  27.58  27.51   0.07  1.30  1.15  2.07  0.82   0.61
 -75.00  24.80  24.37   0.43  1.78  1.67  2.98  0.87   0.64
-100.00  21.63  20.93   0.70  1.78  1.90  3.04  0.88   0.66
-125.00  18.52  17.84   0.68  1.63  1.87  2.77  0.87   0.65
-150.00  15.81  15.22   0.59  1.25  1.68  2.08  0.85   0.64
-200.00  12.31  11.90   0.41  0.80  1.09  1.06  0.80   0.43
-250.00  10.19  10.21  -0.01  0.44  0.58  0.50  0.68   0.23
-300.00   9.14   9.37  -0.23  0.35  0.28  0.30  0.57  -0.39
-500.00   7.30   7.61  -0.31  0.35  0.07  0.16  0.21  -3.94
-750.00   5.76   5.96  -0.21  0.27  0.07  0.18  0.24  -1.28

Location: 0n147e
No. samples: 356
 Depth  M_Mean  D_Mean M_diff  RMSD  stdm  stdd   R     SS
  -1.50  29.61  29.81  -0.19  0.33  0.31  0.35  0.67   0.08
 -25.00  29.44  29.67  -0.23  0.34  0.30  0.30  0.64  -0.29
 -50.00  29.01  29.49  -0.49  0.63  0.45  0.46  0.63  -0.82
 -75.00  28.19  28.60  -0.40  0.92  0.63  1.23  0.78   0.43
-100.00  26.74  25.81   0.92  1.47  0.66  1.65  0.85   0.20
-125.00  24.81  23.50   1.31  1.54  0.64  1.26  0.85  -0.48
-150.00  22.56  21.85   0.71  1.13  0.60  1.02  0.50  -0.23
-200.00  17.86  18.11  -0.26  0.78  0.48  0.87  0.54   0.20
-250.00  13.86  14.27  -0.41  0.70  0.39  0.67  0.54  -0.07
-300.00  11.57  11.88  -0.31  0.50  0.22  0.40  0.33  -0.55
-500.00   8.01   8.39  -0.38  0.42  0.09  0.21  0.61  -2.86
-750.00   5.74   5.88  -0.14  0.19  0.08  0.17  0.69  -0.24

Location: 5s156e
No. samples: 360
 Depth  M_Mean  D_Mean M_diff  RMSD  stdm  stdd   R     SS
  -1.50  29.64  29.72  -0.09  0.27  0.34  0.38  0.74   0.46
 -25.00  29.56  29.61  -0.05  0.20  0.31  0.30  0.81   0.57
 -50.00  29.36  29.49  -0.13  0.33  0.33  0.36  0.62   0.17
 -75.00  28.75  29.13  -0.39  0.58  0.51  0.64  0.73   0.16
-100.00  27.73  28.33  -0.60  0.76  0.76  0.97  0.88   0.38
-125.00  26.39  27.03  -0.64  0.87  1.00  1.36  0.92   0.59
-150.00  24.50  25.16  -0.67  0.92  1.21  1.48  0.91   0.61
-200.00  19.30  18.96   0.34  0.78  1.10  1.41  0.87   0.70
-250.00  14.73  13.46   1.27  1.39  0.72  0.72  0.70  -2.73
-300.00  11.99  11.03   0.96  1.02  0.40  0.37  0.59  -6.74
-500.00   7.94   8.15  -0.22  0.28  0.12  0.22  0.57  -0.69
-750.00   5.58   6.04  -0.46  0.48  0.06  0.15  0.56  -9.04


 M_mean – model mean temperature,       R    - correlation coefficient
 D_mean – data mean temperature,        SS   - skill score
 M_diff – mean difference model – data, RMSD - root mean square difference
 Stdm   - standard deviation model
 Stdd   - standard deviation data
```

```
Table 3. Statistics - MODAS vs. TAO mooring.

  Location: 8n137e
  No. samples: 360
  Depth  M_Mean  D_Mean M_diff  RMSD   stdm   stdd    R      SS
   -1.50  29.15   29.06   0.09   0.33   0.64   0.69   0.89    0.77
  -25.00  28.85   28.90  -0.06   0.27   0.61   0.63   0.91    0.81
  -50.00  27.75   27.51   0.24   1.42   0.87   2.07   0.86    0.53
  -75.00  24.83   24.37   0.46   2.07   1.42   2.98   0.81    0.52
 -100.00  21.54   20.93   0.61   2.22   1.78   3.04   0.73    0.47
 -125.00  18.31   17.84   0.47   2.21   1.87   2.77   0.63    0.37
 -150.00  15.52   15.22   0.30   1.81   1.72   2.08   0.57    0.24
 -200.00  12.09   11.90   0.20   1.09   1.13   1.06   0.52   -0.06
 -250.00  10.07   10.21  -0.14   0.59   0.62   0.50   0.49   -0.38
 -300.00   9.08    9.37  -0.29   0.42   0.32   0.30   0.50   -0.98
 -500.00   7.29    7.61  -0.31   0.35   0.06   0.16   0.19   -4.11
 -750.00   5.76    5.96  -0.21   0.27   0.07   0.18   0.17   -1.33

  Location: 0n147e
  No. samples: 356
  Depth  M_Mean  D_Mean M_diff  RMSD   stdm   stdd    R      SS
   -1.50  29.82   29.81   0.01   0.31   0.39   0.35   0.64    0.18
  -25.00  29.63   29.67  -0.04   0.22   0.34   0.30   0.78    0.47
  -50.00  29.37   29.49  -0.12   0.33   0.37   0.46   0.76    0.50
  -75.00  28.68   28.60   0.08   0.88   0.49   1.23   0.82    0.49
 -100.00  27.37   25.81   1.56   1.97   0.64   1.65   0.80   -0.43
 -125.00  25.58   23.50   2.08   2.25   0.71   1.26   0.75   -2.18
 -150.00  23.34   21.85   1.49   1.74   0.68   1.02   0.50   -1.90
 -200.00  18.30   18.11   0.19   0.77   0.54   0.87   0.52    0.22
 -250.00  14.02   14.27  -0.24   0.70   0.40   0.67   0.35   -0.07
 -300.00  11.63   11.88  -0.25   0.47   0.24   0.40   0.28   -0.40
 -500.00   8.03    8.39  -0.36   0.40   0.07   0.21   0.50   -2.63
 -750.00   5.76    5.88  -0.12   0.19   0.08   0.17   0.59   -0.19

  Location: 5s156e
  No. samples: 360
  Depth  M_Mean  D_Mean M_diff  RMSD   stdm   stdd    R      SS
   -1.50  29.76   29.72   0.04   0.31   0.31   0.38   0.62    0.34
  -25.00  29.54   29.61  -0.07   0.22   0.24   0.30   0.72    0.45
  -50.00  29.21   29.49  -0.28   0.38   0.29   0.36   0.69   -0.11
  -75.00  28.52   29.13  -0.61   0.72   0.49   0.64   0.81   -0.27
 -100.00  27.45   28.33  -0.89   1.01   0.75   0.97   0.87   -0.09
 -125.00  26.04   27.03  -0.99   1.21   0.98   1.36   0.88    0.21
 -150.00  24.07   25.16  -1.09   1.35   1.14   1.48   0.85    0.17
 -200.00  18.89   18.96  -0.07   0.86   1.03   1.41   0.80    0.63
 -250.00  14.44   13.46   0.98   1.13   0.70   0.72   0.68   -1.48
 -300.00  11.81   11.03   0.78   0.87   0.42   0.37   0.54   -4.57
 -500.00   7.86    8.15  -0.29   0.34   0.12   0.22   0.55   -1.51
 -750.00   5.54    6.04  -0.50   0.52   0.06   0.15   0.44  -10.76

  M_mean – model mean temperature,         R    - correlation coefficient
  D_mean – data mean temperature,          SS   - skill score
  M_diff – mean difference model – data,  RMSD - root mean square difference
  Stdm   - standard deviation model
  Stdd   - standard deviation data
```

Table 4. Total statistics for 10 of the moorings, model vs. TAO mooring:

```
 No. samples: 3326
 depth  M_Mean  D_Mean M_diff  RMSD   stdm   stdd    R       SS
  -1.50  29.43   29.56  -0.13   0.30   0.48   0.54   0.87    0.69
 -25.00  29.29   29.38  -0.10   0.32   0.49   0.55   0.84    0.67
 -50.00  28.77   28.95  -0.18   0.80   0.85   1.26   0.79    0.59
 -75.00  27.49   27.71  -0.22   1.19   1.57   2.18   0.85    0.70
-100.00  25.59   25.44   0.15   1.44   2.19   2.81   0.86    0.74
-125.00  23.34   22.94   0.40   1.42   2.70   3.21   0.91    0.81
-150.00  20.84   20.44   0.40   1.38   2.95   3.49   0.93    0.84
-200.00  15.99   15.31   0.69   1.43   2.39   2.90   0.91    0.76
-250.00  12.43   12.12   0.32   1.09   1.58   1.92   0.84    0.68
-300.00  10.59   10.60  -0.01   0.75   1.01   1.24   0.80    0.63
-500.00   7.80    7.97  -0.17   0.34   0.30   0.44   0.75    0.42
-750.00   5.75    5.88  -0.13   0.25   0.11   0.20   0.14   -0.53

 M_mean - model mean temperature
 D_mean - data mean temperature
 M_diff - mean difference model - data
 RMSD   - root mean square difference
 Stdm   - standard deviation model
 Stdd   - standard deviation data
 R      - correlation coefficient
 SS     - skill score
```

Table 5. ILD statistics for EAS16 model vs. TAO moorings

buoy	M_Mean	D_Mean	M_diff	RMSD	stdm	stdd	R	SS
0n147e	-48.34	-60.92	12.58	19.86	12.18	15.87	0.42	-0.57
0n156e	-50.54	-67.31	16.77	20.9	9.32	15.68	0.61	-0.78
2n137e	-43.65	-46.82	3.17	19.61	13.33	19.64	0.36	0
2n147e	-52.17	-34.48	-17.69	19.2	7.28	5.52	0.35	-11.09
2n156e	-59.04	-64.95	5.91	14.77	6.8	13.83	0.29	-0.14
2s156e	-58.14	-76.62	18.48	23.36	9	13.31	0.22	-2.08
5n137e	-35.68	-43.09	7.41	15.04	8.09	12.46	0.25	-0.46
5n147e	-47.17	-57.02	9.85	14.74	7.71	13.59	0.59	-0.18
5n156e	-59.86	-57.54	-2.32	17.64	9.27	21.58	0.61	0.33
5s156e	-63.32	-74.77	11.45	18.42	14.17	21.08	0.73	0.24
8n137e	-36.07	-39.23	3.16	9.18	7.11	10.13	0.55	0.18
8n156e	-45.96	-51.4	5.44	13.32	5.9	14.7	0.59	0.18

Table 6. ILD statistics for MODAS vs. TAO moorings

buoy	M_Mean	D_Mean	M_diff	RMSD	stdm	stdd	R	SS
0n147e	-54.83	-60.92	6.1	16.26	5.3	15.87	0.31	-0.05
0n156e	-50.34	-67.31	16.98	22.09	4.6	15.68	0.47	-0.98
2n137e	-41.99	-46.82	4.83	18.02	6.6	19.64	0.49	0.16
2n147e	-51.6	-34.48	-17.11	18.04	4.82	5.52	0.4	-9.67
2n156e	-52.98	-64.95	11.98	17.67	2.82	13.83	0.39	-0.63
2s156e	-48.88	-76.62	27.74	31.3	6.88	13.31	0.08	-4.53
5n137e	-35.32	-43.09	7.77	14.17	4.24	12.46	0.31	-0.29
5n147e	-44.79	-57.02	12.23	18.16	4.82	13.59	0.21	-0.79
5n156e	-54.06	-57.54	3.48	19.51	7.84	21.58	0.47	0.18
5s156e	-52.59	-74.77	22.18	27.14	11.18	21.08	0.69	-0.66
8n137e	-32.97	-39.23	6.26	11.5	3.21	10.13	0.31	-0.29
8n156e	-42.21	-51.4	9.19	15.11	4.37	14.7	0.71	-0.06

Table 7. Number of samples per season for select regions

Season	N. South China Sea	S. South China Sea	East China Sea	Sea of Japan	Kuroshio extension	Equatorial current	Halmahera Eddy
Winter	3309	870	8434	14260	20495	11079	2718
Spring	794	0	8790	17358	20883	15055	3224
Summer	980	226	8221	19856	22167	15450	5214
Fall	3740	1182	15468	18323	24712	12055	2681

Table 8: Compare currents (cm/sec)

Drifter vs. model	RMSD speed	ME Speed	ME U	ME V	0 to 5 (%)	5 to 10 (%)	10 to 20 (%)	> 20 (%)
Annual	9.69	0.16	1.00	-0.29	57.5	23.0	14.7	5.4
1st quarter	11.00	-1.00	0.38	0.10	46.7	29.3	17.2	6.7
2nd quarter	10.78	-0.13	-1.43	-0.55	46.8	28.0	17.7	7.4
3rd quarter	13.39	-0.17	0.48	-0.47	47.4	25.7	17.7	9.1
4th quarter	10.83	-0.57	-0.05	-0.44	48.8	26.7	17.7	6.8

RMSD – root mean square difference

ME – mean difference

Table 9. Statistics comparing SSH from Hawaii database and EAS16 model

Stations #	lat/lon	mean diff (M)	RMSD (M)	R	SS	#samples
h007	07N134E	-0.021	0.115	0.970	0.937	6488
h008	09N138E	-0.012	0.095	0.969	0.937	6514
h028	15N145E	-0.030	0.080	0.947	0.880	3430
h029	01N154E	0.007	0.103	0.927	0.852	6600
h047	27N142E	-0.017	0.065	0.979	0.956	6600
h049	24N153E	0.058	0.198	0.531	0.198	6600
h053	13N144E	0.006	0.192	0.758	0.575	1902
h168	12S130E	0.039	0.464	0.965	0.916	6600
h347	44N144E	0.002	0.073	0.971	0.942	6600
h348	34N132E	-0.063	0.088	0.947	0.785	6600
h349	36N137E	-0.048	0.071	0.941	0.793	6600
h350	42N144E	0.004	0.077	0.976	0.952	6600
h351	39N141E	-0.019	0.063	0.985	0.968	6600
h352	34N139E	-0.037	0.099	0.973	0.933	6600
h353	33N135E	-0.062	0.098	0.986	0.950	6600
h354	31N131E	-0.045	0.086	0.989	0.968	6600
h355	26N127E	-0.052	0.105	0.984	0.957	6542
h360	45N141E	-0.031	0.067	0.907	0.771	6600
h362	32N129E	-0.065	0.143	0.991	0.958	6540
h364	41N140E	-0.014	0.063	0.968	0.931	6600
h366	10S141E	0.109	0.299	0.970	0.871	6475
h400	02S147E	0.006	0.063	0.970	0.935	6562
h699	01N103E	0.021	0.224	0.955	0.904	6115

```
Table 10. Number of stations with percent error within %error range.
Percent error is between IHO stations and EAS16 model.


                    Tidal Amplitude
                   # of stations                        amp diff< 10 cm
  % error   M2    S2    N2    K2    K1    O1    P1    Q1 |    M2
   0-10    227   226    96   122   319   267   152    67 |   218
  10-20    152   176    66    92   170   197   101    35 |   100
  20-30    103    88    48    63    87   104    73    31 |    37
  30-40     62    63    29    30    45    59    40    17 |    24
  40-50     33    44    24    34    26    25    25     7 |     7
  50-100    70    78    46    57    30    25    32    14 |    14
 >100       41    13    29    24    13    11     8     2
 <20       379   402   162   214   489   464   253   102



                    Tidal Phase
                   # of stations
  % error   M2    S2    N2    K2    K1    O1    P1    Q1
   0-10    426   416   166   252   460   423   274    90
  10-20     88   100    59    65   100   126    73    25
  20-30     42    48    33    23    45    48    30    14
  30-40     39    42    18    26    21    28    19    11
  40-50     23    25    19     9    11    15     7     8
  50-100    44    32    31    27    35    13    17    15
 >100       26    25    12    20    18    35    11    10
 <20       514   516   225   317   560   549   347   115

 total #   688   688   338   422   690   688   431   173
```

Table 11. M2 amplitude and phase at TOPEX/Poseidon crossover points (T/P) and
EAS16 model. T/P values are from Robertson and Ffield (2005).

			M2					
			Amplitude (cm)			Phase (deg)		
Site #	LAT	LON	T/P	EAS	DIFF	T/P	EAS	DIFF
1	5.93	121.88	59.6	59.37	-0.23	290	292.36	2.36
2	2.15	120.47	58.9	58.95	0.05	290	294.88	4.88
3	2.03	123.28	57.2	57.03	-0.17	291	294.94	3.94
4	2.02	128.97	49.3	50.87	1.57	288	282.35	-5.65
5	-2.05	127.55	25.6	25.09	-0.51	160	163.31	3.31
6	-2.15	119.05	46.4	49.49	3.09	277	285.99	8.99
7	-5.9	131.82	58.5	51.12	-7.38	139	142.85	3.85
8	-5.97	114.8	13.4	19.8	6.4	140	200.47	60.47
9	-9.75	127.55	62.2	56.52	-5.68	120	117.64	-2.36
10	-9.75	119.05	83.1	88.71	5.61	54	51.01	-2.99
11	-9.77	133.22	43.5	41.52	-1.98	189	193.26	4.26
12	-13.5	126.13	84.7	85.47	0.77	62	61.86	-0.14
13	-13.52	120.47	89.7	94.48	4.78	56	51.63	-4.37
Rms	Difference: all sites			3.9			17.3	
Rms	Difference: excluding 8			3.6			4.4	

Table 12.

Super Typhoon NIDA Date: 13-21 MAY 2004

ADV	LAT	LON	TIME	WIND (knots)	PR STAT
1	7.30	131.10	05/13/12Z	25	- TROPICAL DEPRESSION
2	8.30	132.10	05/13/18Z	25	- TROPICAL DEPRESSION
4	8.50	131.30	05/14/06Z	60	- TROPICAL STORM
5	8.90	131.00	05/14/12Z	65	- TYPHOON-1
6	9.30	130.40	05/14/18Z	70	- TYPHOON-1
5A	8.90	131.00	05/14/12Z	65	- TYPHOON-1
7	9.60	129.90	05/15/00Z	80	- TYPHOON-1
8	9.60	129.20	05/15/06Z	90	- TYPHOON-2
9	10.10	128.40	05/15/12Z	90	- TYPHOON-2
10	10.60	127.80	05/15/18Z	100	- TYPHOON-3
11	11.30	127.30	05/16/00Z	115	- TYPHOON-4
12	11.80	126.40	05/16/06Z	130	- TYPHOON-4
13	12.50	125.70	05/16/12Z	140	- TYPHOON-5
14	13.40	124.70	05/16/18Z	140	- TYPHOON-5
15	14.00	124.50	05/17/00Z	130	- TYPHOON-4
16	14.70	123.80	05/17/06Z	135	- TYPHOON-4
17	15.20	123.70	05/17/12Z	135	- TYPHOON-4
18	16.10	123.60	05/17/18Z	130	- TYPHOON-4
19	17.00	123.50	05/18/00Z	130	- TYPHOON-4
20	17.60	123.60	05/18/06Z	130	- TYPHOON-4
21	18.50	123.80	05/18/12Z	125	- TYPHOON-4
22	19.30	124.60	05/18/18Z	115	- TYPHOON-4
23	20.20	125.20	05/19/00Z	105	- TYPHOON-3
24	21.20	126.40	05/19/06Z	100	- TYPHOON-3
25	22.60	128.00	05/19/12Z	90	- TYPHOON-2
26	23.60	129.90	05/19/18Z	85	- TYPHOON-2
27	25.10	131.60	05/20/00Z	80	- TYPHOON-1
28	26.70	134.40	05/20/06Z	80	- TYPHOON-1
29	28.90	136.40	05/20/12Z	80	- TYPHOON-1
30	30.40	140.40	05/20/18Z	60	- TROPICAL STORM
31	34.20	143.40	05/21/00Z	55	- TROPICAL STORM
32	37.80	146.50	05/21/06Z	45	- TROPICAL STORM

APPENDIX

Statistics for the rest of the moorings - model vs. TAO mooring.

```
Location: 0n156e
No. samples: 360
depth  M_Mean  D_Mean M_diff   RMSD   stdm   stdd    R      SS
 -1.50  29.78   29.95  -0.17   0.31   0.33   0.36   0.72    0.26
-25.00  29.63   29.83  -0.20   0.31   0.30   0.31   0.70    0.00
-50.00  29.26   29.80  -0.54   0.62   0.35   0.33   0.56   -2.57
-75.00  28.43   28.90  -0.47   0.87   0.51   1.05   0.78    0.32
-100.00 26.88   26.84   0.04   1.11   0.63   1.61   0.88    0.53
-125.00 25.01   24.12   0.89   1.38   0.71   1.57   0.84    0.23
-150.00 22.69   21.58   1.10   1.46   0.66   1.44   0.84   -0.03
-200.00 17.34   16.88   0.46   0.96   0.47   1.01   0.55    0.09
-250.00 13.30   13.52  -0.22   0.54   0.34   0.53   0.42   -0.04
-300.00 11.35   12.09  -0.75   0.81   0.23   0.24   0.11  -10.12
-500.00  8.16    8.36  -0.20   0.31   0.07   0.23   0.08   -0.81
-750.00  5.79    5.87  -0.08   0.13   0.08   0.13   0.61    0.03

Location: 2n137e
No. samples: 360
depth  M_Mean  D_Mean M_diff   RMSD   stdm   stdd    R      SS
 -1.50  29.32   29.50  -0.18   0.34   0.36   0.46   0.77    0.44
-25.00  29.02   29.11  -0.09   0.55   0.38   0.72   0.67    0.41
-50.00  28.54   28.30   0.25   1.32   0.61   1.65   0.70    0.36
-75.00  27.57   27.38   0.20   1.42   0.83   1.98   0.79    0.48
-100.00 25.76   25.18   0.58   1.50   0.82   1.70   0.60    0.22
-125.00 23.84   23.07   0.77   0.99   0.84   0.90   0.74   -0.22
-150.00 21.85   21.56   0.29   0.76   0.65   0.97   0.69    0.39
-200.00 17.51   17.90  -0.39   1.22   0.43   1.12   0.09   -0.20
-250.00 13.69   14.88  -1.19   1.85   0.27   1.42   0.10   -0.70
-300.00 11.20   11.92  -0.71   1.34   0.17   1.12  -0.01   -0.43
-500.00  7.74    8.06  -0.31   0.45   0.13   0.42   0.83   -0.12
-750.00  5.76    5.82  -0.06   0.36   0.08   0.39   0.52    0.14

Location: 2n147e
No. samples: 262
depth  M_Mean  D_Mean M_diff   RMSD   stdm   stdd    R      SS
 -1.50  29.45   29.63  -0.18   0.30   0.27   0.39   0.78    0.40
-25.00  29.37   29.49  -0.12   0.24   0.26   0.37   0.83    0.58
-75.00  28.05   26.97   1.08   1.35   0.40   1.01   0.66   -0.77
-100.00 26.51   25.80   0.71   1.18   0.48   1.19   0.66    0.02
-125.00 24.66   24.00   0.66   1.03   0.55   0.97   0.58   -0.13
-150.00 22.33   22.13   0.19   0.86   0.59   0.90   0.42    0.08
-200.00 17.10   16.78   0.31   1.29   0.57   1.36   0.40    0.11
-250.00 12.86   11.86   1.00   1.19   0.38   0.89   0.76   -0.80
-750.00  5.71    6.03  -0.32   0.35   0.09   0.18   0.70   -2.87
```

```
Location: 2n156e
No. samples 360
depth   M_Mean  D_Mean M_diff  RMSD    stdm    stdd     R       SS
 -1.50   29.66   29.77  -0.11   0.27    0.32    0.34    0.72    0.35
-25.00   29.60   29.66  -0.06   0.20    0.31    0.26    0.79    0.41
-50.00   29.41   29.63  -0.22   0.32    0.34    0.38    0.80    0.29
-75.00   28.59   28.77  -0.19   0.70    0.45    0.82    0.57    0.27
-100.00  27.07   26.54   0.53   1.07    0.58    1.24    0.70    0.25
-125.00  25.08   24.76   0.32   0.93    0.70    1.29    0.77    0.48
-150.00  22.54   22.63  -0.09   1.12    0.74    1.44    0.65    0.40
-200.00  16.65   14.92   1.73   2.16    0.60    1.47    0.47   -1.17
-250.00  12.67   11.72   0.94   1.12    0.43    0.35   -0.19   -9.03
-300.00  10.95   11.05  -0.11   0.48    0.34    0.32   -0.01   -1.28
-500.00   8.11    8.49  -0.38   0.42    0.15    0.17    0.43   -4.98
-750.00   5.84    5.84   0.00   0.17    0.10    0.16    0.22   -0.10


Location: 2s156e
No. samples: 360
depth   M_Mean  D_Mean M_diff  RMSD    stdm    stdd     R       SS
 -1.50  29.80   30.02  -0.21   0.31    0.39    0.41    0.84    0.43
-25.00  29.72   29.94  -0.22   0.28    0.34    0.37    0.88    0.43
-50.00  29.52   29.97  -0.45   0.51    0.27    0.42    0.84   -0.48
-75.00  28.73   29.53  -0.80   0.92    0.32    0.61    0.70   -1.24
-100.00 27.37   28.29  -0.93   1.31    0.45    1.18    0.69   -0.24
-125.00 25.63   26.28  -0.65   1.33    0.52    1.47    0.71    0.18
-150.00 23.36   23.65  -0.29   1.16    0.55    1.48    0.76    0.39
-250.00 13.62   13.47   0.15   1.73    0.38    1.88    0.49    0.15
-300.00 11.53   11.54  -0.01   0.53    0.27    0.58    0.40    0.16
-500.00  8.17    9.29  -1.12   1.58    0.11    1.12    0.15   -0.98
-750.00  5.73    6.40  -0.67   1.38    0.08    1.20   -0.01   -0.32


Location: 5n137e
No. samples: 359
depth   M_Mean  D_Mean M_diff  RMSD    stdm    stdd     R       SS
 -1.50  28.99   29.10  -0.11   0.36    0.49    0.68    0.88    0.73
-25.00  28.84   28.98  -0.13   0.39    0.43    0.61    0.80    0.58
-50.00  27.38   28.04  -0.66   1.29    0.86    1.40    0.60    0.14
-75.00  24.90   25.90  -1.01   2.18    1.56    2.41    0.59    0.18
-100.00 22.38   23.18  -0.80   2.56    1.98    2.95    0.58    0.25
-125.00 20.00   20.45  -0.45   2.48    2.14    3.32    0.68    0.44
-150.00 17.75   17.83  -0.08   2.26    2.07    3.47    0.78    0.58
-200.00 14.00   13.08   0.93   1.57    1.54    2.33    0.86    0.54
-250.00 11.24   10.41   0.83   0.99    0.92    1.06    0.86    0.14
-300.00  9.70    9.37   0.32   0.55    0.49    0.77    0.84    0.49
-500.00  7.43    7.36   0.07   0.17    0.14    0.24    0.82    0.55
-750.00  5.76    5.85  -0.09   0.14    0.06    0.13    0.58   -0.19
```

```
Location: 5n147e
No. samples: 329
 depth  M_Mean  D_Mean M_diff  RMSD   stdm   stdd    R      SS
  -1.50  29.33   29.44  -0.11   0.28   0.35   0.41   0.78    0.53
 -25.00  29.22   29.29  -0.07   0.26   0.31   0.35   0.71    0.43
 -50.00  28.74   29.07  -0.33   0.47   0.23   0.35   0.38   -0.79
 -75.00  27.28   28.03  -0.76   1.18   0.50   0.80   0.09   -1.17
-100.00  25.11   25.91  -0.79   1.42   0.89   1.33   0.50   -0.14
-125.00  22.47   23.01  -0.54   1.41   1.33   2.16   0.83    0.58
-150.00  19.45   19.67  -0.22   1.45   1.68   2.67   0.88    0.71
-200.00  14.39   13.46   0.93   1.56   1.32   2.11   0.83    0.45
-250.00  11.06   10.44   0.62   0.77   0.64   0.72   0.77   -0.15
-300.00   9.64    9.39   0.25   0.33   0.31   0.30   0.76   -0.17
-500.00   7.59    7.52   0.07   0.18   0.12   0.14   0.28   -0.54
-750.00   5.73    5.84  -0.10   0.18   0.09   0.12   0.08   -1.16

Location: 5n156
No. samples: 360
 depth  M_Mean  D_Mean M_diff  RMSD   stdm   stdd    R      SS
  -1.50  29.39   29.54  -0.15   0.29   0.36   0.49   0.87    0.65
 -25.00  29.32   29.29   0.04   0.20   0.34   0.32   0.83    0.61
 -50.00  29.12   29.03   0.09   0.37   0.27   0.43   0.54    0.24
 -75.00  28.27   28.23   0.04   0.83   0.36   0.84   0.25    0.03
-100.00  26.65   26.70  -0.05   1.07   0.69   1.10   0.35    0.04
-125.00  24.39   24.02   0.37   1.15   1.07   1.32   0.61    0.25
-150.00  21.57   20.56   1.02   1.68   1.38   1.81   0.68    0.14
-200.00  15.78   13.97   1.81   2.17   1.12   1.32   0.52   -1.72
-250.00  11.90   10.62   1.28   1.40   0.61   0.44   0.48   -9.05
-300.00  10.22    9.46   0.77   0.86   0.35   0.18   0.10  -20.45
-500.00   7.93    7.62   0.31   0.35   0.15   0.11   0.22   -8.80
-750.00   5.84    5.86  -0.02   0.13   0.10   0.17   0.63    0.39

Location: 8n156e
No. samples: 360
 depth  M_Mean  D_Mean M_diff  RMSD   stdm   stdd    R      SS
  -1.50  29.55   29.62  -0.08   0.21   0.32   0.40   0.88    0.73
 -25.00  29.04   29.10  -0.06   0.16   0.59   0.55   0.97    0.91
 -50.00  28.68   28.82  -0.14   0.35   0.37   0.43   0.69    0.35
 -75.00  27.04   27.51  -0.46   1.08   0.64   1.21   0.60    0.21
-100.00  24.21   24.47  -0.26   1.56   1.25   2.37   0.81    0.57
-125.00  20.66   20.19   0.47   1.44   1.58   2.20   0.79    0.57
-150.00  17.13   16.34   0.79   1.39   1.53   1.65   0.74    0.29
-200.00  12.68   11.96   0.72   0.93   0.87   0.70   0.74   -0.76
-250.00  10.35   10.32   0.03   0.27   0.40   0.25   0.75   -0.13
-300.00   9.38    9.61  -0.23   0.26   0.18   0.14   0.71   -2.50
-500.00   7.61    7.96  -0.34   0.36   0.07   0.17   0.78   -3.66
-750.00   5.71    5.93  -0.22   0.24   0.06   0.15   0.74   -1.64
```

41

```
Statistics for rest of moorings - MODAS vs. TAO mooring.

  Location: 0n156e
  No. samples: 360
  depth  M_Mean  D_Mean M_diff  RMSD   stdm   stdd    R      SS
   -1.50  29.97  29.95   0.02   0.27   0.29   0.36   0.70    0.47
  -25.00  29.73  29.83  -0.10   0.23   0.25   0.31   0.74    0.44
  -50.00  29.41  29.80  -0.39   0.46   0.25   0.33   0.69   -0.91
  -75.00  28.53  28.90  -0.37   0.90   0.35   1.05   0.75    0.26
 -100.00  27.01  26.84   0.17   1.18   0.59   1.61   0.83    0.46
 -125.00  25.12  24.12   1.00   1.47   0.79   1.57   0.78    0.12
 -150.00  22.76  21.58   1.18   1.57   0.87   1.44   0.71   -0.18
 -200.00  17.10  16.88   0.22   0.92   0.60   1.01   0.47    0.16
 -250.00  13.08  13.52  -0.44   0.68   0.32   0.53   0.35   -0.63
 -300.00  11.24  12.09  -0.85   0.90   0.20   0.24   0.11  -12.76
 -500.00   8.11   8.36  -0.25   0.35   0.07   0.23  -0.09   -1.37
 -750.00   5.74   5.87  -0.13   0.17   0.07   0.13   0.62   -0.65

  Location: 2n137e
  No. samples: 360
  depth  M_Mean  D_Mean M_diff  RMSD   stdm   stdd    R      SS
   -1.50  29.62  29.50   0.12   0.37   0.52   0.46   0.76    0.36
  -25.00  29.32  29.11   0.20   0.48   0.47   0.72   0.81    0.56
  -50.00  28.82  28.30   0.52   1.30   0.60   1.65   0.84    0.37
  -75.00  27.76  27.38   0.39   1.39   0.80   1.98   0.87    0.51
 -100.00  26.22  25.18   1.04   1.55   0.89   1.70   0.78    0.17
 -125.00  24.33  23.07   1.27   1.46   0.90   0.90   0.68   -1.63
 -150.00  22.27  21.56   0.71   1.08   0.85   0.97   0.60   -0.25
 -200.00  17.68  17.90  -0.22   1.20   0.63   1.12   0.18   -0.16
 -250.00  13.74  14.88  -1.14   1.86   0.43   1.42   0.04   -0.71
 -300.00  11.23  11.92  -0.69   1.30   0.27   1.12   0.19   -0.34
 -500.00   7.77   8.06  -0.29   0.46   0.12   0.42   0.67   -0.18
 -750.00   5.79   5.82  -0.04   0.38   0.07   0.39   0.26    0.05

  Location: 2n147e
  No. samples: 262
  depth  M_Mean  D_Mean M_diff  RMSD   stdm   stdd    R      SS
   -1.50  29.64  29.63   0.02   0.28   0.33   0.39   0.72    0.50
  -25.00  29.46  29.49  -0.03   0.21   0.30   0.37   0.82    0.67
  -75.00  28.25  26.97   1.27   1.43   0.48   1.01   0.84   -1.00
 -100.00  26.74  25.80   0.93   1.22   0.63   1.19   0.79   -0.05
 -125.00  24.86  24.00   0.86   1.19   0.76   0.97   0.57   -0.50
 -150.00  22.50  22.13   0.36   1.02   0.85   0.90   0.41   -0.28
 -200.00  17.21  16.78   0.42   1.31   0.75   1.36   0.44    0.08
 -250.00  12.93  11.86   1.07   1.29   0.47   0.89   0.58   -1.13
 -750.00   5.76   6.03  -0.27   0.30   0.08   0.18   0.72   -1.85
```

```
Location: 2n156e
No. samples: 360
 depth  M_Mean  D_Mean M_diff   RMSD    stdm    stdd     R       SS
 -1.50   29.81   29.77   0.03    0.27    0.32    0.34    0.68     0.38
-25.00   29.61   29.66  -0.04    0.21    0.28    0.26    0.72     0.35
-50.00   29.33   29.63  -0.30    0.43    0.29    0.38    0.62    -0.27
-75.00   28.46   28.77  -0.31    0.75    0.40    0.82    0.55     0.15
-100.00  26.91   26.54   0.37    1.00    0.58    1.24    0.70     0.35
-125.00  24.93   24.76   0.16    0.88    0.74    1.29    0.76     0.53
-150.00  22.41   22.63  -0.22    1.19    0.79    1.44    0.58     0.31
-200.00  16.56   14.92   1.64    2.10    0.64    1.47    0.45    -1.05
-250.00  12.61   11.72   0.89    1.09    0.44    0.35   -0.27    -8.53
-300.00  10.90   11.05  -0.15    0.51    0.34    0.32   -0.07    -1.56
-500.00   8.05    8.49  -0.44    0.48    0.12    0.17    0.31    -6.69
-750.00   5.76    5.84  -0.08    0.19    0.08    0.16    0.15    -0.35

Location: 2s156e
No. samples: 360
 depth  M_Mean  D_Mean M_diff   RMSD    stdm    stdd     R       SS
 -1.50   29.98   30.02  -0.04    0.32    0.42    0.41    0.70     0.38
-25.00   29.72   29.94  -0.22    0.36    0.33    0.37    0.69     0.09
-50.00   29.38   29.97  -0.59    0.66    0.28    0.42    0.70    -1.44
-75.00   28.54   29.53  -0.99    1.09    0.29    0.61    0.72    -2.14
-100.00  27.13   28.29  -1.16    1.51    0.44    1.18    0.62    -0.65
-125.00  25.37   26.28  -0.91    1.50    0.59    1.47    0.62    -0.05
-150.00  23.09   23.65  -0.56    1.30    0.66    1.48    0.65     0.23
-250.00  13.51   13.47   0.04    1.75    0.38    1.88    0.43     0.13
-300.00  11.45   11.54  -0.09    0.55    0.23    0.58    0.33     0.08
-500.00   8.07    9.29  -1.22    1.66    0.07    1.12   -0.08    -1.20
-750.00   5.68    6.40  -0.72    1.41    0.06    1.20   -0.07    -0.37

Location: 5n137e
No. samples: 359
 depth  M_Mean  D_Mean M_diff   RMSD    stdm    stdd     R       SS
 -1.50   29.24   29.10   0.14    0.41    0.58    0.68    0.82     0.64
-25.00   29.01   28.98   0.03    0.30    0.49    0.61    0.88     0.76
-50.00   28.15   28.04   0.11    1.04    0.60    1.40    0.74     0.45
-75.00   25.92   25.90   0.02    1.81    1.00    2.41    0.73     0.44
-100.00  23.28   23.18   0.10    2.21    1.48    2.95    0.69     0.44
-125.00  20.55   20.45   0.10    2.37    1.87    3.32    0.72     0.49
-150.00  17.96   17.83   0.13    2.34    1.99    3.47    0.76     0.54
-200.00  13.98   13.08   0.90    1.66    1.53    2.33    0.81     0.49
-250.00  11.18   10.41   0.77    1.00    0.91    1.06    0.80     0.11
-300.00   9.66    9.37   0.29    0.58    0.49    0.77    0.76     0.42
-500.00   7.42    7.36   0.06    0.17    0.14    0.24    0.80     0.52
-750.00   5.76    5.85  -0.09    0.15    0.05    0.13    0.52    -0.24
```

```
Location: 5n147e
No. samples: 329
depth  M_Mean  D_Mean M_diff  RMSD  stdm  stdd   R    SS
 -1.50  29.54   29.44   0.11   0.31  0.38  0.41  0.73   0.42
-25.00  29.33   29.29   0.04   0.27  0.34  0.35  0.70   0.41
-50.00  28.87   29.07  -0.20   0.43  0.32  0.35  0.36  -0.50
-75.00  27.32   28.03  -0.72   1.09  0.55  0.80  0.31  -0.86
-100.00 24.99   25.91  -0.91   1.36  1.05  1.33  0.67  -0.05
-125.00 22.25   23.01  -0.76   1.41  1.59  2.16  0.84   0.57
-150.00 19.22   19.67  -0.45   1.54  1.90  2.67  0.84   0.67
-200.00 14.24   13.46   0.78   1.53  1.38  2.11  0.79   0.47
-250.00 10.97   10.44   0.53   0.71  0.63  0.72  0.76   0.03
-300.00  9.60    9.39   0.21   0.30  0.29  0.30  0.73  -0.01
-500.00  7.59    7.52   0.07   0.17  0.12  0.14  0.27  -0.49
-750.00  5.73    5.84  -0.10   0.17  0.08  0.12  0.05  -1.10


Location: 5n156e
No. samples: 360
depth  M_Mean  D_Mean M_diff  RMSD  stdm  stdd   R    SS
 -1.50  29.50   29.54  -0.05   0.26  0.39  0.49  0.85   0.71
-25.00  29.34   29.29   0.05   0.19  0.32  0.32  0.83   0.63
-50.00  29.05   29.03   0.02   0.35  0.28  0.43  0.58   0.32
-75.00  28.00   28.23  -0.24   0.85  0.44  0.84  0.31  -0.03
-100.00 26.09   26.70  -0.62   1.25  0.87  1.10  0.41  -0.29
-125.00 23.55   24.02  -0.47   1.27  1.33  1.32  0.60   0.08
-150.00 20.55   20.56  -0.01   1.38  1.58  1.81  0.68   0.42
-200.00 14.82   13.97   0.84   1.38  1.10  1.32  0.61  -0.09
-250.00 11.32   10.62   0.69   0.82  0.50  0.44  0.57  -2.47
-300.00  9.93    9.46   0.47   0.56  0.28  0.18  0.18  -8.28
-500.00  7.81    7.62   0.19   0.25  0.13  0.11  0.18  -3.90
-750.00  5.76    5.86  -0.10   0.17  0.10  0.17  0.62   0.03


Location: 8n156e
No. samples: 360
depth  M_Mean  D_Mean M_diff  RMSD  stdm  stdd   R    SS
 -1.50  29.60   29.62  -0.02   0.22  0.31  0.40  0.84   0.70
-25.00  28.99   29.10  -0.10   0.17  0.52  0.55  0.97   0.90
-50.00  28.57   28.82  -0.25   0.37  0.42  0.43  0.80   0.25
-75.00  26.79   27.51  -0.71   1.15  0.76  1.21  0.66   0.09
-100.00 23.77   24.47  -0.70   1.77  1.31  2.37  0.76   0.44
-125.00 20.13   20.19  -0.06   1.55  1.54  2.20  0.71   0.50
-150.00 16.66   16.34   0.32   1.35  1.47  1.65  0.65   0.33
-200.00 12.43   11.96   0.47   0.85  0.86  0.70  0.61  -0.46
-250.00 10.25   10.32  -0.08   0.33  0.40  0.25  0.59  -0.78
-300.00  9.34    9.61  -0.27   0.32  0.19  0.14  0.56  -4.08
-500.00  7.60    7.96  -0.36   0.38  0.07  0.17  0.66  -4.10
-750.00  5.71    5.93  -0.22   0.26  0.06  0.15  0.53  -1.94


M_mean – model mean temperature
D_mean – data mean temperature
M_diff – mean difference model – data
RMSD   - root mean square difference
Stdm   - standard deviation model
Stdd   - standard deviation data
R      - correlation coefficient
SS     - skill score
```

44

REFERENCES

Asselin, R., 1972: Frequency filter for time integrations. *Mon. Wea. Rev.*, **100**, 487-490.

Barron, C.N., Kara, B.A., Rhodes, R.C., Rowley, C. and Smedstad, L.F., 2004: Validation Test Report for the 1/8° Global Navy Coastal Ocean Model Nowcast/Forecast System.

Blumberg, A.F., and H.J. Herring, 1987: Circulation modelling using orthogonal curvilinear coordinates. In: Nihoul, J., and B. Jamart (Eds.), *Three-Dimensional Models of Marine and Estuarine Dynamics*, Elsevier Oceanography Series, **45**, 55-88.

Blumberg, A.F., and G.L. Mellor, 1987: A description of a three-dimensional coastal ocean circulation model. In: Heaps, N. (Ed.) *Three-Dimensional Coastal Ocean Models*, Amer. Geophys. Union, New York, 208 pp.

Boebel, O., and C. Barron, 2003: A comparison of in-situ float velocities with altimeter derived geostrophic velocities. *Deep Sea Res. II*, **50**, 119-139.

Bretherton, F.P., R.E. Davis, and C.B. Fandry, 1976: A technique for objective analysis and design of oceanographic experiments applied to MODE-73. *Deep Sea Res.,* **23**, 559-582.

Chapman, D.C., D-S Ko and R.H. Preller. 2004: A High-Resolution Numerical Modeling Study of the Subtidal Circulation in the Northern South China Sea. *J. Oceanic Eng.*, **29**, 1087-1103.

Craig, P.D., and M.L. Banner, 1994: Modeling wave-induced turbulence in the ocean surface layer. *J. Phys. Oceanogr.,* **24**, 2546-2559.

Egbert, G.D., A F. Bennett, and M.G.G. Foreman, 1994: TOPEX/Poseidon tides estimated using a global inverse model. *J. Geophys. Res.,* **99**, 24821–24852.

Egbert, G. and L. Erofeeva, 2002: Efficient inverse modeling of barotropic ocean tides. *J. Atmos. Oceanic Technol.*, **19**, 183-204.

Fox, D.N., W.J. Teague, C.N. Barron, M.R. Carnes, and C.M. Lee, 2002a: The Modular Ocean Data Assimilation System (MODAS). *J. Atmos. Oceanic Technol.,* **19**, 240-252.

Fox, D.N., C.N. Barron, M.R. Carnes, M. Booda, G. Peggion, and J.V. Gurley, 2002b: The Modular Ocean Data Assimilation System. *Oceanography,* **15**, 22-28.

Friedrich, H., and S. Levitus, 1972: An approximation to the equation of state for sea water, suitable for numerical ocean models. *J. Phys. Oceanogr.,* **2**, 514-517.

Holland, W.R., J.C. Chow, and F.O. Bryan, 1998: Application of a third-order upwind scheme in the NCAR ocean model. *J. Climate,* **11**, 1487-1493.

Jacobs, G.A., C.N. Barron, D.N. Fox, K.R. Whitmer, S. Klingenberger, D. May, and J.P. Blaha, 2002: Operational altimeter sea level products. *Oceanography,* **15**, 13-21.

Jacobs, G.A, D.S. Ko, H. Ngodock, R.H. Preller and S.K. Riedlinger, 2005: Synoptic Forcing of Korea Strait Transport, *Deep Sea Res. Part II*, **52,** 1490-1504 .

Kara, A. B., Rochford, P.A., and Hurlburt, H.E., 2000: An optimal definition for ocean mixed layer depth, *J. Geophys. Res.,* **105** 16803-16821.

Kara, A. B., C. N. Barron, P. J. Martin, L. F. Smedstad, and R. C. Rhodes, 2006: Validation of Interannual Simulations from the 1/8° Global Navy Coastal Ocean Model (NCOM), *Ocean Modelling*, **11,** 376-398.

Ko, D-S, R.H. Preller, G.A. Jacob s, T.Y. Tang and S.F.Lin, 2003: Transport Reversals at Taiwan Strait during October and November, 1999, *J. Geophys. Res.* **108**, 3370.

Large, W.G. McWillaims, J.C., and Doney, S.C. 1994: Oceanic vertical mixing: a review and a model with a nonlocal boundary layer parameterization. *Review of Geophysics*, **32** (4), 363-403.

LeFevre, F., F.G. Lyard, and C. Le Provost, 2002: A Global Tide Finite Element Solution Assimilating Tide Gauge and Altimeter Information. *J. Atmos. Oceanic Technol*., **19,** 1345-1356.

Martin, P.J., 2000: Description of the Navy Coastal Ocean Model Version 1.0. NRL Report No. NRL/FR/7322/00/9962, 45pp. [Available from NRL, Code7322, Bldg. 1009, Stennis Space Center, MS 39529-5004, USA.]

Martin, P.J., G. Peggion, and K.J. Yip, 1998: A comparison of several coastal ocean models. NRL Report No. NRL/FR/7322/97/9692, 96pp. [Available from NRL, Code7322, Bldg. 1009, Stennis Space Center, MS 39529-5004, USA.]

May, D.A., M.M. Parmeter, D.S. Olszewski, and B.D. McKenzie, 1998: Operational processing of satellite sea surface temperature retrievals at the Naval Oceanographic Office. *Bull. Amer. Met. Soc.,* **79**, 397-407.

McPhaden, M.J., A.J. Busalacchi, R., Cheney, J.R. Donguy, K.S. Gage, D. Halpern, M. Ji, P. Julian, G. Meyers, G.T. Mitchum, P.P. Niiler, J. Picaut, R.W. Reynolds, N. Smith, and K. Takeuchi, 1998: The Tropical Ocean-Global Atmosphere (TOGA) observing system: A decade of progress. *J. Geophys. Res.,* **103**, 14169-14240.

Mellor, G.L., 1991: An equation of state for numerical models of oceans and estuaries. *J. Atmos. Oceanic Technol.,* **8**, 609-611.

Mellor, G.L., and T. Yamada, 1982: Development of a turbulence closure model for geophysical fluid problems. *Rev. Geophys. Space Phys.,* **20**, 851-875.

Mellor, G.L., and T. Yamada, 1974: A hierarchy of turbulence closure models for planetary boundary layers. *J. Atmos. Sci.,* **31**, 1791-1806.

Millero, F.J., and A. Poisson, 1981: International one-atmosphere equation of state of seawater. *Deep Sea Res. I,* **28**, 625-629.

Millero, F.J., C.-T. Chen, A. Bradshaw, and K. Schleicher, 1980: A new high pressure equation of state for seawater. *Deep Sea Res. I,* **27**, 255-264.

Murphy, A.H., and E.S. Epstein, 1989: Skill scores and correlation coefficients in model verification. *Mon. Wea. Rev.* **117**, 572-581.

Naganuma, K., 1977: The oceanographic fluctuations in the Japan Sea, *Kaiyo Kauaku*, **9**, 137-141.

Pazan, S.E. and P. Niiler, 2004: New Global Drifter Data Set Available. *EOS, Transactions, American Geophysical Union*. **85**, 2, 17.

Perry, G.D., P.B. Duffy, and N.L. Miller, 1996: An extended data set of river discharges for validation of general circulation models. *J. Geophys. Res*., **101**, 21339-21349.

Rhodes, R.C., H.E. Hurlburt, A.J. Wallcraft, C.N. Barron, P.J. Martin, E.J. Metzger, J.F. Shriver, D.S. Ko, O.M. Smedstad, S.L. Cross, and A.B. Kara, 2002: Navy real-time global modeling systems. *Oceanography,* **15**, 29-43.

Robertson, R. and A. Ffield, 2005: M2 Baroclinic Tides in the Indonesian Seas. *Oceanography*, **18**, 62-73.

Rosmond, T.E., J. Teixeira, M. Peng, T.F. Hogan, and R. Pauley, 2002: Navy Operational Global Atmospheric Prediction System (NOGAPS): Forcing for ocean models. *Oceanography,* **15**, 99-108.

Senjyu, T., 1999: The Japan Sea Intermediate Water; its characteristics and circulation, *J. Oceanogr.*, **55**, 111-122.

Simpson, J.J. and T.D. Dickey, 1981: Alternative Parameterizations of downward irradiance and their dynamical significance, *J. Phys. Oceanogr*., **11**, 876-882.

Shriver, J.F. and H.E. Hurlburt, 2000: The effect of upper ocean eddies on the non-steric contribution to the barotropic mode. *Geophys. Res. Lett.*, **27**, 2713-2716.

Smagorinsky, J., 1963: General circulation experiments with the primitive equations. I: The basic experiment. *Mon. Wea. Rev.,* **91**, 99-164.

Smedstad, O.M., H.E. Hurlburt, E.J. Metzger, R.C. Rhodes, J.F. Shriver, A.J. Wallcraft, and A.B. Kara, 2003: An operational eddy-resolving 1/16° global ocean nowcast forecast system. *J. Mar. Res.,* 40-41, 341-361.

Tropical Atmosphere-Ocean (TAO) array**, http://www.pmel.noaa.gov/tao.**

Teague W.J., G.A. Jacobs, D.S. Ko, T.Y. Tang, K.I. Chang, and M. Suk, 2003: Connectivity of the Taiwan, Cheju, and Korea Straits, *Continental Shelf Research*, **23**, 63-67.

University Of Hawaii Sea Level Center. http://ilikai.soeast.hawaii.edu/uhslc/data.html.

Wyrtki, K. 1961: Scientific Results of Marine Investigations of the South China Sea and the Gulf of Tailand 1959-1961, NAGA REPORT, V2,195p.

Yang, Y., J. Su, 1984: *Numerical modeling of the circulation in the East China Sea, in Ocean Hydrodynamics of the Japan and East China Sea, Elsevier Oceanogr. Ser.*, vol. 39, edited by T. Ichiye, pp. 167-186, Elsevier, New York.

Zalesak, S.T., 1979: Fully multidimensional flux-corrected transport algorithms for fluid. *J. Comp. Phys.,* ***31,33.***
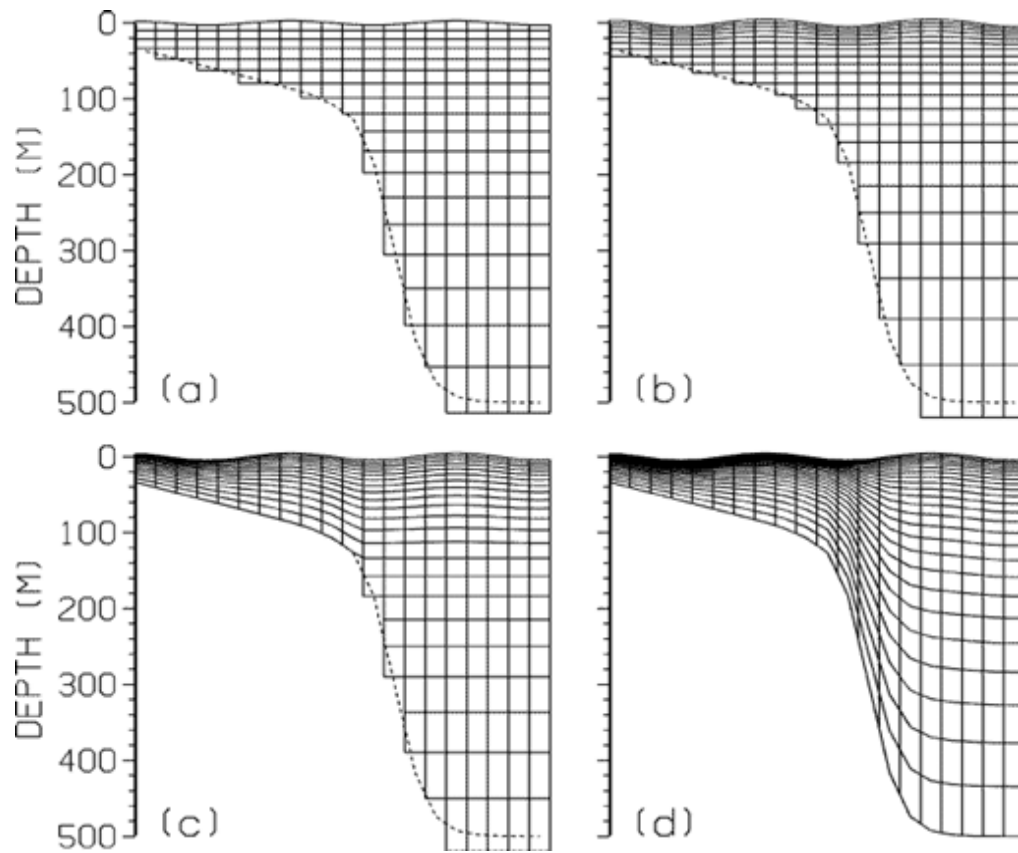
Figure 1. Examples of vertical coordinates available in NCOM: a) fixed z coordinates with free surface at level one, b) hybrid σ-z with σ confined to a few of the upper levels, c) hybrid σ-z with σ down to the shelf break and fixed z from shelf break to bottom, d) full σ. The EAS16 model uses case c with σ-z transition at 137 m depth.
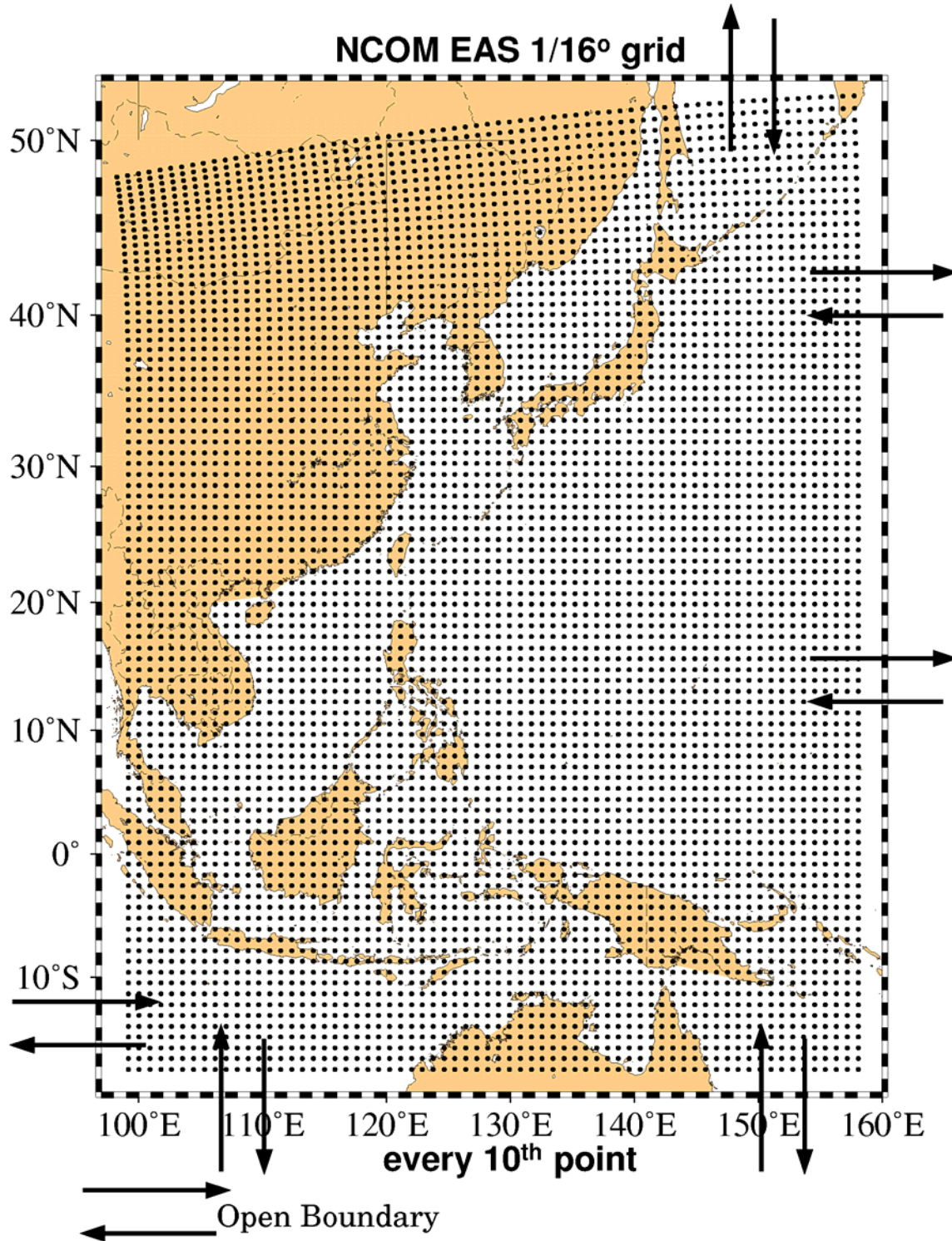
Figure 2. Horizontal grid used in the East Asian Sea model. Grid spacing is 1/16° which translates to 9 km over much of the area decreasing to 6 km toward the northern boundary. Arrows denote the open boundaries. Every 10th grid point is shown.
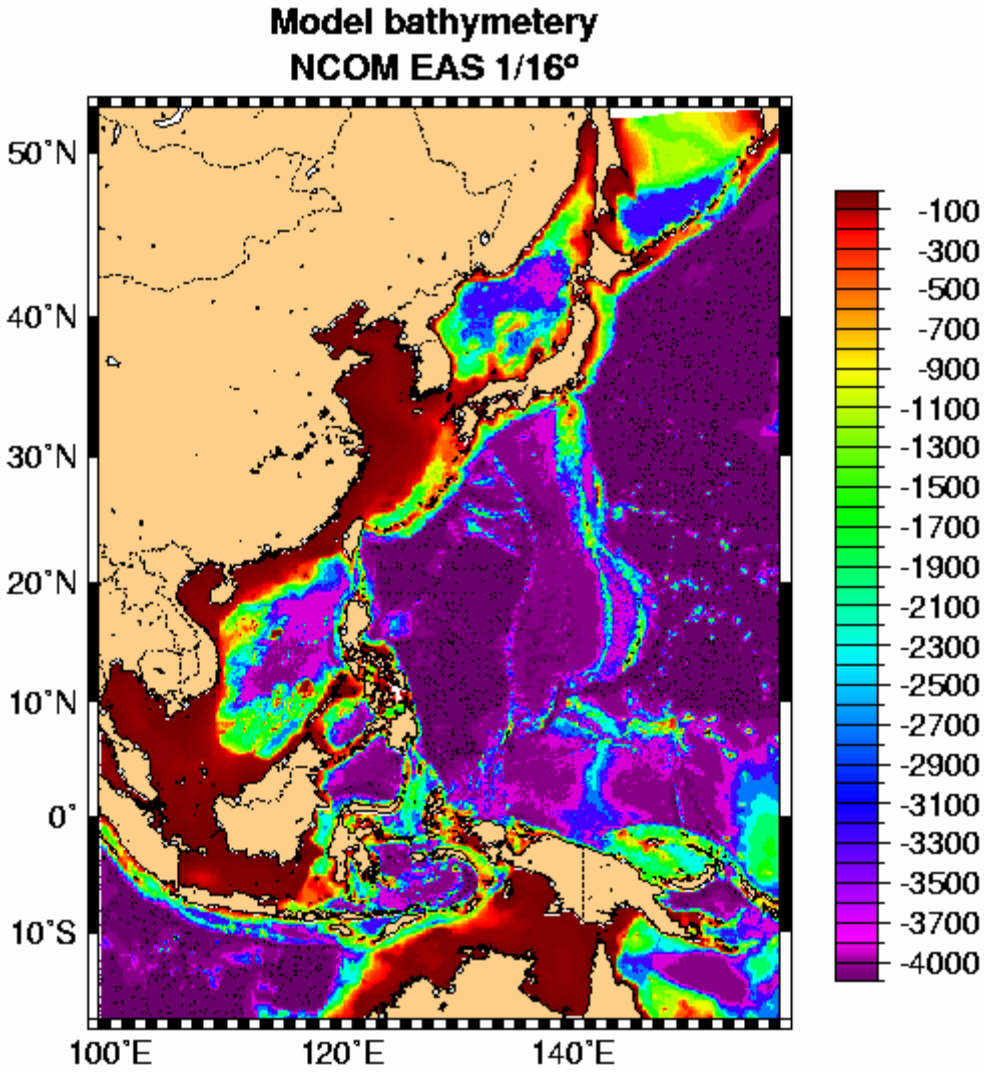
Figure 3. Bathymetry (meters) used in the EAS16 model. Depth values are from the NRL 2-minute gridded bottom topography (DBDB2)
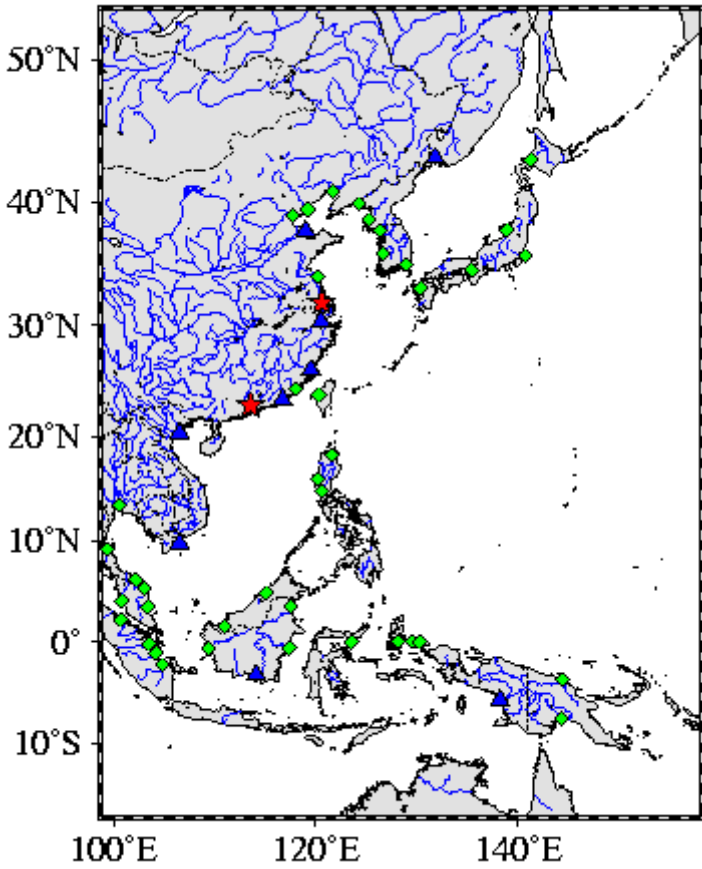
Figure 4. Location of rivers included in the EAS16 model. Red stars denote the rivers with the largest flow rates (>1X10^4 m^3/sec). Blue triangles denote rivers with flow rates of 1 to 2X10^3 m^3/sec. Smaller rivers denoted by green diamonds.
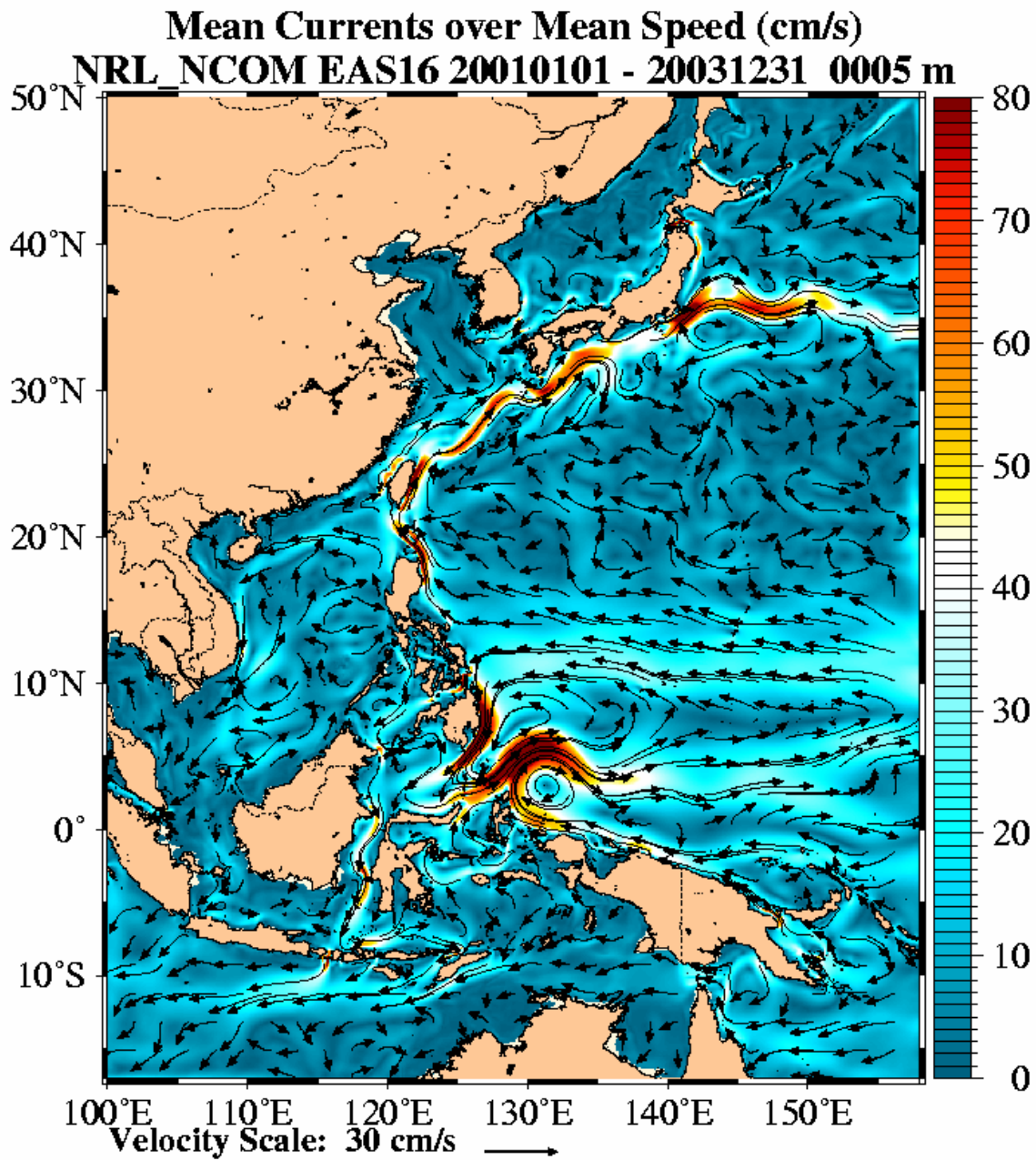
Figure 5. Mean 5 meter currents from the EAS16 model for 2001-2003. Color scale is speed in cm/sec
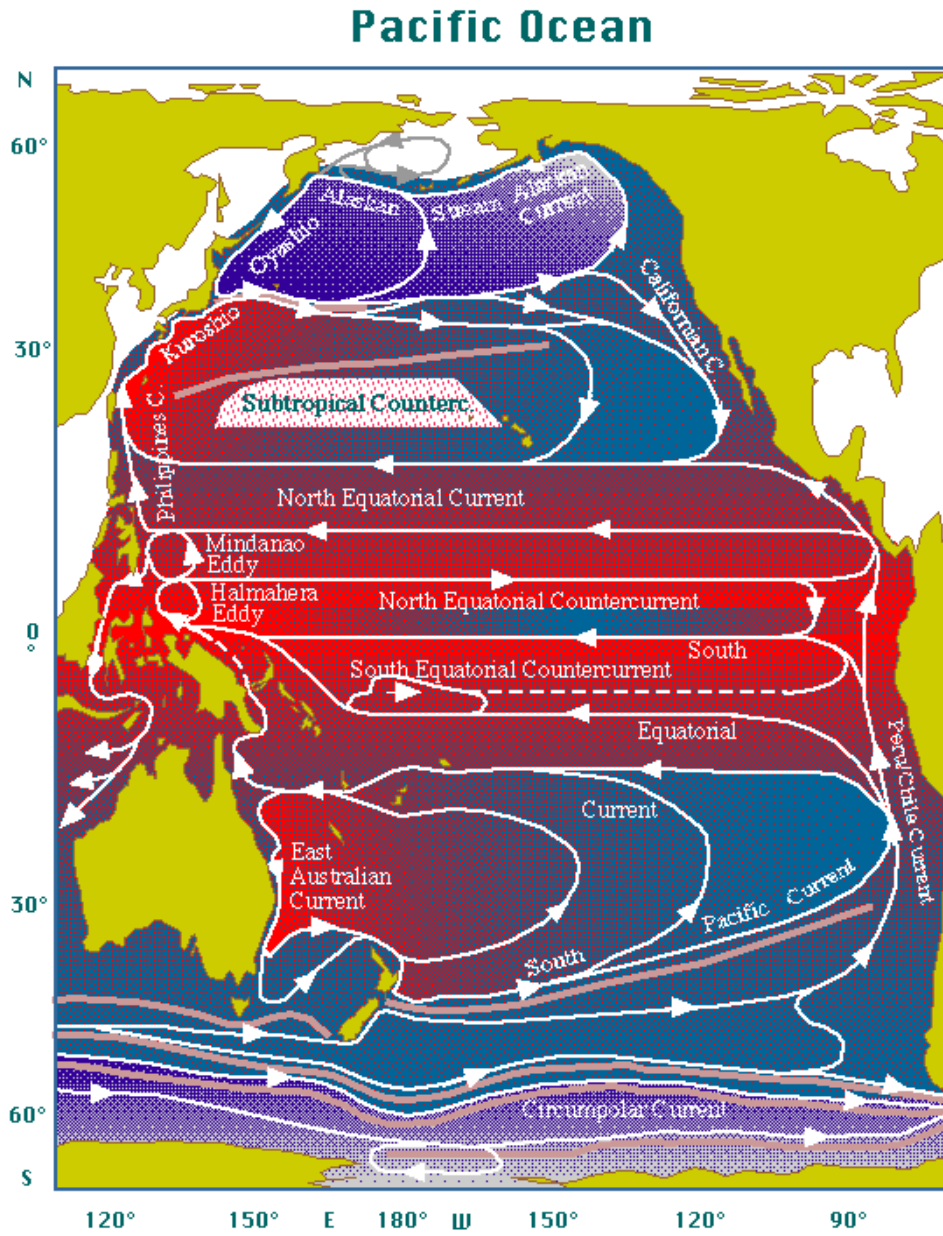
Figure 6. A schematic of the general circulation in the Pacific.

.
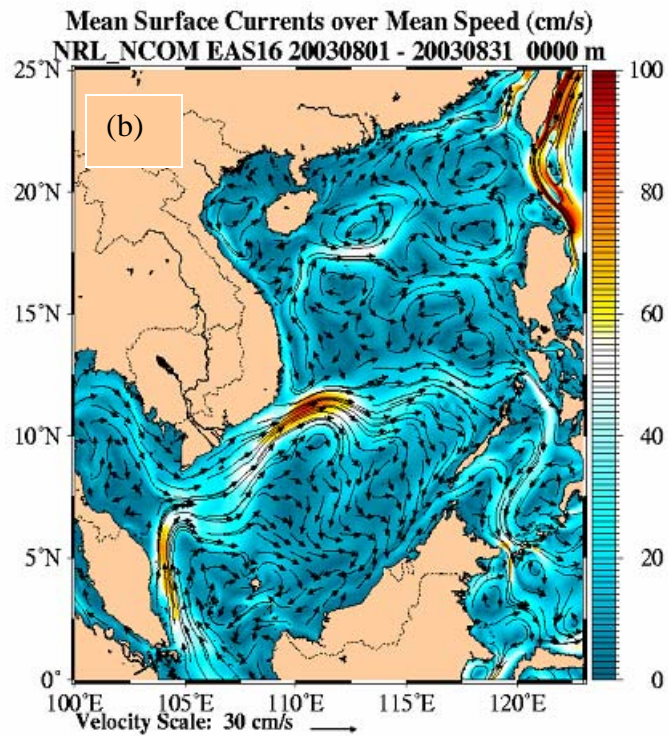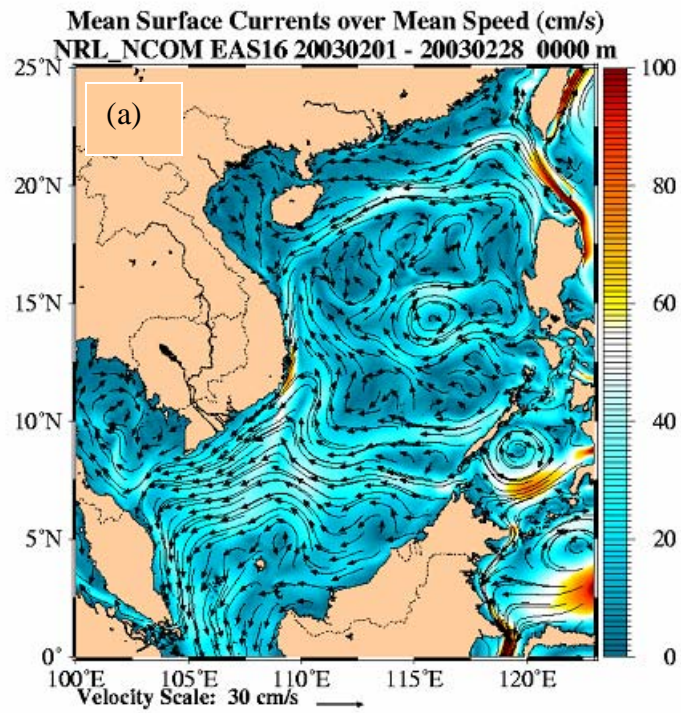
Figure 7 a-b. Monthly mean surface current from EAS16 for the South China Sea, a) February 2003, b) August 2003.
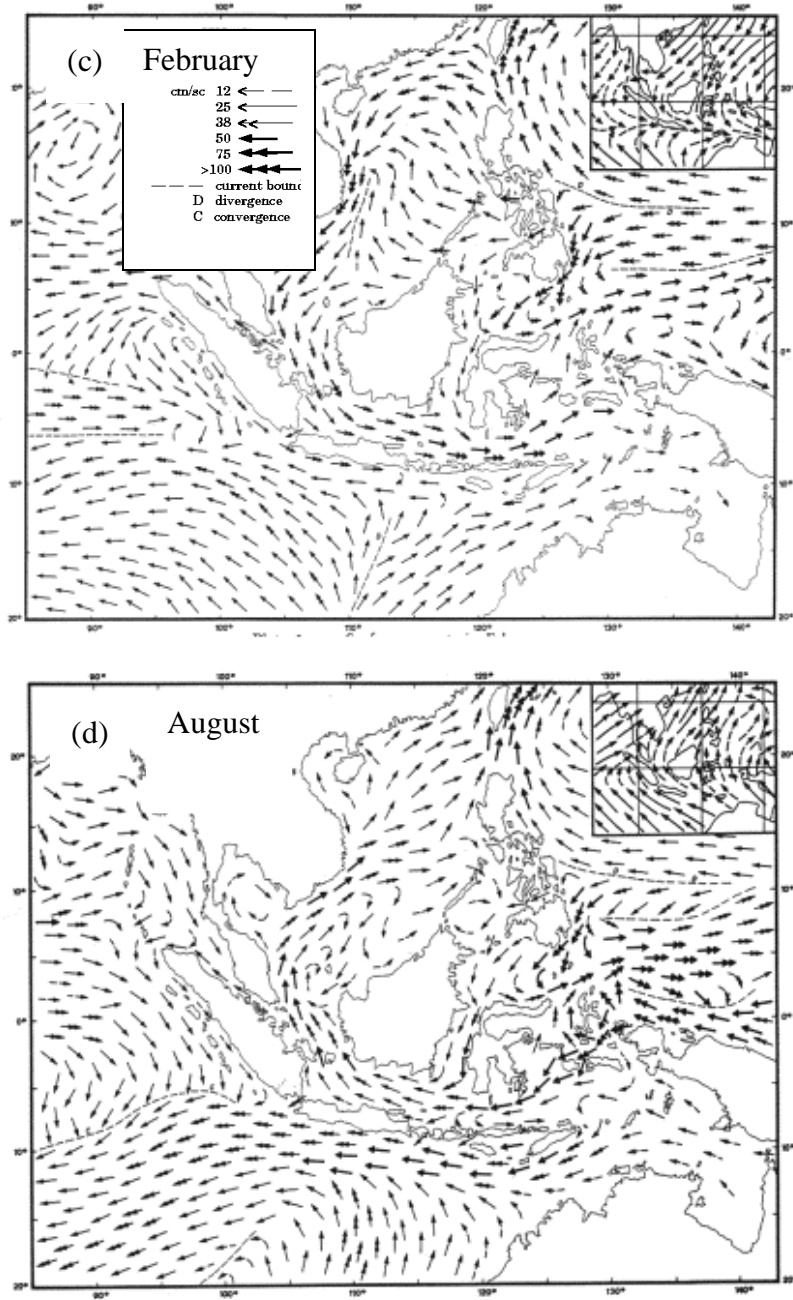
Figure 7 c-d . Schematic of the mean circulation in the South China Sea, a) February 2003, b) August 2003. Taken from Wyrtki 1961.

(a)

Mean Surface Currents over Mean Speed (cm/s)
NRL_NCOM EAS16 20030201 - 20030228 0000 m

Velocity Scale: 30 cm/s

(b)

Mean Surface Currents over Mean Speed (cm/s)
NRL_NCOM EAS16 20030801 - 20030831 0000 m

Velocity Scale: 30 cm/s
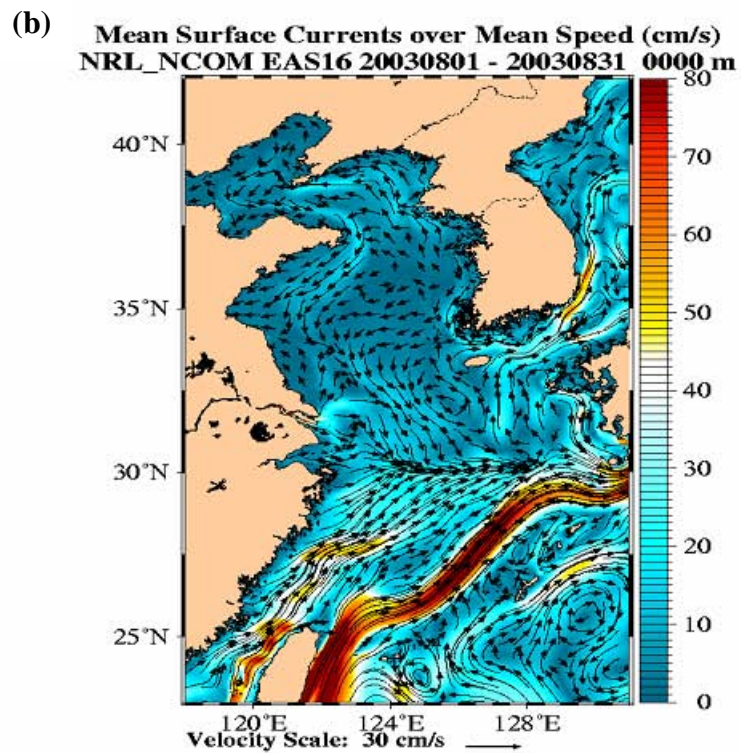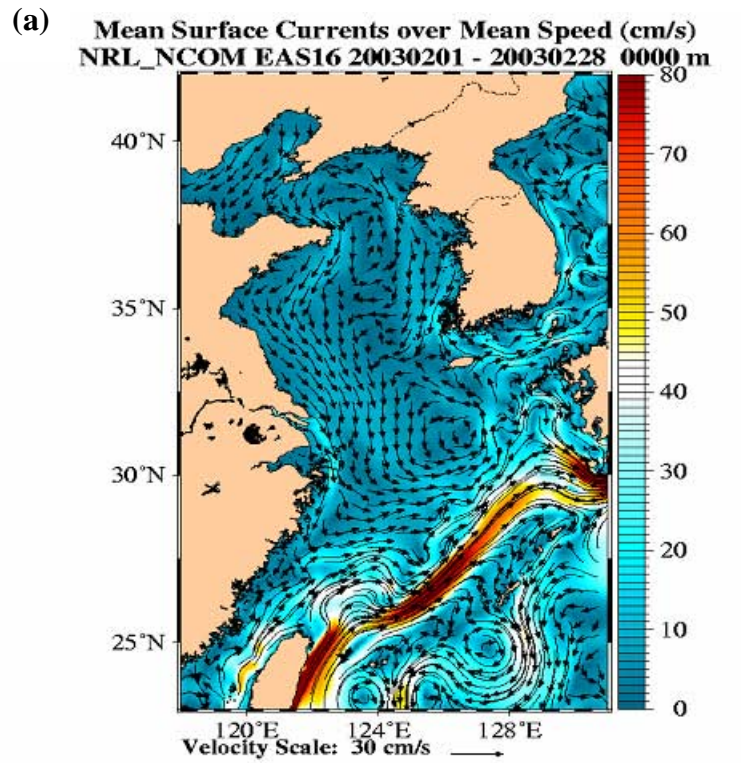
Figure 8 a-b. Monthly mean surface current from EAS16 model for the Yellow Sea/ East China Sea, a) February 2003, b) August 2003.

(c)   **(d)**
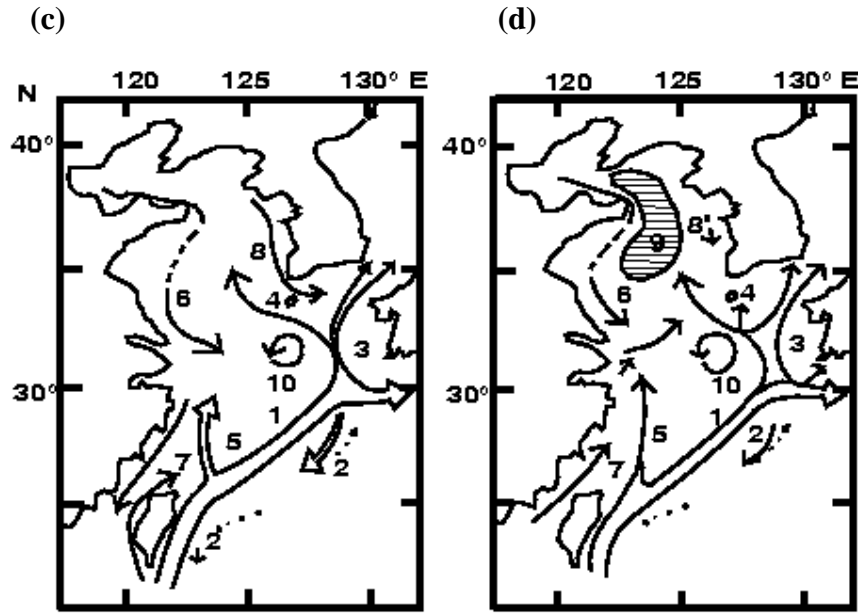
Figure 8 c-d. Schematic of the major currents in the Yellow Sea/East China Sea, a) winter, b) summer. (redrawn from Yuan & Su 1984)
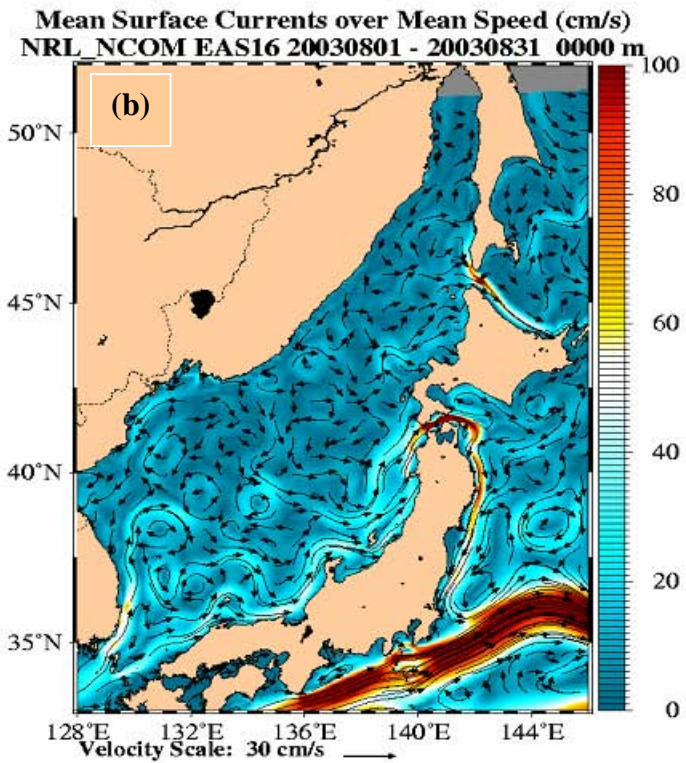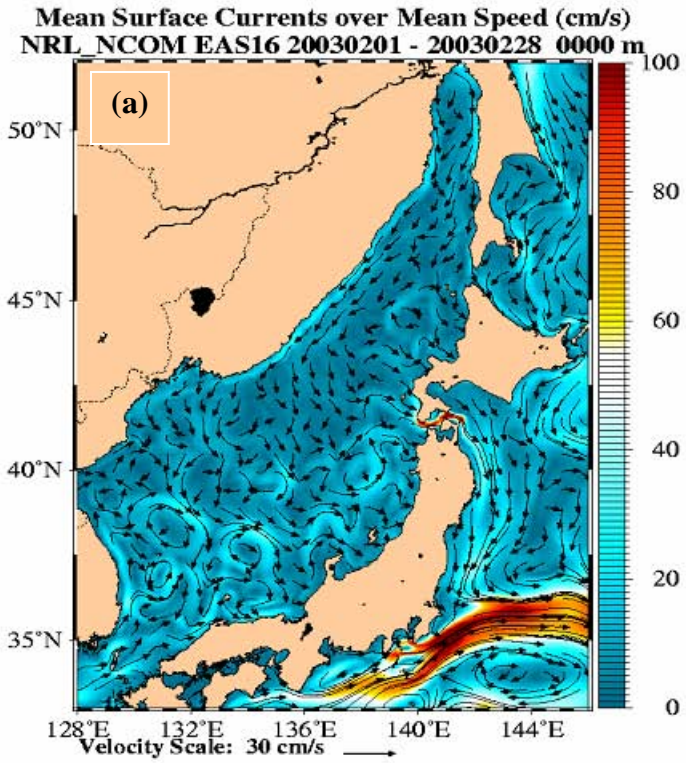
Figure 9 a-b. Monthly mean surface currents from EAS16 model for the Sea of Japan, a) February 2003, b) August 2003.

(c)
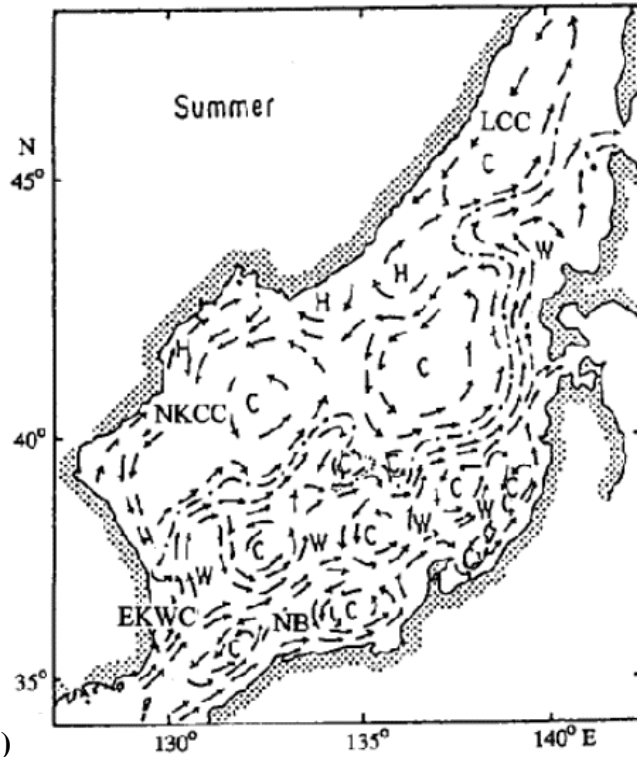
(d)
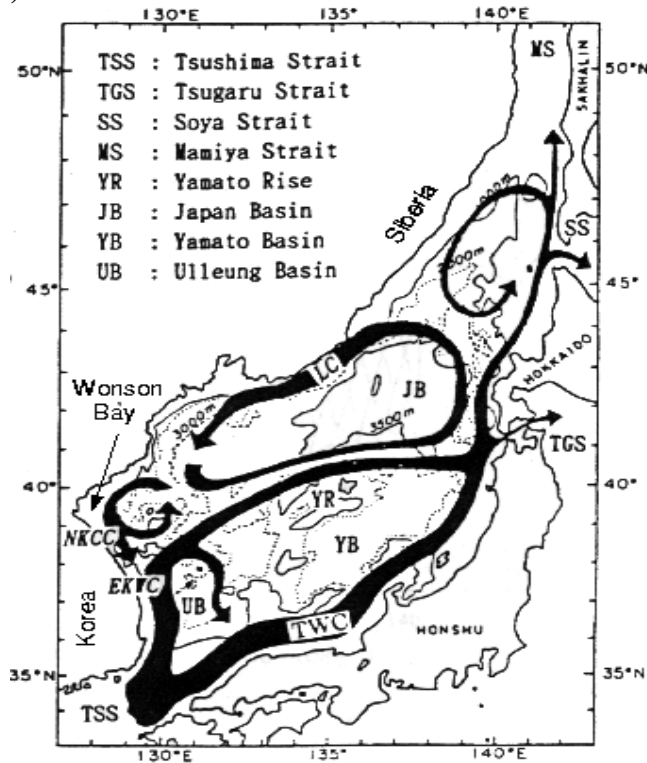
Figure 9c-d. Schematic of the major currents in the Sea of Japan, a) summer by Naganuma (1977), b) winter by Senjyu (1999)
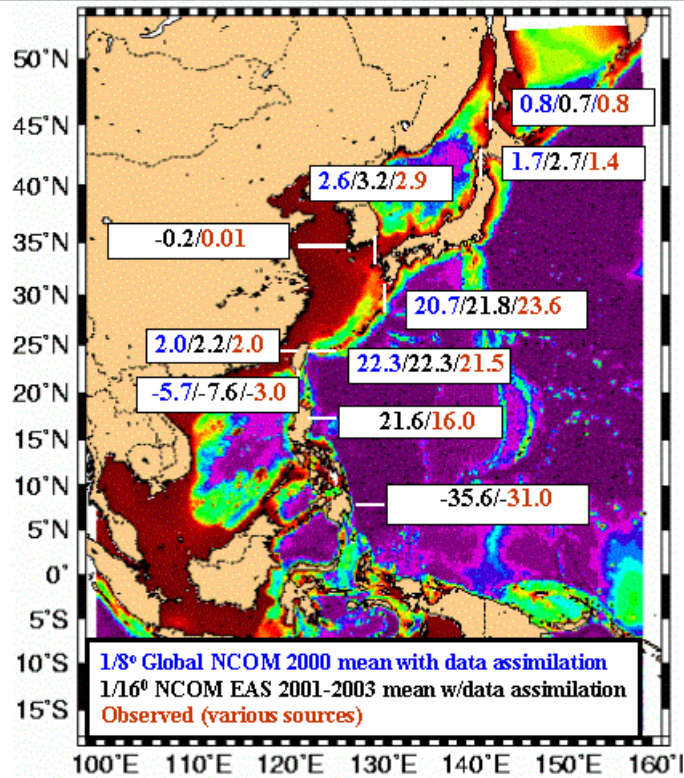
Figure 10. Transports (1×10^6 m^3/s) from various open literature sources (red numbers). Transports from 1/8° global NCOM for the year 2000 are denoted by blue numbers and from 1/16° EAS NCOM for 2001-2003 denoted by black numbers. Positive transports denote northward and eastward net flow.
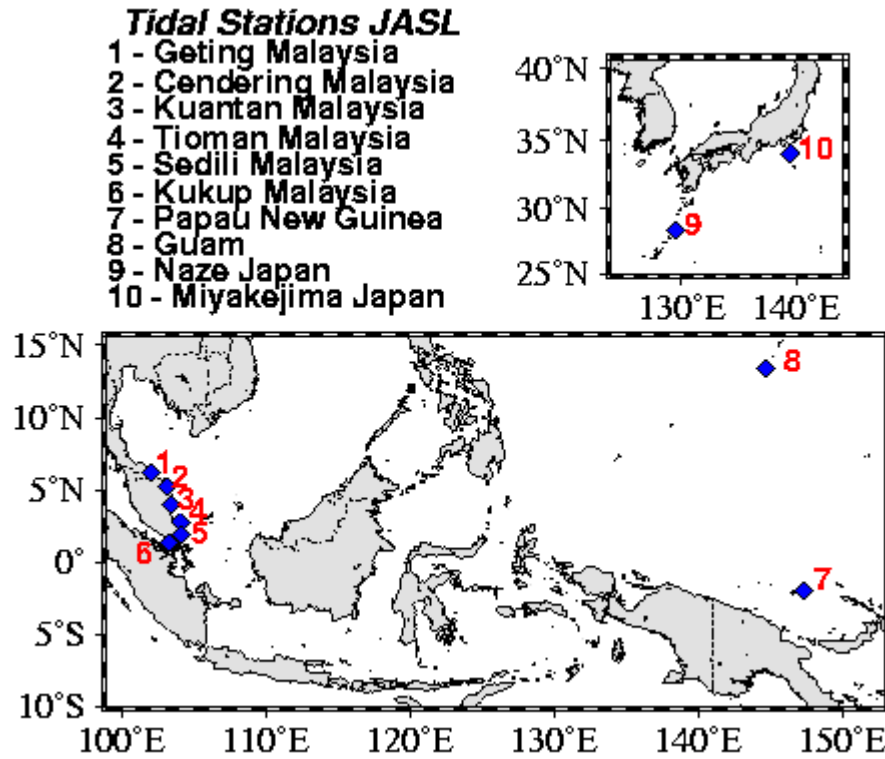
Figure 11a. Location of tide gauges used for comparison of sea surface height from EAS16 model.
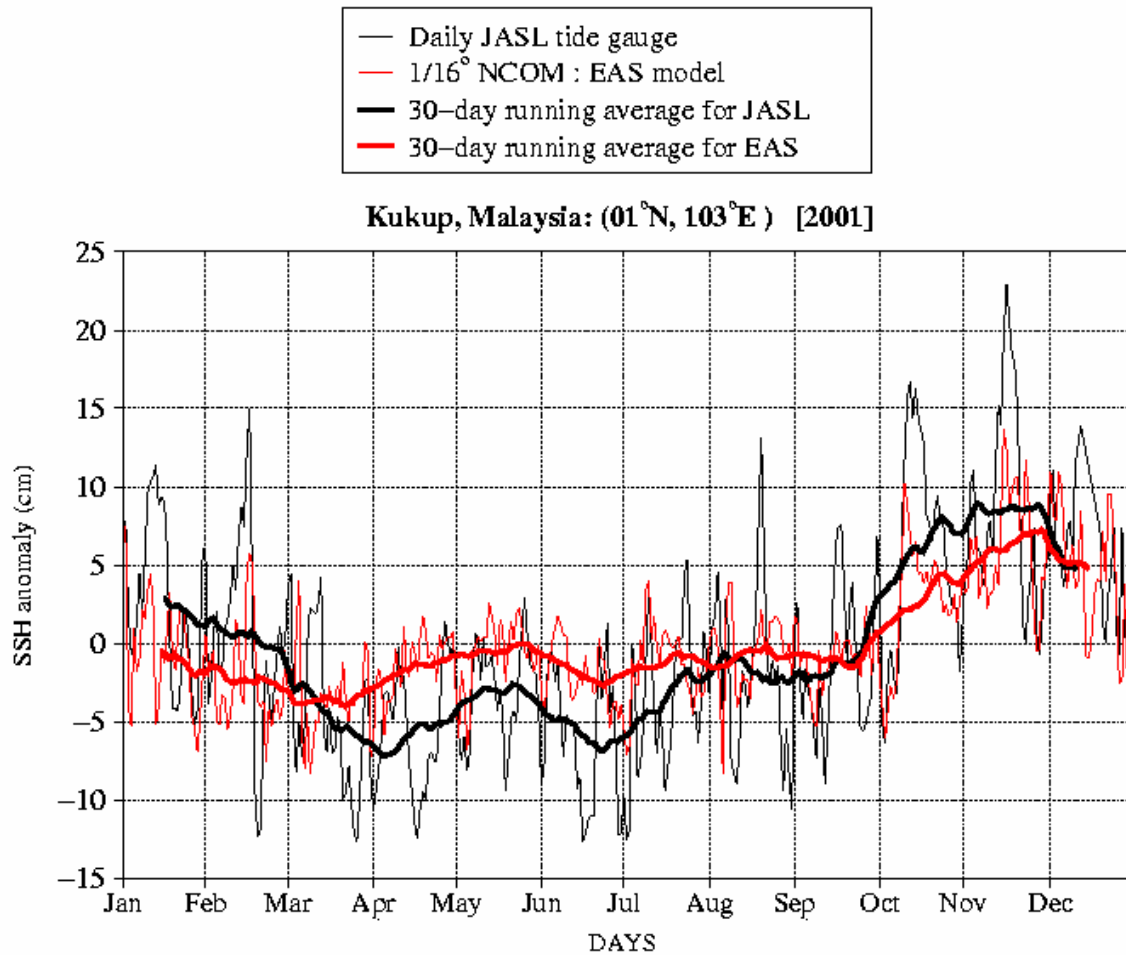
Figure 11b. Daily sea surface height at Kukup, Malaysia, for EAS16 model (thin red line) and de-tided JASL tide gauge data (thin black line). Thirty day running mean of sea surface height for EAS16 model (thick red line) and for de-tided JASL tide gauge data (thick black line).
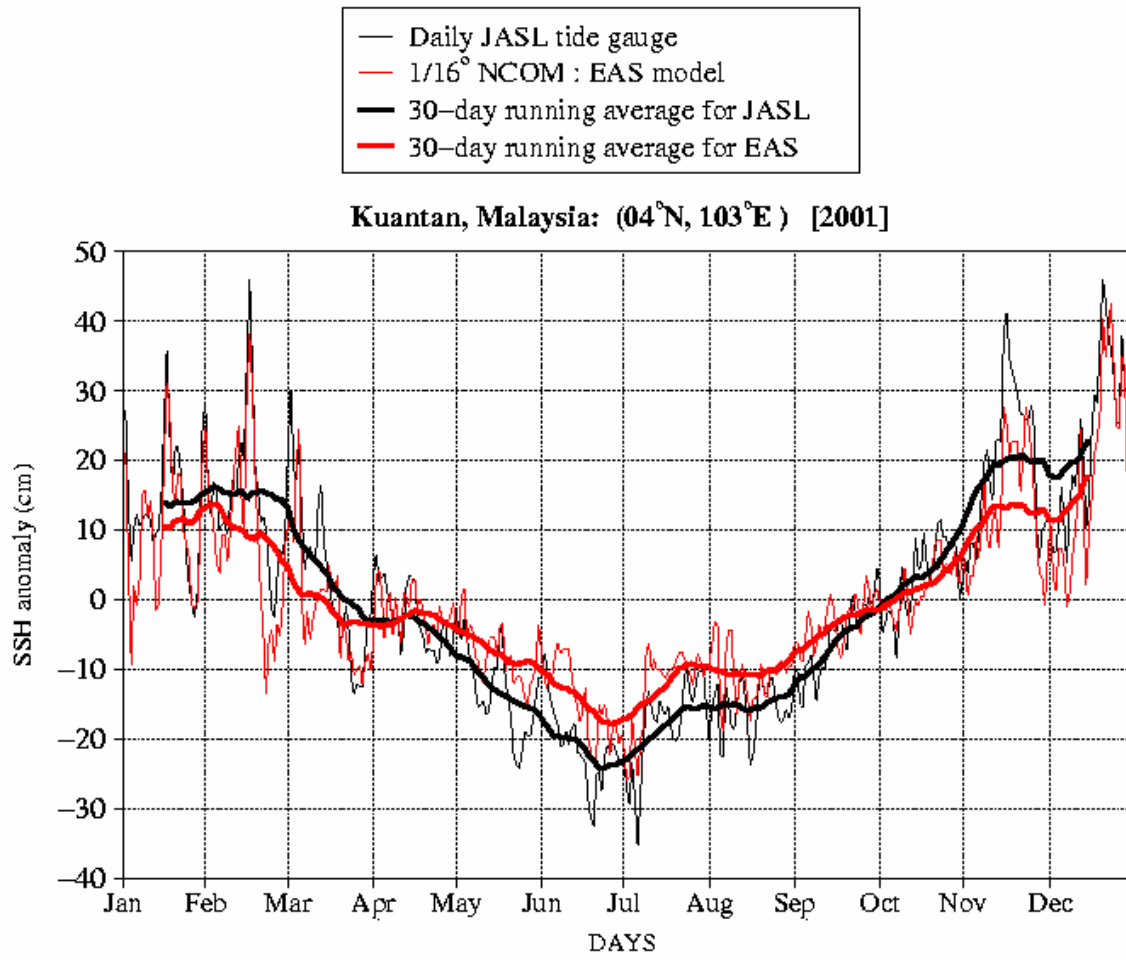
Figure 11c. Same as 11b for Kuantan, Malaysia.
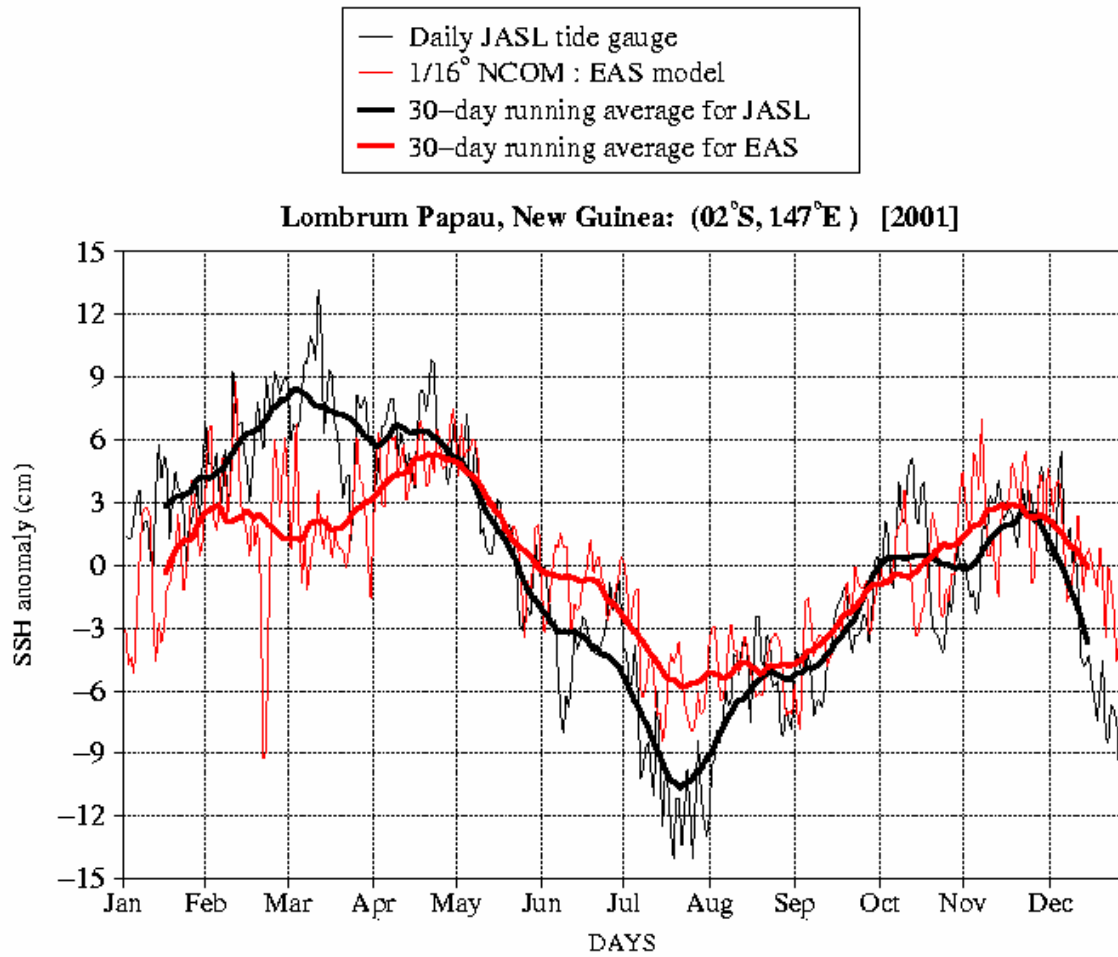
Figure 11d . Same at 11b for Lombrum, Papau New Guinea
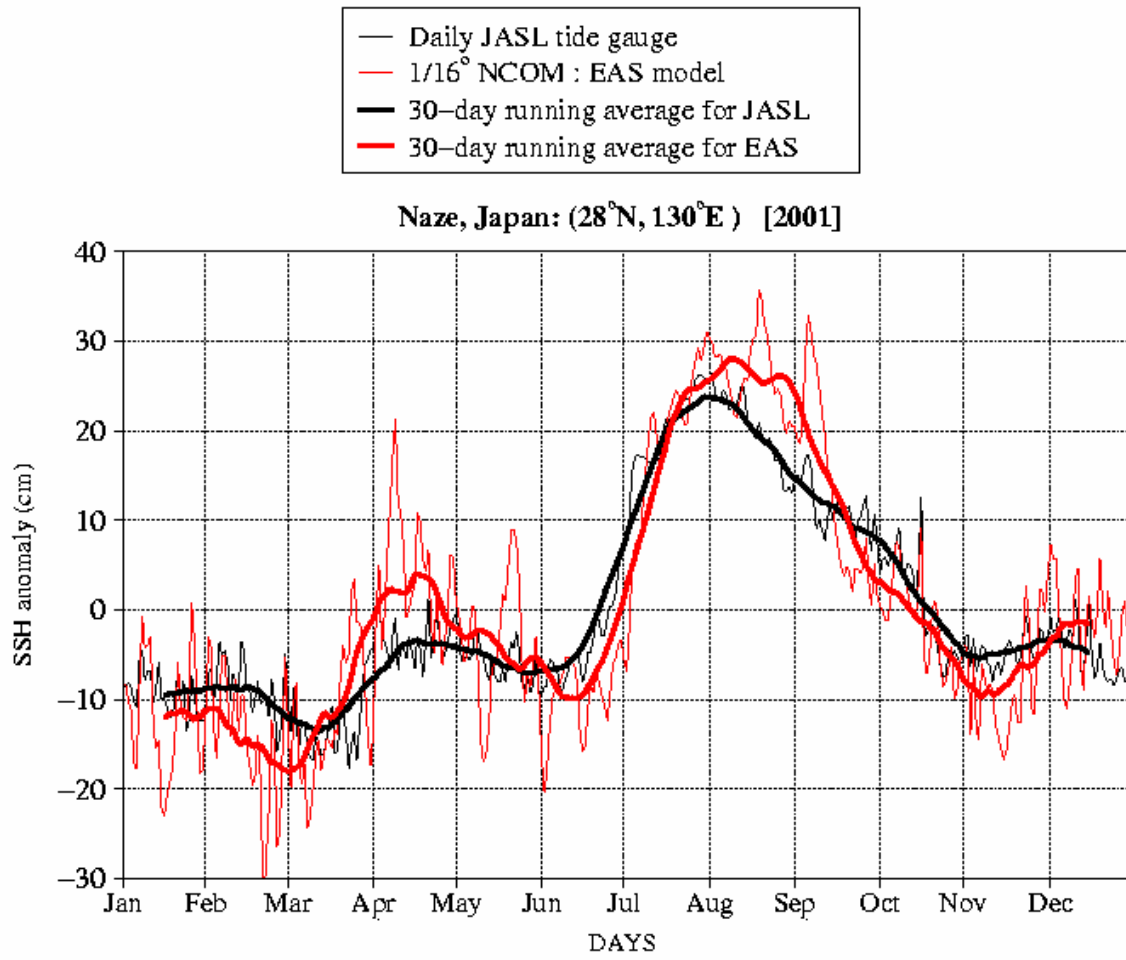
Figure 11e. Same as 11b for Naze, Japan
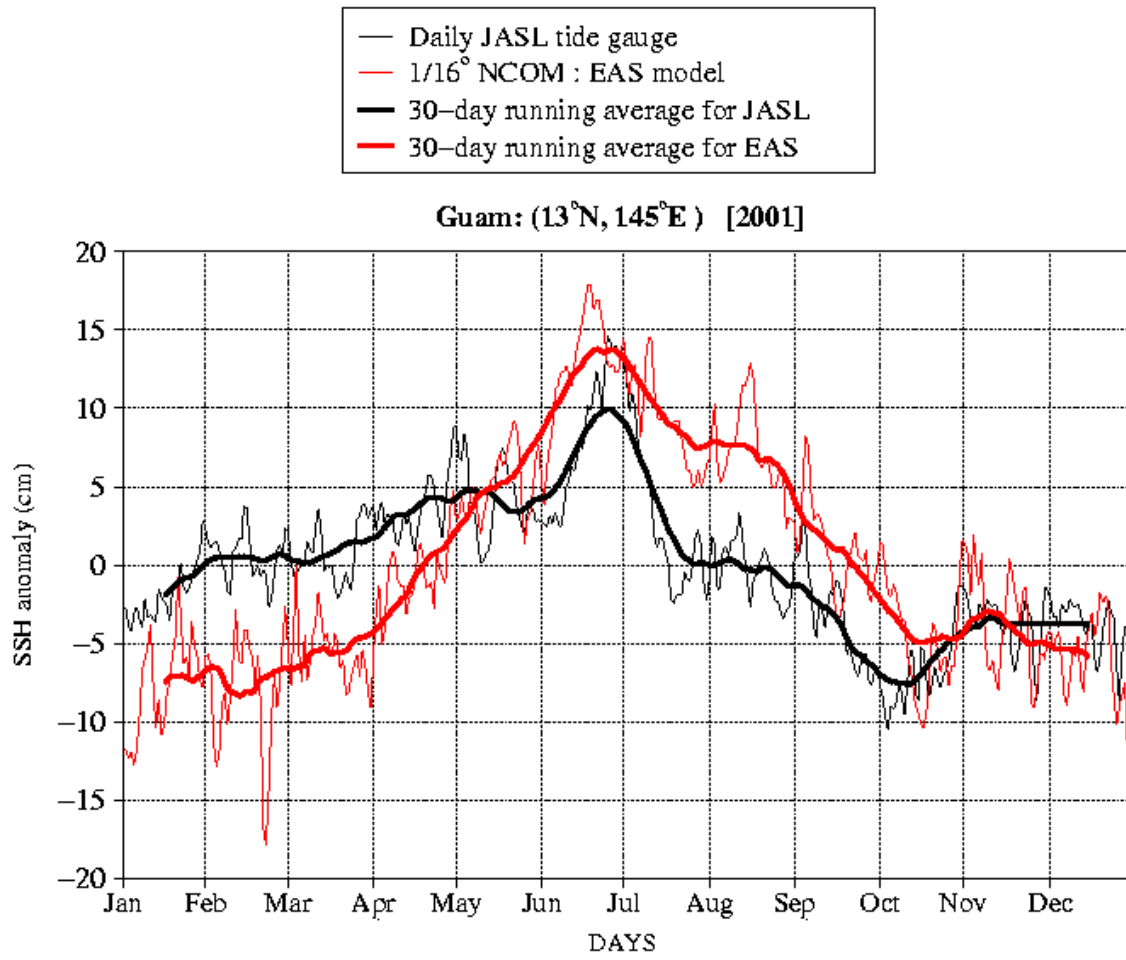
Figure 11f   Same as 11b for Guam.
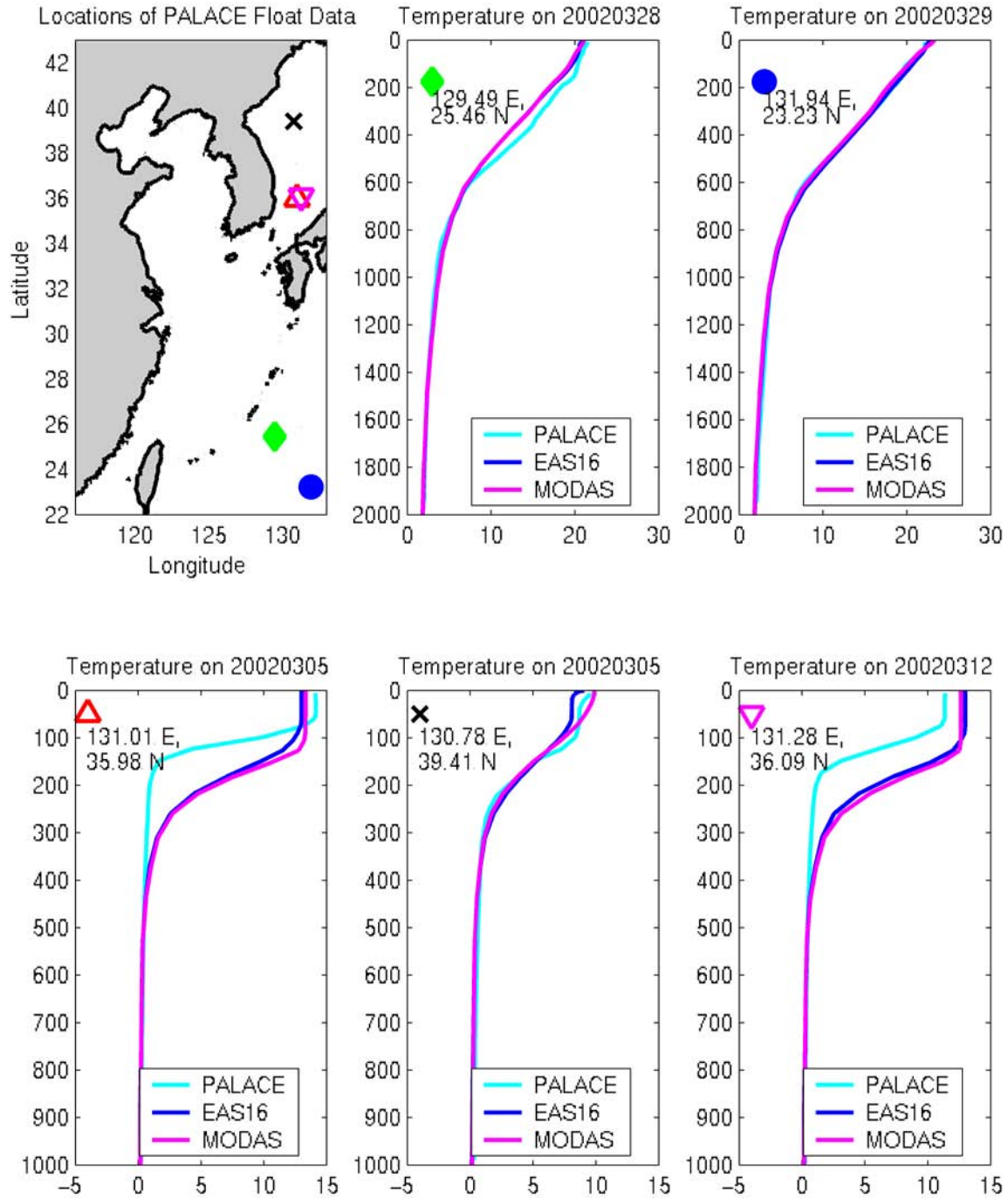
Figure 12. Comparison of temperature profiles from model (dark blue line), PALACE floats (cyan line), and MODAS (pink line) at locations in the Sea of Japan and Pacific south of Ryukyu Islands. (Plots provided by Andrea Mask.)
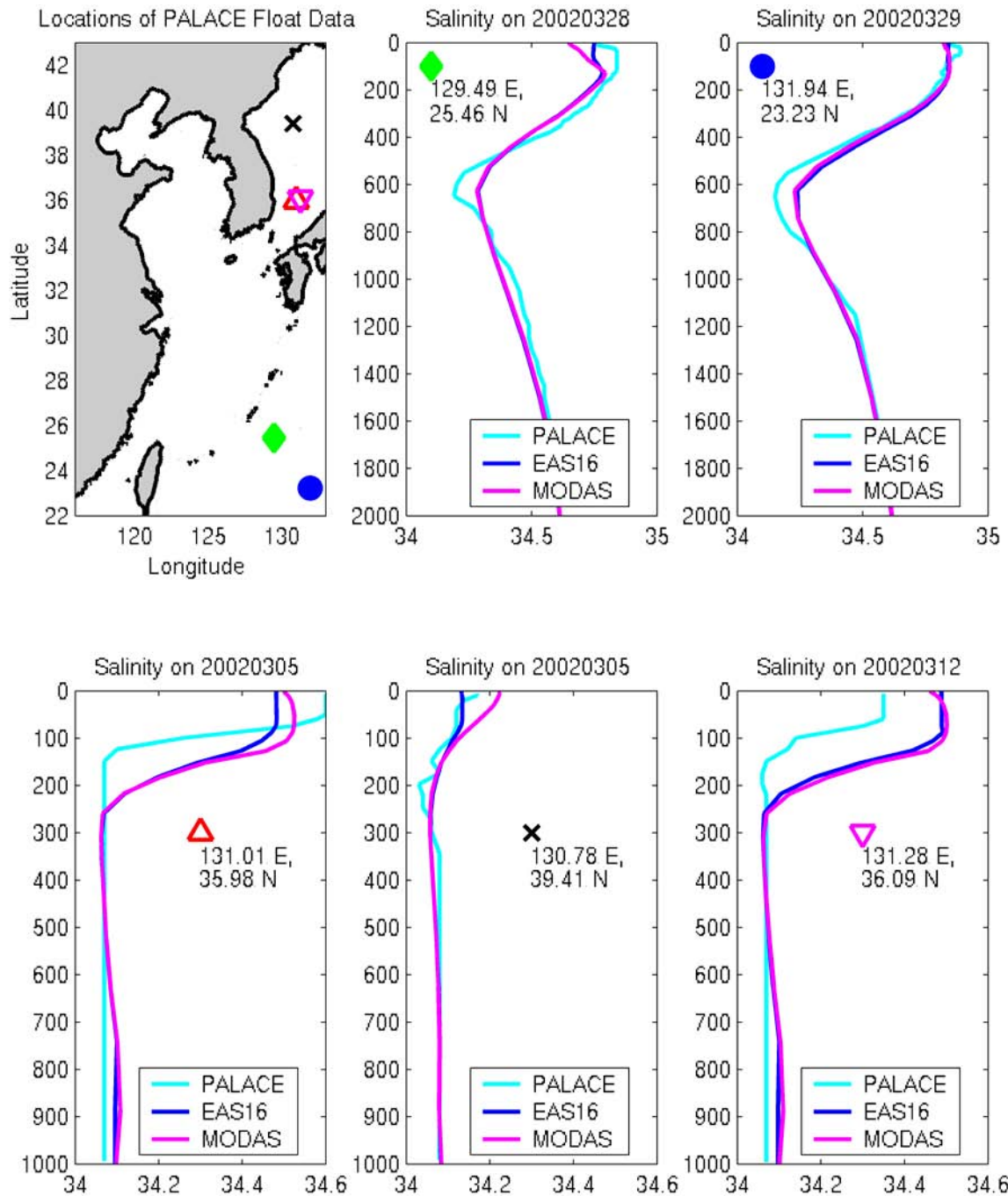
Figure 13. Comparison of salinity profiles from model (dark blue line), PALACE floats (cyan line), and MODAS (pink line) at locations in the Sea of Japan and Pacific south of Ryukyu Islands. (Plots provided by Andrea Mask.)
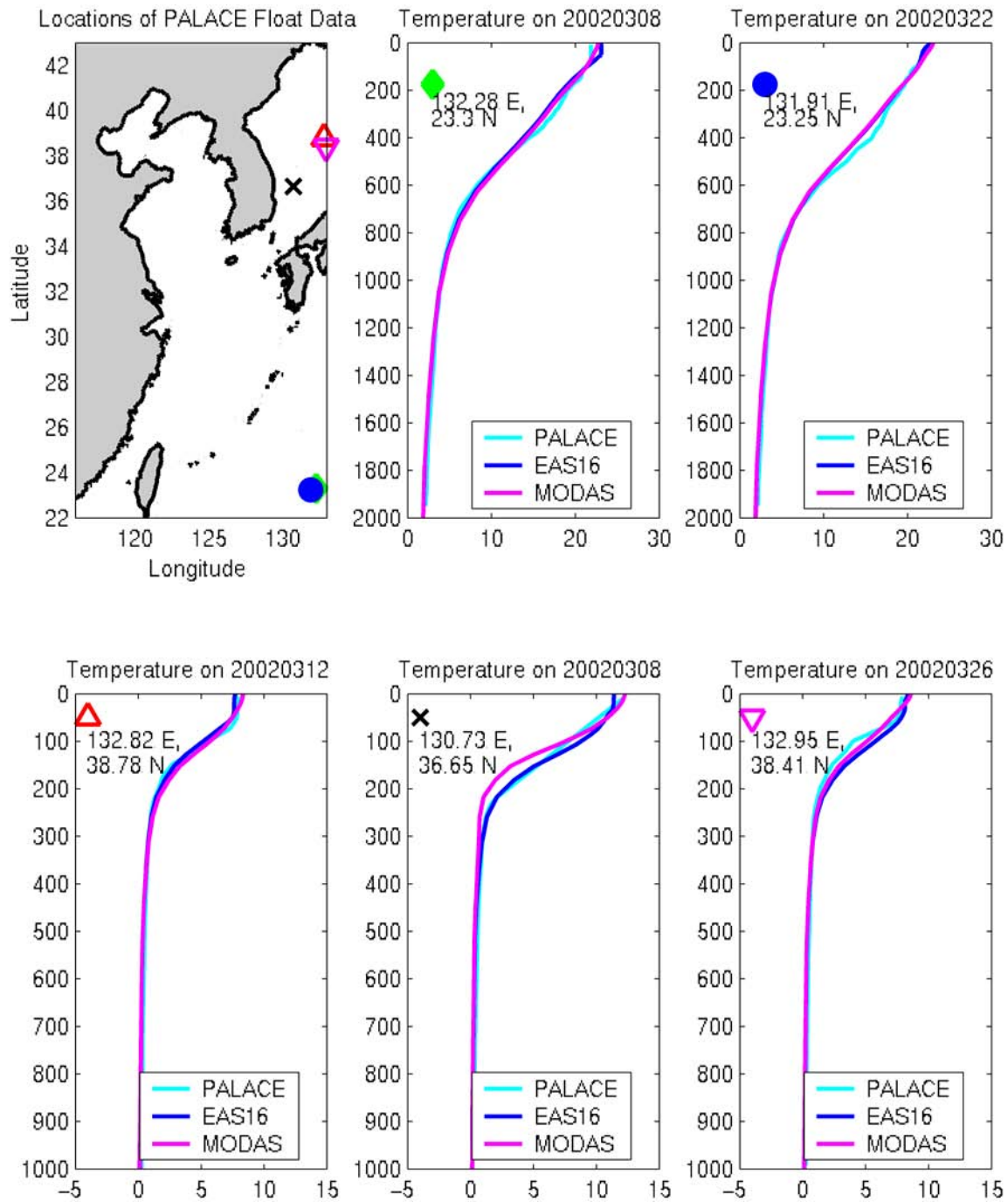
Figure 14. Comparison of temperature profiles from model (dark blue line), PALACE floats (cyan line), and MODAS (pink line) at locations in the Sea of Japan and Pacific south of Ryukyu Islands. (Plots provided by Andrea Mask.)
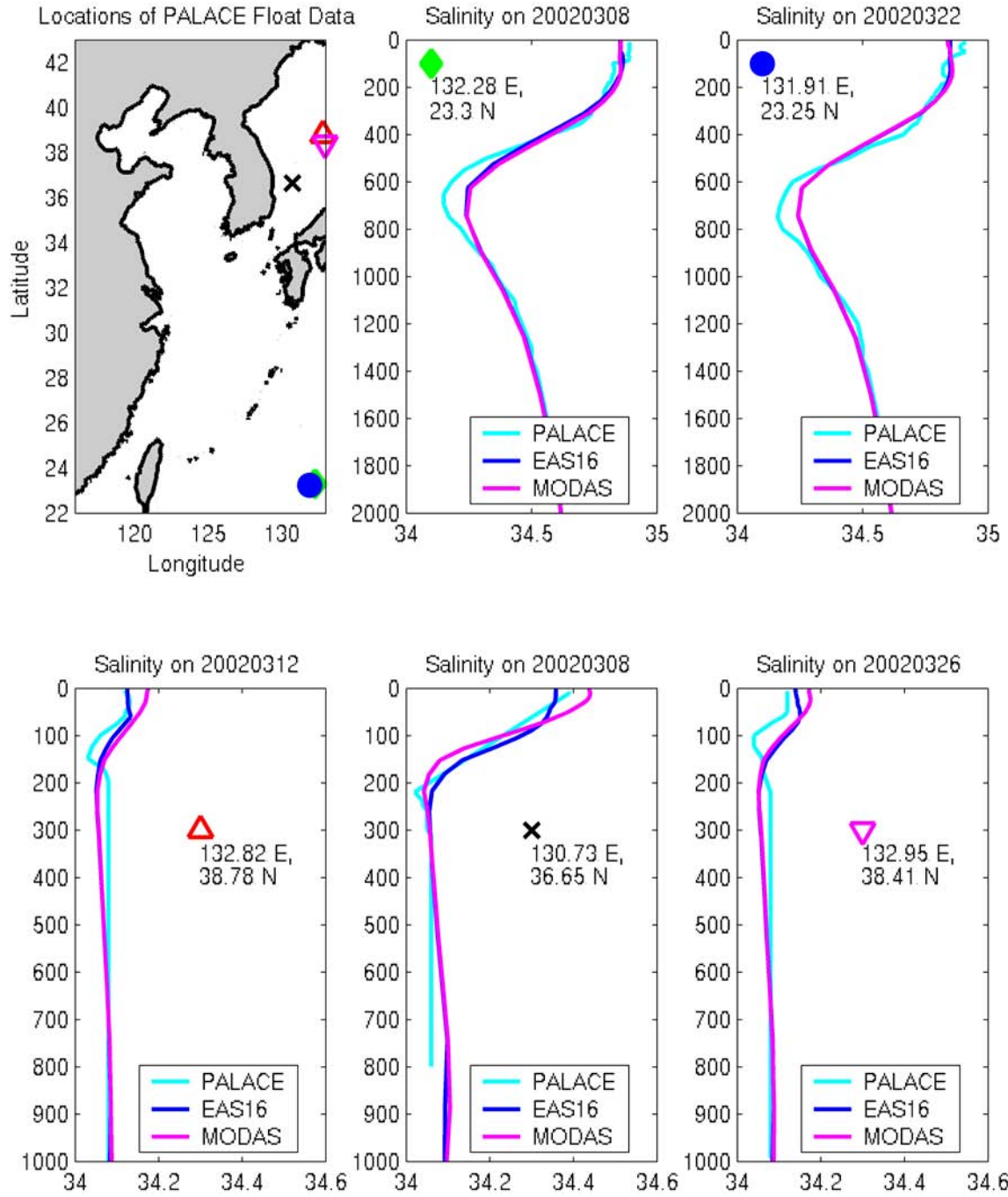
Figure 15. Comparison of salinity profiles from model (dark blue line), PALACE floats (cyan line), and MODAS (pink line) at locations in the Sea of Japan and Pacific south of Ryukyu Islands. (Plots provided by Andrea Mask.)
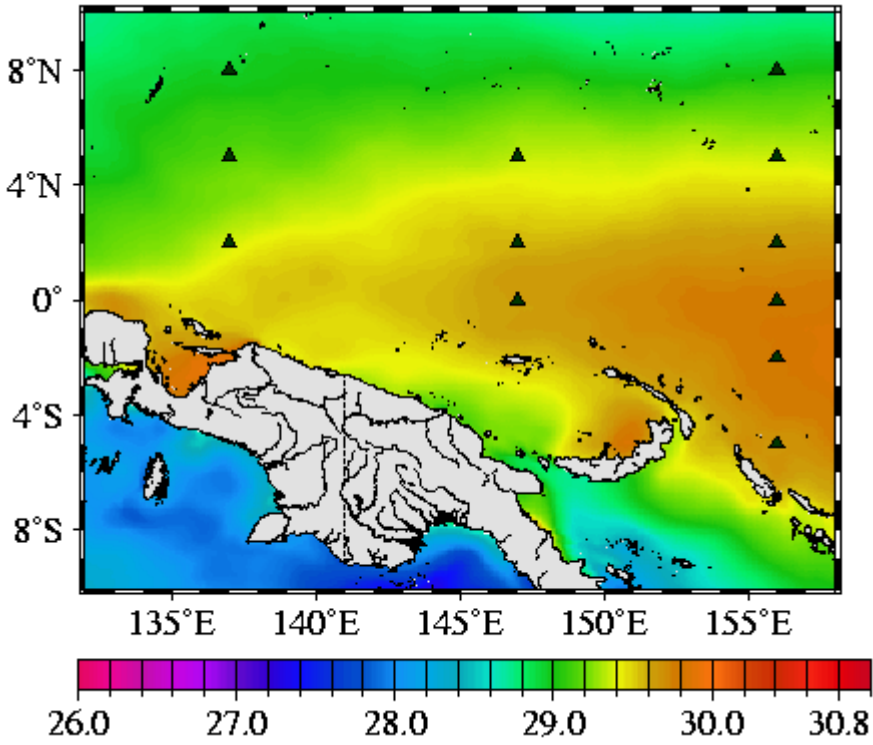
Figure 16. Location of the 12 TAO moorings (triangle), which fall within the EAS16 domain. Locations are overlaid on annual mean surface temperature (^{o}C) from EAS16.
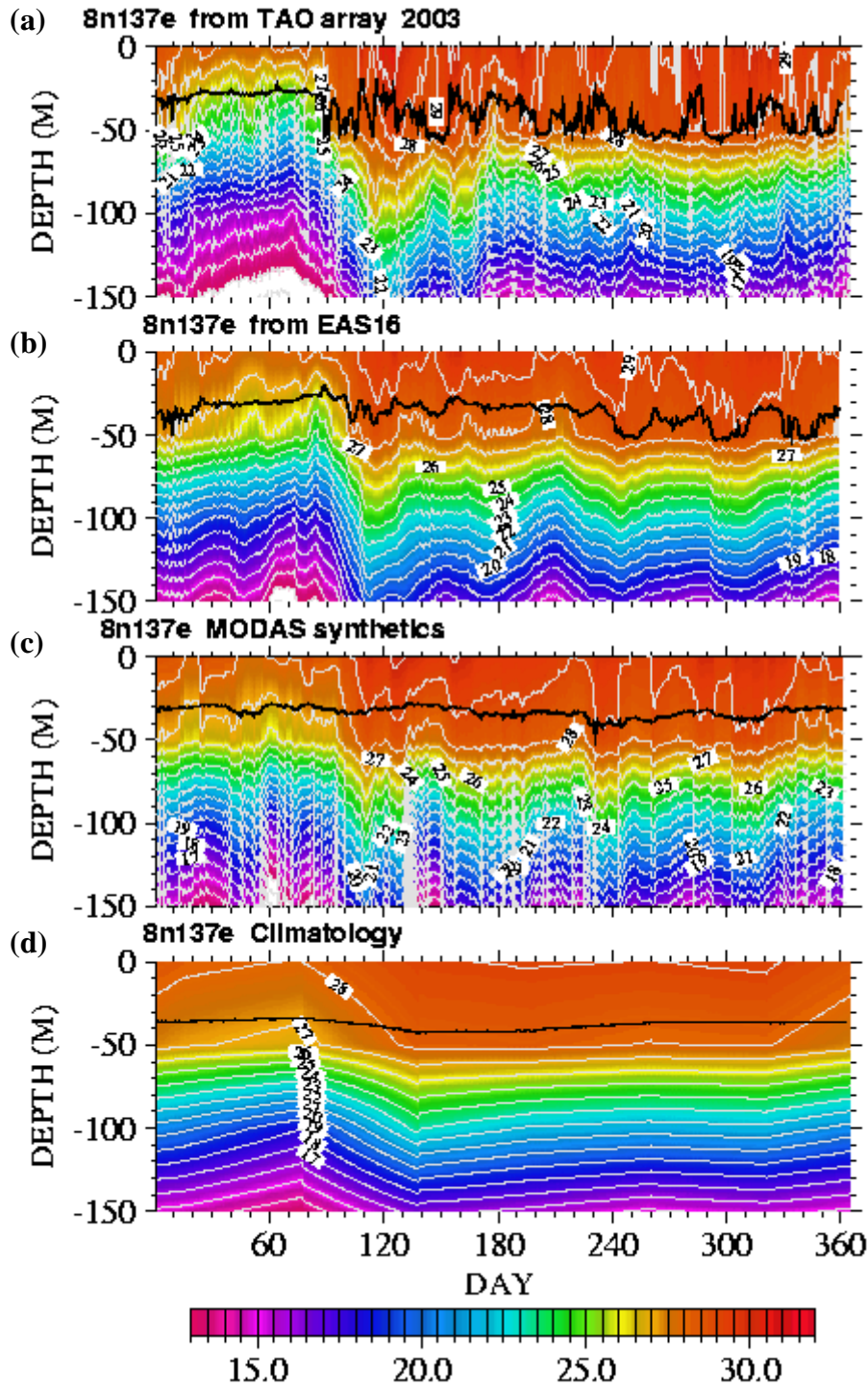
Figure 17. Time series of temperature from 1.5m to 150m a) from TAO moorings at 8ᵒN 137ᵒE, b) same location from EAS16 model, c) same for MODAS and d) same for climatology. Black line represents the depth of the isothermal layer.

73
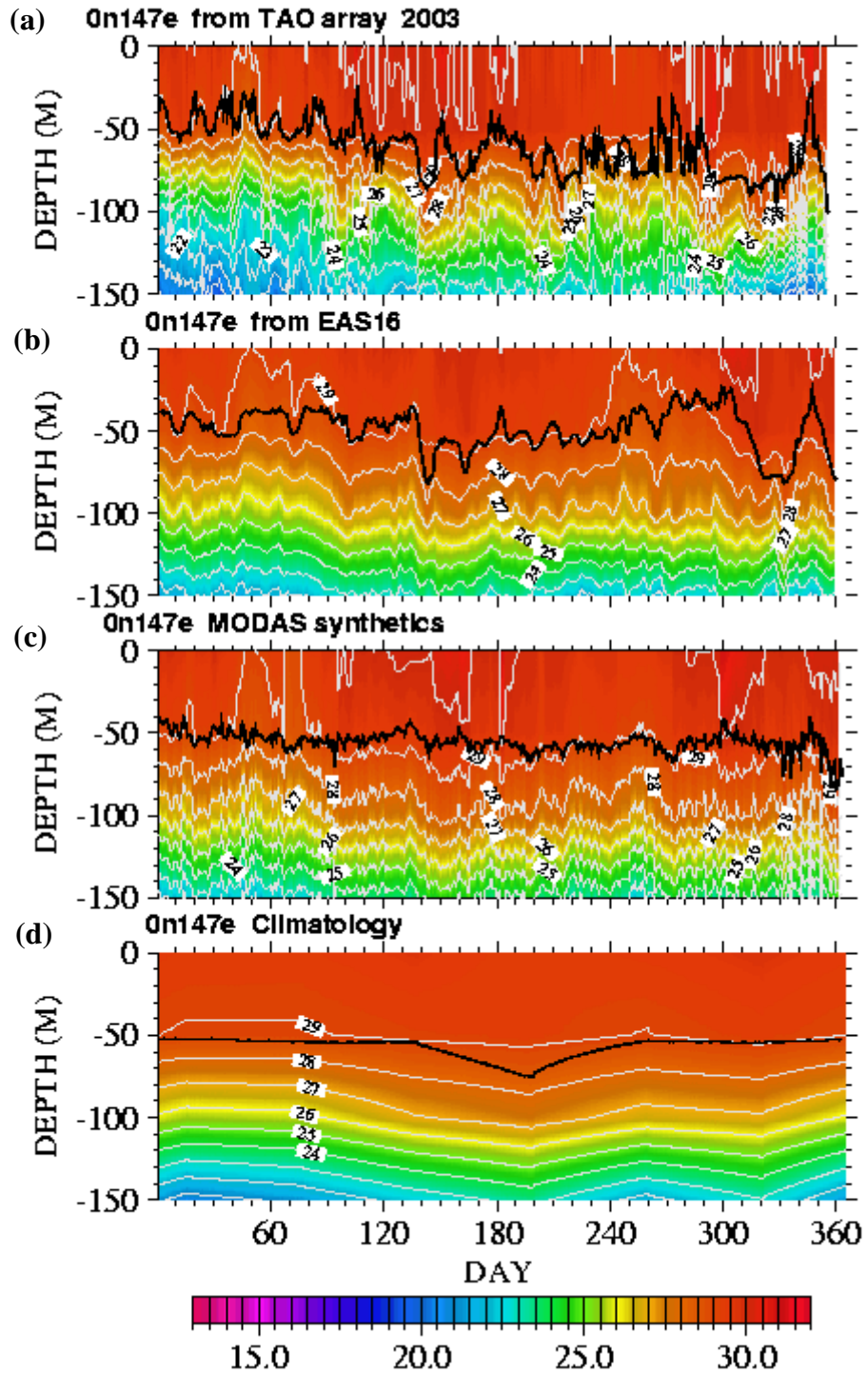
Figure 18. Time series of temperature from 1.5m to 150m a) from TAO moorings at 0^oN 147^oE, b) same location from EAS16 model, c) same for MODAS and d) same for climatology. Black line represents the depth of the isothermal layer.

74
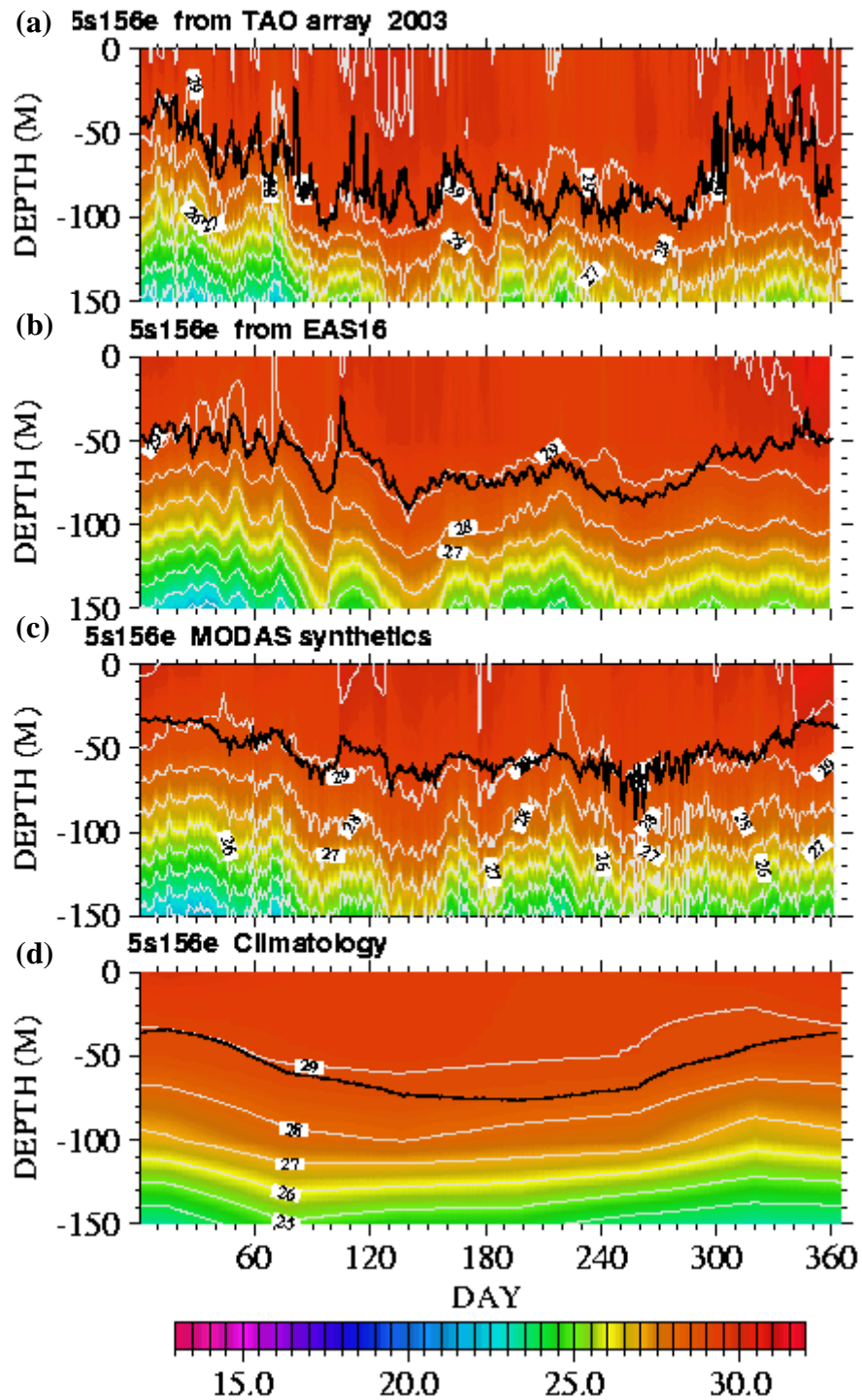
Figure 19. Time series of temperature from 1.5m to 150m a) from TAO moorings at 5°S 156°E, b) same location from EAS16 model, c) same for MODAS and d) same for climatology. Black line represents the depth of the isothermal layer.
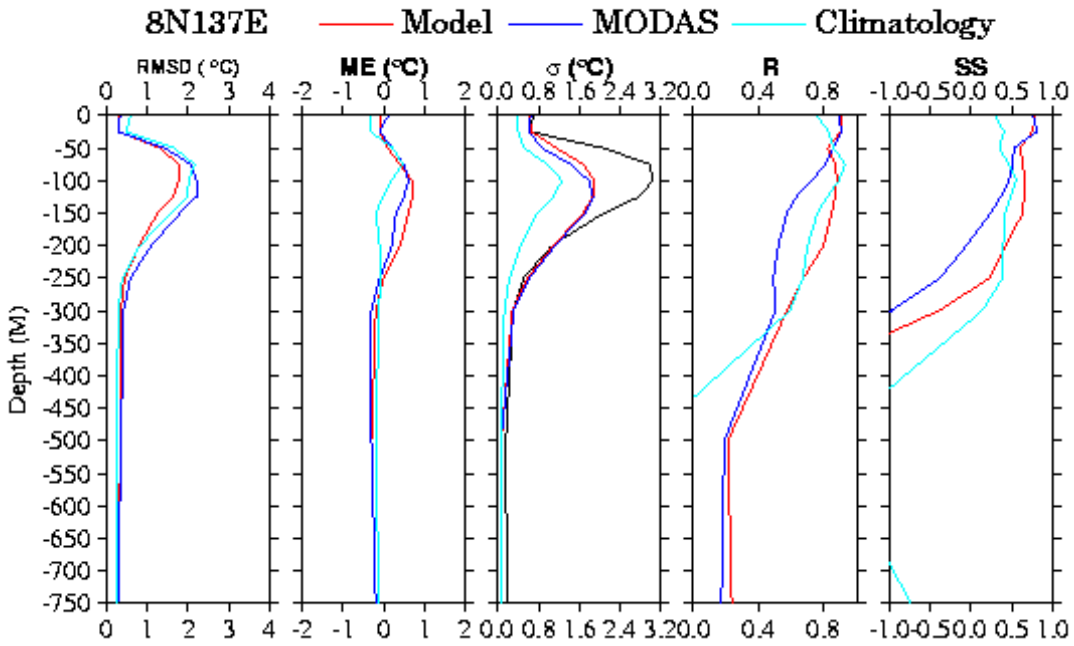
Figure 20. Statistical values plotted vs. depth for temperature comparison at mooring 8°N 137°E. Plots are for EAS16 model (red line), MODAS (blue line) and climatology (cyan line). RMSD is root mean square difference, ME is mean error, σ is standard deviation, R is correlation coefficient, and SS is skill score. For standard deviation the black line is TAO data.
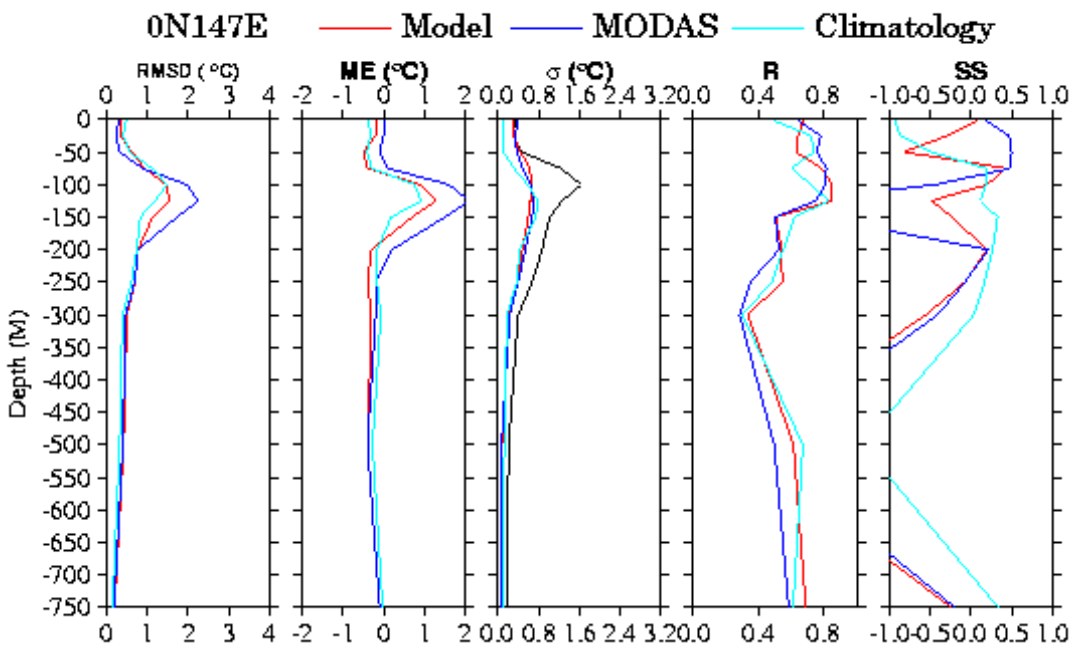
Figure 21. Statistical values plotted vs. depth for temperature comparison at mooring 0°N 147°E. Plots are for EAS16 model (red line), MODAS (blue line) and climatology (cyan line). RMSD is root mean square difference, ME is mean error, σ is standard deviation, R is correlation coefficient, and SS is skill score. For standard deviation the black line is TAO data.
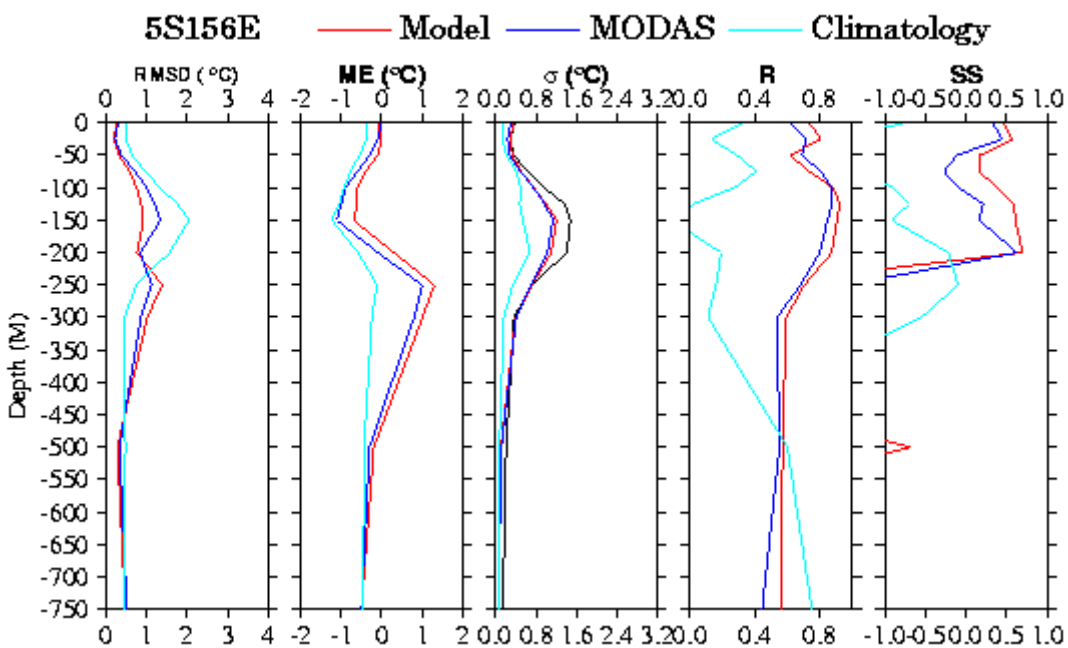
Figure 22. Statistical values plotted vs. depth for temperature comparison at mooring 5ºS 156ºE. Plots are for EAS16 model (red line), MODAS (blue line) and climatology (cyan line). RMSD is root mean square difference, ME is mean error, σ is standard deviation, R is correlation coefficient, and SS is skill score. For standard deviation the black line is TAO data.
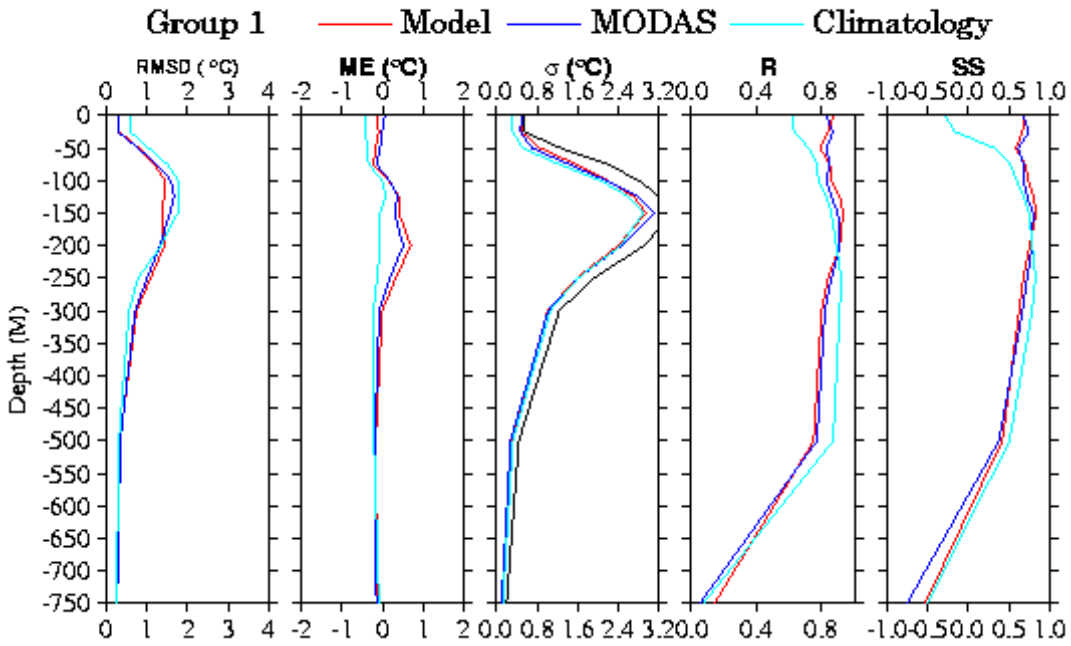
Figure 23. Total statistical values plotted vs. depth for temperature comparison for 10 of the mooring. Plots are for EAS16 model (red line), MODAS (blue line) and climatology (cyan line). RMSD is root mean square difference, ME is mean error, σ is standard deviation, R is correlation coefficient, and SS is skill score. For standard deviation the black line is TAO data.
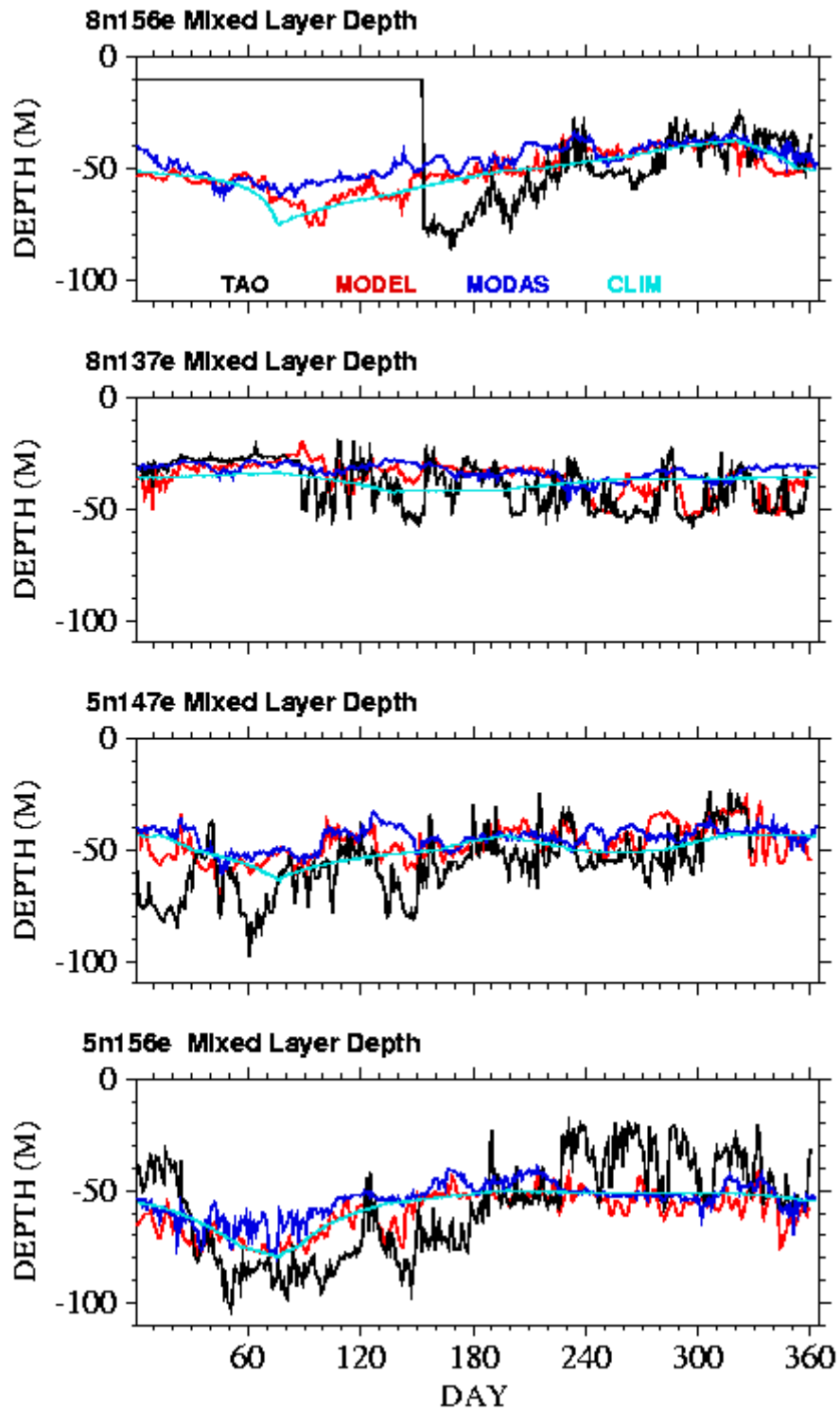
Figure 24a. Effective mixed layer depth computed from temperature profiles (Isothermal layer depth) from TAO moorings (black line), from EAS16 model (red line), from MODAS (blue line) and from climatology (cyan line), for the year 2003. (Missing data days 1-150 for 8n156e)

80
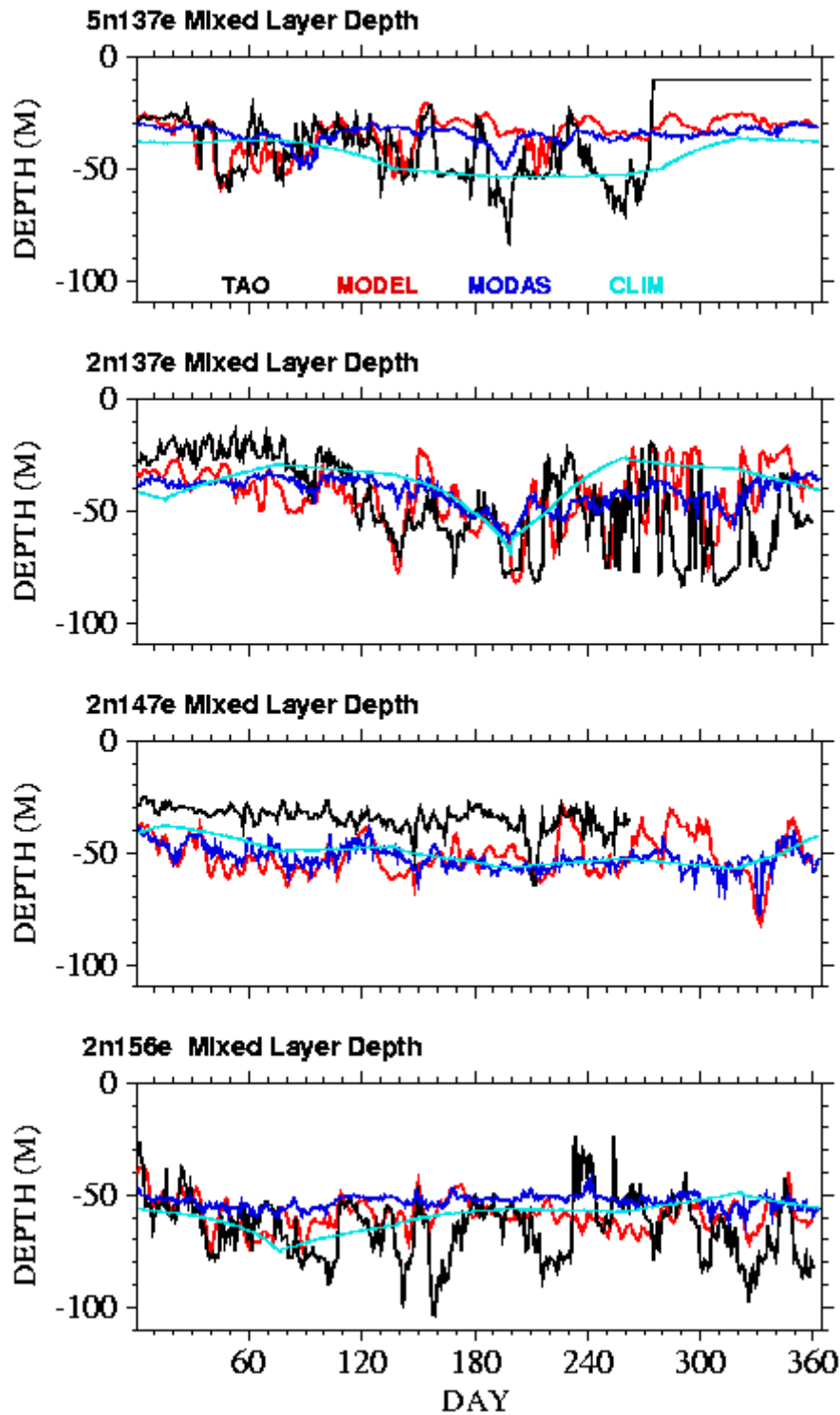
Figure 24b. Effective mixed layer depth computed from temperature profiles (Isothermal layer depth) from TAO moorings (black line), from EAS16 model (red line), from MODAS (blue line) and from climatology (cyan line), for the year 2003. (Missing data days 270-360 for 5n137e)

81
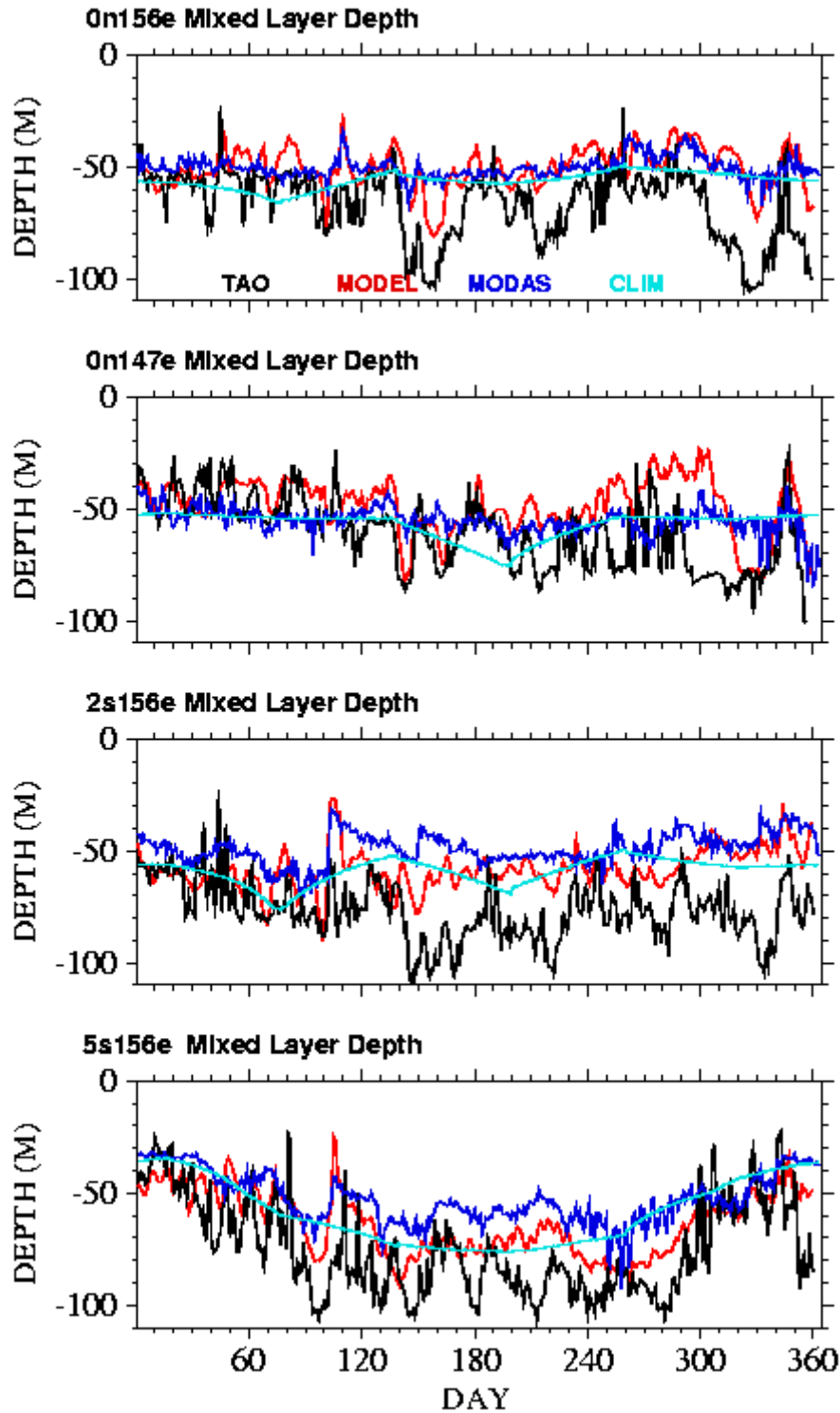
Figure 24c. Effective mixed layer depth computed from temperature profiles (Isothermal layer depth) from TAO moorings (black line), from EAS16 model (red line), from MODAS (blue line) and from climatology (cyan line), for the year 2003.
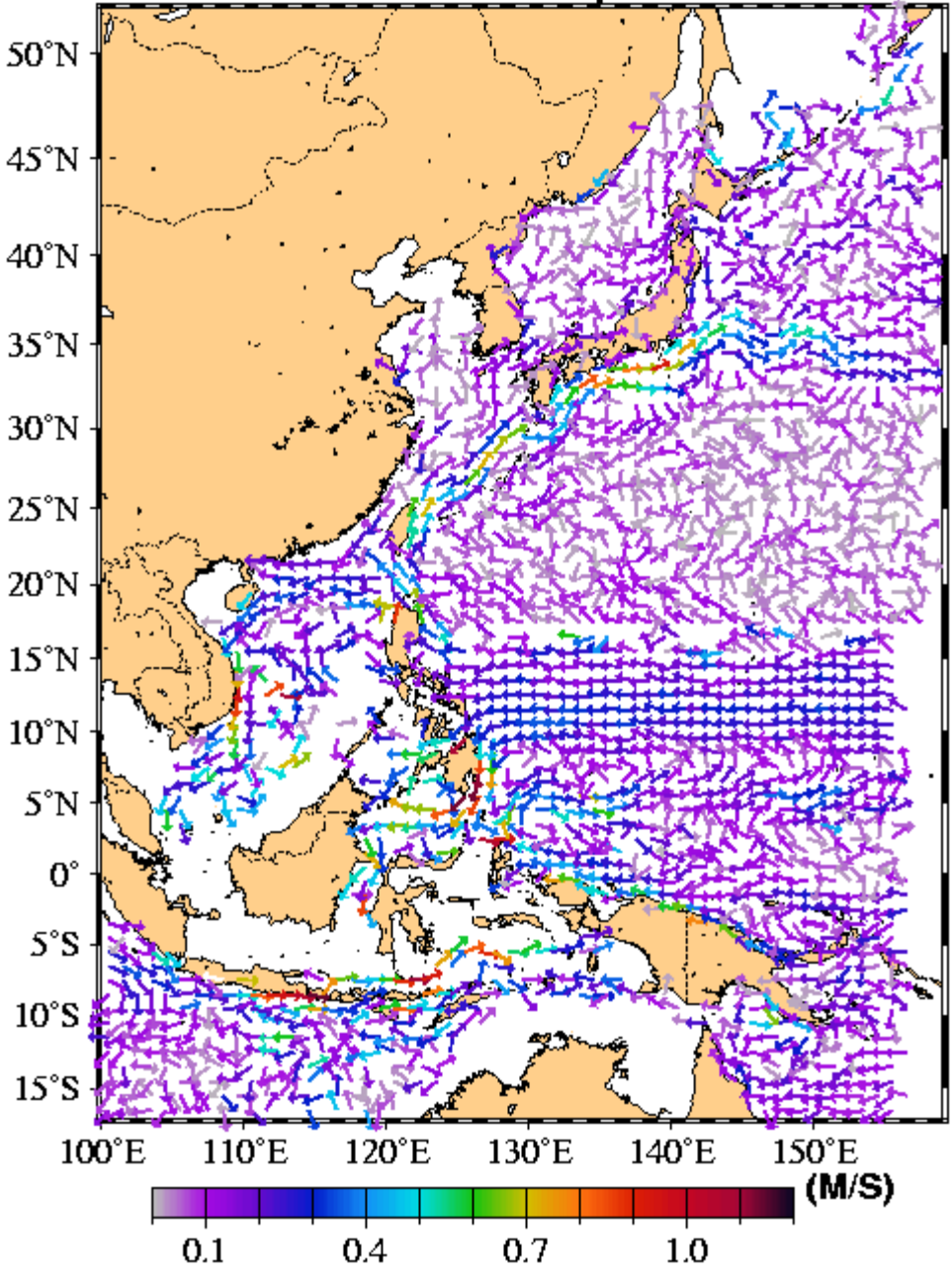
Figure 25a. Mean currents computed from Niiler drifter data in 1°X1° bins (all years and all months.) Empty bins occur as there are no drifter measurements in those areas. Color scale is speed in m/sec.
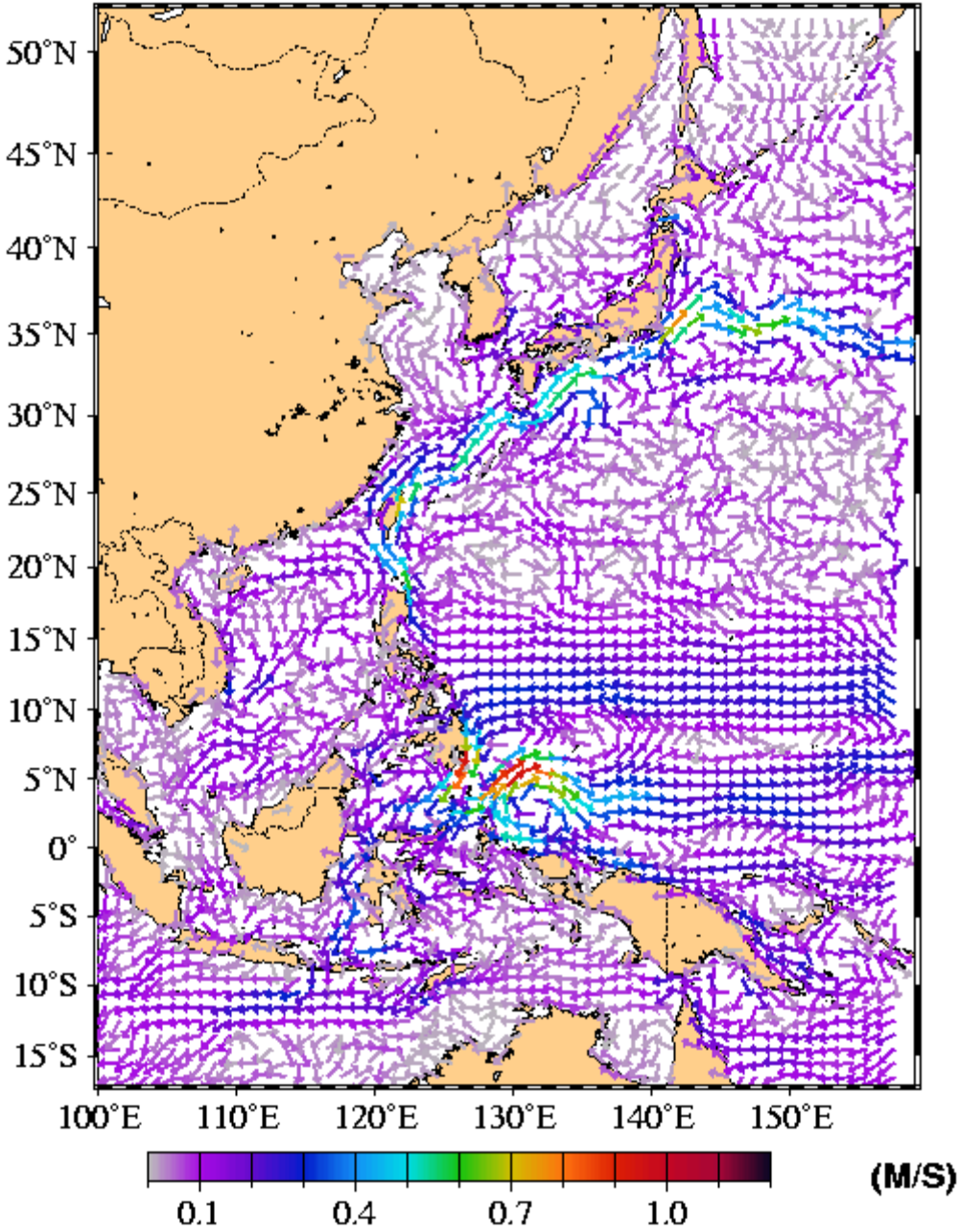
Figure 25b. Mean currents computed from EAS16 model in 1°X1° bins (all years and all months). Color scale is speed in m/sec.
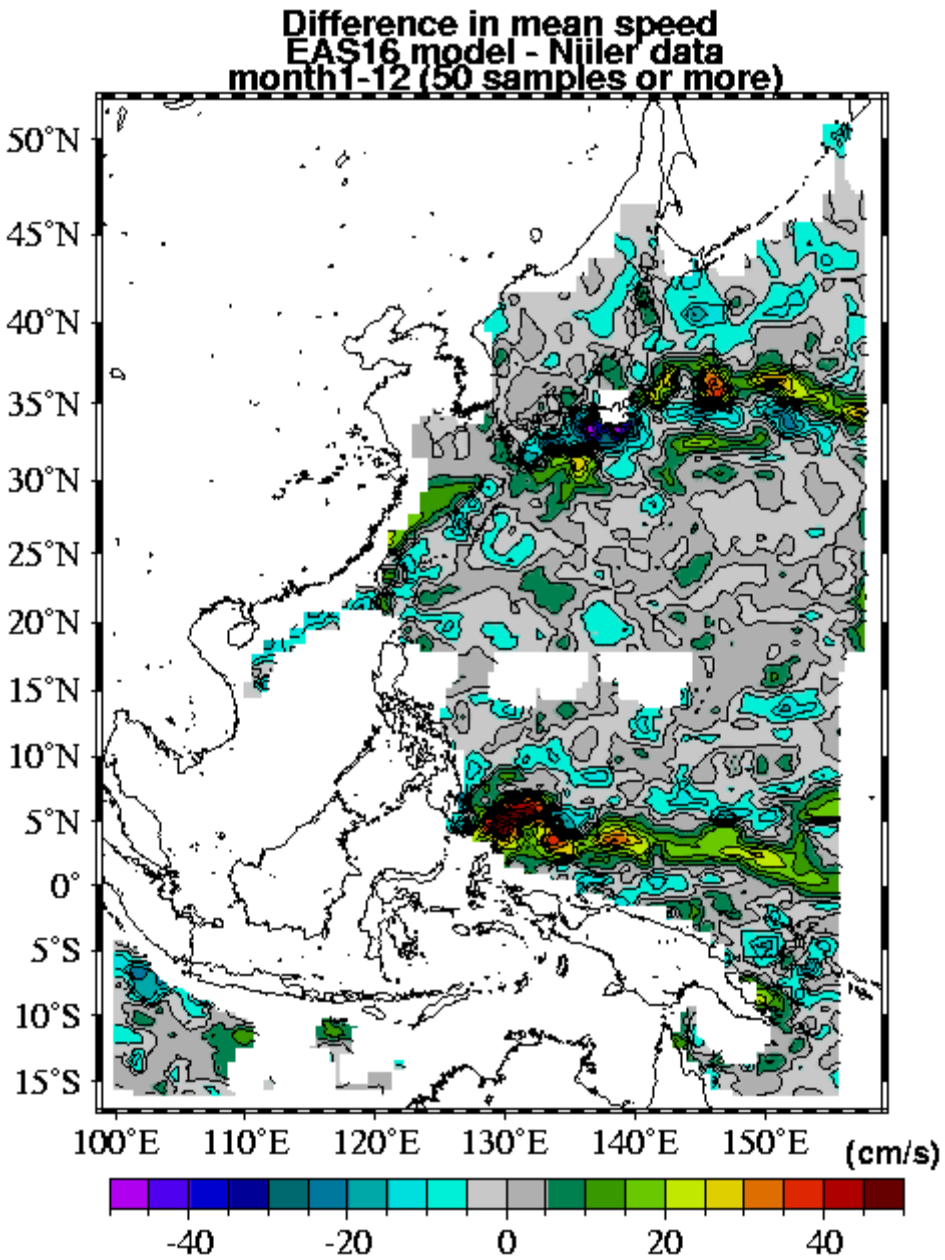
Figure 26. Difference in mean speed, EAS16 model – Niiler data, for the average of months 1 through 12. For Niller data, all available years were used for EAS16 model, results from years 2001 through 2003 were used. Only bins with more than 50 u&v pair were used.
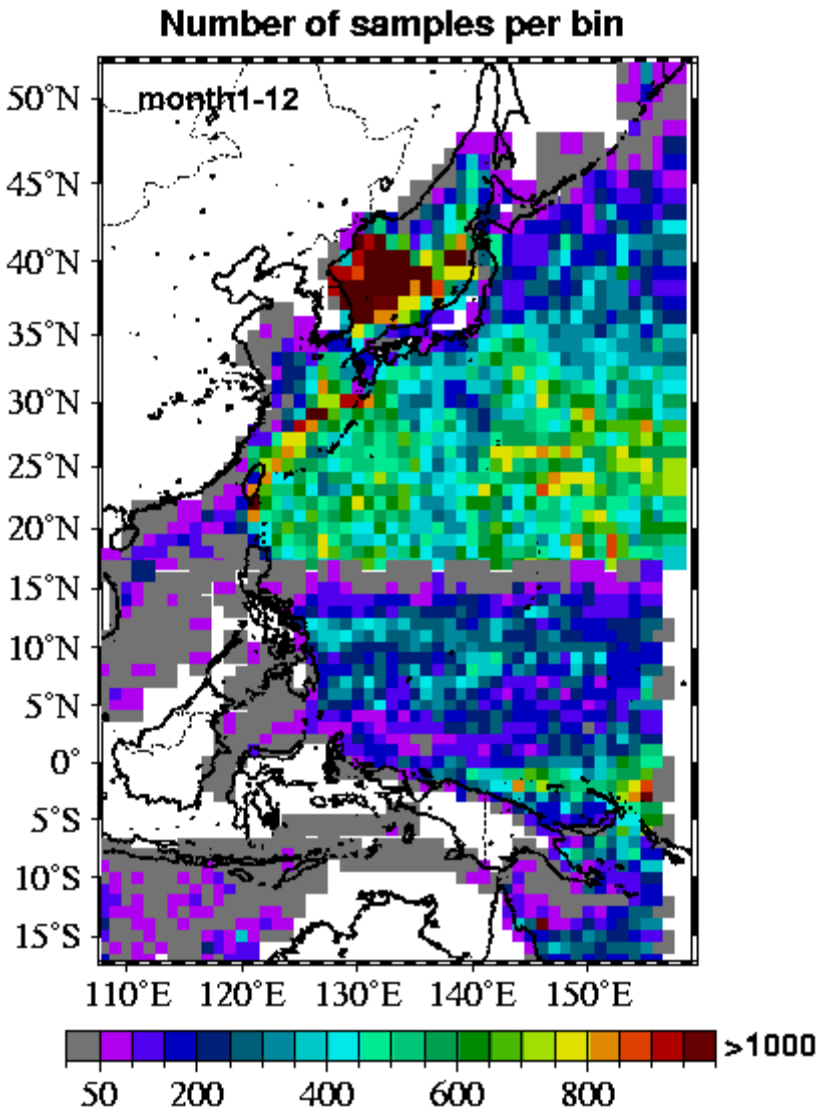
Figure 27. Number of u&v pair per 1°X1^{o} bin for Niiler drifter data.
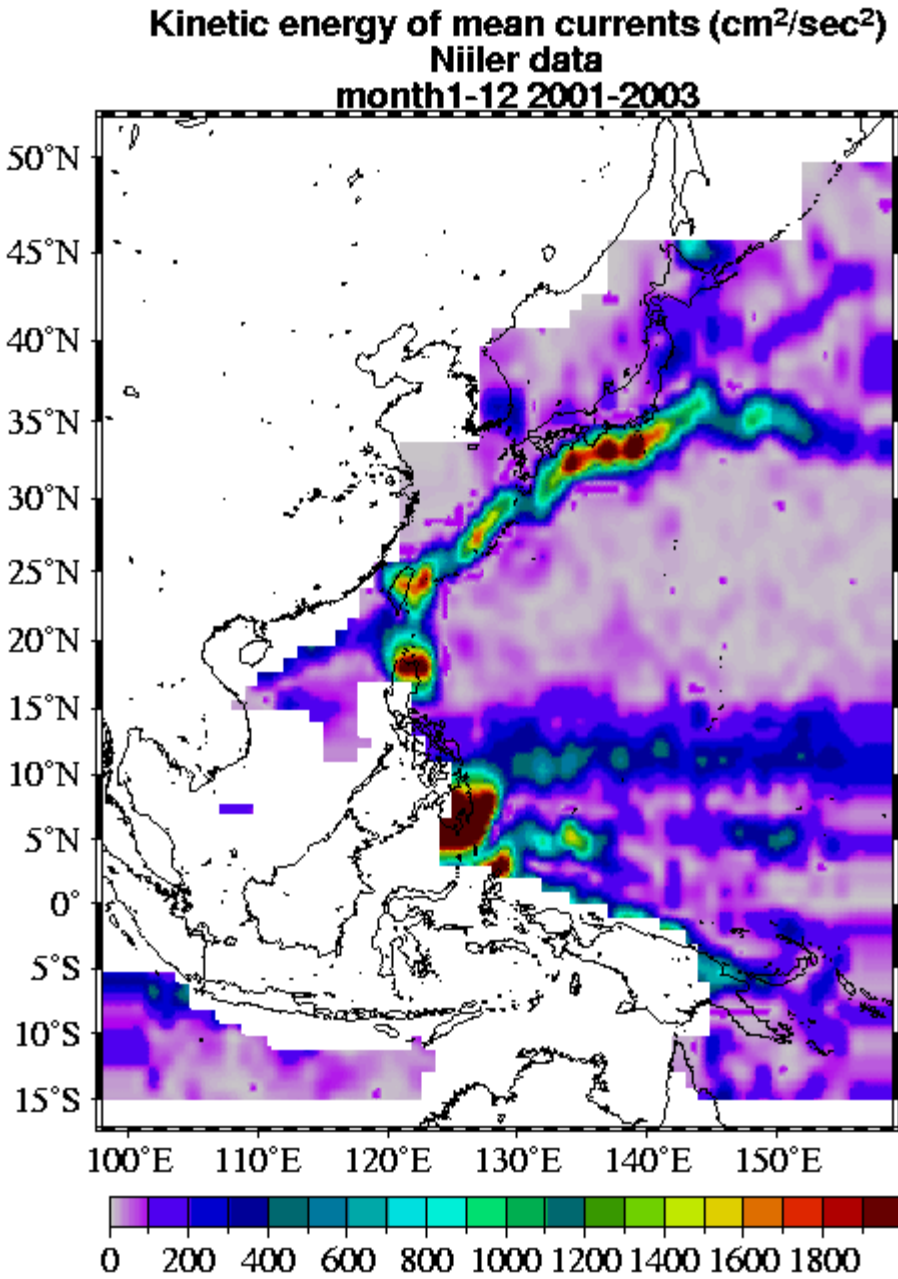
Figure 28a. Kinetic energy computed for each bin from the u&v pairs from the Niiler drifter data.
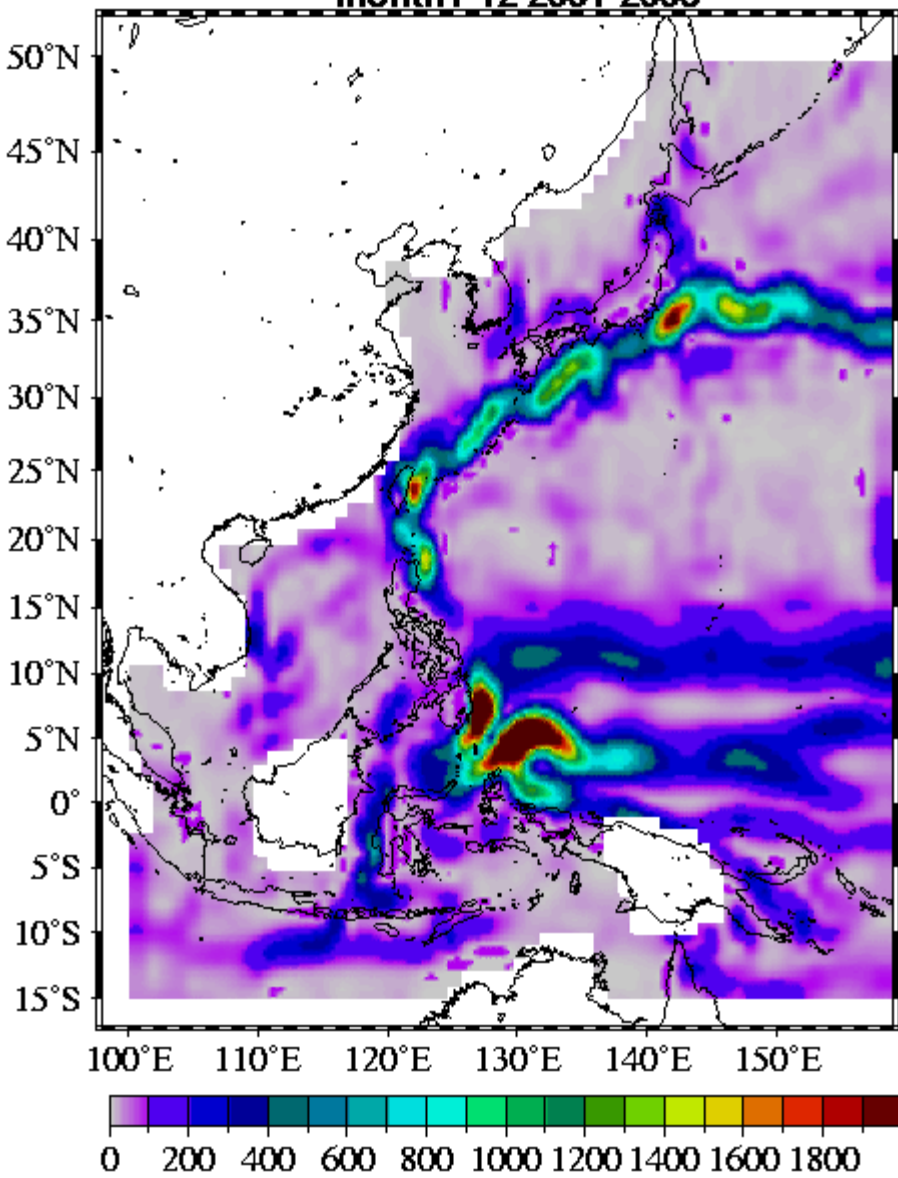
Figure 28b. Kinetic energy computed for each bin from the u&v pairs from the EAS16 model.
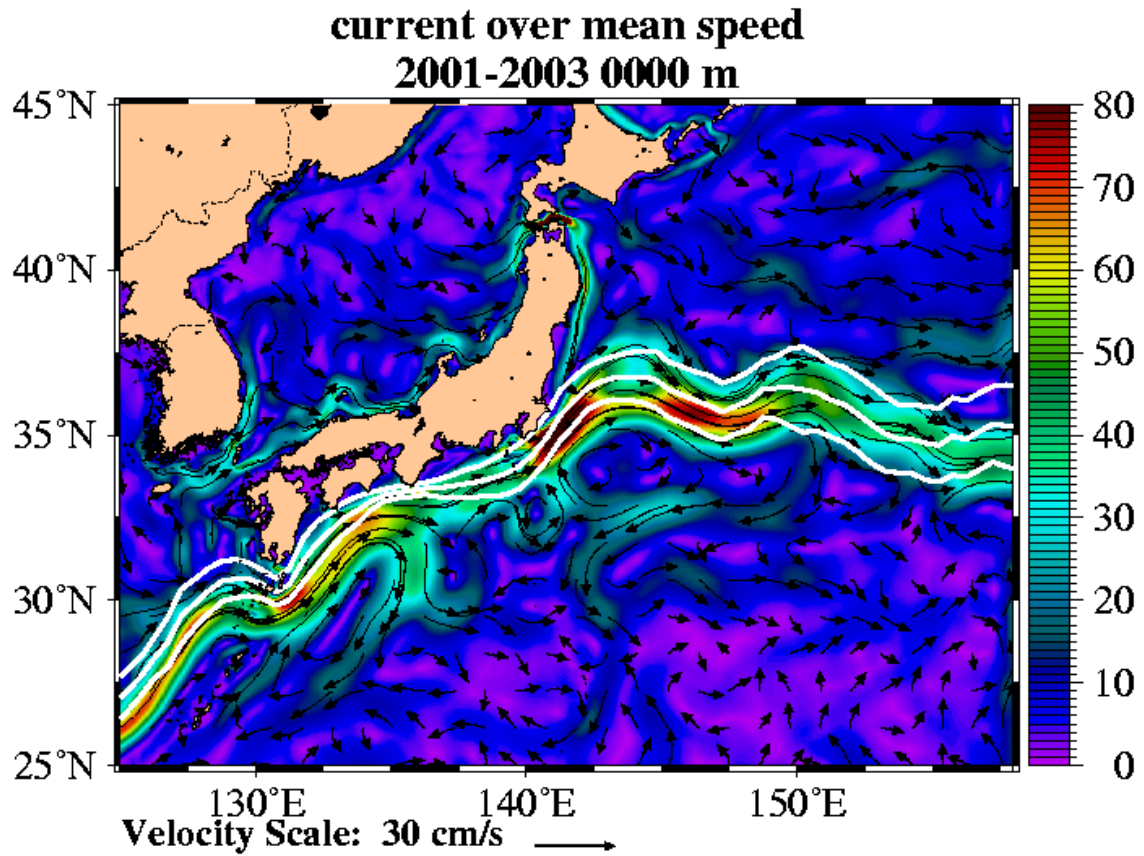
Figure 29a. Annual mean currents from EAS16 NCOM for years 2001-2003. Bogus of mean position of the Kuroshio from NAVO for years 2001-2003 with +- 1 standard deviation (white lines).
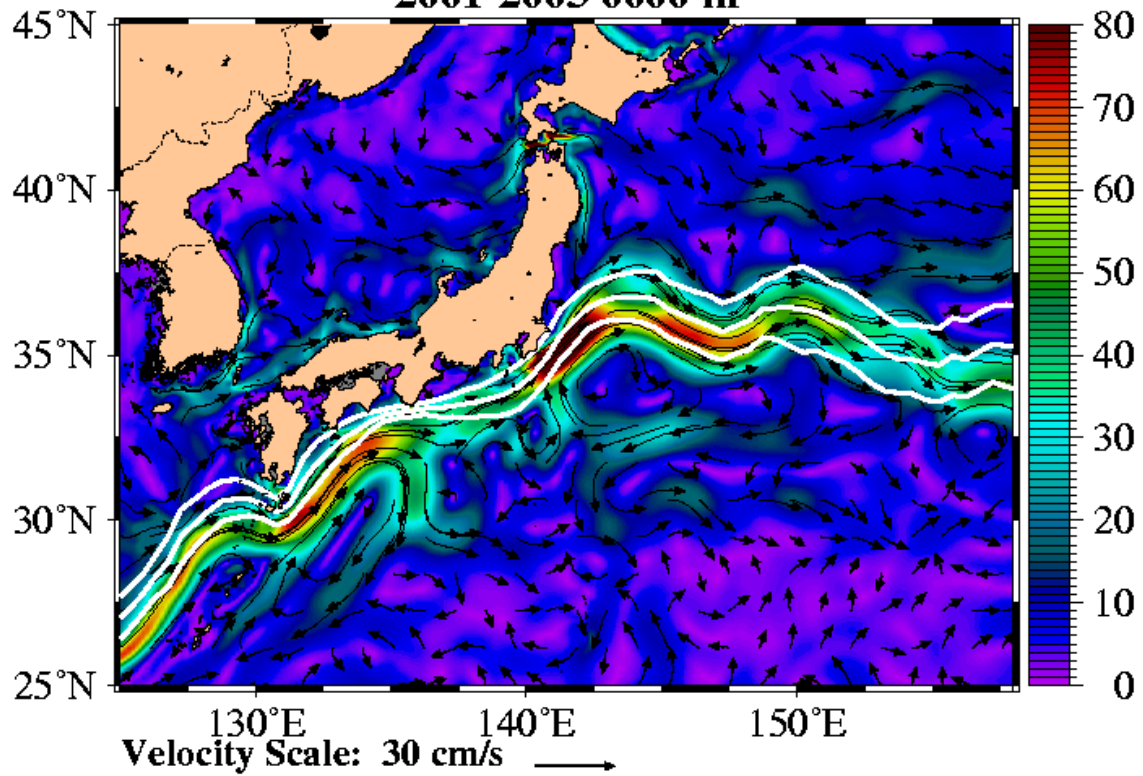
Figure 29b. Annual mean currents from Global NCOM for years 2001-2003. Bogus of mean position of the Kuroshio from NAVO for years 2001-2003 with +- 1 standard deviation (white lines).
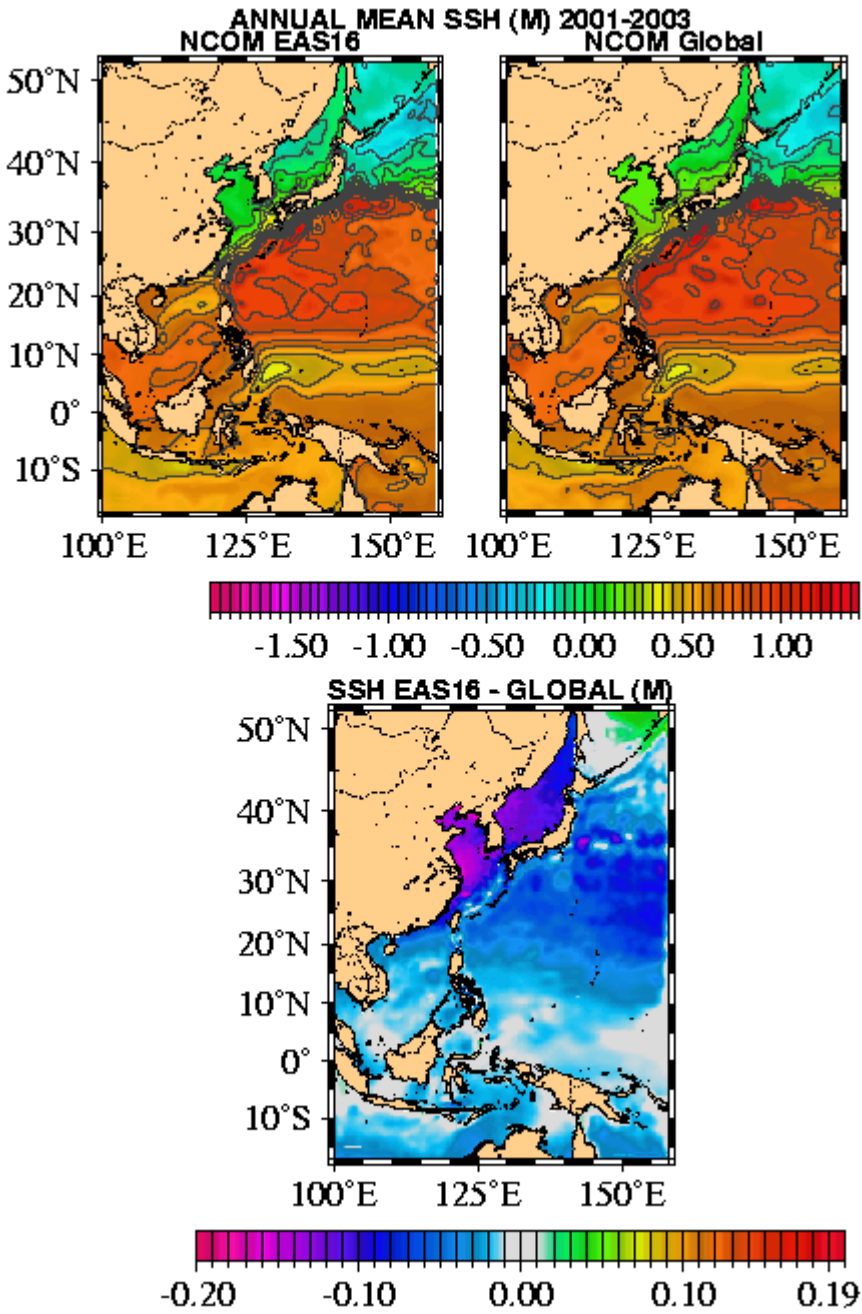
Figure 30. Comparison of sea surface height from EAS16 model and Global model (upper panels). Difference between EAS16 and Global ssh (m) (lower panel).
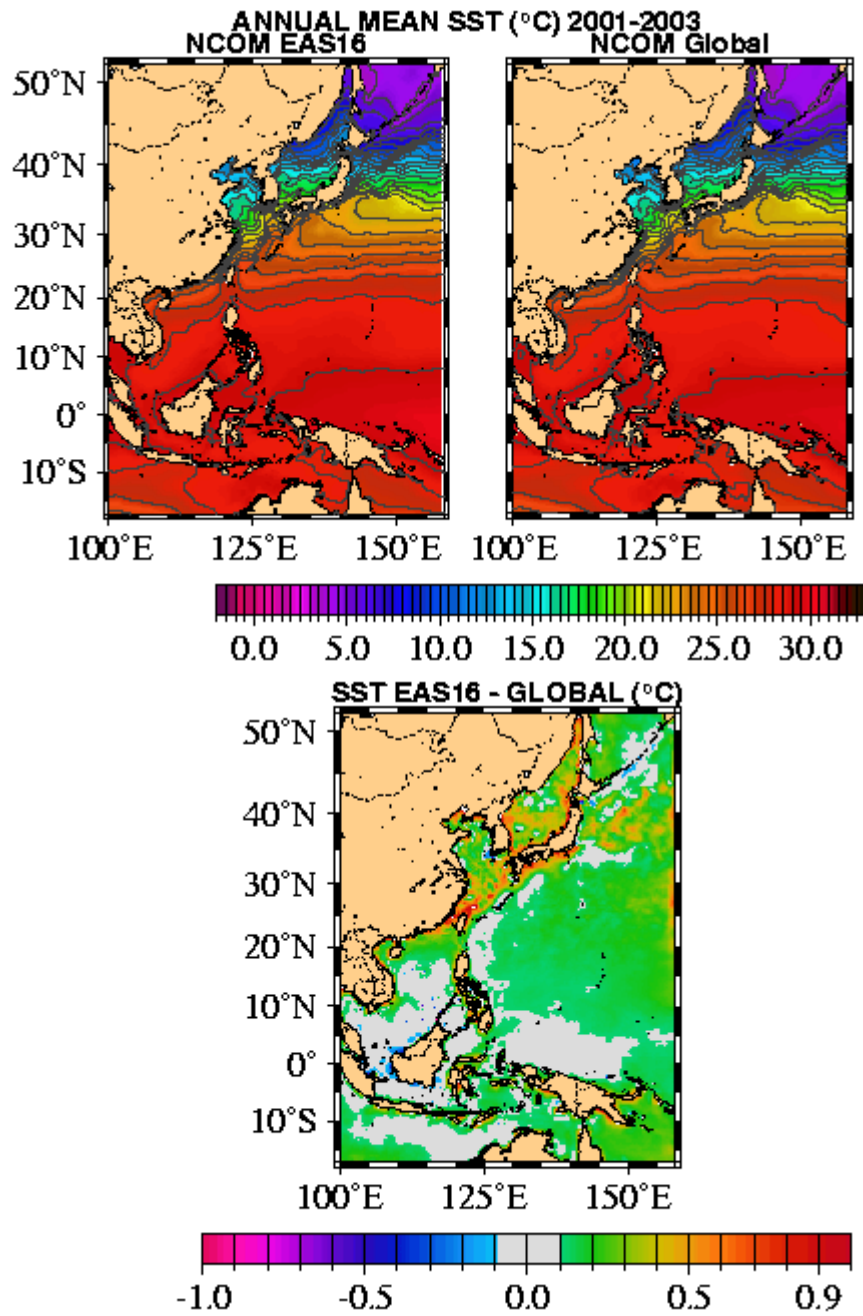
Figure 31. Comparison of sea surface temperature from EAS16 model and Global model (upper panels). Difference between EAS16 and Global sst (^{o}C) (lower panel).
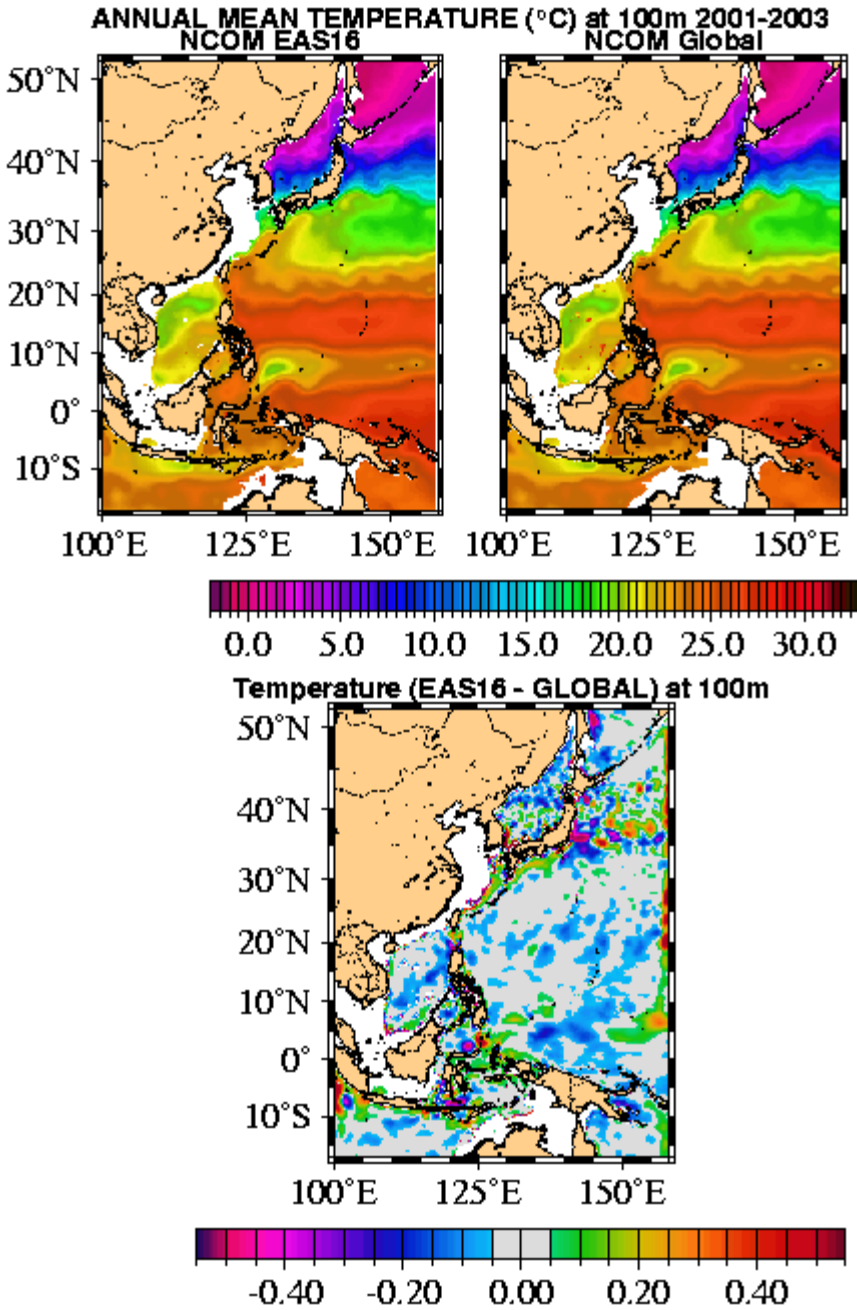
Figure 32. Comparison of temperature at 100 m from EAS16 model and Global model (upper panels). Difference between EAS16 and Global temperature at 100m (^{o}C) (lower panel).
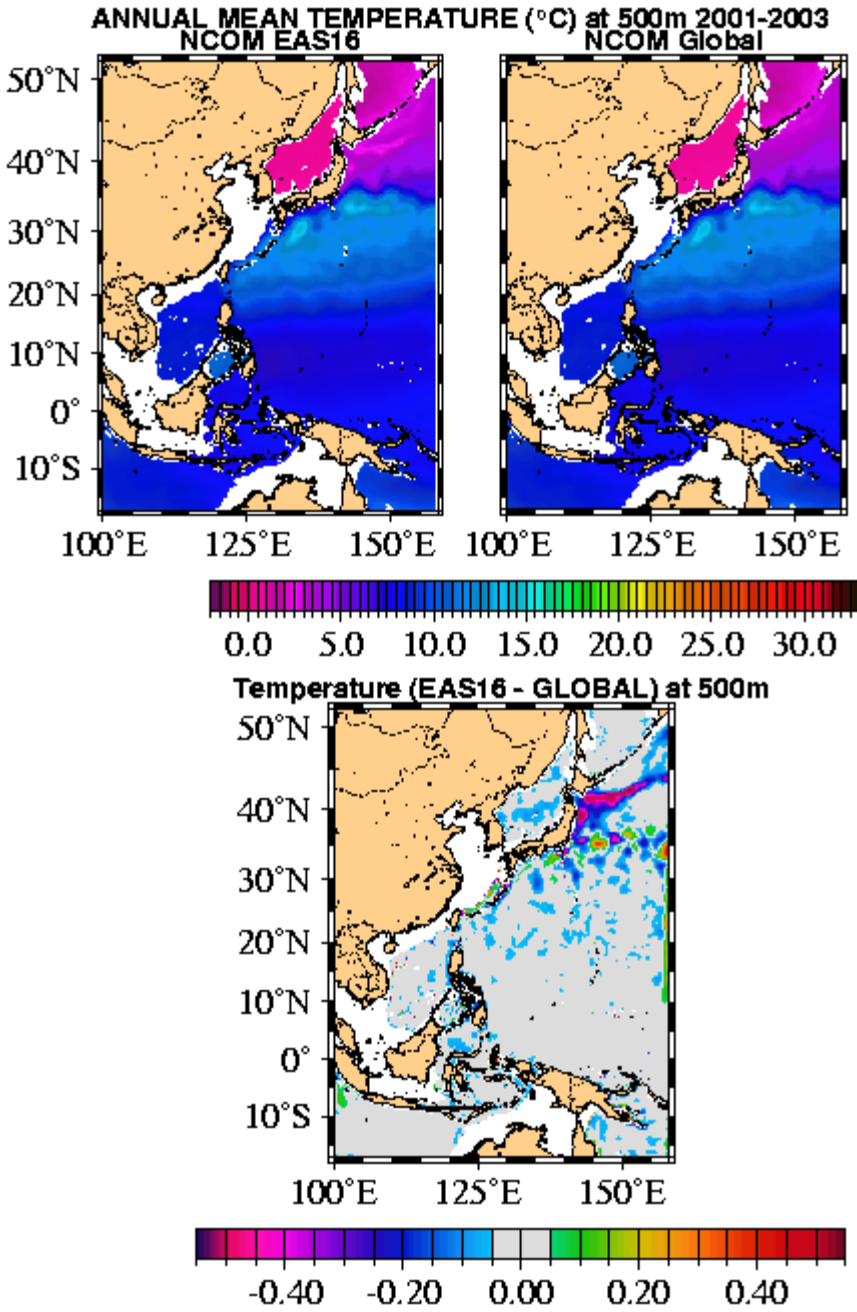
Figure 33. Comparison of temperature at 500 m from EAS16 model and Global model (upper panels). Difference between EAS16 and Global temperature at 500m (^{o}C) (lower panel).
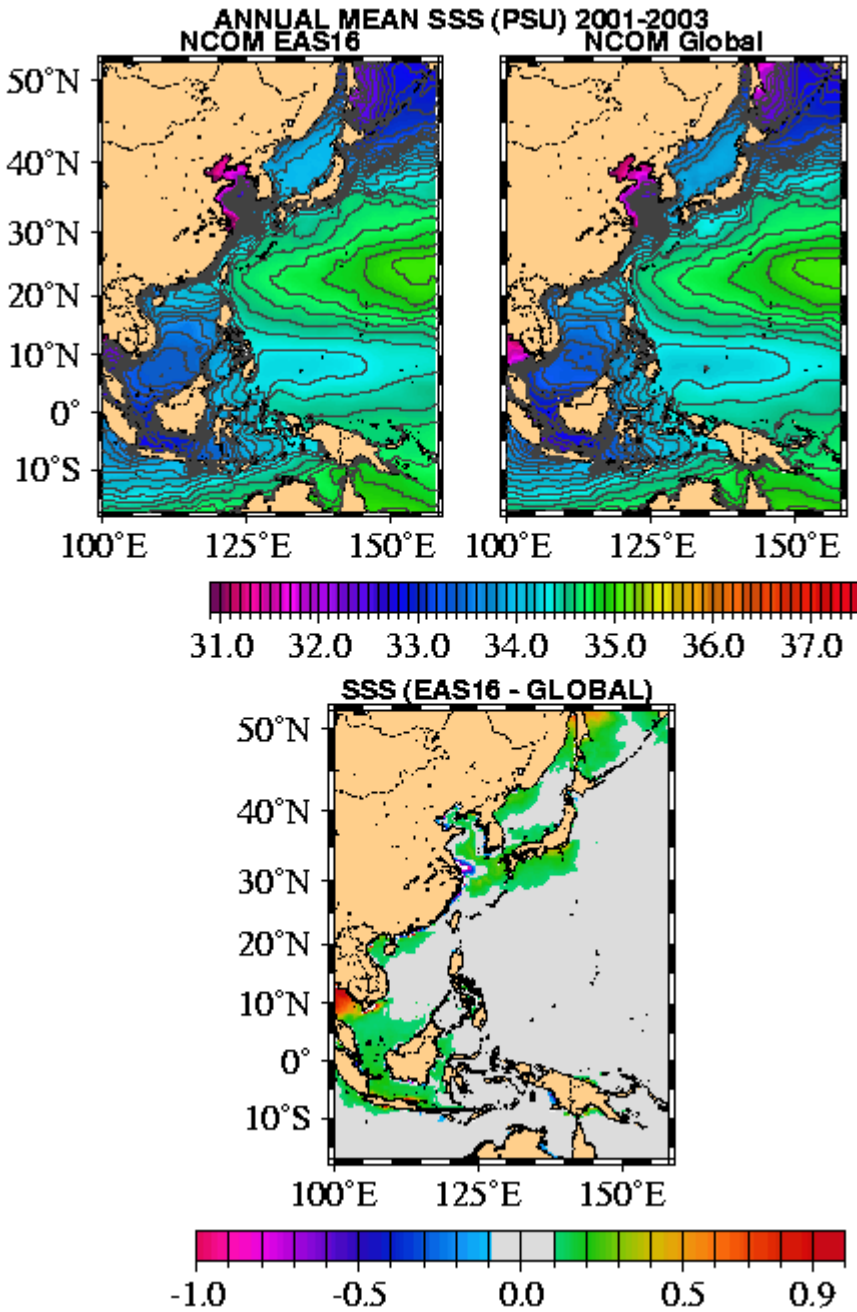
Figure 34. Comparison of surface salinity from EAS16 model and Global model (upper panels). Difference between EAS16 and Global surface salinity (ppt) (lower panel).
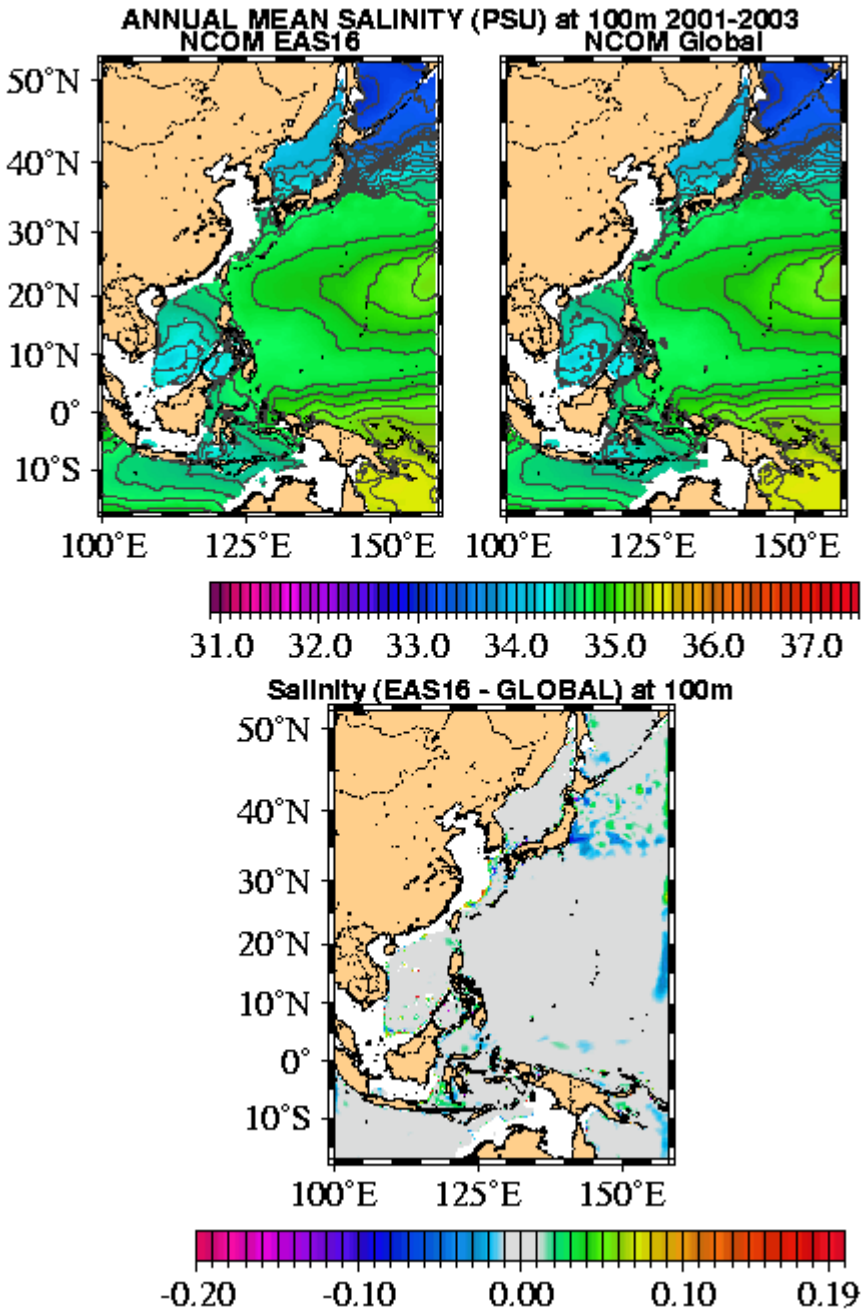
Figure 35. Comparison of salinity at 100m from EAS16 model and Global model (upper panels). Difference between EAS16 and Global salinity at 100m (ppt) (lower panel).
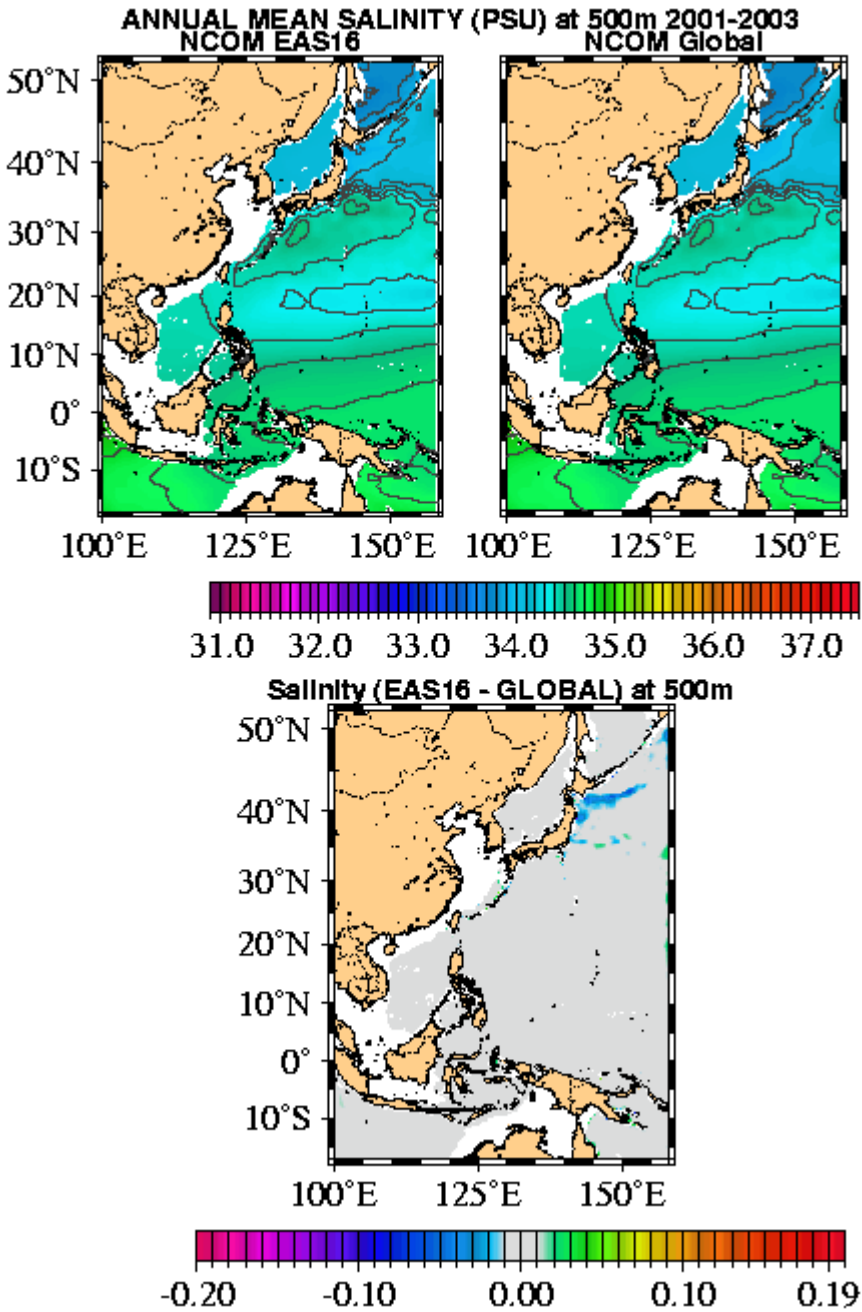
Figure 36. Comparison of salinity at 500m from EAS16 model and Global model (upper panels). Difference between EAS16 and Global salinity at 500m (ppt) (lower panel).
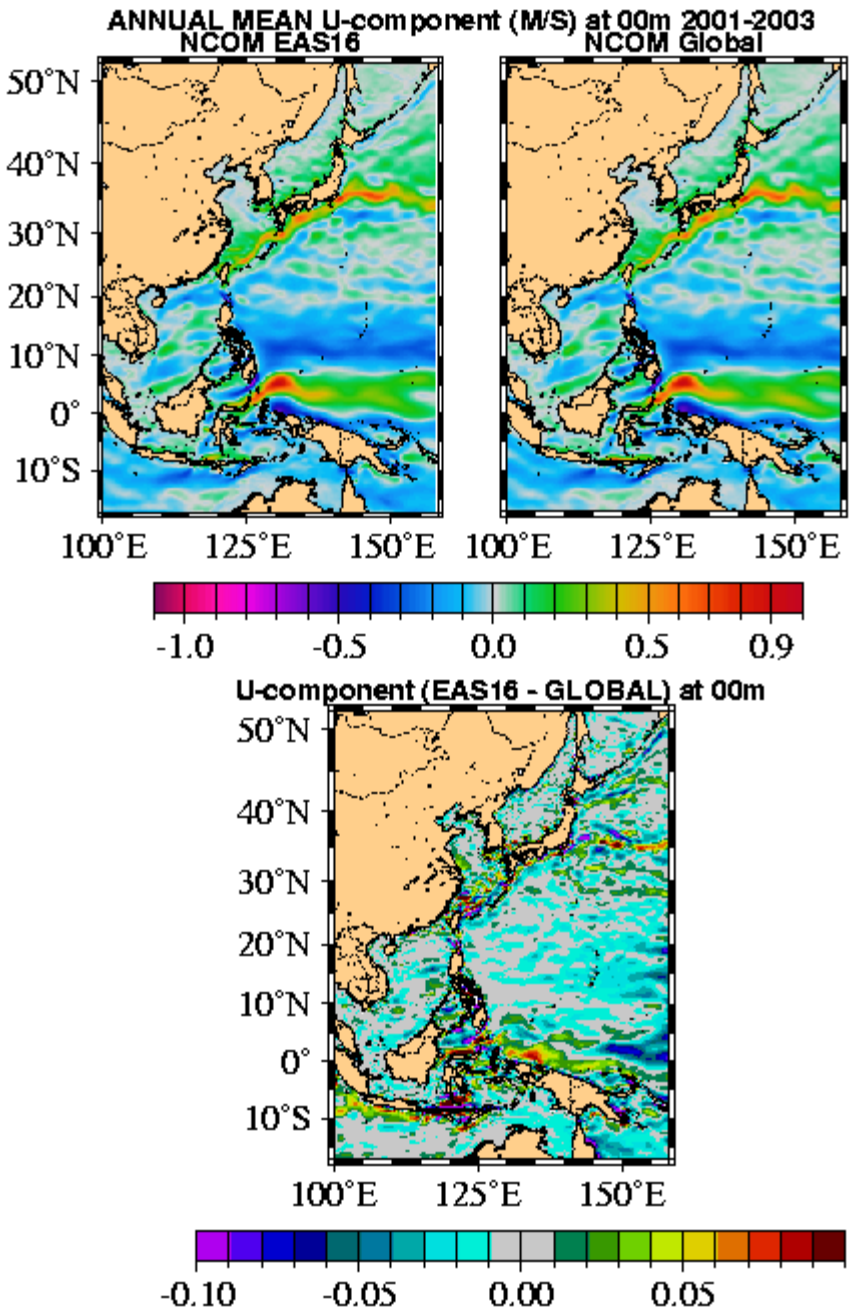
Figure 37. Comparison of surface U-component of velocity from EAS16 model and Global model (upper panels). Difference between EAS16 and Global surface U-component of velocity (m/sec) (lower panel).
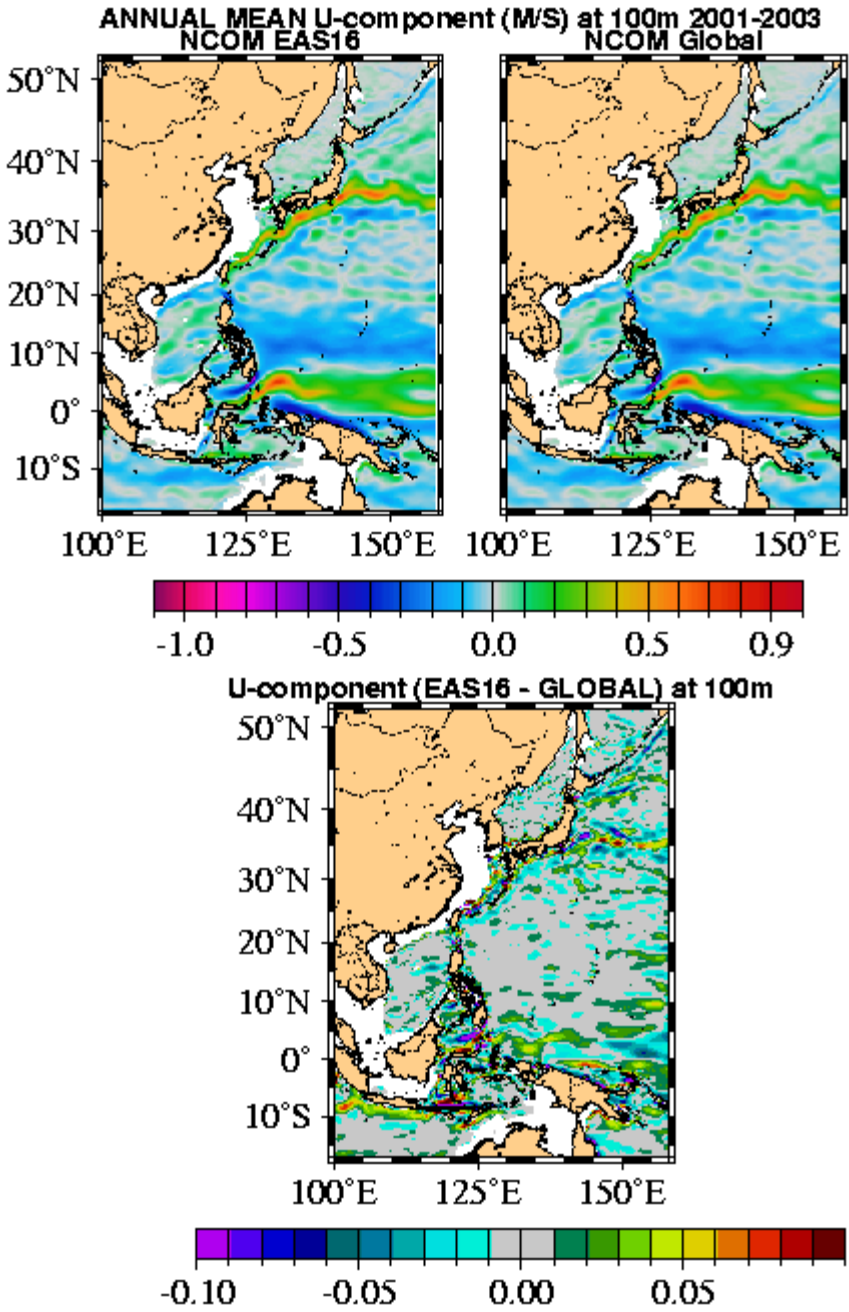
Figure 38. Comparison of U-component of velocity at 100m from EAS16 model and Global model (upper panels). Difference between EAS16 and Global U-component of velocity (m/sec) at 100m (lower panel).
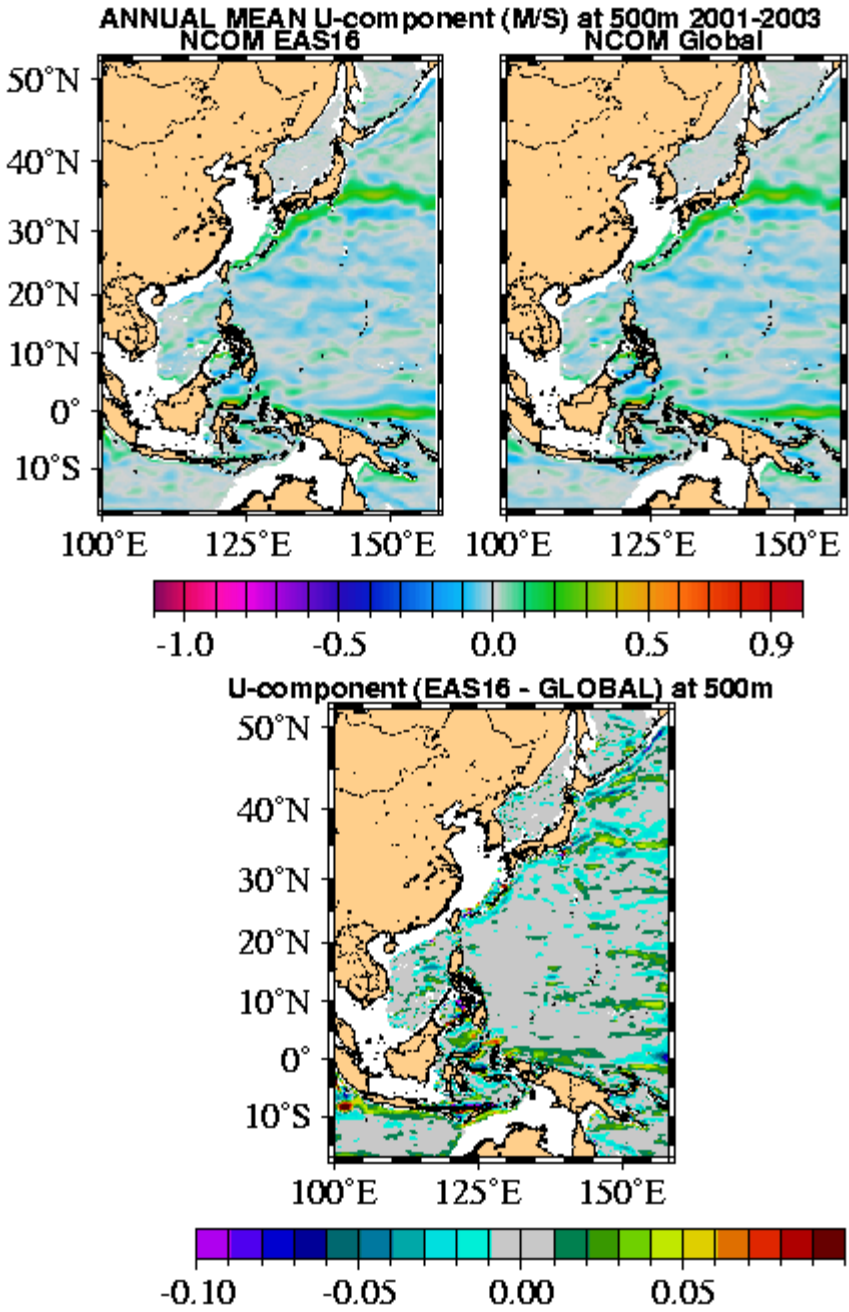
Figure 39. Comparison of U-component of velocity at 500m from EAS16 model and Global model (upper panels). Difference between EAS16 and Global U-component of velocity (m/sec) at 500m (lower panel).
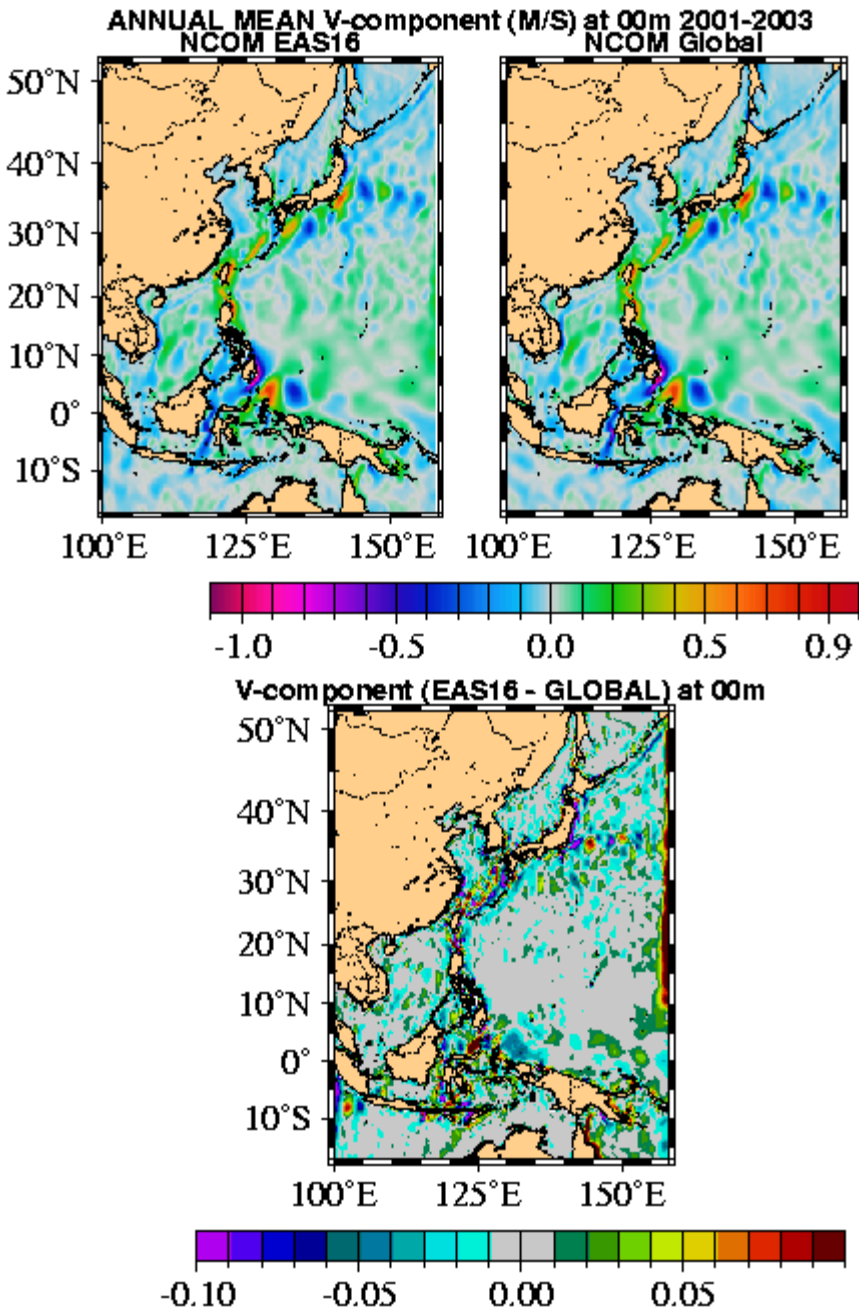
Figure 40. Comparison of surface V-component of velocity from EAS16 model and Global model (upper panels). Difference between EAS16 and Global surface V-component of velocity (m/sec) (lower panel).
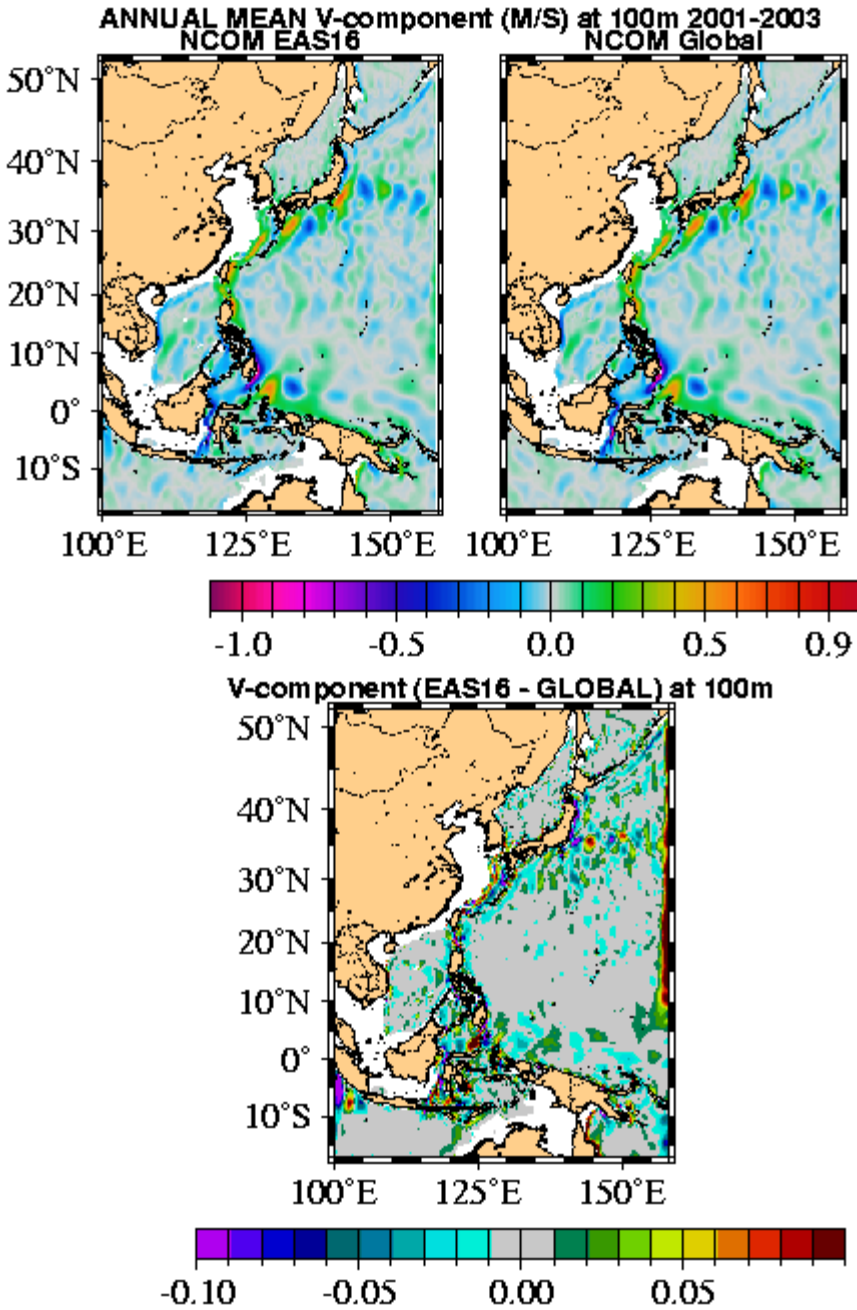
Figure 41. Comparison of V-component of velocity at 100m from EAS16 model and Global model (upper panel). Difference between EAS16 and Global V-component of velocity (m/sec) at 100m (lower panel).
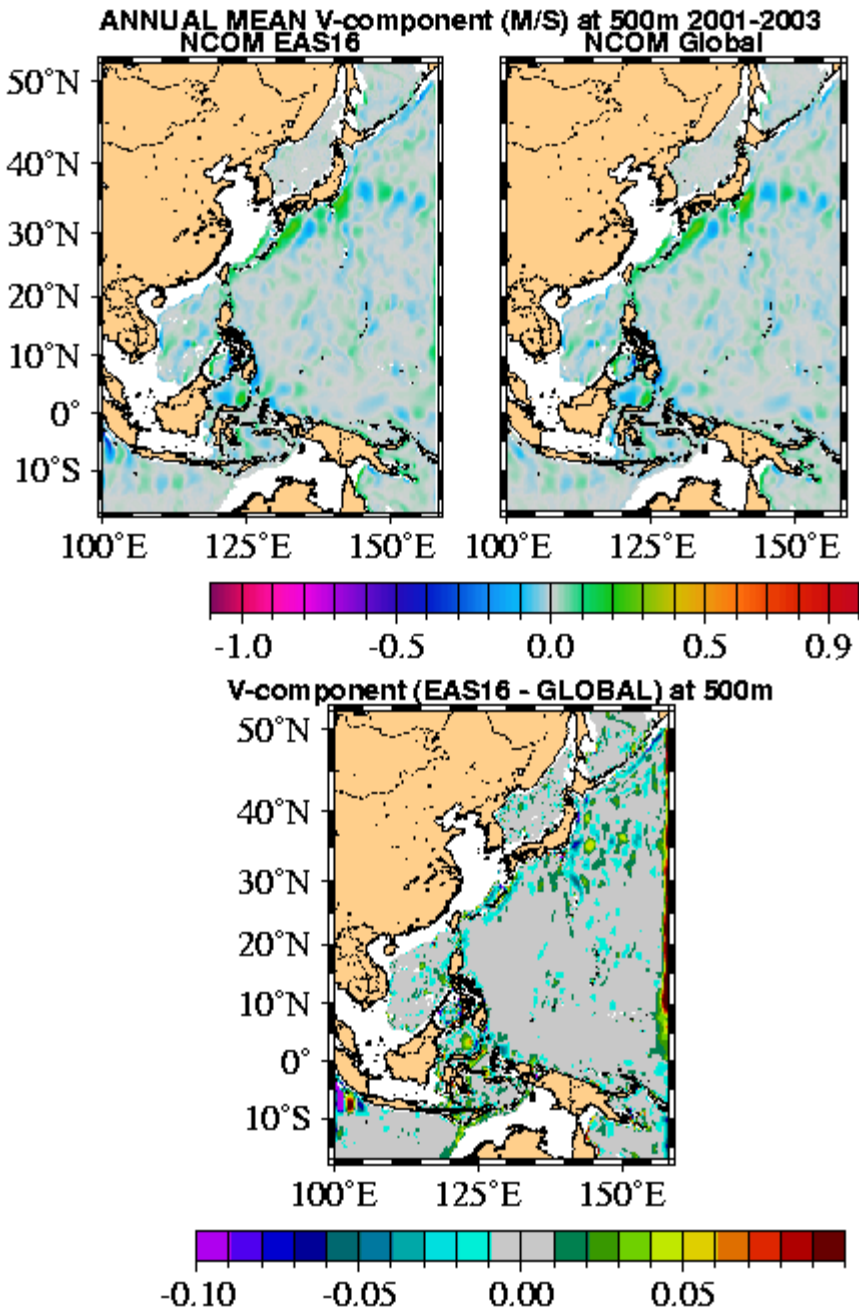
Figure 42. Comparison of V-component of velocity at 500m from EAS16 model and Global model (upper panel). Difference between EAS16 and Global V-component of velocity (m/sec) at 500m (lower panel).
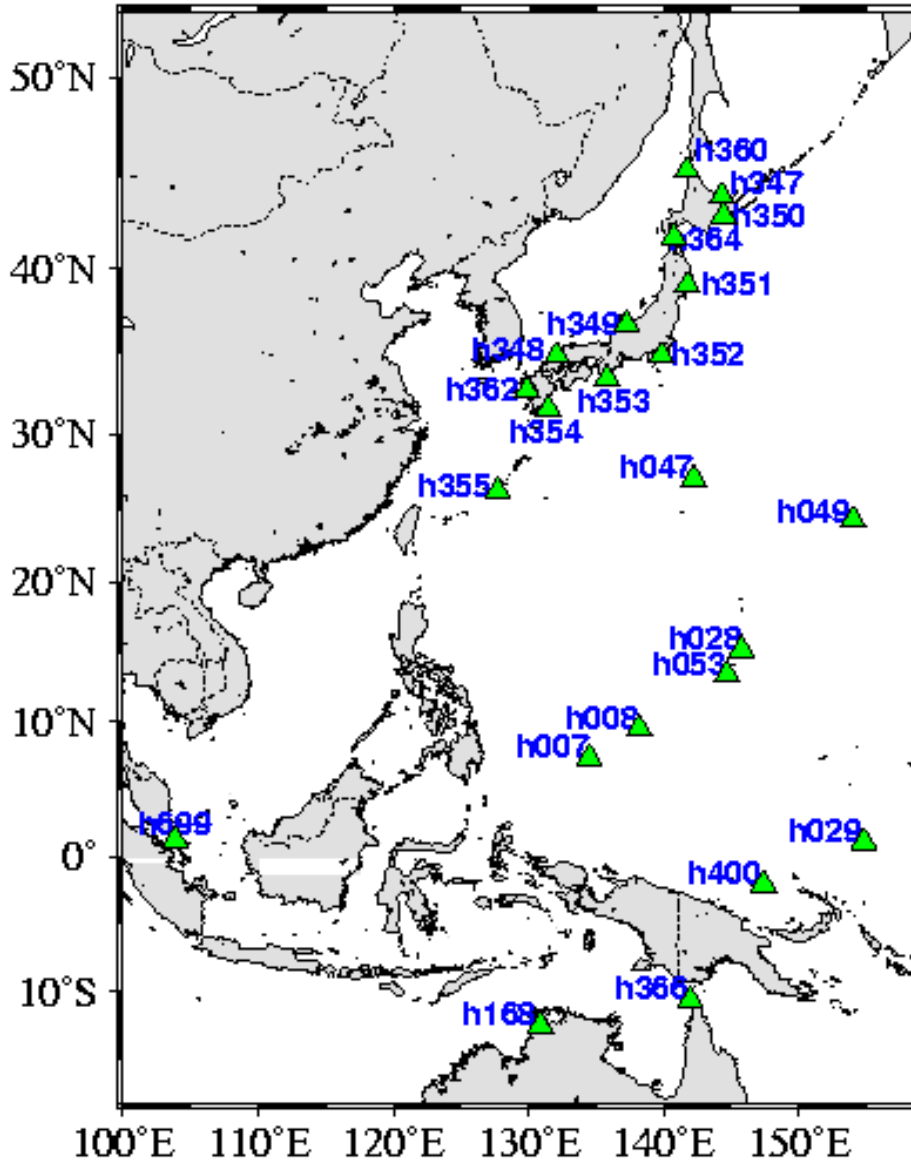
Figure 43. Location of tide gauges from University of Hawaii sea level database for 2004.
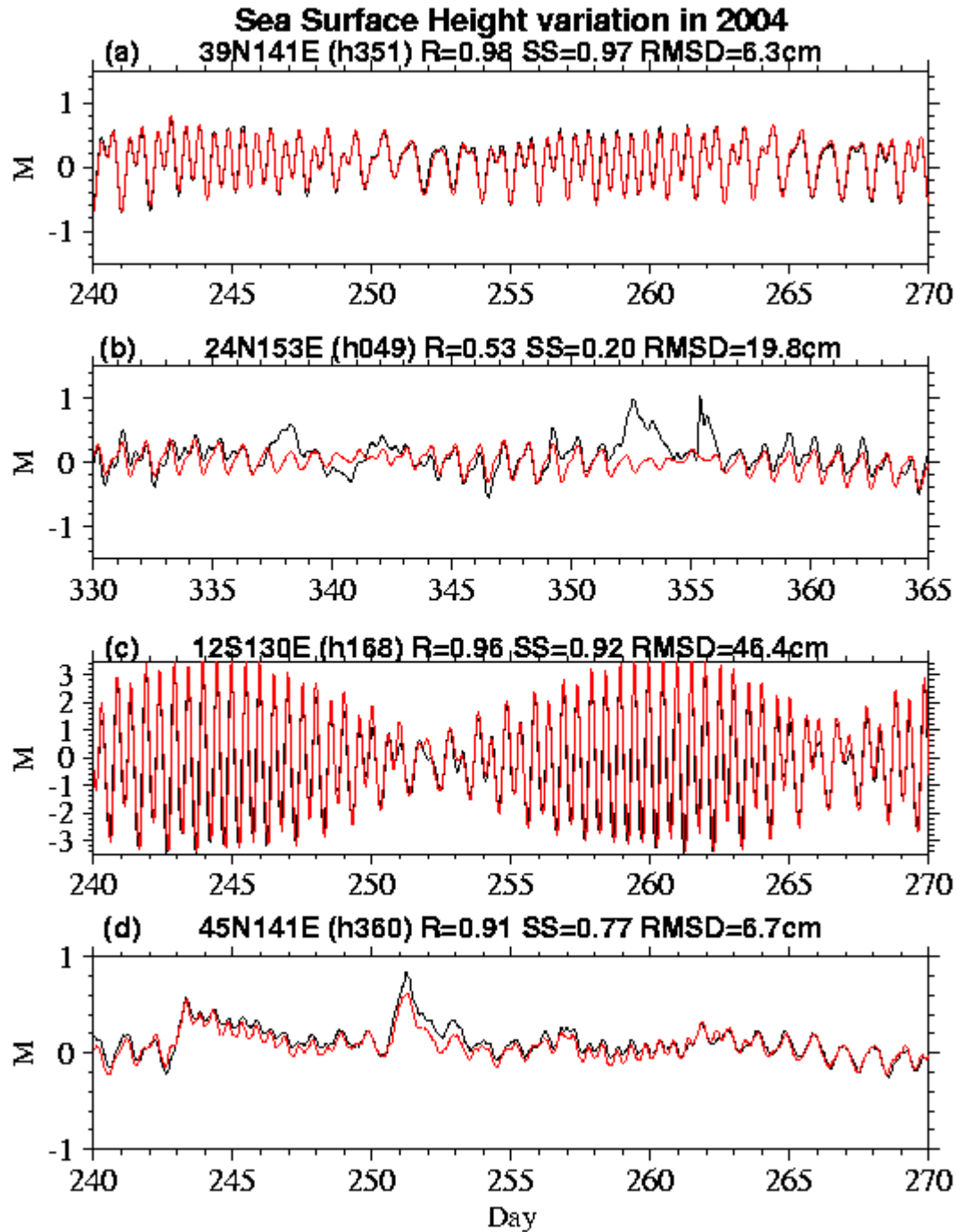
Figure 44. Thirty day time series of sea level variation for four stations from 2004. Tide gauge (black line), EAS16 model (red line). R is correlations coefficient, SS is skill score, and RMSD is root mean square difference. (Mean has been removed from each data set)
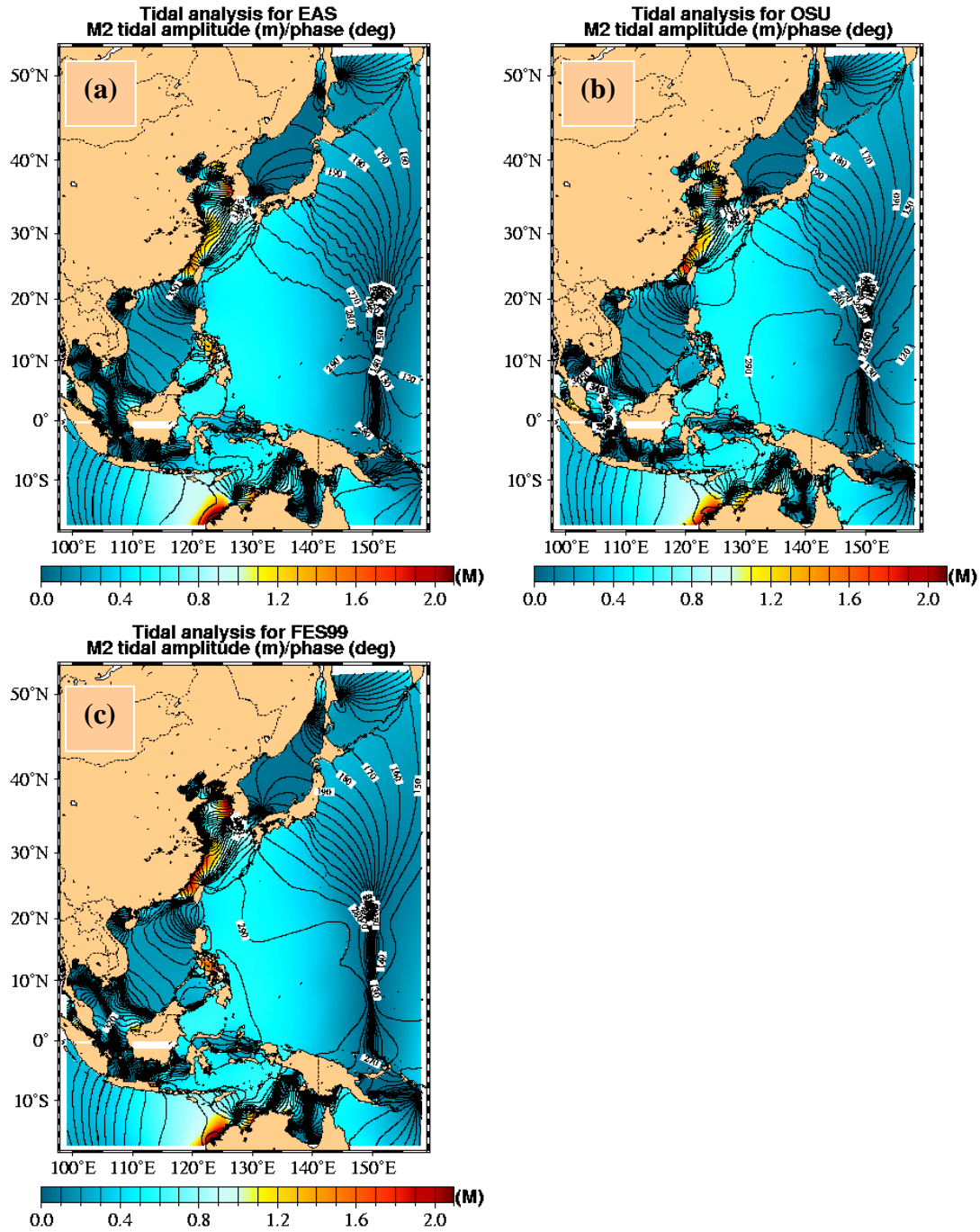
Figure 45. Co-tidal plots from M2 tidal constituent for (a) EAS16 model, (b) Oregon State University model and (c) FES99 model. Amplitudes are in meters and phases are in degrees.
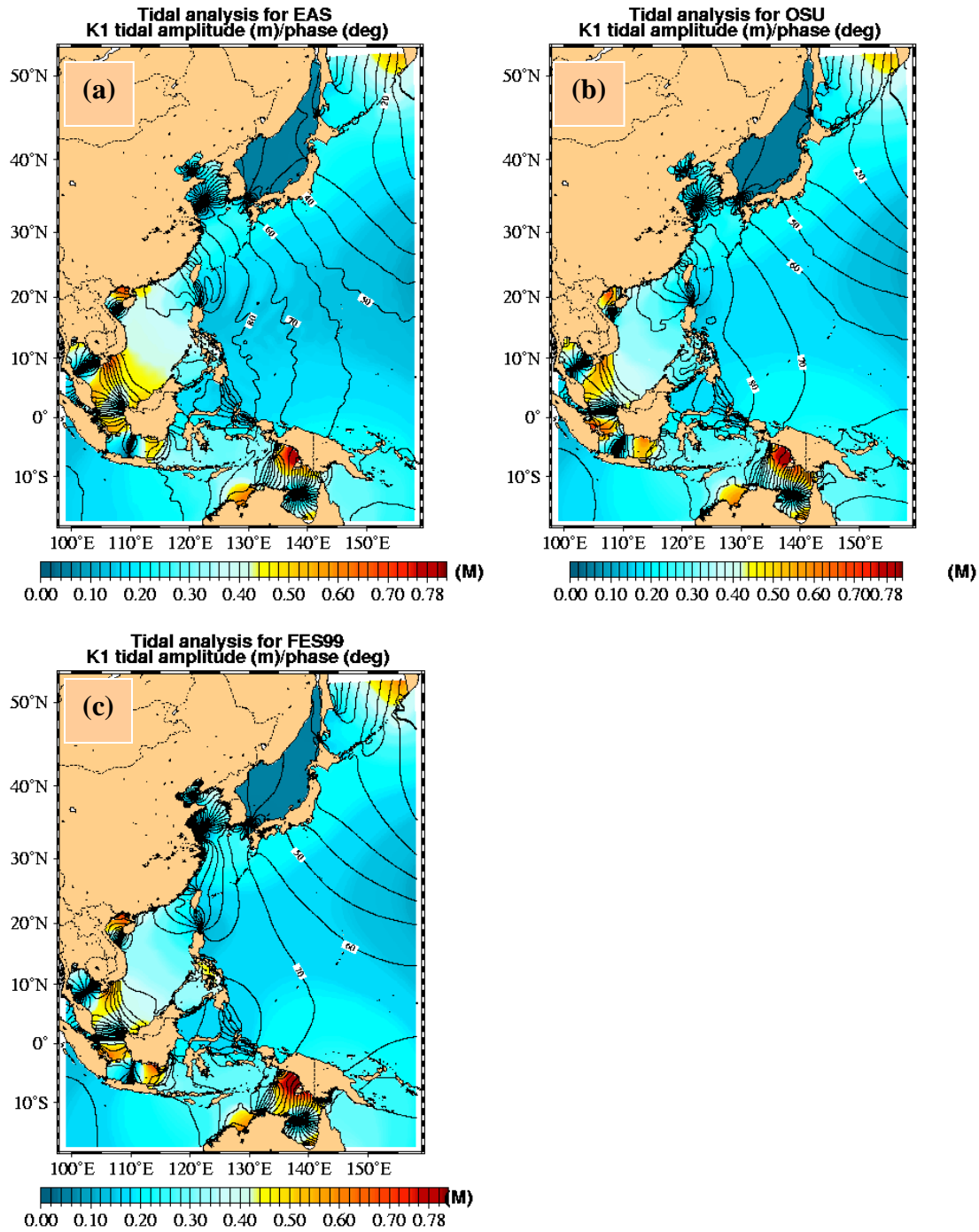
Figure 46. Co-tidal plots from K1 tidal constituent for (a) EAS16 model, (b) Oregon State University model and (c) FES99 model. Amplitudes are in meters and phases are in degrees.
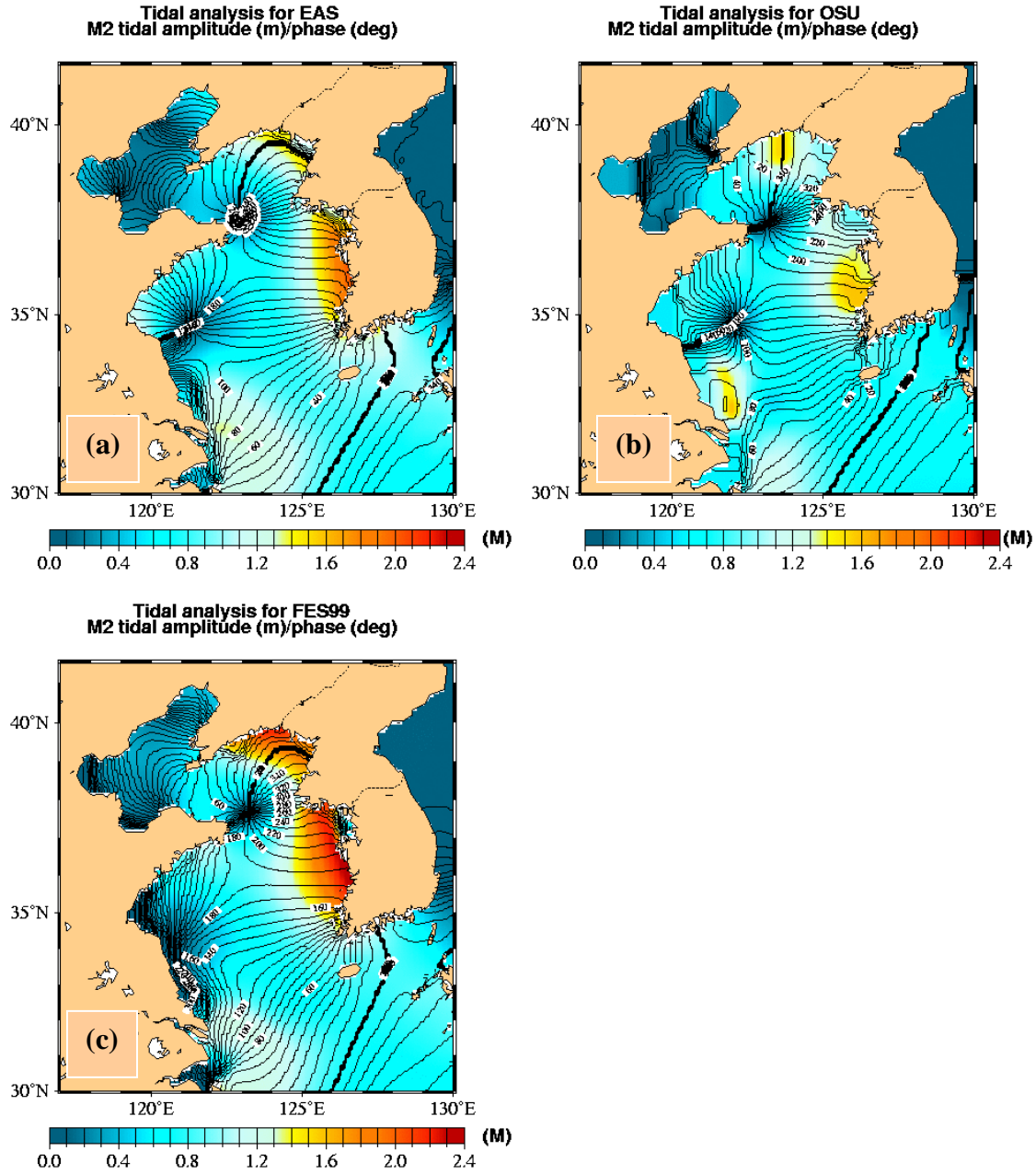
Figure 47. Co-tidal plots from M2 tidal constituent for (a) EAS16 model, (b) Oregon State University model and (c) FES99 model. A closer look at the Yellow Sea and Bohai Bay. Amplitudes are in meters and phases are in degrees.
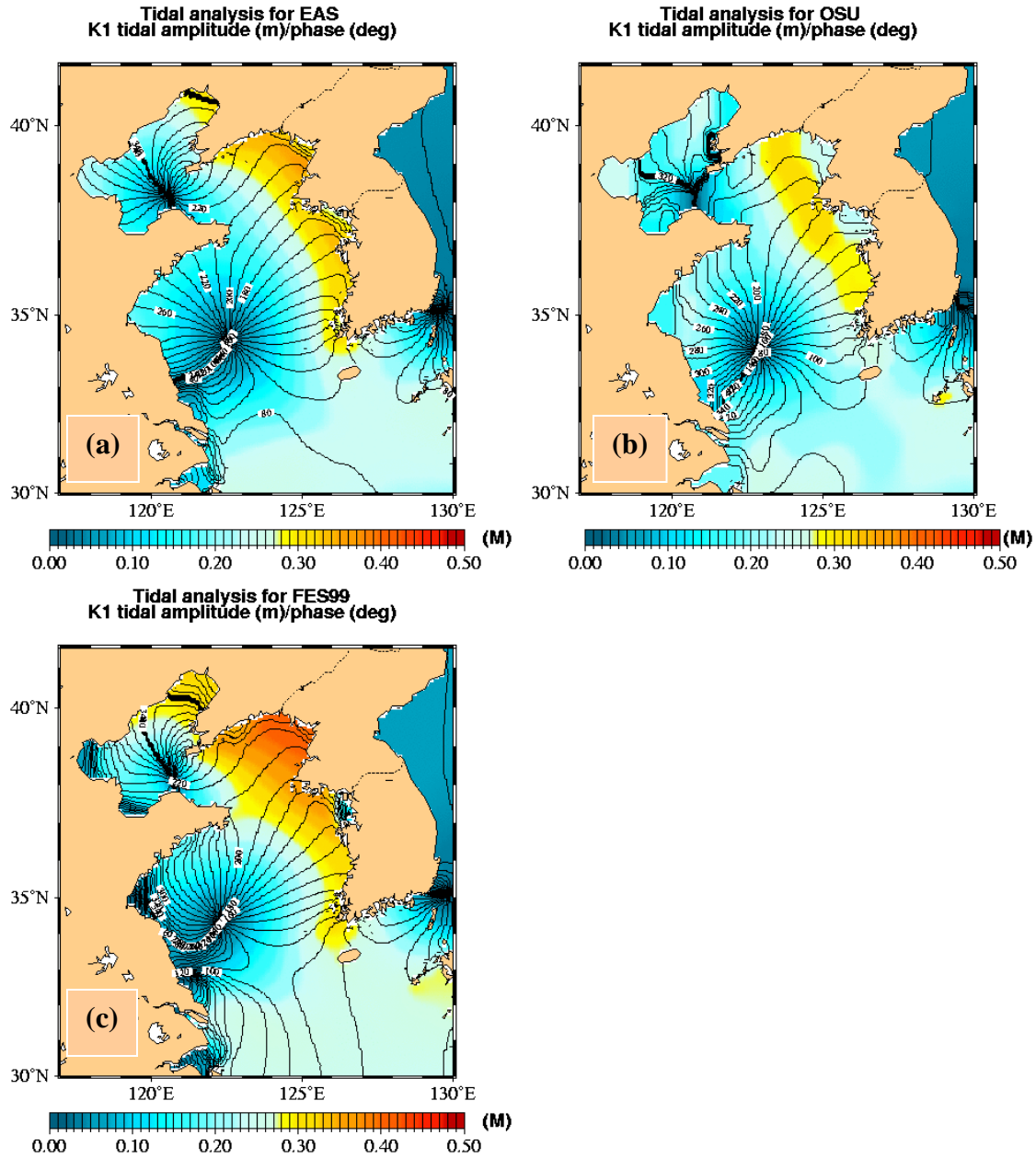
Figure 48. Co-tidal plots from K1 tidal constituent for (a) EAS16 model, (b) Oregon State University model and (c) FES99 model. A closer look at the Yellow Sea and Bohai Bay. Amplitudes are in meters and phases are in degrees.
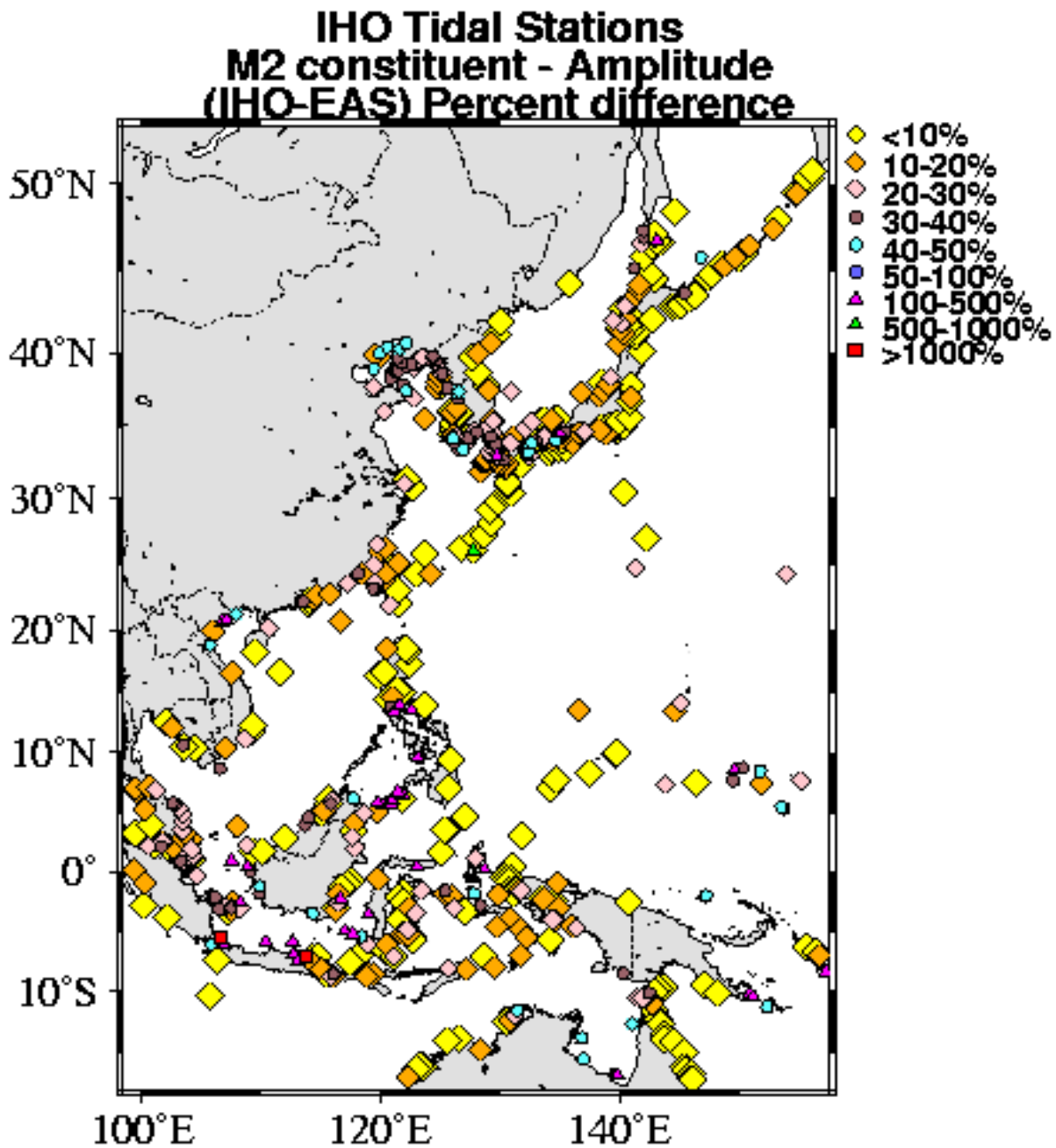
Figure 49. Percent error in tidal amplitude (M2 constituent) between IHO data values and EAS16 model values. The yellow and orange diamonds denote locations with percent error of less than 10 and 20 respectively. Pink diamonds 20-30% error. Colored circles denote % error of 30 to 100, triangles >100 and red squares >1000.
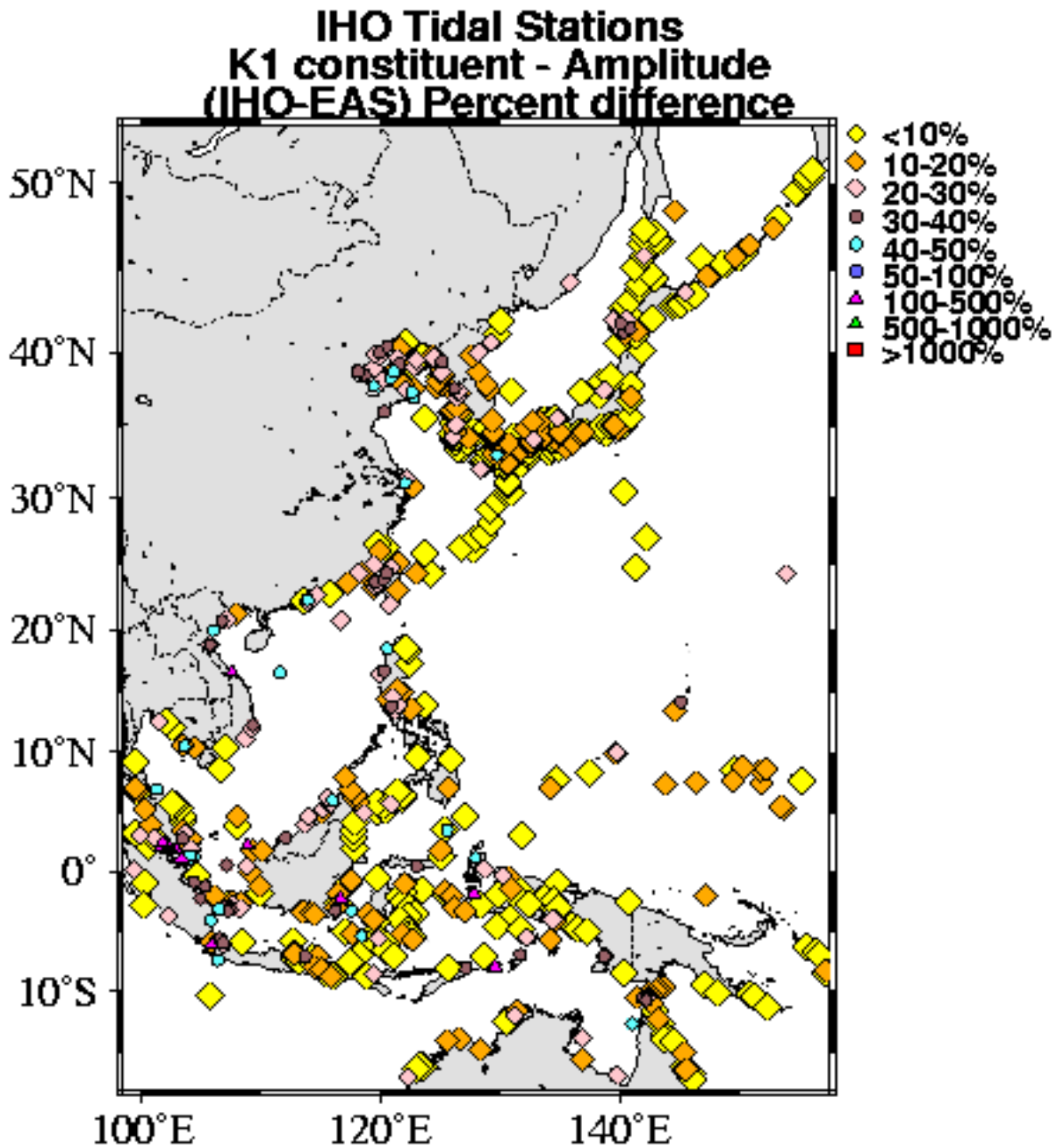
Figure 50. Percent error in tidal amplitude (K1 constituent) between IHO data values and EAS16 model values. The yellow and orange diamonds denote locations with percent error of less than 10 and 20 respectively. Pink diamonds 20-30% error. Colored circles denote % error of 30 to 100, triangles >100 and red squares >1000.
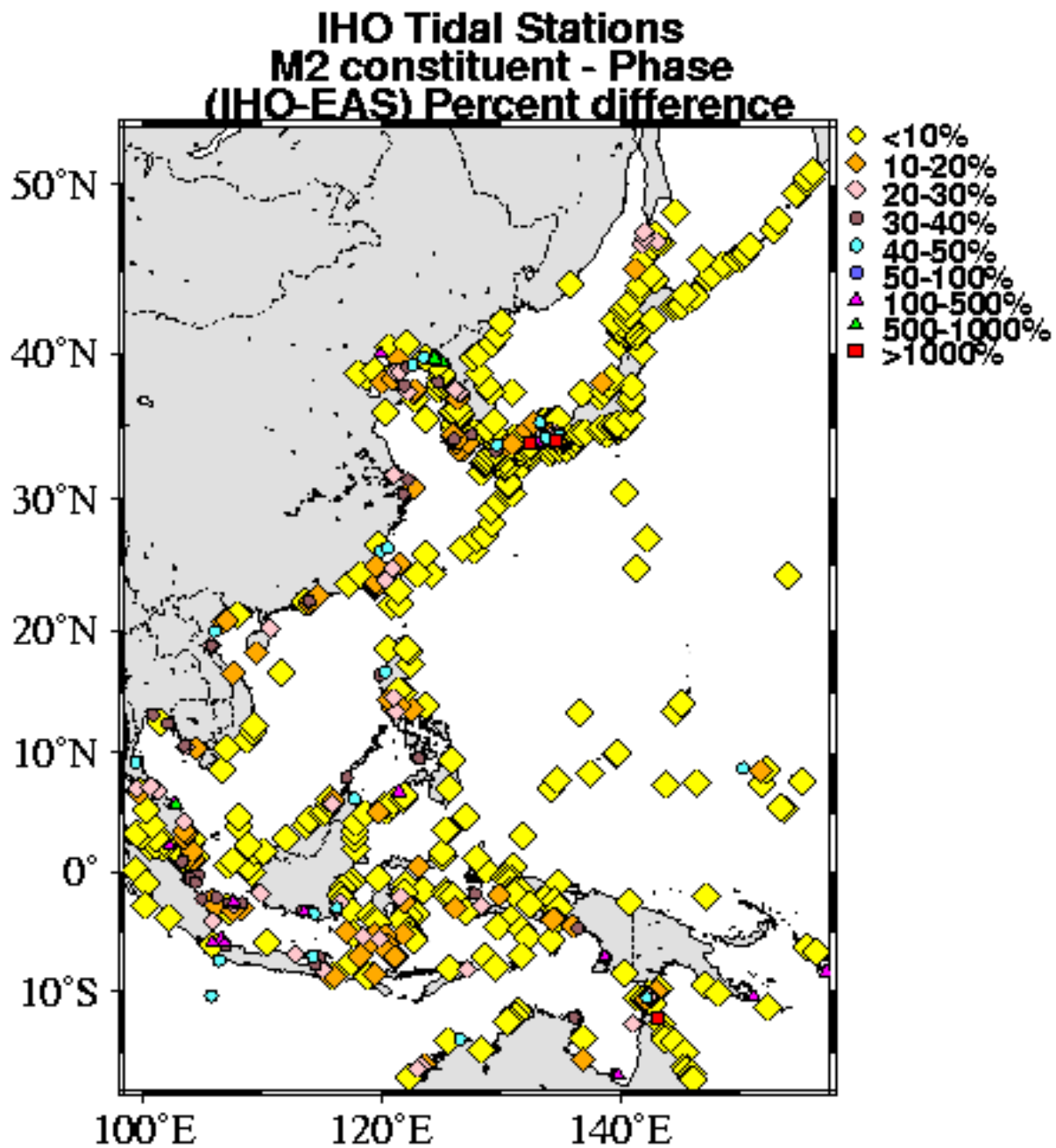
Figure 51. Percent error in tidal phase (M2 constituent) between IHO data values and EAS16 model values. The yellow and orange diamonds denote locations with percent error of less than 10 and 20 respectively. Pink diamonds 20-30% error. Colored circles denote % error of 30 to 100, triangles >100 and red squares >1000.
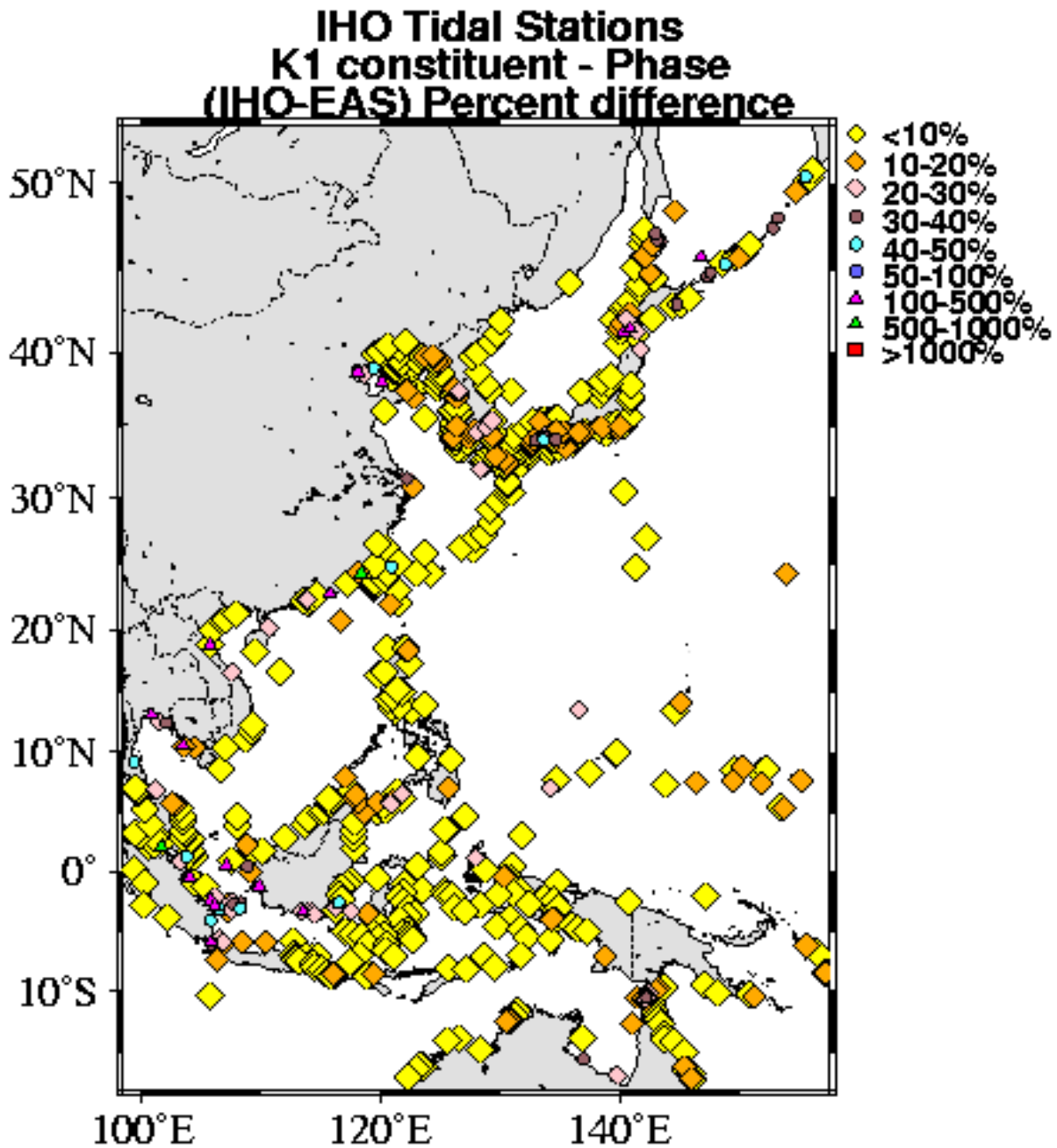
Figure 52. Percent error in tidal phase (K1 constituent) between IHO data values and EAS16 model values. The yellow and orange diamonds denote locations with percent error of less than 10 and 20 respectively. Pink diamonds 20-30% error. Colored circles denote % error of 30 to 100, triangles >100 and red squares >1000.

113
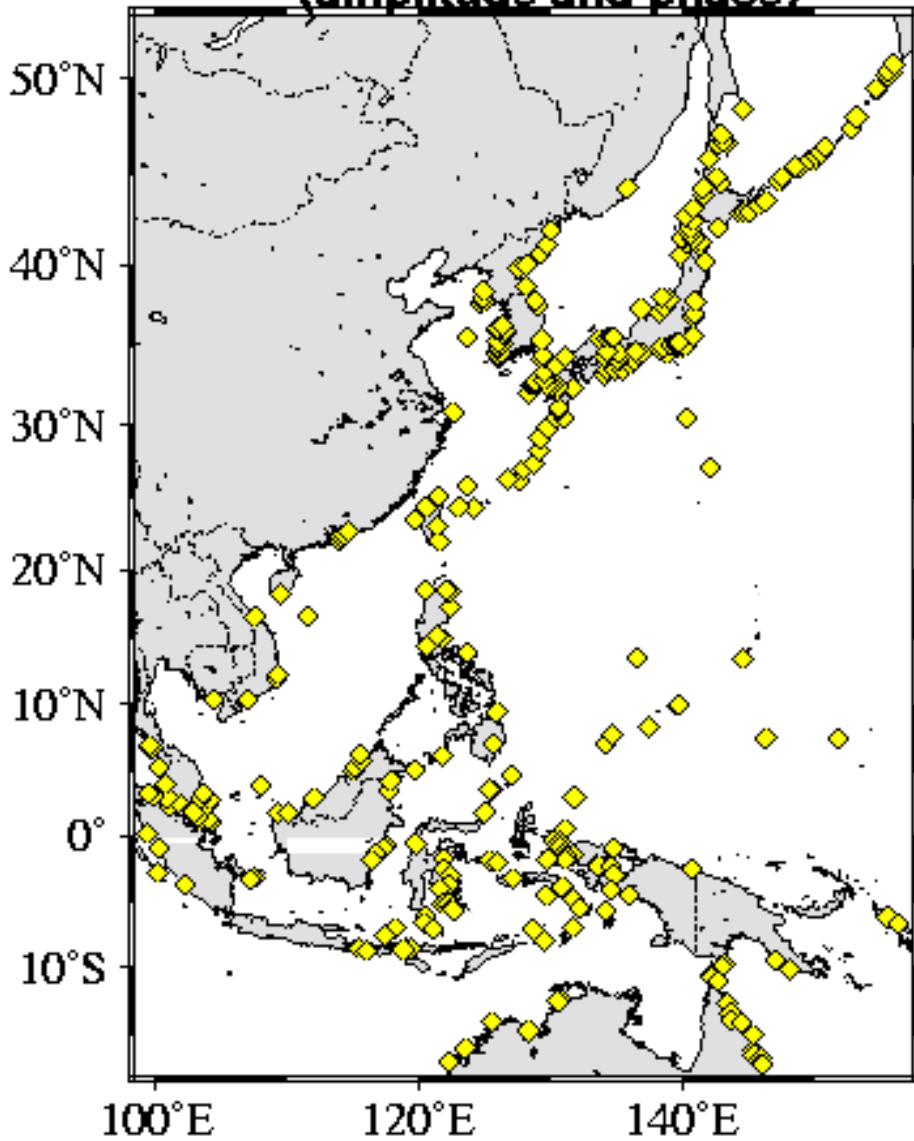
Figure 53. Stations were the percent error for M2 between IHO and EAS16 model values, is less than 20% for both amplitude and phase.
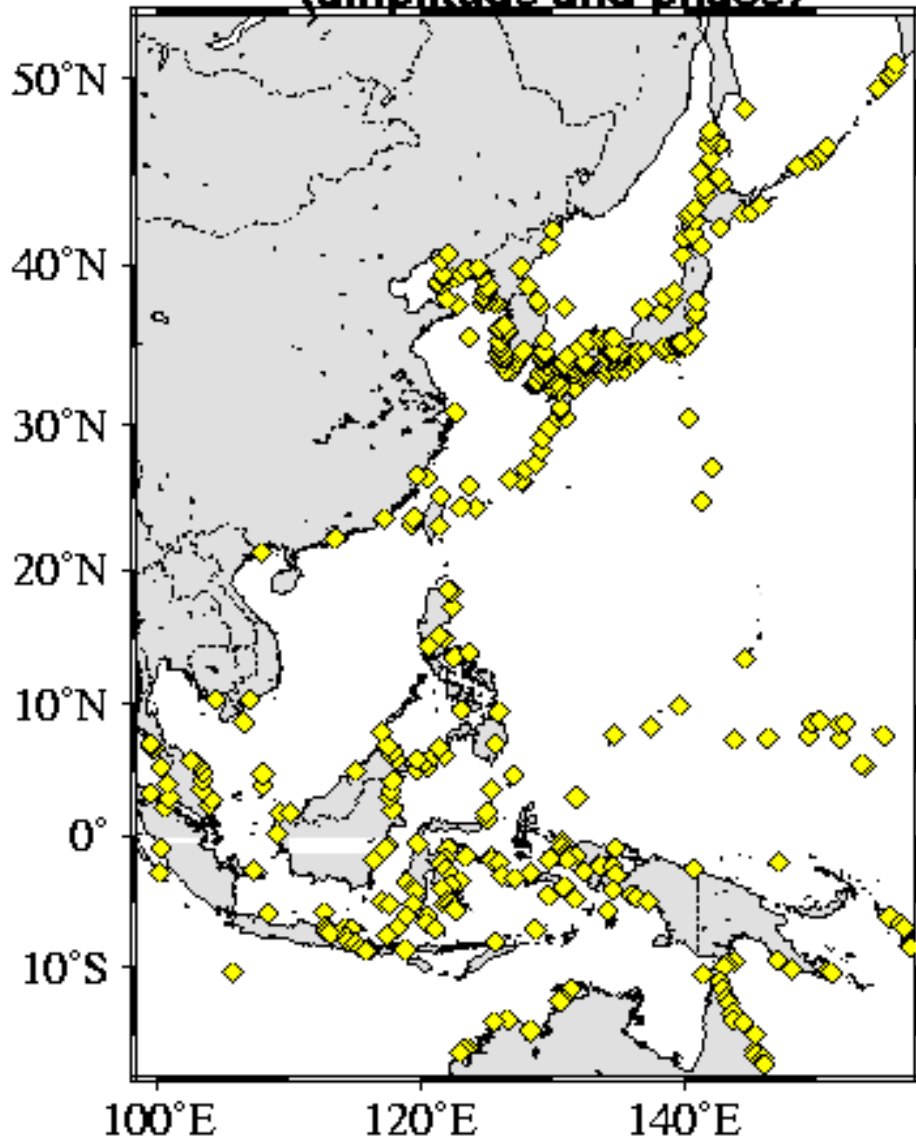
Figure 54. Stations were the percent error for K1, between IHO and EAS16 model values, is less than 20% for both amplitude and phase.
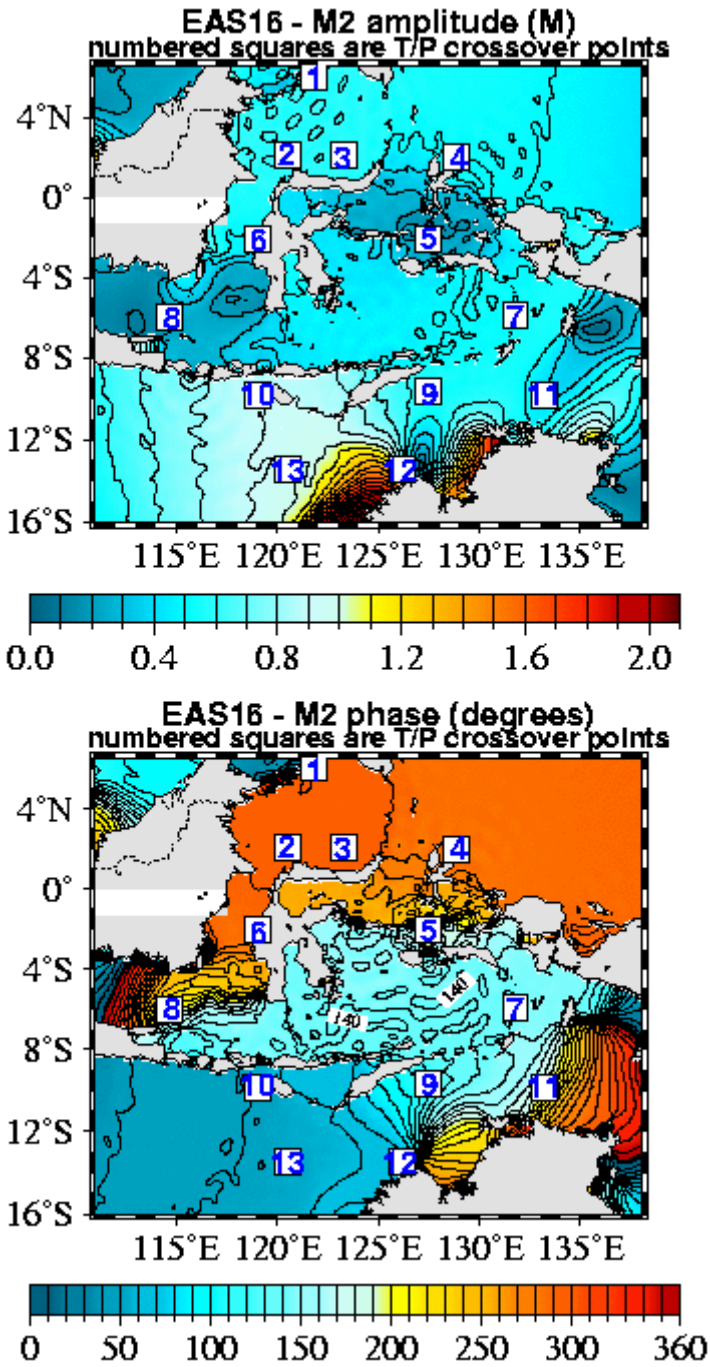
Figure 55. Amplitude and phase from EAS16 model in the Indonesia seas. Numbers denote TOPEX/Poseidon crossover points.
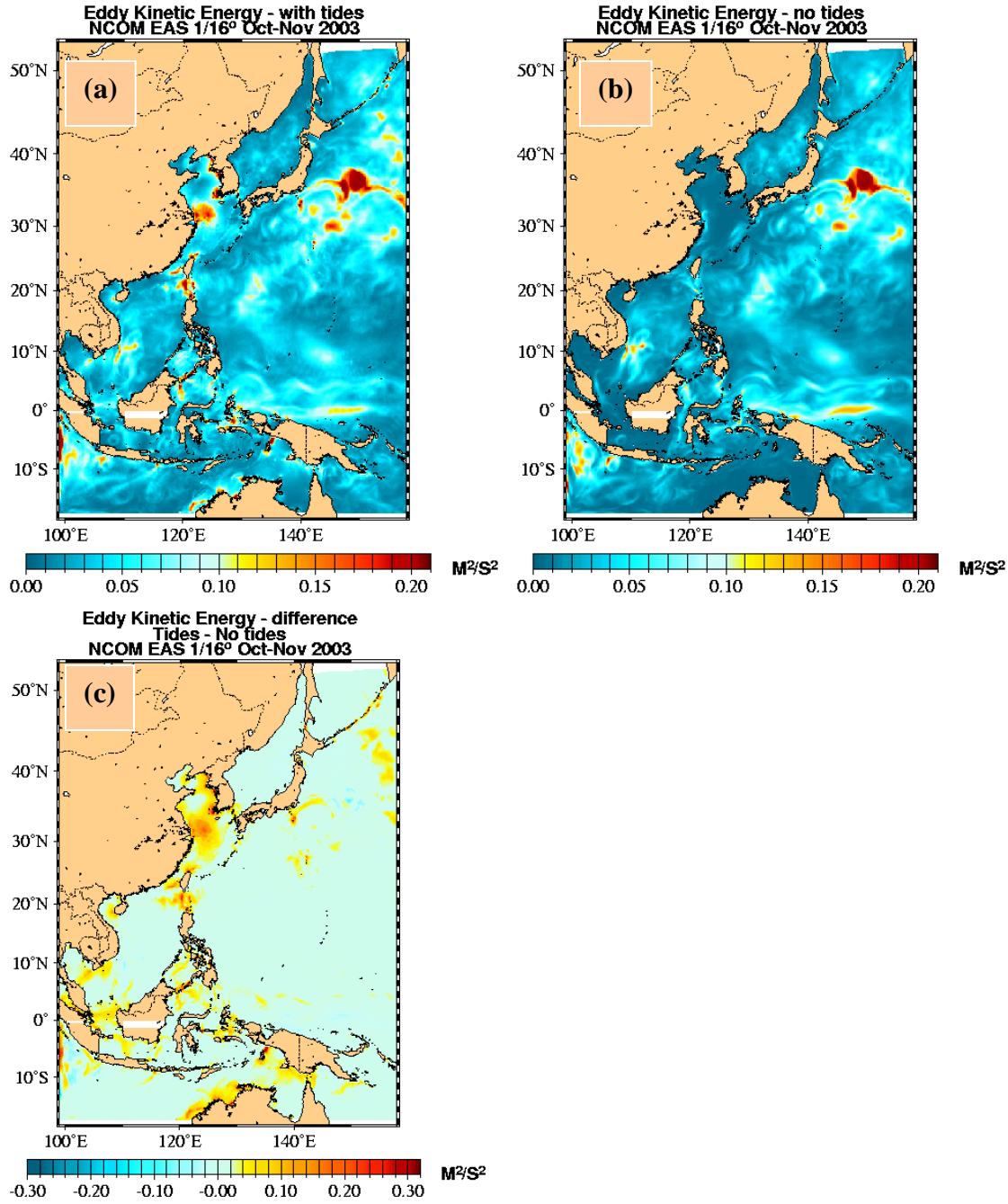
Figure 56. (a) Eddy kinetic energy of surface currents for EAS16 model run with tides, (b) Eddy kinetic energy of surface currents for EAS16 model run without tides, (c) difference between model run with tides and without tides for October through November 2003.
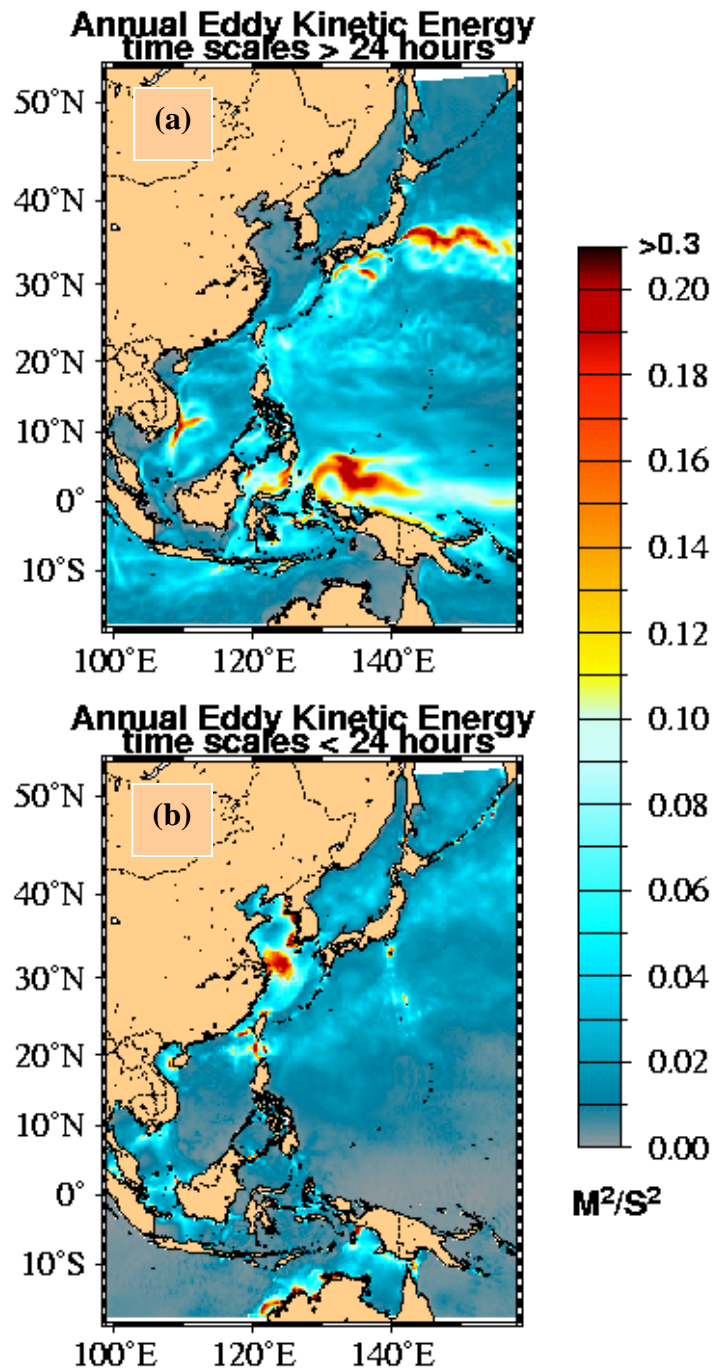
Figure 57. (a) Eddy kinetic energy for time scales of 1 day to 1 year. (b) eddy kinetic energy for time scales less than 1 day.
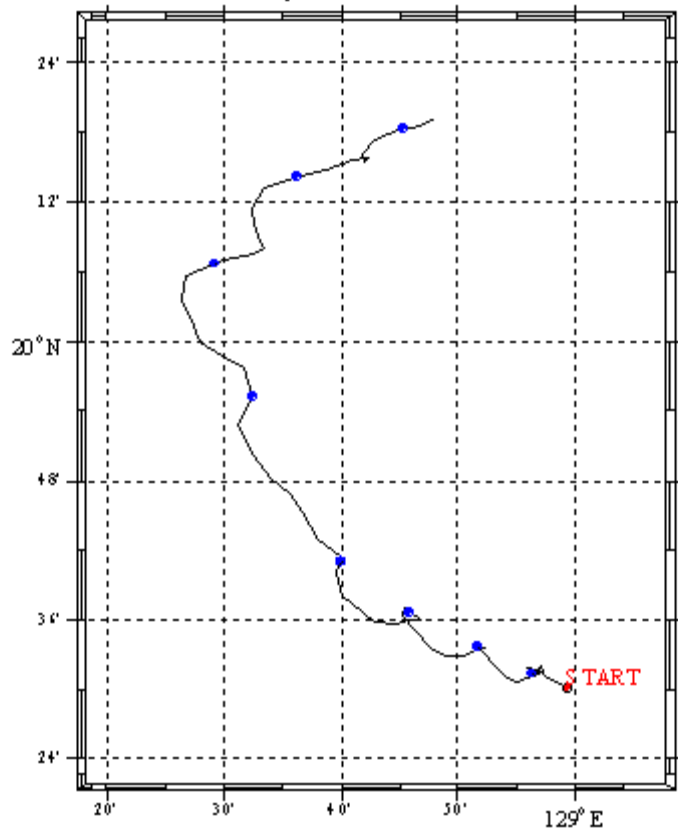
Figure 58. Drifter track for glider we04 from May 8 to May 17, 2004. Plot provided by Dr. Mike Carnes (NAVOCEANO).
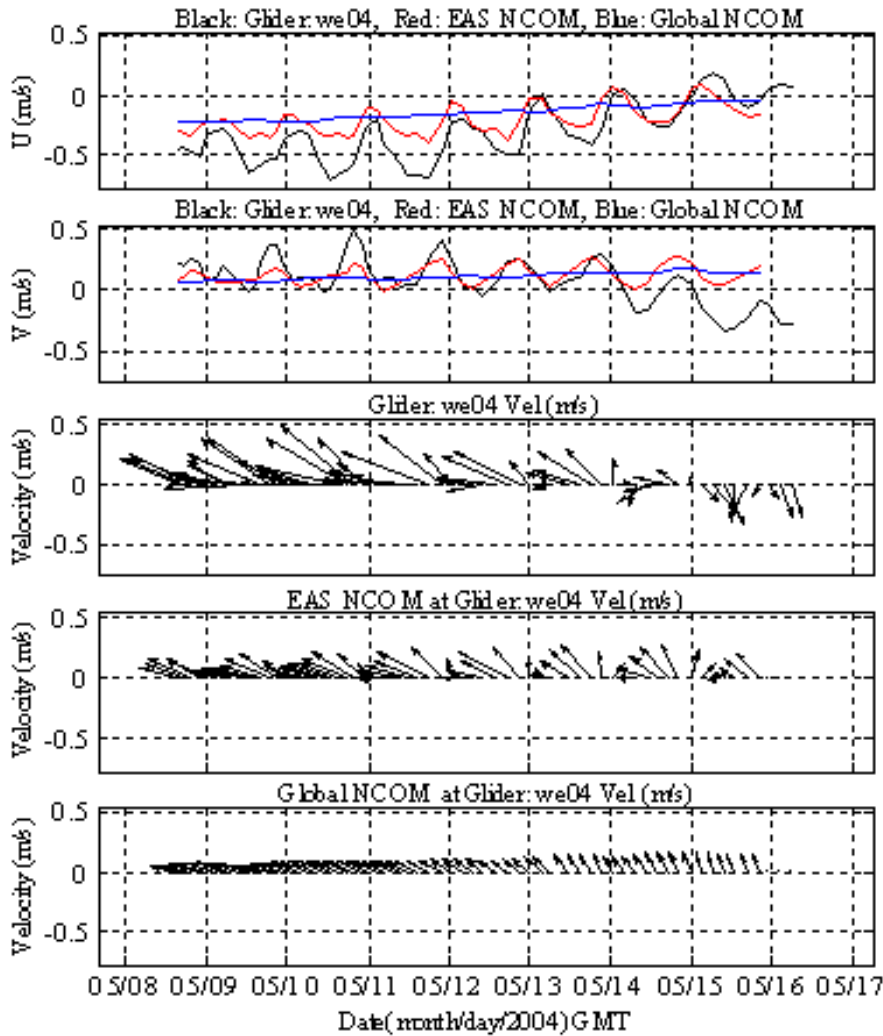
Figure 59a. Upper two panels show the U and V component of velocity in m/s from Glider we04 (black line), corresponding velocity for EAS16 model (red line) and corresponding velocity from Global model (blue line). Lower three panels show the velocity vector for glider, EAS16 mode and global model. Plot provided by Dr. Mike Carnes (NAVOCEANO).

120
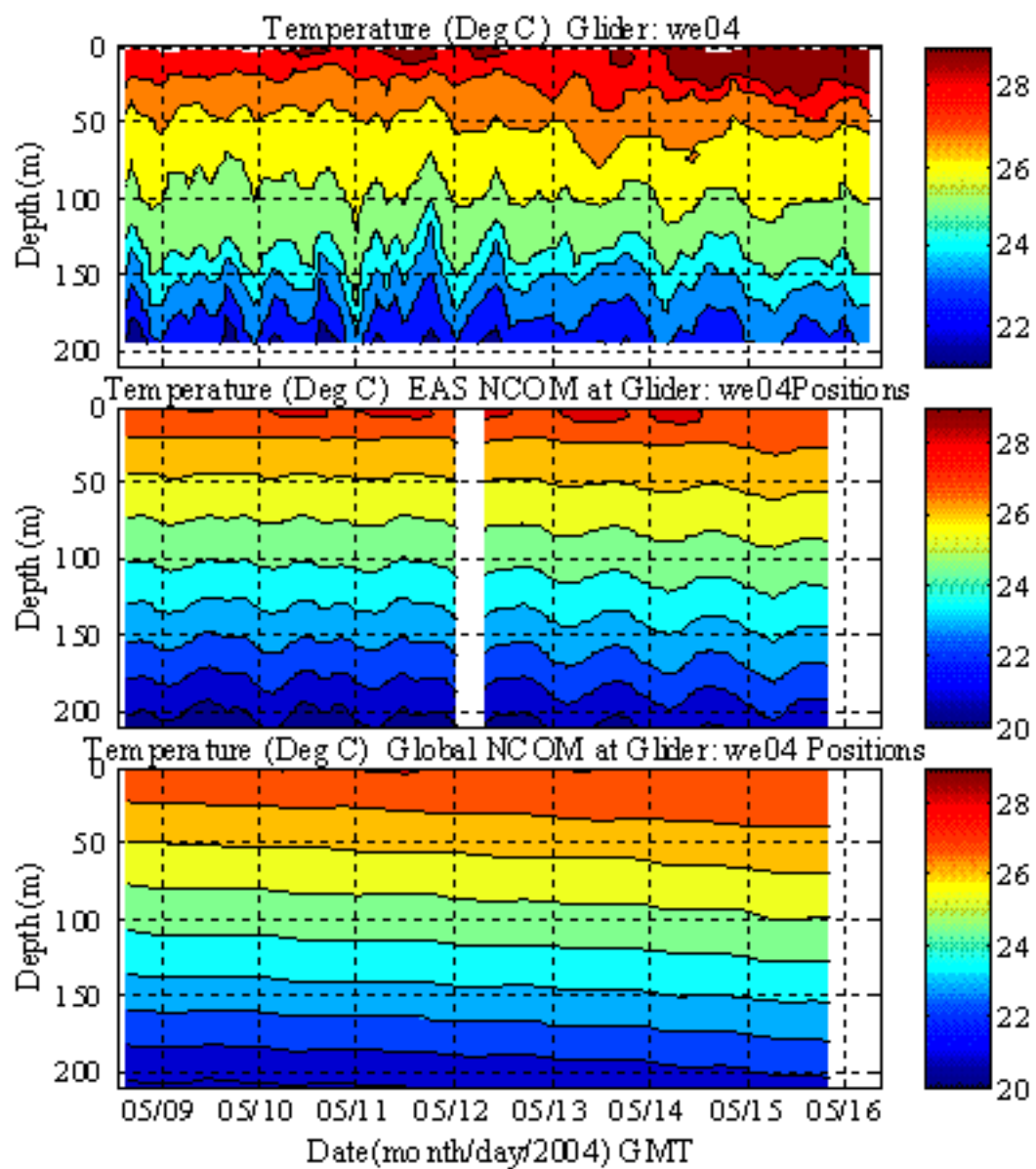
Figure 59b. Temperature with depth (°C) for the upper 200 meters. Upper panel shows temperatures from Glider we04, middle is for EAS16 model (missing data near May 12) and lower panel is for Global model. Plot provided by Dr. Mike Carnes (NAVOCEANO).
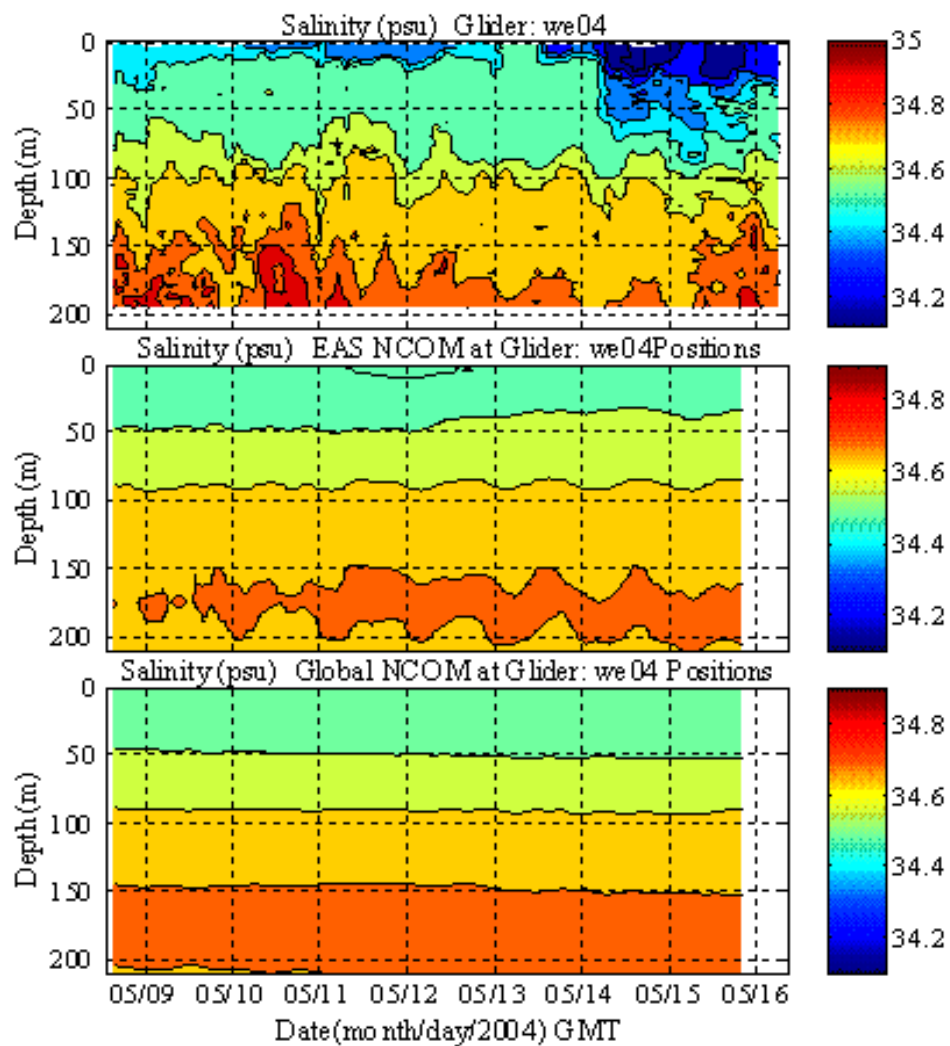
Figure 59c. Salinity with depth (ppt) for the upper 200 m. Upper panel shows salinity from Glider we04, middle is for EAS16 model and lower panel is for Global model. Plot provided by Dr. Mike Carnes (NAVOCEANO).
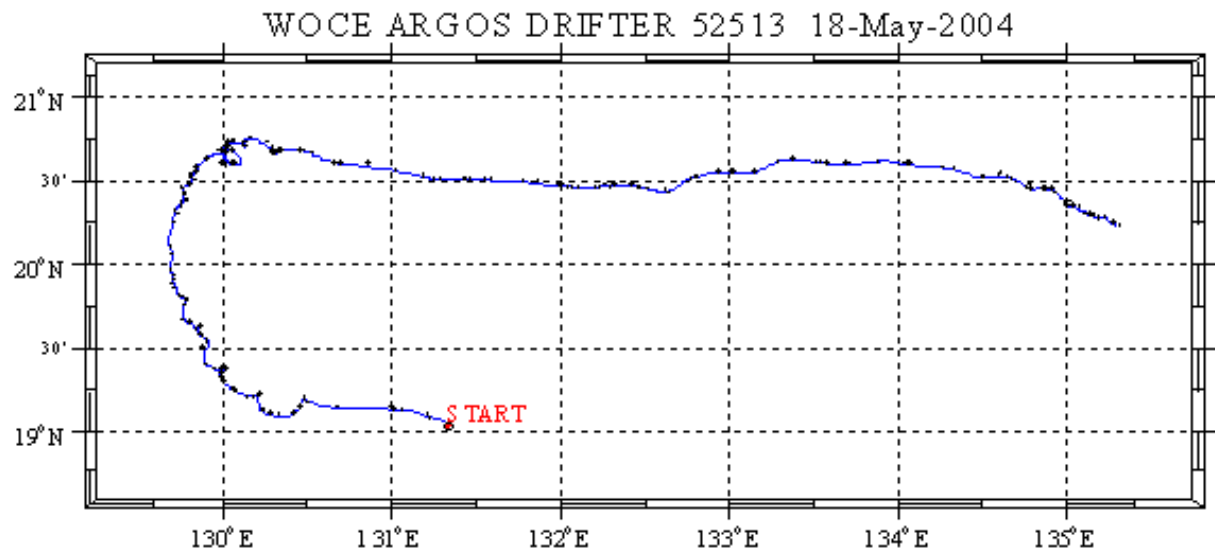
Figure 60a. Drifter path for WOCE ARGOS drifter #52513 from April 13 through May 18, 2004. Plot provided by Dr. Mike Carnes (NAVOCEANO).
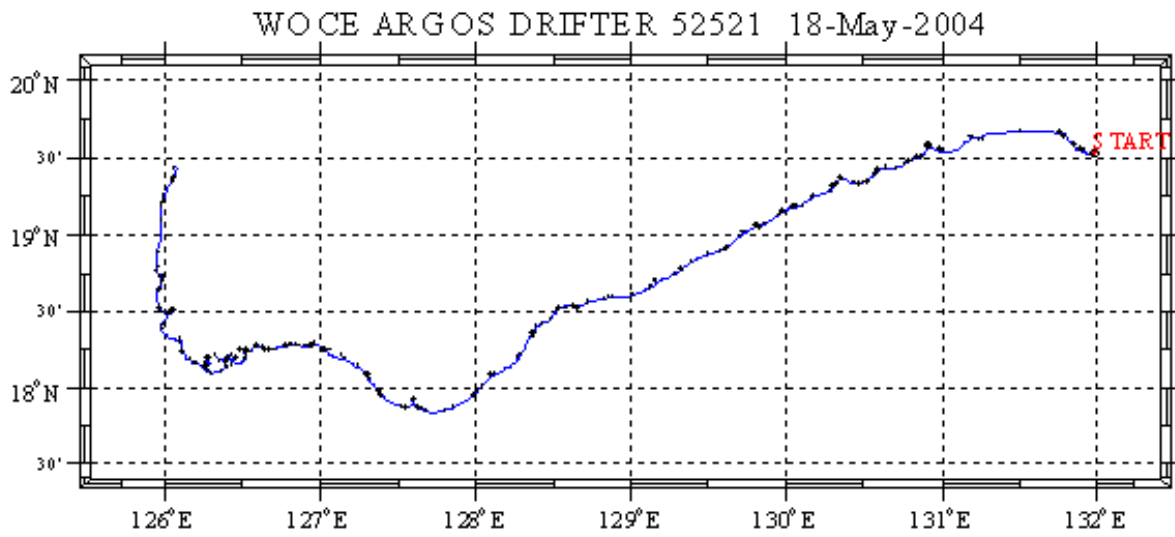
Figure 60b. Drifter path for WOCE ARGOS drifter #52521 from April 13 through May 18, 2004. Plot provided by Dr. Mike Carnes (NAVOCEANO).
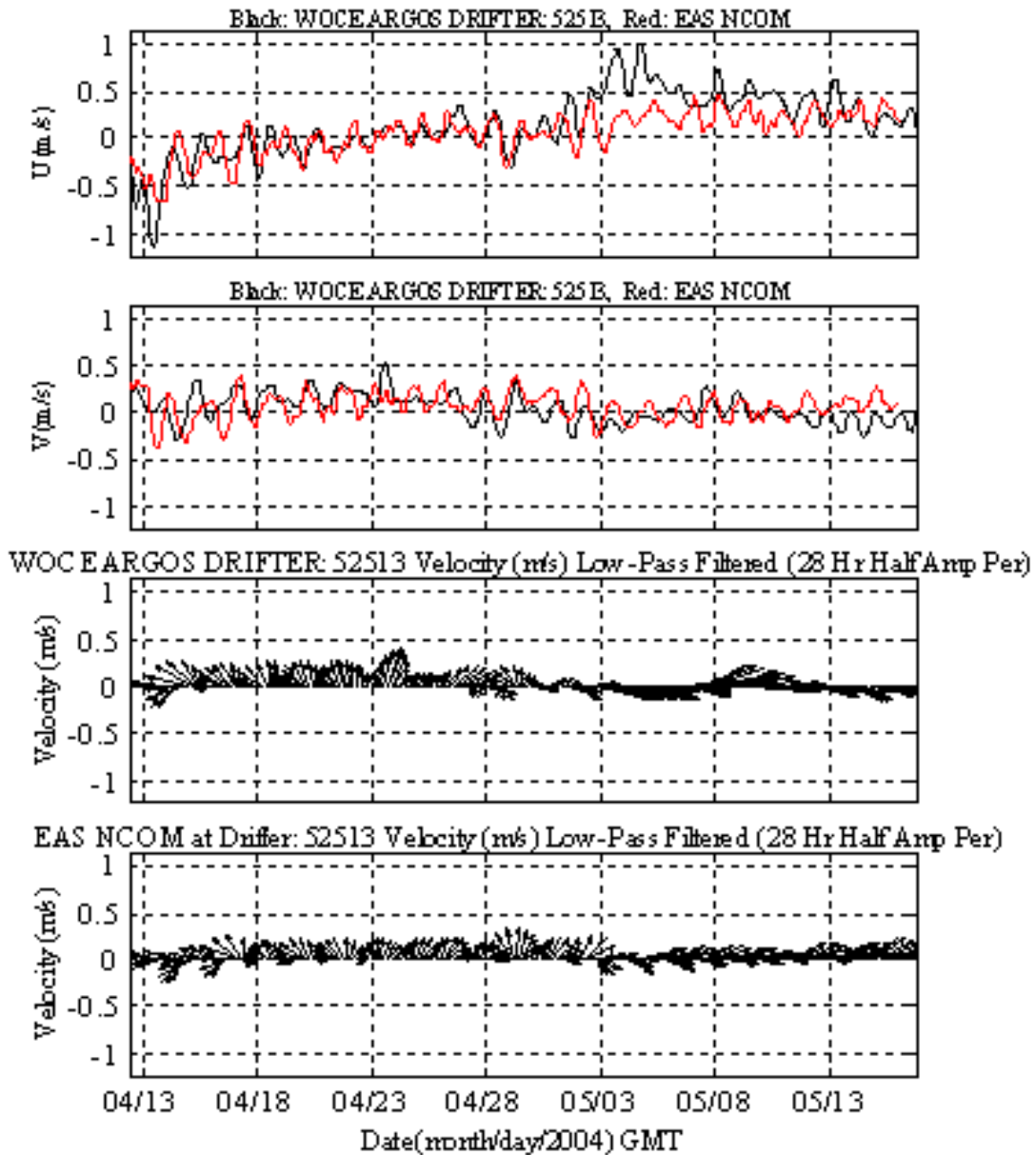
Figure 61a. Velocity time series for drifter #52513. Upper two panels show U&V component of velocity for drifter (black line) and EAS16 model (red line). Lower two panels show the velocity vectors for the drifter and EAS16 model. Plot provided by Dr. Mike Carnes (NAVOCEANO).
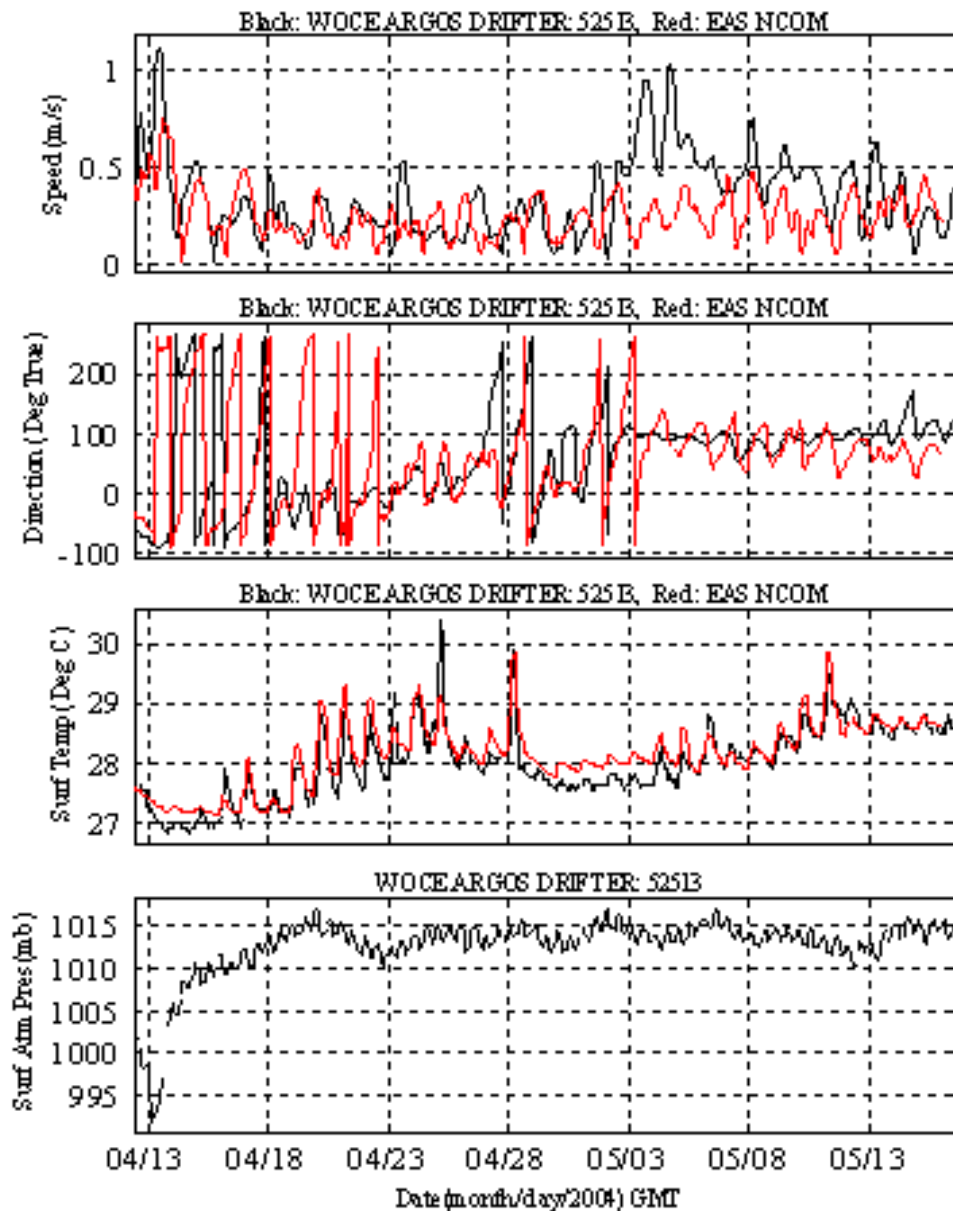
**Figure 61b. Upper two panels show the speed (m/s) and direction from drifter #52513 (black line) and EAS16 model (red line). Third panel shows the temperature from drifter #52513 (black line) and EAS16 model (red line). Bottom panel shows the surface air pressure from the drifter. All values are for the time period April 13, 2004 through May 18, 2004. Plot provided by Dr. Mike Carnes (NAVOCEANO).**

126
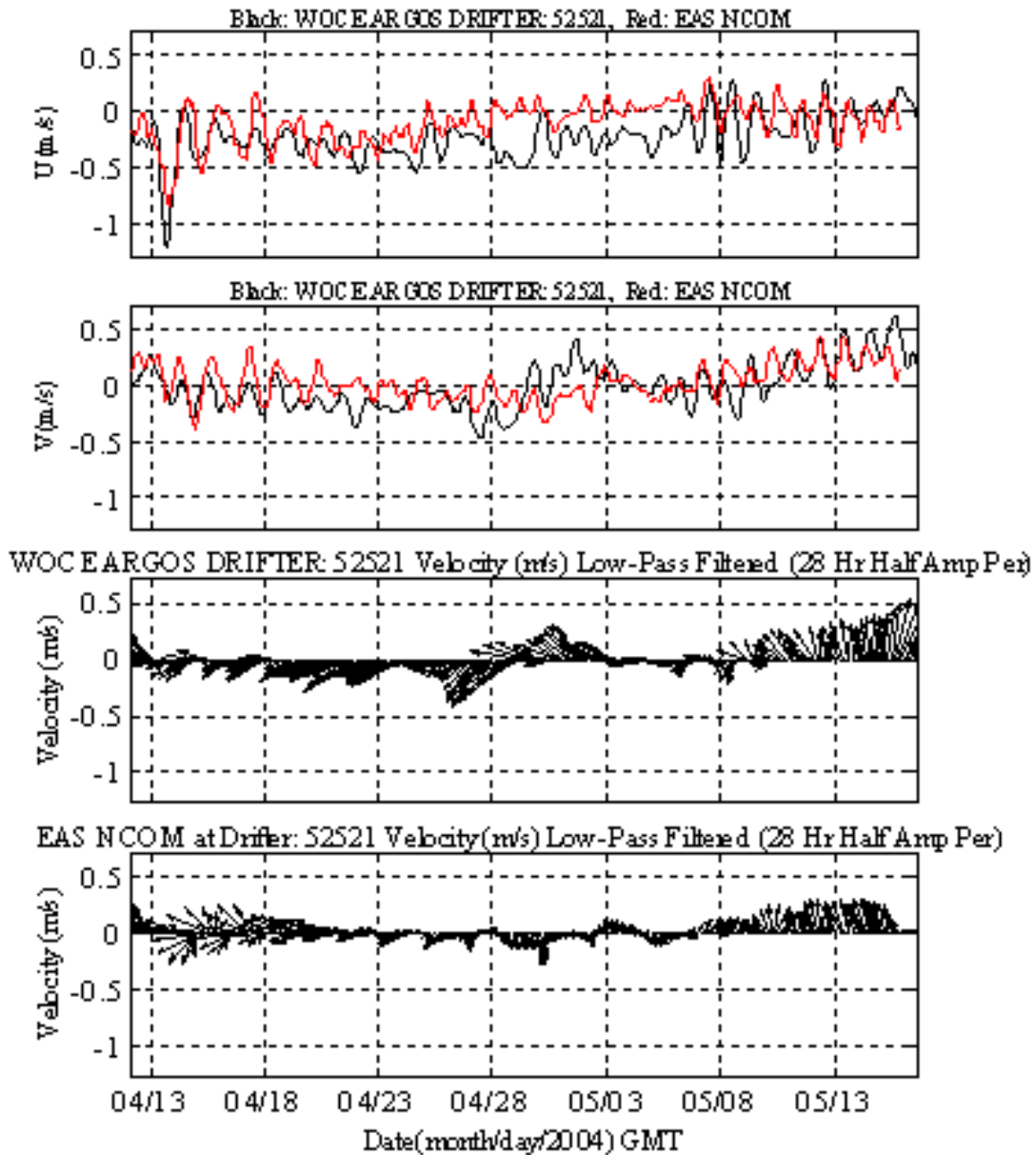
Figure 62a. Velocity time series for drifter #52521. Upper two panels show U&V component of velocity for drifter (black line) and EAS16 model (red line). Lower two panels show the velocity vectors for the drifter and EAS16 model. Plot provided by Dr. Mike Carnes (NAVOCEANO).

127
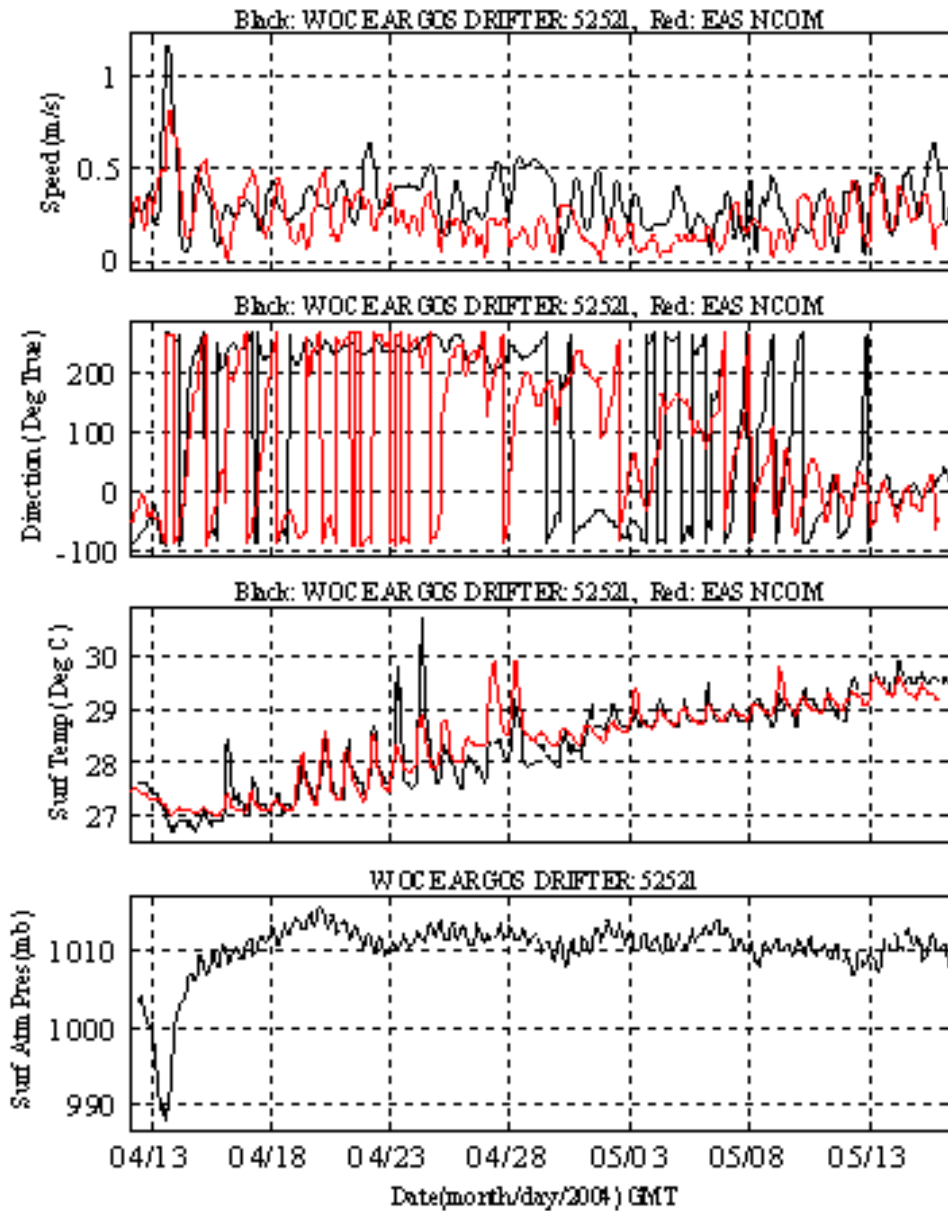
**Figure 62b. Upper two panels show the speed (m/s) and direction from drifter #52521 (black line) and EAS16 model (red line). Third panel shows the temperature from drifter #52521 (black line) and EAS16 model (red line). Bottom panel shows the surface air pressure from the drifter. All values are for the time period April 13, 2004 through May 18, 2004. Plot provided by Dr. Mike Carnes (NAVOCEANO).**
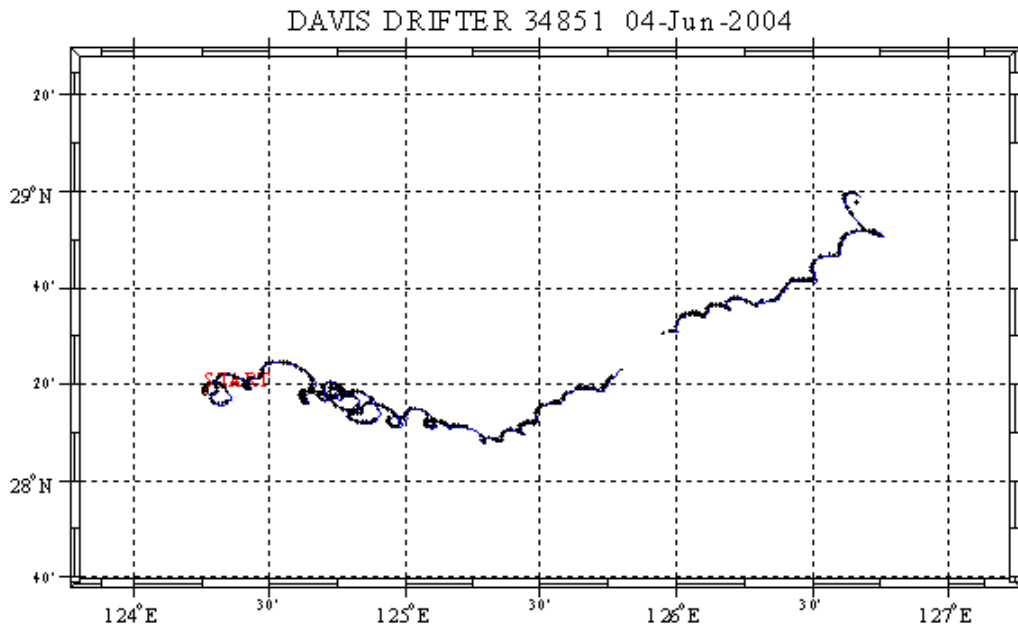
Figure 63. Location of Davis drifter #34851 from May 13, 2004 through June 2, 2004. Gap in drifter path indicates missing data. Plot provided by Dr. Mike Carnes (NAVOCEANO).
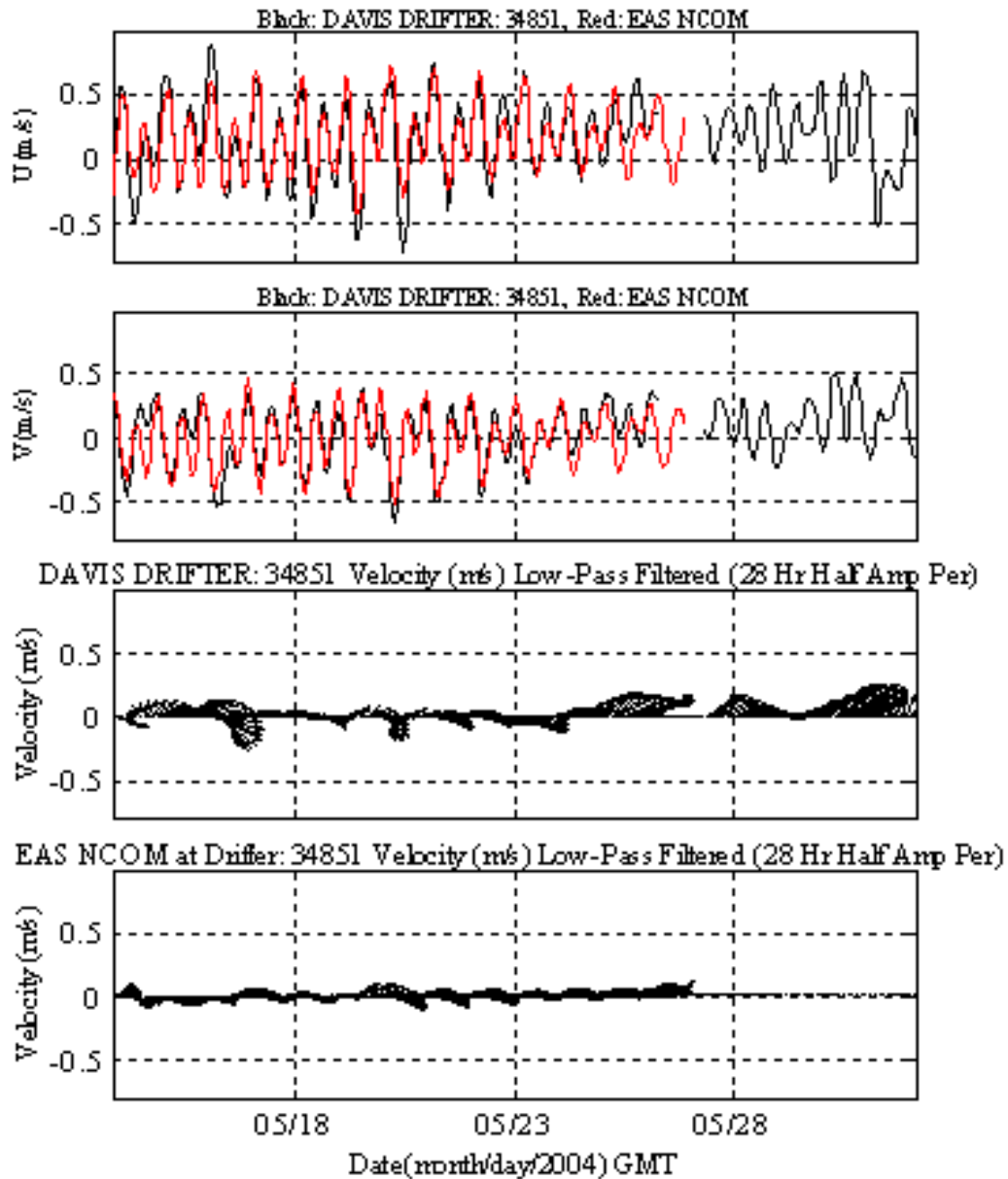
**Figure 64a. Velocities from Davis drifter #34851 (black line) and EAS16 model (red line). Upper two panels show the U&V component of velocity. The lower two panels show the velocity vectors for the drifter and EAS16 model. Plot provided by Dr. Mike Carnes (NAVOCEANO).**
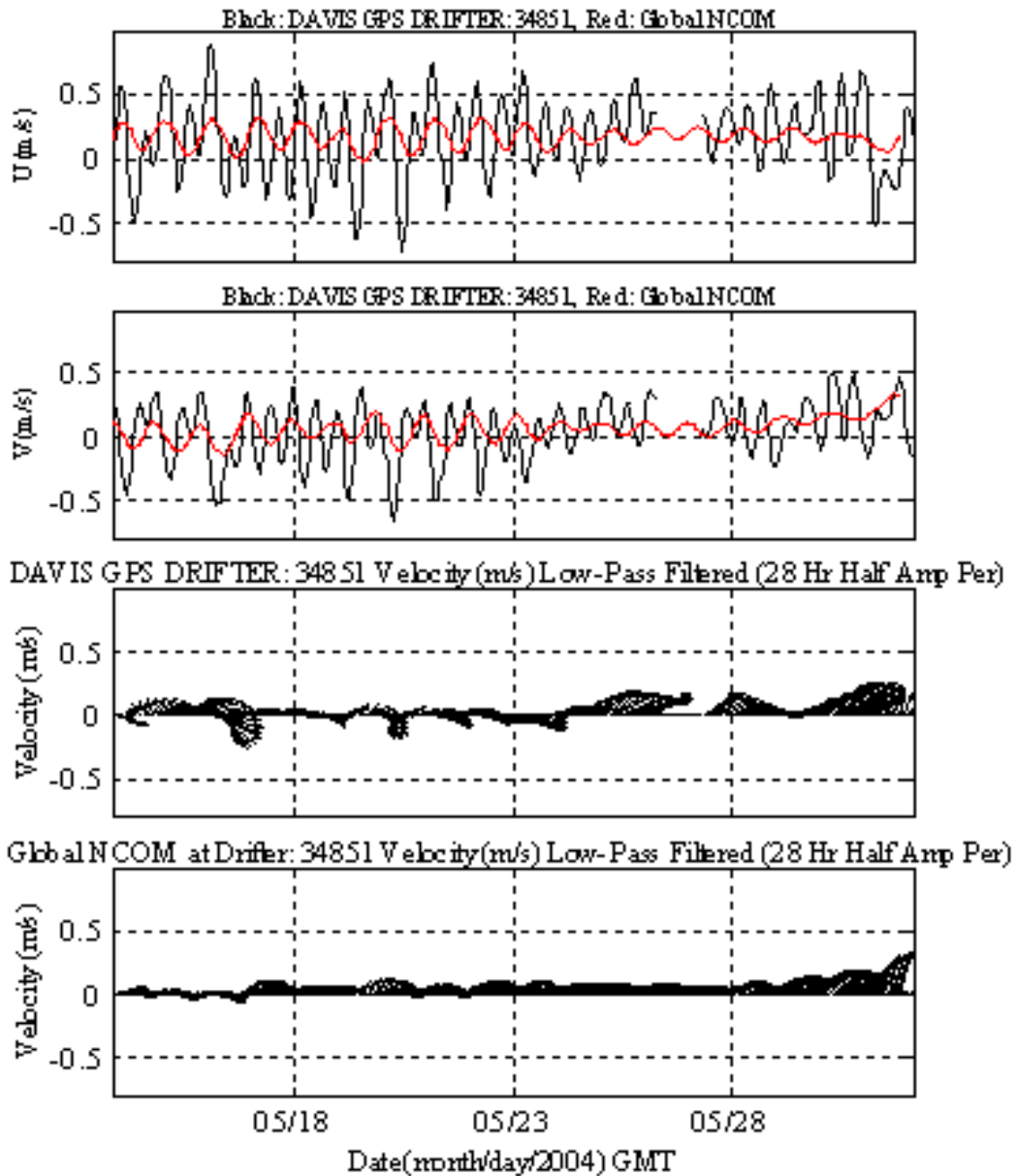
Figure 64b. Velocities from Davis drifter #34851(black line) and Global model (red line). Upper two panels show the U&V component of velocity. The lower two panels show the velocity vectors for the drifter and Global model. Plot provided by Dr. Mike Carnes (NAVOCEANO).
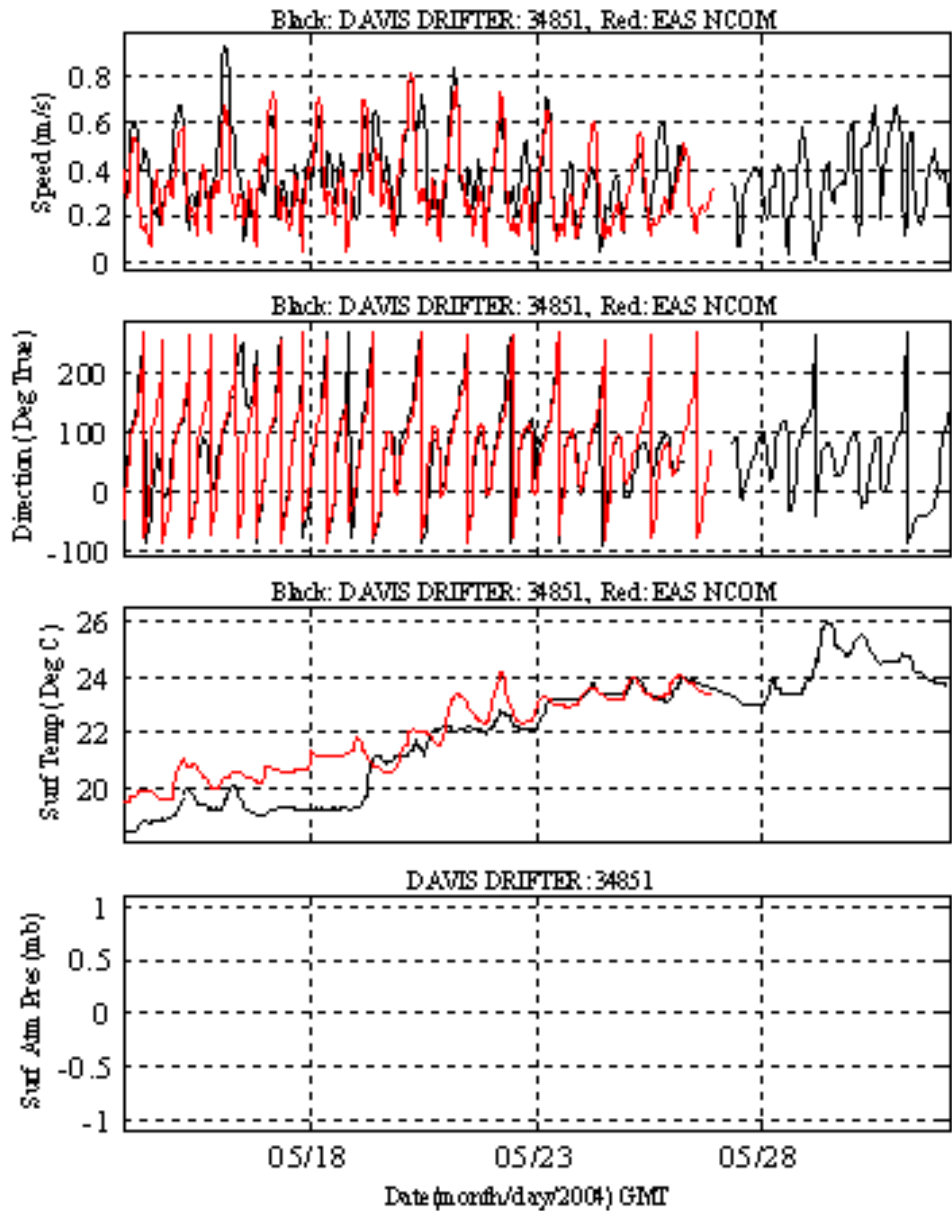
Figure 65a. Upper two panels show the speed and direction for the Davis drifter #34851 (black line) and the EAS16 model (red line). The third panel shows the surface temperature for the drifter (black line) and EAS16 model (red line). Plot provided by Dr. Mike Carnes (NAVOCEANO).

132
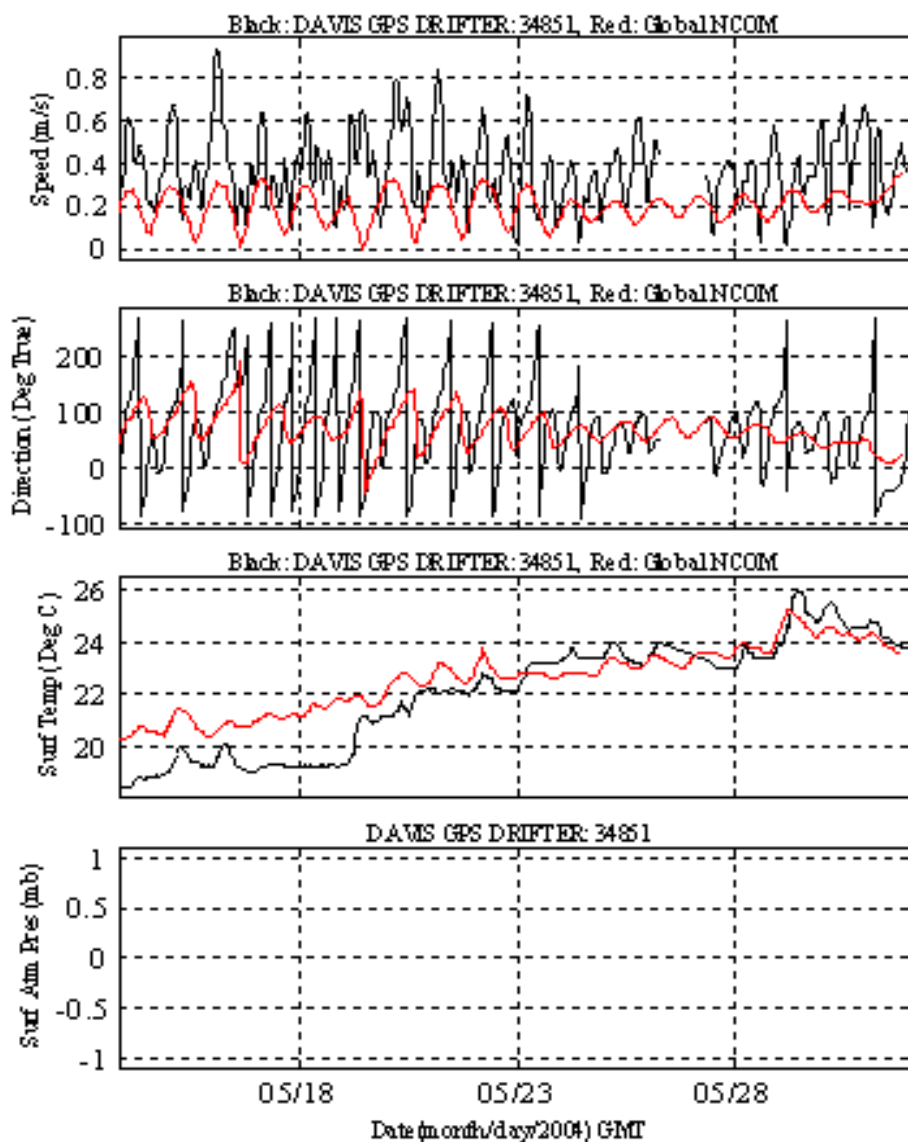
Figure 65b. Upper two panels show the speed and direction for the Davis drifter #34851 (black line) and the Global model (red line). The third panel shows the surface temperature for the drifter (black line) and Global model (red line).

133
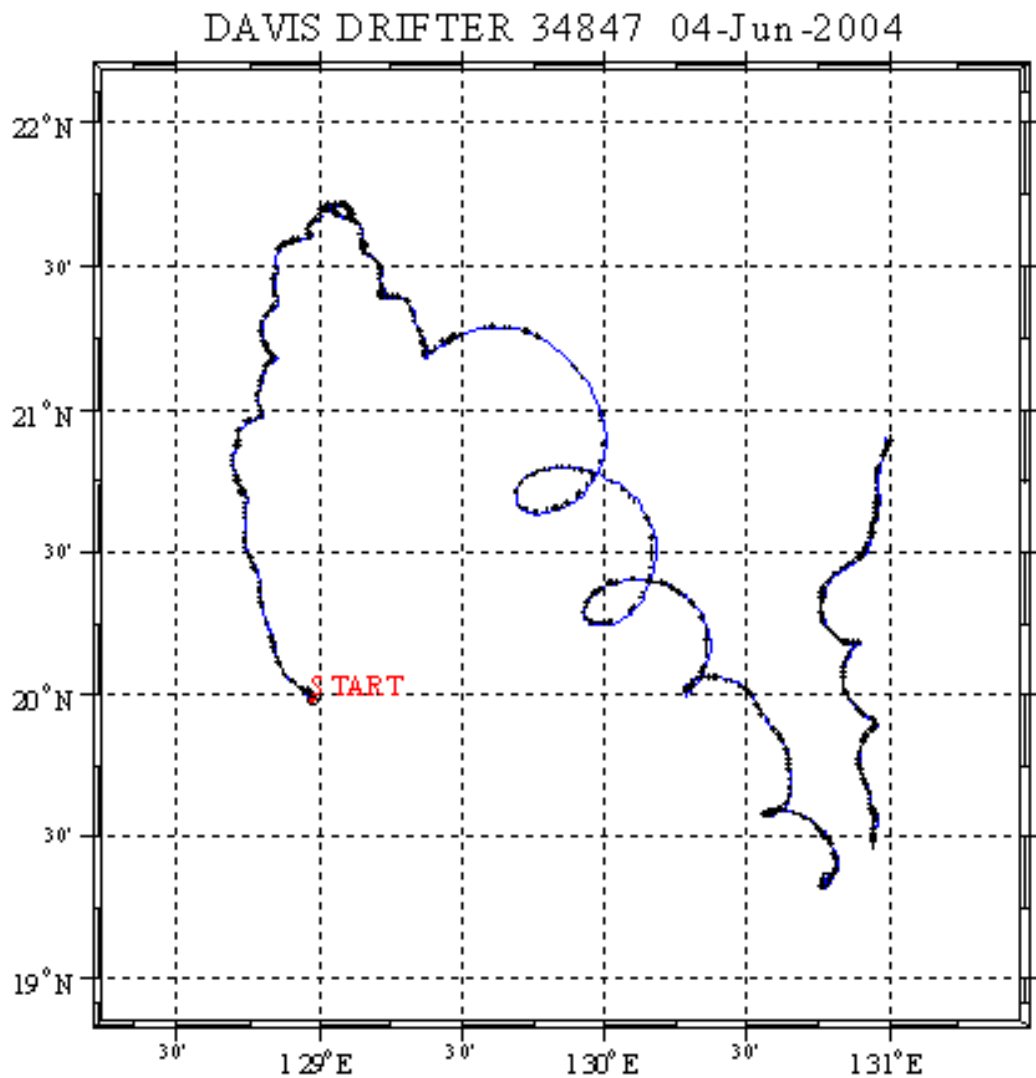
Figure 66. Location of Davis drifter #34847 from May 8, 2004 through June 4, 2004. Gap in drifter path indicates missing data. Plot provided by Dr. Mike Carnes (NAVOCEANO).
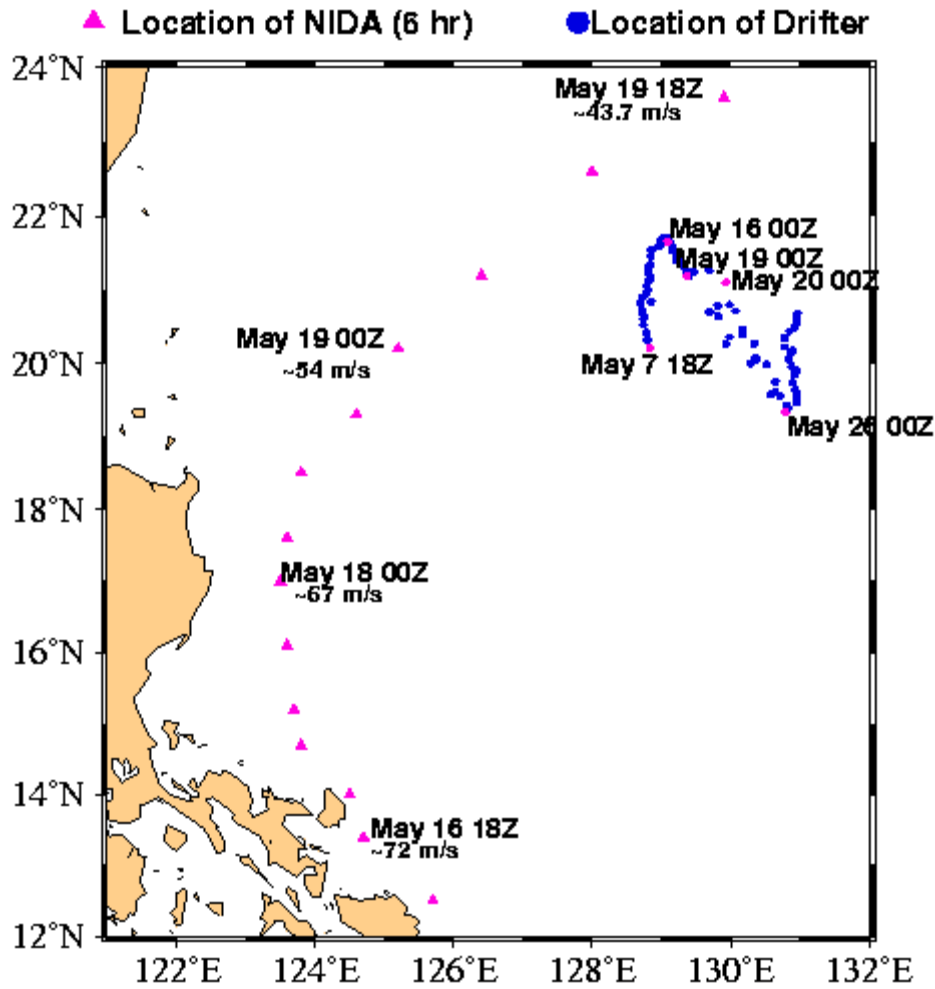
Figure 67. Track for Super Typhoon NIDA from May 16 through May 19 (pink triangles). Speed associated with the date shown is the approximated maximum wind speed for NIDA at that time. The blue squares show the drifter track. Pink squares show location of drifter on corresponding dates
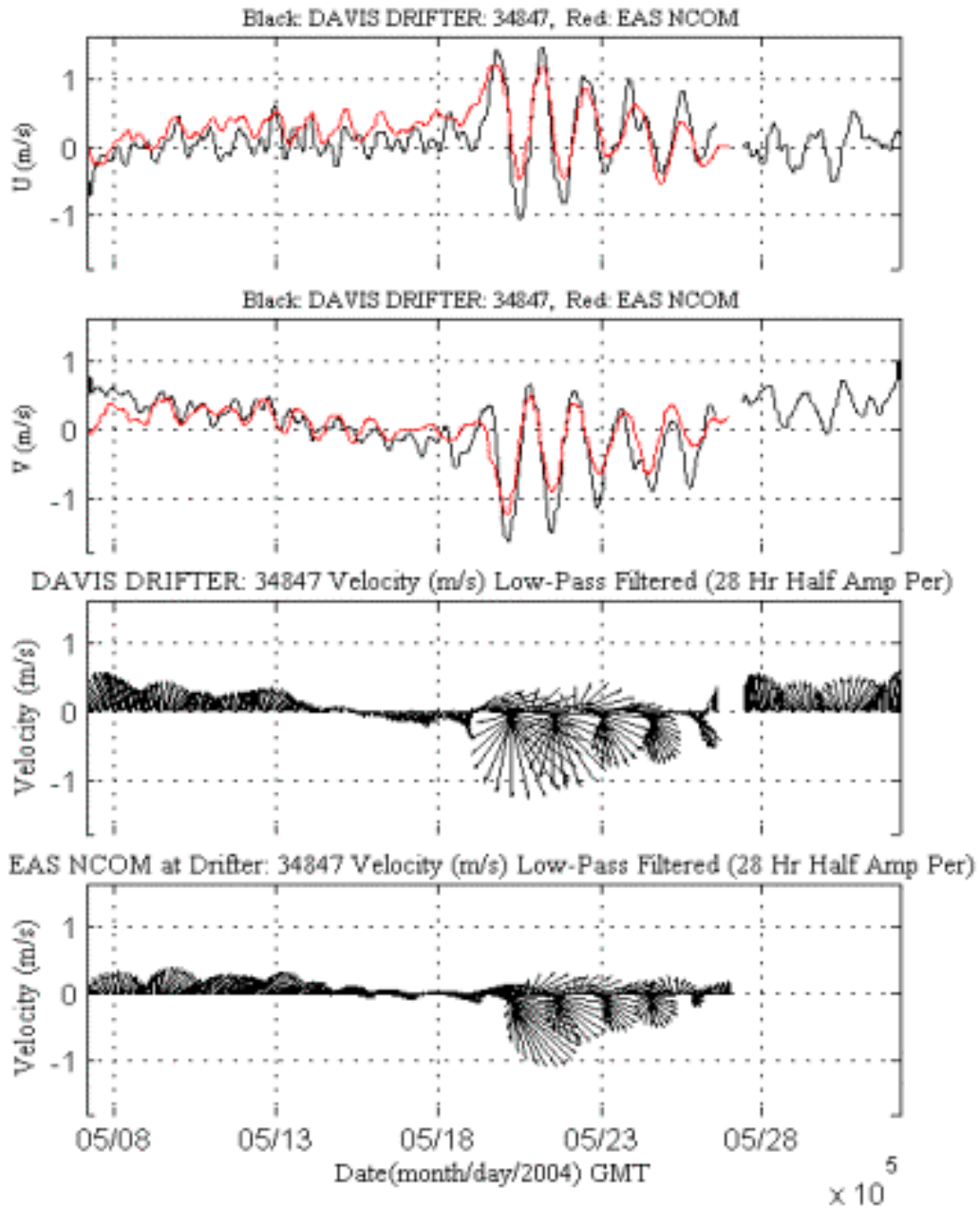
Figure 68a. Upper panels show the U&V component of velocity from Davis drifter #34857 (black line) and EAS16 model (red line). Lower two panels show the velocity vectors for the Davis drifter and EAS16. From My 8, 2004 through June 4, 2004. Plot provided by Dr. Mike Carnes (NAVOCEANO).
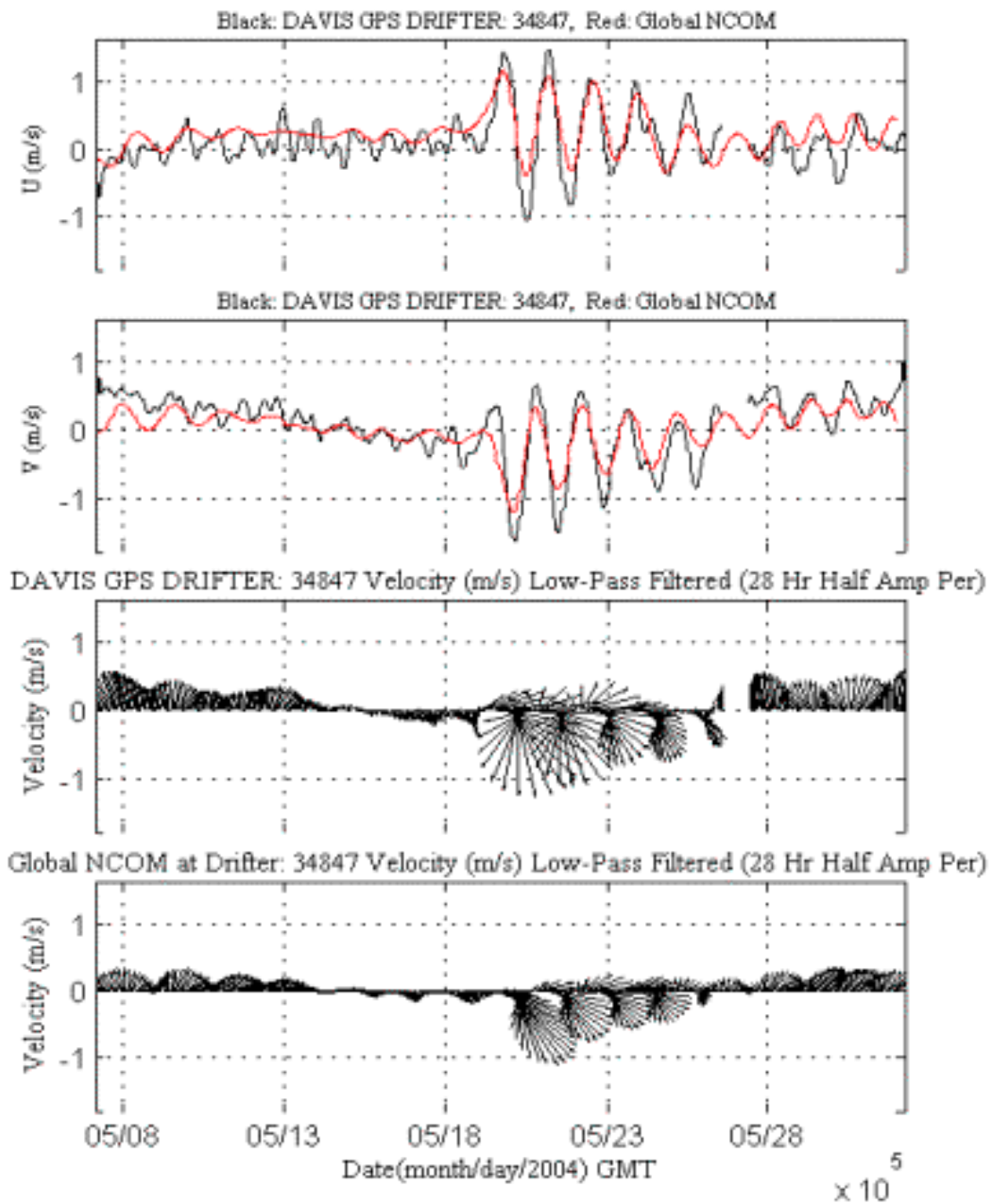
Figure 68b. Upper panels show the U&V component of velocity from Davis drifter #34857 (black line) and Global model (red line). Lower panels show the velocity vectors for the Davis drifter and Global model. From My 8, 2004 through June 4, 2004. Plot provided by Dr. Mike Carnes (NAVOCEANO).
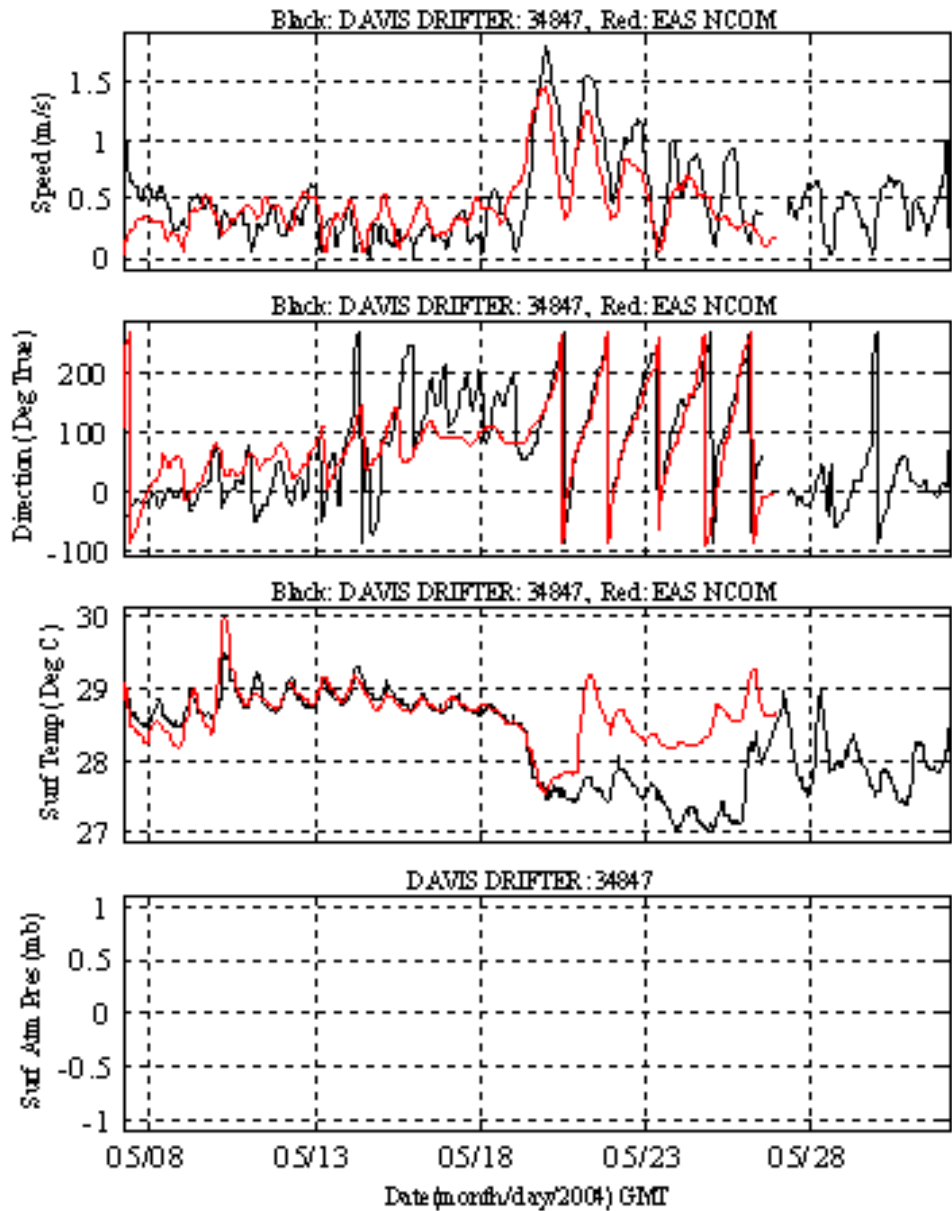
Figure 69a. Upper two panels show the speed and direction from Davis drifter #34847 (black line) and EAS16 model (red line). Third panel shows surface temperature. From May 8, 2004 through June 4. 2004. Plot provided by Dr. Mike Carnes (NAVOCEANO).
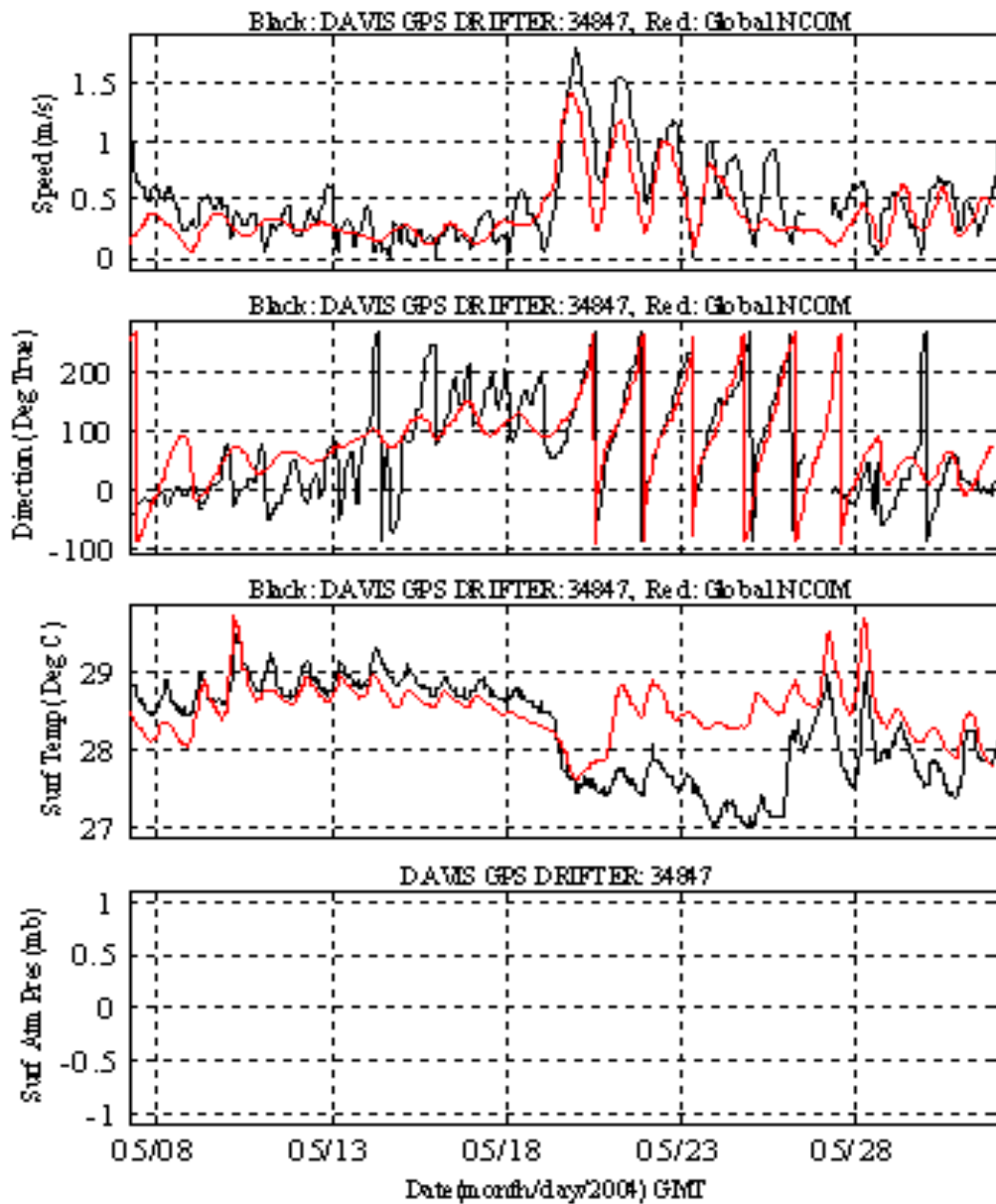
Figure 69b. Upper two panels show the speed and direction from Davis drifter #34847 (black line) and Global model (red line). Third panel shows the surface temperature. From May 8, 2004 through June 4. 2004. Plot provided by Dr. Mike Carnes (NAVOCEANO).
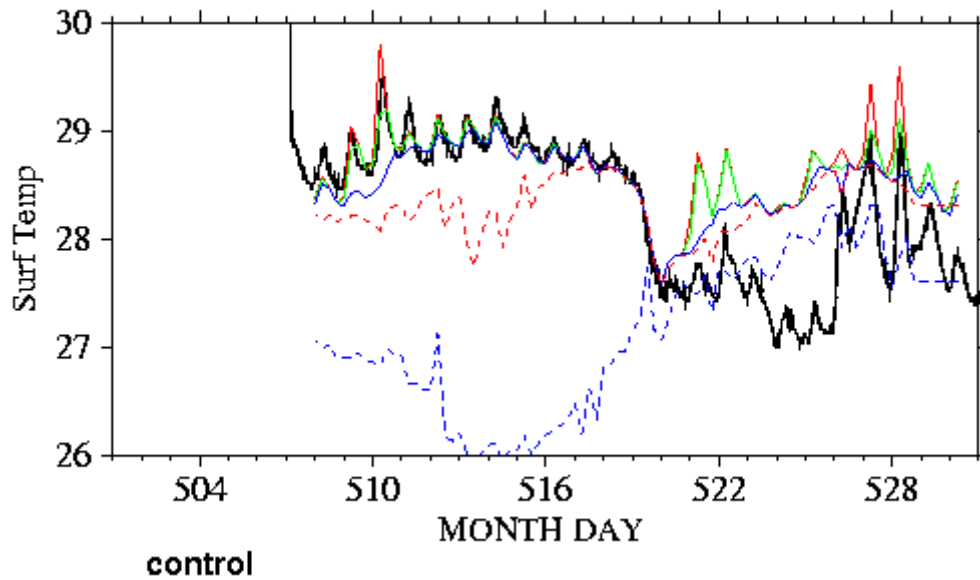
Figure 70. Comparing sea surface temperature for May 6, 2004 through May 30, 2004 for drifter (black line), EAS16 model, surface (red line), 1 meter (green line), 5 meters (blue line), 15 meters (red dashed line) and 40 meters (blue dashed line).